AD-A073 818 PENNSYLVANIA STATE UNIV UNIVERSITY PARK APPLIED RESE--ETC F/G 20/1
TRANSIENT RESPONSE OPTIMIZATION OF PIEZOELECTRIC DISC TRANSDUCE--ETC(U)
JUL 79 H A WOLF N00024-79-C-6043
UNCLASSIFIED ARL/PSU/TM-79-139 NL

1 OF 3

AD A073818

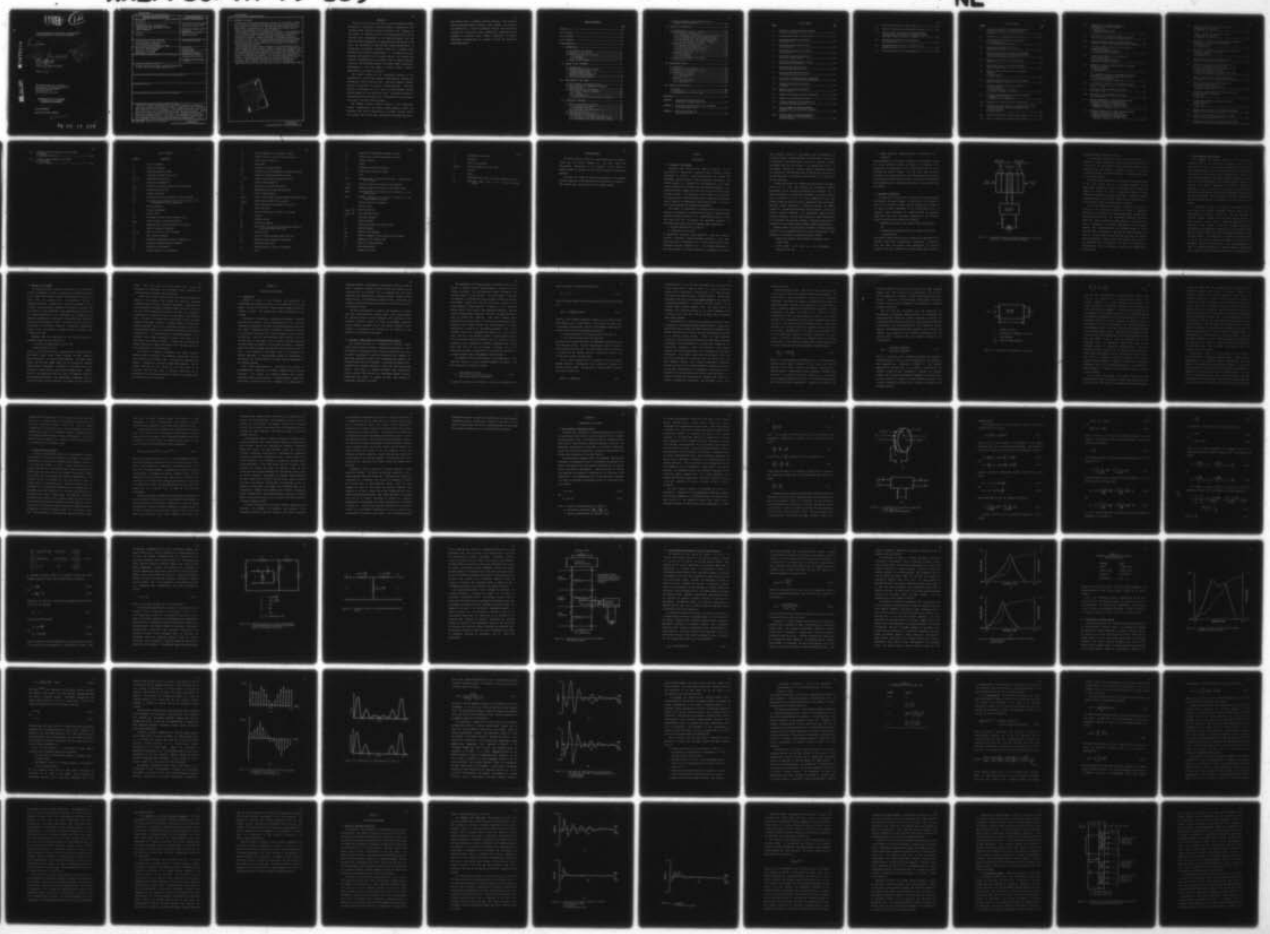

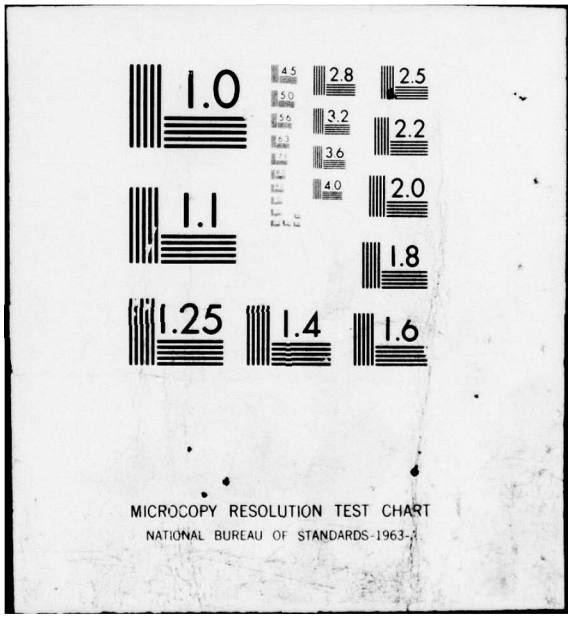
1.0
1.1
1.25
1.4
1.6
1.8
2.0
2.2
2.5
2.8
3.2
3.6
4.0
4.5
5.0
5.6
6.3
MICROCOPY RESOLUTION TEST CHART
NATIONAL BUREAU OF STANDARDS-1963-A

LEVEL II

TRANSIENT RESPONSE OPTIMIZATION OF PIEZOELECTRIC DISC TRANSDUCERS BY TIME DOMAIN TECHNIQUES.

Henry Alan Wolf

Technical Memorandum

File No. TM-79-139
July 23, 1979
Contract No. N00024-79-C-6043

Copy No. 13

The Pennsylvania State University
Institute for Science and Engineering
APPLIED RESEARCH LABORATORY
Post Office Box 30
State College, PA 16801

APPROVED FOR PUBLIC RELEASE
DISTRIBUTION UNLIMITED

NAVY DEPARTMENT

NAVAL SEA SYSTEMS COMMAND

AD A073818

DDC FILE COPY

DDC RECEIVED SEP 17 1979 C

311001

79 09 14 054

UNCLASSIFIED

SECURITY CLASSIFICATION OF THIS PAGE *(When Data Entered)*

REPORT DOCUMENTATION PAGE		READ INSTRUCTIONS BEFORE COMPLETING FORM
1. REPORT NUMBER TM 79-139	2. GOVT ACCESSION NO.	3. RECIPIENT'S CATALOG NUMBER
4. TITLE *(and Subtitle)* TRANSIENT RESPONSE OPTIMIZATION OF PIECOELECTRIC DISC TRANSDUCERS BY TIME DOMAIN TECHNIQUES		5. TYPE OF REPORT & PERIOD COVERED PhD Thesis, August 1979 6. PERFORMING ORG. REPORT NUMBER TM 79-139
7. AUTHOR(s) Alan Wolf		8. CONTRACT OR GRANT NUMBER(s) N00024-79-C-6043
9. PERFORMING ORGANIZATION NAME AND ADDRESS The Pennsylvania State University Applied Research Laboratory P. O. Box 30, State College, PA 16801		10. PROGRAM ELEMENT, PROJECT, TASK AREA & WORK UNIT NUMBERS
11. CONTROLLING OFFICE NAME AND ADDRESS Naval Sea Systems Command Department of the Navy Washington, DC 20362		12. REPORT DATE July 23, 1979 13. NUMBER OF PAGES 250 pages & figures
14. MONITORING AGENCY NAME & ADDRESS*(if different from Controlling Office)*		15. SECURITY CLASS. *(of this report)* Unclassified, Unlimited 15a. DECLASSIFICATION/DOWNGRADING SCHEDULE

16. DISTRIBUTION STATEMENT *(of this Report)*

Approved for public release, distribution unlimited, per NSSC (Naval Sea Systems Command) 8/3/79

17. DISTRIBUTION STATEMENT *(of the abstract entered in Block 20, if different from Report)*

18. SUPPLEMENTARY NOTES

19. KEY WORDS *(Continue on reverse side if necessary and identify by block number)*

20. ABSTRACT *(Continue on reverse side if necessary and identify by block number)*

The goals of this research have been to find and demonstrate design procedures for reducing the mechanical ringing of piezoelectric disc transducers under impulsive electrical excitation. The transducer has been treated as a three-port device: the two mechanical ports and one electrical port. Improvements to the transient response have been sought through determination of appropriate matching networks at the ports. The optimization of specified time domain characteristics is accomplished by performing a gradient search over a parameter space defining the port matching configurations. It is

DD FORM 1 JAN 73 1473 EDITION OF 1 NOV 65 IS OBSOLETE

UNCLASSIFIED

SECURITY CLASSIFICATION OF THIS PAGE *(When Data Entered)*

20. ABSTRACT (Continued)

assumed that only one mechanical port radiates into the acoustic medium. The transducer and mechanical matching sections are modeled using the Mason equivalent circuit and the distributed parameter wave guide model, respectively. Transformation to the time domain is achieved using a numerical approximation to the Laplace transform.

The primary criterion of the optimization procedure is the minimization of face velocity ring-down peaks under the constraint of limiting loss from the peak velocity. Back-side mechanical matching methods are restricted to anechoic, resistive backings. Front-side matching is considered for one-, two-, and three-cascaded matching sections between the disc and acoustic load. Conventional inductance tuned matching at the electrical port is demonstrated to be detrimental to the goal of reducing transient ringing.

The findings indicate a natural division of the optimization process. Lightly backed and heavily backed transducers define the categories, each with an appropriate set of design criteria. Within each category, the new time domain optimization procedures described in this research result in improved transient performance over previously reported techniques based on frequency domain analysis. The procedures also demonstrate the utility of suboptimal solutions when the variable parameters are constrained. Those findings offer considerable design flexibility in situations where material availability is limited. Experimental demonstrations are provided to verify the theoretical design improvements.

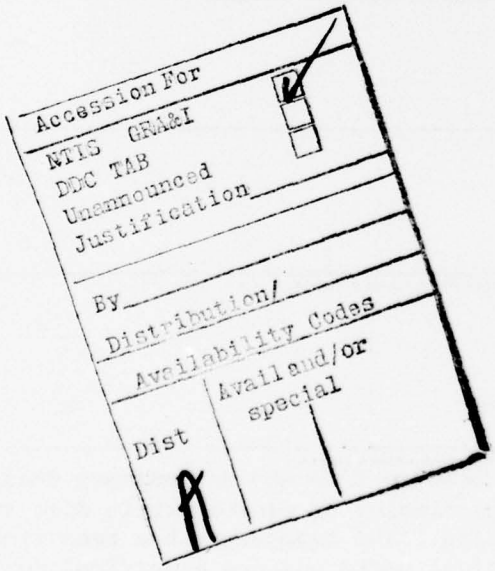

Abstract

The goals of this research have been to find and demonstrate design procedures for reducing the mechanical ringing of piezoelectric disc transducers under impulsive electrical excitation. The transducer has been treated as a three-port device: the two mechanical ports and one electrical port. Improvements to the transient response have been sought through the determination of appropriate matching networks at the ports. The optimization of specified time domain characteristics is accomplished by performing a gradient search over a parameter space defining the port matching configurations. It is assumed that only one mechanical port radiates into the acoustic medium. The transducer and mechanical matching sections are modeled using the Mason equivalent circuit and the distributed parameter wave guide model, respectively. Transformation to the time domain is achieved using a numerical approximation to the Laplace transform.

The primary criterion of the optimization procedure is the minimization of face velocity ring-down peaks under the constraint of limiting loss from the peak velocity. Back-side mechanical matching methods are restricted to anechoic, resistive backings. Front-side matching is considered for one-, two-, and three-cascaded matching sections between the disc and acoustic load. Conventional inductance-tuned matching at the electrical port is demonstrated to be detrimental to the goal of reducing transient ringing.

The findings indicate a natural division of the optimization process. Lightly backed and heavily backed transducers define the categories, each with an appropriate set of design criteria. Within each category, the new time domain optimization procedures described in

this research result in improved transient performance over previously reported techniques based on frequency domain analysis. The procedures also demonstrate the utility of suboptimal solutions when the variable parameters are constrained. Those findings offer considerable design flexibilty in situations where material availability is limited. Experimental demonstrations are provided to verify the theoretical design improvements.

TABLE OF CONTENTS

Page

Abstract....iii

List of Tables....vii

List of Figures....ix

List of Symbols....xv

Acknowledgements....xix

I. INTRODUCTION....1

1.1 Statement of the Problem....1
1.2 Statement of Objectives....3
1.3 General Approach and Procedures....6
1.3.1 Approach....6
1.3.2 Procedures....7
1.4 Nature of the Findings....9

II. REVIEW OF THE LITERATURE....11

2.1 Introduction....11
2.2 Frequency Domain Design of Front-Side Matching Sections....12
2.3 Frequency Domain Design of an Electrical Matching Network....21
2.4 Transient Response Analysis....23

III. DEVELOPMENT OF THE THEORY....28

3.1 The Transducer's Equivalent Circuit....28
3.2 Characterizing the Transducer's Frequency Domain Response....43
3.3 Calculation of the Time Response....47
3.3.1 Discrete Fourier Transform....50
3.3.2 Z-Forms....57
3.3.3 Pade Expansion....60
3.3.4 Summary of the Time Inversion Techniques....60

IV. OPTIMIZATION PROCEDURE....68

4.1 Effects of Matching at Each Port....68
4.1.1 Loading at the Back Face....69
4.1.2 Front-Side Matching....74
4.1.3 Matching at the Electrical Port....78
4.2 Optimization Criteria....85
4.3 Implementing the Optimization....93
4.3.1 Selection of the Search Procedure....93
4.3.2 Optimization with Light Back-Side Loading....98
4.3.3 Optimization with Heavy Back-Side Loading....101

4.4 Additional Remarks and Limitations on the Gradient Search Procedure.....104

V. RESULTS OF OPTIMIZATION.....109

5.1 Introduction.....109
5.2 Lightly Backed Transducer Systems.....111
5.2.1 Preview of the Results.....111
5.2.2 Air Backing with a Single Front-Side Section.....112
5.2.3 Air Backing with Two Front-Side Sections.....118
5.2.4 Air Backing with Three Front-Side Sections.....125
5.2.5 The Use of Light, but Non-Zero Backing.....127
5.3 Heavily Backed Transducer Systems.....131
5.3.1 Preview of the Results.....131
5.3.2 With a Single Front-Side Section.....134
5.3.3 With Two Front-Side Sections.....138
5.3.4 With Three Front-Side Sections.....146
5.4 Parameter Sensitivity.....149
5.4.1 Air Loading.....152
5.4.2 Heavy Backing.....155
5.5 Effects of Including the Electrodes in the Model.....157

VI. EXPERIMENTAL RESULTS.....163

6.1 Objectives.....163
6.2 Designing the Test Examples.....165
6.3 Assembly of the Transducer Systems.....167
6.4 Experimental Procedure.....170
6.4.1 Frequency Domain.....170
6.4.2 Time Domain.....175
6.5 Results.....176
6.5.1 Frequency Domain.....176
6.5.2 Time Domain.....183

VII. SUMMARY AND CONCLUSIONS.....201

7.1 Summary.....201
7.2 Conclusions.....203
7.3 Recommendations for Future Study.....207

REFERENCES.....211

APPENDIX A Low-Frequency Evaluation of the Piezoceramic Coupling Coefficient.....215

APPENDIX B Experimental Determination of the Parameters in the Equivalent Circuit.....219

APPENDIX C Calculation of the Pade Poles and Residues.....229

LIST OF TABLES

Table		Page
3.1	Parameters of the Quarter-Wave Matching Section for System B	47
3.2	An Abbreviated Table of z-Form Pairs	59
5.1	Air-Backed Systems with One Front-Side Section	113
5.2	Air-Backed Systems with Two Front-Side Sections	119
5.3	Air-Backed Sytems with Three Front-Side Sections	126
5.4	Air-Backed Systems Re-optimized to Account for Light Backing	132
5.5	Heavily Backed Systems with a Single Front-Side Matching Section	135
5.6	Heavily Backed Systems for Two Front-Side Matching Sections	139
5.7	Heavily Backed Systems with Three Front-Side Matching Sections	147
5.8	A Comparison of Heavily Backed Systems with One-, Two-, and Three-Section Transformers	151
5.9	Examples for Sensitivity Analysis: Air-Backed	153
5.10	Examples for Sensitivity Analysis: Heavily Backed	155
5.11	Effects of Including the Silver Electrodes	158
6.1	Summary of the Experimental Cases	164
6.2	Physical Properties of the Backing and Front-Side Matching Sections	166
6.3a	Section Lengths and Impulse Response Characteristics of the Various Transducer Systems	168
6.3b	Section Lengths and Impulse Response Characteristics of the Suboptimal Two-Section Systems	168

6.4 Physical Constants of the Epoxy Bonds.....182

6.5 Results of Optimizing the Experimental Systems.....198

6.6 Section Lengths and Theoretical Impulse Response Characteristics of the Various Transducer Systems (with Epoxy Bonds Included in the Model).....200

B.1 Definition of Constants for Describing a Piezoceramic Disc.....220

B.2 Estimated and Final Values of Constants for an Unmounted Disc.....223

C.1 Poles and Residues of the Pade Expansion.....230

LIST OF FIGURES

Figure		Page
1.1	Conventional methods of supplying mechanical or electrical matching to a piezoceramic disc transducer	4
2.1	Parameters of a transmission line section	18
3.1	The mechanics for describing a planar disc a. The actual disc b. Its schematic representation	31
3.2	Generalized equivalent circuit of a piezoelectric element	36
3.3	Equivalent circuit for a planar disc operating in the thickness mode with poling and electric field in the thickness direction	39
3.4	Equivalent circuit for a nonpiezoelectric section	40
3.5	Equivalent circuit for the disc transducer and matching systems	42
3.6	Effect of silver electrodes on the frequency response a. Without silver b. With silver	46
3.7	Frequency response of system B with the quartz matching section of Table 3.1	48
3.8	Frequency response of systems A and B up to the tenth harmonic a. Amplitude response of system A b. Amplitude response of system B	49
3.9	Frequency domain symmetry for IDFT time response a. Symmetry of the real part b. Symmetry of the imaginary part	53
3.10	Demonstration of band-limiting at frequency f_c	54
3.11	Evaluating the time response of system B using a 2048-IDFT with Δf=50 KHz, including components up to a. Second harmonic b. Sixth harmonic	56
3.12	System A evaluated for different Pade orders	63
3.13	System B evaluated for different Pade orders	64

4.1 Comparison of the impulse response of system A with different backings
a. Air-backed
b. Matched backing, Z_B=1.0
c. Backing set to Z_B=2.0.....70

4.2 The paths of the acoustical signals in a system with a single quarter-wave matching section.....75

4.3 A simple matching network for broad-banding the amplitude response and linearizing the phase response.....80

4.4 A frequency domain comparison of the effects of electrical matching
a. No matching network employed
b. With the network of Figure 4.3.....81

4.5 A time domain comparison of the effects of electrical matching
a. No matching network employed
b. With the network of Figure 4.3.....82

4.6 Response of a backed transducer with the matching network of Figure 4.3
a. Frequency domain
b. Time domain.....83

4.7 Time responses overlaid to demonstrate the effects of electrical matching; backing fixed to Z_B=1.0
a. No electrical matching
b. Electrical matching of Figure 4.3.....84

4.8 A typical time response for illustrating $t_s(n=3)$, v_{peak}, and v_{ring}.....88

4.9 Flow chart of the optimization procedure for light backing.....102

4.10 Flow chart of the optimization procedure for heavy backing.....105

5.1 Impulse response with a single matching section
a. Length optimized to maximize opt(3)
b. Impedance optimized to maximized opt(3)
c. Impedance optimized to maximize energy delivered to the load.....114

5.2 Frequency response with a single matching section
a. Length optimized to maximize opt(3)
b. Impedance optimized to maximize opt(3)
c. Impedance optimized to maximize energy delivered to the load.....116

5.3 Frequency response of a two-section system
a. Maximally flat bandwidth
b. Bandwidth, W, equal to 1.0.....120

5.4 Impulse response of a two-section system
a. Maximally flat bandwidth
b. Bandwidth, W, equal to 1.0.....121

5.5 Response as a result of optimizing both the impedances and lengths of a two-section transformer
a. Frequency domain
b. Time domain.....123

5.6 Response of a two-section system with the impedances adjusted to maximize total energy
a. Frequency domain
b. Time domain.....124

5.7 Impulse response using three quarter-wave sections with optimized impedances.....128

5.8 Peak power and peaks ratio as a function of Z_B with the following front-side designs
a. One-section impedance optimized (case 5.1:3)
b. Two-section W=0.6 (case 5.2:2)
c. Two-section impedance optimized (case 5.2:4)
d. Three-section impedance optimized (case 5.3:7).....130

5.9 Impulse response using a single quarter-wave matching section with no optimization and Z_B=1.0.....136

5.10 Impulse responses with either impedance or length optimization (Z_B=1.0)
a. Impedance optimized (case 5.5:4)
b. Length optimized (case 5.5:5).....137

5.11 A frequency domain comparison between two locally optimal time domain solutions
a. Case 5.6:5
b. Case 5.6:6.....141

5.12 A time domain comparison between two locally optimal solutions
a. Case 5.6:7
b. Case 5.6:8.....143

5.13 Impulse response of case 5.6:9 utilizing optimized impedances and lengths with Z_B fixed at 1.19.....145

5.14 Optimized impulse response using two front-side sections and with Z_B fixed at 1.40.....146

5.15 Impulse response with a three-section quarter-wave transformer with optimized impedances (case 5.7:7).....149

5.16 The effects of electrodes on the impulse response of air-backed systems (solid curves represent the nonsilvered)
a. With one front-side section
b. With two front-side sections.....159

5.17 The effects of the electrodes on the impulse response of heavily backed systems (solid curves represent the nonsilvered)
a. With one front-side section
b. With two front-side sections.....161

6.1 Experimental setup for measuring the frequency response.....174

6.2 A comparison between the theoretical (solid curves) and measured power responses (P_v); with a single front-side section and light backing
a. Nonoptimized (case L-1)
b. Optimized (case L-1-O).....179

6.3 A comparison between the theoretical (solid curves) and measured power responses (P_v); with two front-side sections and light backing
a. Nonoptimized (case L-2)
b. Optimized (case L-2-SO).....180

6.4 A comparison between the theoretical (solid curves) and measured power responses (P_v); with a single front-side section and heavy backing
a. Nonoptimized (case H-1)
b. Optimized (case H-1-O).....181

6.5 A comparison between the theoretical (solid curves) and measured power responses (P_v); with two front-side sections and heavy backing
a. Nonoptimized (case H-2)
b. Optimized (case H-2-SO).....182

6.6 The experimental excitation
a. As measured at the generator
b. As measured at the transducer.....184

6.7 The effects on the face velocity of system H-1 (with epoxy bond included) of a finite width excitation pulse
a. Theoretical impulse response
b. Theoretical response to a finite width pulse.....186

6.8 On-axis pressure response from a disc transducer having an impulsive face velocity.....187

6.9 Comparison between the experimental and predicted on-axis transient pressure of system L-1
a. Experimental
b. Predicted.....189

6.10 Comparison between the experimental and predicted on-axis transient pressure of system L-1-O
a. Experimental
b. Predicted.....190

6.11 Comparison between the experimental and predicted on-axis transient pressure of system L-2
a. Experimental
b. Predicted.....191

6.12 Comparison between the experimental and predicted on-axis transient pressure of system L-2-SO
a. Experimental
b. Predicted.....192

6.13 Comparison between the experimental and predicted on-axis transient pressure of system H-1
a. Experimental
b. Predicted.....193

6.14 Comparison between the experimental and predicted on-axis transient pressure of system H-1-O
a. Experimental
b. Predicted.....194

6.15 Comparison between the experimental and predicted on-axis transient pressure of system H-2
a. Experimental
b. Predicted.....195

6.16 Comparison between the experimental and predicted on-axis transient pressure of system H-2-SO
a. Experimental
b. Predicted.....196

A.1 Equivalent circuit for air loading on each face
a. Mason equivalent circuit
b. Low-frequency approximation
c. Low-frequency approximation after removal of transformer.....216

B.1 Electrical input impedances for air loading
a. Measured (unmounted disc)
b. Predicted (γ=0.015)
c. Measured (disc mounted in housing).....222

B.2 Housing to waterproof one face of the disc.....225

B.3 Electrical input impedance for water loading
a. Measured
b. Predicted (γ=0.015).....226

B.4 Predicted input impedances for γ=0.018
a. Air loading
b. Water loading.....228

LIST OF SYMBOLS

Symbol	Definition
A	Area of transducer
a	Radius of transducer
a_1	Tchebychev pass band ripple
a_2	Tchebychev frequency scale factor
B_1, B_2	Undetermined coefficients
b	Dielectric impermeability
C_{eff}	Effective low-frequency capacitance of transducer
C_i^n	Binomial coefficient $\binom{n}{i}$
C_o	Clamped capacitance
C_m	Effective mechanical capacitance at low frequencies
C_m'	Capacitance C_m transformed to the electrical side of the mechanical-electrical transformer
c	Elastic stiffness
D	Electric displacement
E	Electric field
$E\%$	Percentage of energy delivered before $t_s(n)$
E_{out}	Output voltage of receiving transducer
E_t	Normalized total energy delivered to the load Z_L
e	Base of the natural logarithm
F_1, F_2	Force at the faces of the transducer
f_c	Band-limiting frequency
f_s	Frequency corresponding to the DFT sampling rate
f_z	Frequency of maximum motional impedance
h	Piezoelectric coefficient
I	Current supplied to the transducer

I_L	Current supplied to the mechanical load Z_L
J_1	Bessel function of the first kind of order one
j	Square root of minus one
k	Wave number
k_i	Residue of the Pade expansion
k_t	Piezoelectric electromechanical coupling coefficient
L_i	Length of a front-side matching section
l (ℓ)	Length of an arbitrary mechanical section
M	Order of Pade denominator
M_o	Open-circuit receiving sensitivity
MF	Maximally flat pass band characteristic
N	Order of Pade numerator
opt(n)	ratio of total energy to peak ring-down power after $t_s(n)$
P_{avail}	Total power available from a generator
P_D	Power deivered by the transducer to the load
P_L	Power loss factor
P_v	Power delivered, per volt drive, to the load
p	Pressure
$\underline{p}$	Parameter vector
p_o	On-axis rms pressure
PR	Peaks ratio: the ratio of the peak face velocity to the velocity peak after $t_s(n)$
Q	Quality factor
q	Factor to control gradient search step size
R_g	Effective series resistance of generator
r	Reflection coefficient
r_o	On-axis distance to center of transducer
S	Strain

S_o	Open-circuit transmitting response (on-axis)
S_s	Short-circuit transmitting response (on-axis)
s	Complex frequency
T	Stress
T_n	Tchebychev polynomial of degree n
T_o	Transit time through the ceramic
t	Time
$t_s(n)$	Separation time early and late energy, occurring after the n^{th} pulse
U_1, U_2	Particle velocity at the faces of the transducer
$U_L(w)$	Frequency domain face velocity at the acoustic load
$U_F(w)$	Frequency domain face velocity, per volt drive, at the acoustic load
$u_F(t)$	Impulse response of the face velocity at the transducer-medium interface
V	Voltage drive to the transducer
v	Speed of sound
v_{peak} (v_p)	Peak face velocity
v_{ring} (v_r)	Peak ring-down velocity
W	Tchebychev bandwidth
w	Angular frequency
x	Direction of poling and electric field
Z_B	Backing impedance
Z_{eff}	Effective load impedance
Z_{in}	Effective impedance at the center of the KLM model
Z_L	Impedance of the acoustic load
z_i	Poles of the Pade expansion
α	Perturbation factor
γ	Ceramic loss factor

T	Transmission coefficient
λ	Wavelength
ξ	Particle displacement
$\xi_{N,M}(z)$	Pade approximation of order (N,M)
π	3.14159 . . .
ρ	Density
ϕ	Transformer turns ratio in the Mason equivalent circuit
ϕ_E	Transformer turns ratio in the electrical matching network

ACKNOWLEDGEMENTS

The author wishes to express his sincere gratitude to Dr. James L. Lawther and Dr. William Thompson, Jr., for their advice and encouragement. Appreciation is also extended to Drs. Carter L. Ackerman, Robert W. Farwell, and Jiri Tichy for serving on the Doctoral Committee.

The writer also wishes to express his appreciation to the Applied Reasearch Laboratory of The Pennsylvania State University for support of this research under contract with Naval Sea Systems Command.

CHAPTER I

INTRODUCTION

1.1 Statement of the Problem

Ultrasonic flaw detection and medical ultrasonics are two applications of piezoelectric transducers where transient response performance is critical. Certain characteristics are required for maximizing spatial resolution during conventional echo imaging. The impulse response of a transducer can be characterized by the shape, height, and duration of its major pulse and subsequent ring-down. It is generally desired to maximize the peak level of the face velocity and to minimize the width of the peak pulse and the energy in the ring-down. In situations where signal attenuation may be significant, penetration depth is improved by maximizing the peak acoustical power, at least as long as load materials are relatively nondispersive.

With respect to a piezoelectric transducer driven by an electrical impulse, the requirement of minimizing the acoustical ring-down energy presents an inherent difficulty. For a band-limited excitation, it has been shown [18] that the necessary and sufficient conditions for minimizing distortion are that the frequency domain response have:

1. constant amplitude over the band and
2. linear phase over the band.

An impulse-like excitation signal represents a very wide spectrum waveform. Piezoelectric thickness-expander transducers, on the other hand, have zeros of transmission at d.c. and at even harmonics of their fundamental operating frequency [21]. It is therefore impossible to have wide transducer pass bands compared to the bandwidth of a pulse-

like excitation. Because of this inherent pass band limitation, a transducer having a constant amplitude and linear phase response near its fundamental operating frequency can still be expected to exhibit considerable distortion with respect to an impulsive excitation. In echo imaging, reduction of ring-down energy is especially important. For a generalized wide-band excitation, Sittig [46] has shown that the specific distortion of ring down is closely linked to the linearity of the pass band phase.

Unloaded piezoceramic disc transducers typically have a resonance Q greater than 50 [21]. This research has specifically examined piezoceramic devices although the modeling and procedures are, in general, applicable to piezoelectric trnasducers. Even when loaded by water, an overall Q of 10 to 15 is not uncommon, due to the high mismatch between the specific acoustic impedances of water and ceramic. Therefore, without mechanical or electrical matching, the impulse response of a piezoelectric transducer rings for several cycles at the half-wave resonance frequency. This dissertation examines various methods for improving the time domain response of those transducers by use of mechanical and electrical matching. A procedure is developed for optimizing a few of several possible impulse response characteristics.

Numerous authors have examined the problem of providing matching schemes at the two mechanical ports and at the electrical port. Their approaches to increasing the transducer bandwidth include:

1. quarter-wave matching layers between the transducer and the acoustic load,
2. lossy loading on the back, i.e., the nonradiating, mechanical port, and

3. lumped electrical components between the generator and transducer.

These techniques for a piezoceramic transducer are illustrated in Figure 1.1 and are discussed in detail in Chapter II. Previously, these schemes have been implemented in the frequency domain with the aim of improving the impulse response. For the first time, procedures developed in this dissertation base the design directly upon optimizing certain impulse response characteristics. In addition, the consequences and interdependencies of simultaneously matching at the available ports are examined.

1.2 Statement of Objectives

The objectives of this work are to devise and contrast procedures for improving the impulse response of piezoelectric disc transducers. Since it is not possible to design such a transducer with no ringing in the impulse response, compromises in the response quality must be tolerated. These compromises are generally based on engineering judgment and depend upon the specific application of the transducer. Typical optimization goals include the following:

1. maximizing the ratio of peak power to peak ring-down power and
2. maximizing the energy delivered to the acoustic load within a specified time.

In addition to single objective goals as stated above, parameters can be optimized under various constraints and restrictions. It should be clear that there are several other possibilities for objective functions. This work examines both of those listed above, but directs

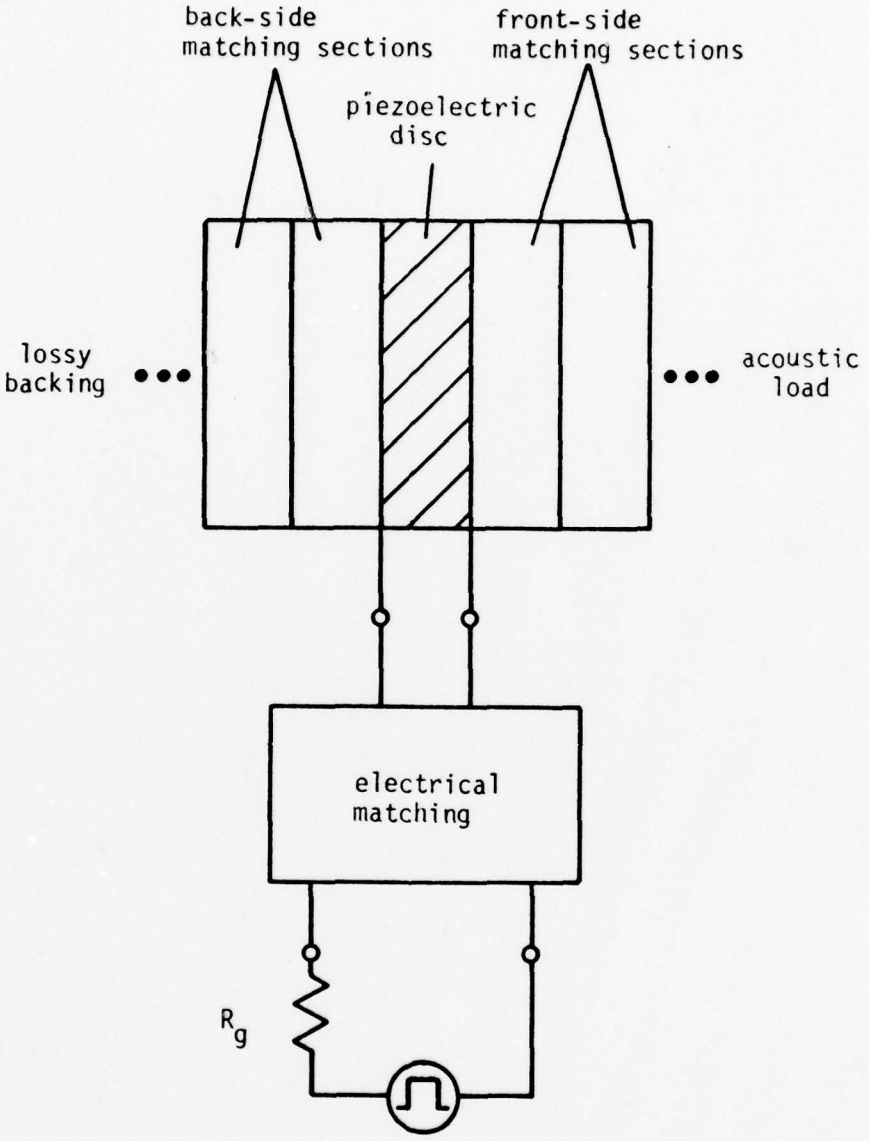

Figure 1.1. Conventional methods of supplying mechanical or electrical matching to a piezoceramic disc transducer

its primary effort toward the first goal.

An alternative design goal, which might have been posed, is to design for an impulse response with specified levels and restrictions on the waveform. The chief drawback of that alternative is that physically realizable goals are difficult to establish a priori. It therefore seems more practical to optimize and improve the characteristics which are of specific interest.

Since the ultimate design goal is to improve the pulse-like quality of the face velocity, use of an impulsive excitation may be unnecessarily restrictive. The use of other excitations is suggested in Chapter IV. However, to offer a standardized comparison between different electromechanical systems, this study is limited to impulsive excitations, which is also the most common means of transducer drive in both the medical science and nondestructive evaluation.

It is a final objective of this work to check both the validity and utility of the theoretical procedures by means of appropriate experiments. To this end, a few lead metaniobate disc transducers have been constructed and tested. The experimental findings are reported in Chapter VI. Various mechanical matching schemes are utilized with the discs to demonstrate the possible improvements to the transient response. These experimental discs are half-wave resonant in the low megahertz range. This range is a convenient one from the materials cost point of view and requires modest-sized test facilities and fixtures. At those frequencies, however, special considerations must be given to the electrodes and the thickness of the bonds. The importance of including these factors in the design process is also demonstrated in later sections.

1.3 General Approach and Procedures

1.3.1 Approach. The impulse response is to be improved by adjustments made at the electrical or mechanical ports. At the front-side of the disc, as many as three matching sections are analyzed. Later discussions detail the theoretical and practical restrictions of using more than three sections. Both the impedance and length of each section can be considered as variables. Resistive backings covering the range from air loading through the mechanically matched condition are included. The possible combinations of mechanical matching are presented in a way to cover most of the cases of practical interest. Electrical matching networks with low-pass and band-pass characteristics have also been examined. There are special difficulties associated with electrical matching and these are mentioned in the final section of this chapter.

As described by others [11,19,30,35,47], quarter-wave matching layers between the ceramic and acoustic load are known means of broad-banding the frequency response and hence of improving the transient response. Although these procedures do not optimize the impulse response, they do offer a significant improvement and are described in later chapters. These early findings motivated the expectation that an appropriate optimization of the front-side matching sections in the time domain can offer still greater improvements to the transient response. It is assumed that the number of matching sections as well as the acoustic impedance and length of each section are adjustable. Cases are presented where some of these parameters are fixed. A practical application is a situation where the designer has only a limited selection of materials available for the matching layers.

With that constraint, only the number of sections and layer lengths are available for optimization.

The options for front-side matching are first examined for an air backed transducer, and then reexamined for a back loaded transducer. Back-side loading is modeled as being purely resistive and is selectable by the designer. As with the air backed case, it is meaningful to examine a number of different situations separately. Any of the aforementioned impedances or lengths can be considered constrained or fixed. A few of the most practical situations are examined in Chapter V. For both the backed and nonbacked cases, the sensitivity to parameter perturbation is also examined.

1.3.2 Procedures. The Mason equivalent circuit [3] and the classical distributed parameter wave guide model are used for analyzing the piezoelectric element and mechanical matching sections, respectively. Lumped elements are used to model the electrical matching network. Use of the Mason circuit implies that plane wave propagation is assumed. In the experimental work, the diameters of the disc transducers are selected to be several times their thicknesses so that the radial components will be small compared to the plane wave component. The Mason model also assumes that the disc is laterally fixed at its edges. Although this requirement may be difficult to achieve in general, a large diameter-to-thickness ratio means that lateral motion at the edges will be secondary even though the disc is not physically constrained. The model parameters are developed for poling and motion in the thickness direction. The mathematical development linking the piezoelectric equations and boundary conditions to the equivalent circuit are developed fully in Chapter III.

To emphasize energy transfer as a result of optimized matching schemes, the transducer and matching sections are modeled as lossless materials. The layers are thin and any losses are assumed small. In any case, for the broad-band systems under consideration, small losses do not seriously affect the shape of the impulse response as demonstrated in Chapter V. To further simplify the demonstration and understanding of the design procedure, the epoxy bonds and silver electrodes are not included in the model. However, these factors, as well as ceramic losses, are considered in the sections of this work which describe transducers that have been designed, built, and tested according to the procedures reported herein.

By virtue of its distributed elements, the Mason circuit represents a piezoelectric transducer throughout a multiplicity of resonances. Applying the usual transformation from real frequencies to the complex plane allows time responses to be computed from Laplace transform calculus. Due to the complexity of the inversion, numerical approximations must be employed in lieu of closed form solutions. Two different approximations to the Laplace inversion are examined in this research: the z-form and Pade methods. A third inversion technique, the fast Fourier transform, which approximates the analog response by its digital representation, is also considered. Armed with a suitable inversion method and optimization goal, a gradient search adjusts the variable parameters toward that optimum solution. A computer program has been written to perform the circuit analysis, the Laplace inversion, and the gradient search.

1.4 Nature of the Findings

The design procedures developed in this research are sufficiently general to accommodate a variety of physical and acoustical situations. It is presumed that the basic transducer applications and objectives are known. From that starting point, a piezoelectric material, a fundamental resonance frequency, and a typical load impedance must be selected. The characteristic impedance of the electric generator must also be known. Having established these fundamentals, the specifics of the design configuration can be determined. For demonstrating the numerical procedures and experimental verification, lead metaniobate discs, half wave resonant at 3.5 MHz, are chosen to drive a water load. Acoustically, that situation represents a mismatch of approximately fifteen to one. The generator is assumed to have a resistive input impedance of 50 ohms.

Depending upon the application, two very broad categories of transducer systems have been identified:

1. air backed or lightly damped, $Z_B < 0.25$ and
2. heavily damped, $Z_B > 0.75$,

where Z_B is the specific acoustic impedance of the backing normalized with respect to that of the ceramic. Although the above ranges are meant as guidelines, there <u>is</u> a definite midrange. The heavily damped systems are used when higher losses can be tolerated for improved impulse response performance. In Chapter V, it is shown that certain optimization goals preclude designs using midranged values. Another reason for distinguishing between the above two categories relates to the optimization procedure. With lightly backed transducers, there is little interaction between optimizing the backing and the front-side

match. This is not so for the heavily backed cases. Due to the differences in performance and optimization, these categories are treated separately throughout this dissertation.

Within each category, numerous designs and results are presented in Chapter V. The designs in that chapter are limited to optimizing mechanical matching with no electrical compensation. Comparisons are presented between previously established designs and those offered by the time domain optimization developed in this work. The emphasis of optimization is to increase the ratio of peak power to peak ring-down power. In general, it is found that the application of this time domain optimization technique results in transducer designs with performance measures surpassing those of the best designs previously reported. A second important finding is the considerable design flexibility afforded by optimization. If a desired backing or front-side impedance is not available, other design adjustments can often offset much of the deterioration in the impulse response. In Chapter VI, the experimental findings confirm that length adjustments to the front-side sections do effect improvements to the time response.

The results in Chapter IV demonstrate that lumped electrical elements between the generator and transducer can increase the total energy delivered to the acoustic load. The increase is achieved at the expense of extending the duration of significant ring-down. Since a suitable resolution to this conflict has not been found, it is conjectured that the usual types of matching networks may not be appropriate for the present application and seems to be consistent with the findings of other investigators.

CHAPTER II

REVIEW OF THE LITERATURE

2.1 Introduction

Remarks in Chapter I have indicated the desirability of broad-banding the frequency response to effect improvements in the time domain. A review of the relevant frequency domain design procedures is therefore in order. The important time domain procedures are also reviewed.

The question of obtaining a broad-band match between a resistive generator and an arbitrary load is certainly not a new one. The first significant contribution in analyzing this problem has been made by Bode [4]. Bode's development provides a fundamental theoretical limitation on the reflection coefficient for a load consisting of a shunt resistor and capacitor. Fano [14] has generalized Bode's solution to include arbitrary loads by developing a set of integral equations specifying relations between the bandwidth and reflection coefficient. Subsequent studies have greatly expanded and simplified the procedures of Bode and Fano. To the knowledge of this author, none of the techniques are directly applicable to the generalized problem of broad-banding a piezoelectric disc with the intent of achieving specific improvements to the transient response.

With certain approximations or restrictions, the problem of broad-banding the transducer can be readily examined by some of those techniques. As an example, an air-backed transducer with lossless mechanical sections can be treated as a lossless two-port. Under those restrictions, procedures have been developed for synthesizing an

electrical matching network between the generator and the transducer [8,22]. Similarly, a mechanical network between the transducer and the acoustical load can be devised if it is recognized that only certain topologies can be realized with mechanical elements. Another technique assumes that the electromechanical coupling is weak. Accordingly, the transducer and mechanical matching sections can be analyzed as a series of wave guide sections.

The above representations, as well as the transducer as a three-port, have been discussed by numerous authors. This chapter examines the important features of their approaches. The objectives of this literature review are twofold. It allows for meaningful comparison between previous procedures and the new methods presented herein. Secondly, it demonstrates the rationale for the selection of one approach over the possible alternatives.

2.2 Frequency Domain Design of Front-Side Matching Sections

The physical structure of a transducer with matching sections renders certain aspects of two-port matching theory appropriate. Since the transducer and matching sections constitute a mechanical delay line, the system is analogous to electrical transmission line segments. By neglecting piezoelectric effects and electromechanical coupling, the mechanical delay line of the transducer is precisely equivalent to the transmission line networks discussed by Collin [10], Cohn [9],and Young [50,51]. With respect to impedance matching, these piezoelectric effects are weak. Other authors have successfully applied classical transmission line theory to shaping the pass band response of piezoceramic transducers [11,19,20].

The transmission line design procedure developed by Collin is to provide an optimum matching network between a resistive load and resistive generator. The resulting design yields a Tchebychev type amplitude response in the pass band: for a fixed number of sections, the bandwidth is maximized for a given pass band voltage standing wave ratio (VSWR). However, this does not insure that any aspect of the impulse response has been optimized. In Chapter V, it is shown that Collin's results can be used to give approximate Tchebychev pass band results for piezoceramic transducers. Moreover, the pass band phase is shown to exhibit good linearity. Since these frequency domain characterisics do possess some of the intuitively desired properties for achieving a good impulse response, the Collin's design is a likely starting point in many of our optimization procedures. There are two additional reasons for considering his solution as a good starting point. The first is for comparative reasons. In some applications, the Tchebychev solution may be the desired one. The second is that the technique is well documented and has been tabulated by Cohn [9] and Young [50]. With its role of providing a starting point in the optimization procedure, the importance of the Tchebychev transformer is of special interest and its development is briefly reviewed.

One parameter which is often discussed in matching theory is the power loss factor; it is also utilized throughout this thesis. The power loss factor is defined as follows:

$$P_L = \frac{\text{power delivered to load}}{\text{total power available from generator}} \quad . \qquad (2.1)$$

In terms of the reflection coefficient, r, as seen by the generator, the

power loss factor is equivalently expressed by:

$$P_L = 1 - r^2 \quad . \tag{2.2}$$

From filter design theory, Collin rationalizes that P_L^{-1} can be expressed as:

$$P_L^{-1} = 1 + a_1^2 T_n^2 [a_2^{-1}(\cos(kl)] \quad , \tag{2.3}$$

where T_n is the Tchebychev polynomial of degree n, a_1 is called the pass band tolerance, a_2 is a scale factor, k is the usual wave number and l is the length of the matching sections. The Tchebychev polynomials are selected since they have the desirable properties of:

1. oscillating between ± 1 for arguments within that range and
2. all n zeros occurring within that same range.

The scale factor therefore determines the bandwidth over which the above two conditions are met. The pass band tolerance sets the amount of ripple allowed within the band. The "quarter-wave" nature of the design is evident from the symmetry condition occurring for cos(kl)=0 (at kl=~/2) at the center of the pass band.

At d.c., where cos(kl)=1, P_L^{-1} is equivalent to the value with no matching sections. Alternatively, this condition is achieved for sections with zero length. Denoting that d.c. value as $P_L^{-1}(0)$, Equation (2.3) can be rewritten as:

$$P_L^{-1}(0) = 1 + a_1^2 T_n^2 (1/a_2) \quad . \tag{2.4}$$

From Equation (2.4) it is seen that specifying either the scale factor or pass band tolerance fixes the other. For a given load/generator impedance ratio [equivalently, fixing $P_L^{-1}(0)$], an n^{th} order polynomial is uniquely determined by fixing n additional points. Collin further demonstrates that those n points are uniquely defined by the requirement of maximizing bandwidth for a given VSWR, or by the converse. For the situation where adjacent impedance steps are modest, Collin has developed a set of equations relating a_1, a_2, and the impedances of the n matching sections (for $n \leq 4$). Cohn [9] and Young [50] have tabulated these design equations.

A comprehensive work by Young [51] expands the results of Collin. In addition to considering half-wave band-pass filters, Young provides formulae and tables covering very large load-to-source impedance ratios. However, like Collin, he is solely concerned with shaping the amplitude of the frequency domain response. Riblet [43] adds theoretical credibility to Collin's work by proving that the quarter-wave Tchebychev and maximally flat transformers are realizable with nonnegative, real characteristic impedances. Riblet also develops a true synthesis procedure rather than depending upon Collin's procedure of undetermined coefficients. The procedure starts with the functional form of the reflection coefficient and proceeds to relate the coefficients of the input impedance function to the unknown characteristic impedances. Gleedhill and Issa [17] have simplified Riblet's synthesis procedure and have provided design formulae for commensurate quarter-wave sections. Kinariwala [27] has generalized these results by the development of a synthesis procedure for determining the impedances and lengths of a stepped, noncommensurate transmission line transformer given a valid

impedance function.

Recently, Desilets, Fraser, and Kino [11] have described a method for improving the shape of the frequency domain amplitude response. The design yields a more Gaussian-like response than the Tchebychev transformer. The authors have therefore concluded that this design will improve the impulse response. Their approach is to use the Krimholtz, Leedom, and Mattaie (KLM) model for piezoceramic transducers. The KLM transmission line model is derived via a series of network transformations from the Mason equivalent circuit. The principal advantage of the transformation is that both the transducer and matching sections are more readily viewed as transmission lines. Their design innovation is to calculate an effective impedance as seen at the center of the ceramic. The front half of the ceramic is then considered to be the first quarter-wave section of a matching transformer. The authors present a table for calculating the impedance values for matching sections up to a three-section transformer (two matching sections plus the ceramic) based upon the following binomial transformer design:

$$\ln \frac{Z_i}{Z_{i+1}} = 2^{-n} C_i^n \ln \frac{Z_L}{Z_{in}} \quad , \tag{2.5}$$

where Z_L is the terminating load impedance, Z_i is the i^{th} quarter-wave matching section (with i=1 adjacent to Z_L), Z_{in} is the effective impedance at the center, and C_i^n is the binomial coefficient for n matching sections. Unless otherwise noted, impedances throughout this work refer to a component's mechanical impedance; i.e., its specific acoustic impedance multiplied by its area. The authors demonstrate that their design procedure approximately satisfies the criterion for

optimizing bandwidth and efficiency tradeoffs for light back-side loading. Their basic criterion is the equalization of the electrical and the mechanical Qs. No attempt is made at time domain optimization. Chapter V compares the time and frequency domain results using their procedure with the results obtained by the optimization techniques described in this work.

Goll and Auld [20], and Goll[19] have also demonstrated the effectiveness of mechanical matching sections for broadbanding air backed piezoceramic transducers. Souquet, Defranould, and Desbois [47] have expanded those efforts to include the study of more front matching sections and the use of backing materials. Goll performs the analysis using the one-dimensional piezoelectric equations. The effective load impedance, Z_{eff}, presented by the mechanical matchings sections and acoustic load is calculated from the standard transmission line transformation:

$$Z_{eff} = Z_1 \frac{Z_L \cos(kl) + jZ_1 \sin(kl)}{Z_1 \cos(kl) + jZ_L \sin(kl)} \quad , \tag{2.6}$$

where Z_1, k, and l refer to the impedance, wave number, and length of a transformer section; and Z_L is the load impedance on the transformer. These parameters are illustrated in Figure 2.1. By successive application of Equation (2.6), it is possible to transform the load impedance through multiple transformers to determine the effective loading. Their method for selecting the impedances of the quarter-wave matching sections is to design for a perfect match near resonance. From classical transmission line theory, this condition is satisfied for the following condition:

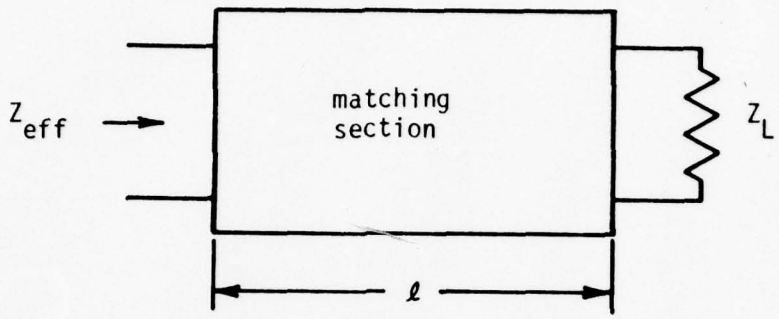

ℓ = length of section

Z = characteristic impedance of section

Z_L = load impedance

Z_{eff} = effective input impedance

Figure 2.1. Parameters of a transmission line section

$$\frac{Z_1}{Z_2} \cdot \frac{Z_3}{Z_4} \cdot \frac{Z_5}{} \cdots \frac{Z_n}{\sqrt{Z_L}} = 1 \quad , \tag{2.7}$$

where the Z_i are the impedances of n matching sections starting from a load Z_L. The impedances are all normalized with respect to the ceramic's impedance. For a single matching section, Equation (2.7) fixes the impedance of the matching transformer to be the geometric mean of the load and source impedances. For more than one matching section, the impedances are not uniquely determined. Goll has demonstrated the effectiveness of employing one and two matching sections for a PZT disc transducer operating in a water load having an impedance mismatch of approximately 25 without the transformer. The theoretical predictions and experimental results of Goll and Auld show a 40% possible bandwidth with one matching section and 70% bandwidth with two matching sections. A trial and error type procedure which provides good bandwidth and small pass band ripple is used to select the impedances for the two transformer case. The impedances selected from this procedure correspond closely to commercially available quartz and lucite. Moreover, the results show that the pass band phase has good linearity. Having selected the impedances for the two-layer match, they proceed to show that it is possible to improve the symmetry of the frequency response by small adjustments to lengths of the sections. These length adjustments tend to make sections quarter-wave at the frequency of maximum response. No analysis of the time domain response is included in their findings.

In an earlier work, Kossoff [30] presents results describing frequency domain effects of back-side loading, front-side matching, and electrical tuning. The analysis is performed using the Mason equivalent

circuit on a PZT7a disc. His findings show that bandwidth can be considerably improved with the use of back-side loading on the transducer. However, this increased bandwidth is at the expense of increased insertion loss. Kossoff also details certain advantages to quarter wave matching low impedance, lossy materials to the back of the ceramic. This type of configuration provides a wider bandwidth with increased ripple than by employing resistive back-side loading which is matched to the ceramic at all frequencies. The increased bandwidth and ripple is understood by recalling that the two situations are identical at resonance but that the case with quarter-wave matching provides less loss off-resonance since the ceramic and back-side load are no longer matched. In addition to a matching section between the transducer and backing, Kossoff examines the use of front-side matching sections. He demonstrates that a single front-side section can provide a bandwidth improvement comparable to direct back-side loading with substantially less insertion loss. Using both a single front-side matching section and back-side loading, large bandwidths with reasonable ripple and insertion loss can be achieved.

The previously cited works are not intended to be an exhaustive list of references in quarter-wave matching theory. However, they are representative of the different research approaches that have been applied to broad-band piezoceramic transducer design. It is observed that the literature extensively examines the effects of the lengths and impedances of the matching sections in the frequency domain. The usual goal is to broad-band the device with good phase linearity. This type of frequency domain design has also been examined for piezoceramic disc receivers [40], acoustic delay lines [1], and cylindrical piezoceramic

transducers [2]. To attain specific impulse response characteristics, additional constraints must be imposed.

2.3 Frequency Domain Design of an Electrical Matching Network

As already discussed, it is possible to include an electrical matching network between the generator and transducer. Two frequency domain numerical procedures have been developed for optimizing the element values for a matching network of fixed topology. One method, developed by Carlin [8], uses tabulated impedance data of the transducer or its model along with an objective such as maximizing minimum pass band gain. Another method described by Hjellen et al. [22] requires tabulated impedance data of the transducer and an electrical model providing impedance data. The objective of each method is to optimize some aspect of the frequency domain response.

Carlin chooses to maximize the minimum pass band gain under the constraint that the power loss factor is approximately flat over the pass band. Hjellen et al. adjust the transducer's frequency response by improving alignment with the desired response offered by the model. However, these frequency domain methods are not, in general, reliable for improving the time domain response of a transducer. Since a piezoelectric transducer with mechanical matching sections is a nonminimum phase system, the amplitude response, P_L, is not sufficient to define the phase response uniquely. Hence, improvements to the time response cannot be guaranteed.

Kossoff, Goll, and Desilets et al. have also demonstrated the use of a series or shunt inductor for reducing insertion loss. Although they cite reductions of insertion loss, Kossoff cautions of possible

resonance problems in pulse detection work. Desilets et al. have indicated the need for more complicated networks when considerable mechanical matching is provided.

Lakestani, Beboux, and Fleischman [31] have described the design of a transmission line at the electrical port for broad-banding a piezoceramic receiving transducer. For the simple case of a disc acoustically loaded by infinitely long mechanical transmission lines at each face, the amplitudes of the face velocity pulse train are readily calculated from the reflection and transmission coefficients between the ceramic and acoustic media. The reflection coefficient, r, and transmission coefficient, T, are calculated by the well-known expressions:

$$r = \frac{Z_2 - Z_1}{Z_2 + Z_1} \tag{2.8a}$$

and

$$T = \frac{2Z_2}{Z_2 + Z_1} \quad , \tag{2.8b}$$

where a pulse is incident upon the medium of acoustic impedance Z_2 from the medium with impedance Z_1. When performing these calculations, it is assumed that the piezoelectric coupling can be neglected. The individual pulses can be summed and Laplace transformed to form an overall frequency domain transfer function.

The authors approach the problem of broad-banding the transducer by implementing a transfer function which is approximately the reciprocal of the transducer's transfer function. The product of these two functions is then approximately independent of frequency. If the network of the inverse function can be appended to the transducer, the

resulting structure should have a flat response over a very broad band. This concept is theoretically and experimentally verified using a PZT transducer symmetrically loaded on each face. For the symmetric configuration, the authors show that a single transmission line circuit appropriately coupled to the transducer through a transistor provides the necessary inverse function, up to the second harmonic. For the case where the acoustic loading is not symmetric, a second transmission line must be included in the matching circuit.

2.4 Transient Response Analysis

In theory, the time domain solution to the piezoelectric transducer with mechanical and electrical matching can be found by performing an inverse Laplace transform on the frequency domain response. However, it is not generally possible to find a closed form solution to the inversion problem. For a few special cases, closed form solutions are possible, but even then, they are quite tedious to bring about. Redwood [42] considers the exact solution of a stressed piezoceramic bar. The transient solution is calculated for the case when the stress is suddenly removed and, simultaneously, a resistor is shunted between the electrodes. In a separate work, Redwood [41] has developed exact and approximate time domain solutions of an electrical step excitation to a piezoceramic plate with a rigid backing. The equations utilized for describing these solutions are the boundary conditions, laws of motion, and piezoceramic equations for developing the Mason equivalent circuit. Procedures for calculating the inverse transform for simple piezoceramic configurations have been extended by Onoe [37] to ultrasonic delay lines. Onoe and Redwood have recognized the importance of using a model

valid over the whole frequency domain for analysis of pulse transmission. To meet this requirement, they present an approach linking the Mason equivalent circuit with Laplace transform calculus.

The approaches of Onoe and Redwood are to manipulate the equations into a form suitable for calculating the inverse Laplace transform. However, even for the simple cases, considerable algebraic manipulation is required. In the final form, the frequency domain response is shown to be an infinite sum of harmonically related exponentials:

$$U(s) = C_o(s) + C_1(s)e^{-sT_o} + C_2(s)e^{-2sT_o} + \ldots \quad , \qquad (2.9)$$

where $U(s)$ is the face velocity, $C_i(s)$ is a function dependent upon the particular transducer configuration, and T_o is the time required for the wave to travel between the moving faces. From Equation (2.9), it is clear that the impulse response is represented by the sum of shifted time functions. For example, the inverse transform of $C_1(s)$ does not contribute to the time domain solution until time T_o. Physically, this corresponds to a mechanical wave undergoing reflection and transmission at the ends of the ceramic. Redwood demonstrates that it is possible to express the C_i of Equation (2.9) in terms of the reflection coefficients.

Although the methods of Redwood and Onoe provide the formalism, as well as a physical interpretation, for calculating the time response, in practical situations with arbitrary mechanical and electrical loading the methods are difficult to apply. Reducing the transfer function to the form of Equation (2.9) may be quite tedious. Even for the cases which can be expressed in the form of Equation (2.9), closed form

solutions of the separate Laplace inversions do not necessarily exist. In spite of these difficulties, some meaningful numerical results are possible with these methods. For example, from the first experiment described above, Redwood demonstrates that the mechanical energy is released very slowly compared to the electrical energy for low-valued shunting resistors.

Another approach using an iterative procedure is offered by Kasai, Okuyama, and Kikuchi [26]. Their procedure utilizes a network derived from the Mason circuit for calculating the reflection coefficients between the ceramic and both mechanical loads. The effects of electrical loading are incorporated by calculating the transmission coefficient between the two mechanical ports. From a known set of initial conditions, it is possible to calculate the frequency domain current distribution in the model during each time interval a pulse traverses the ceramic. The method is iterative in that the next solution uses the currents determined from the previous solution as the new initial conditions. Upon summing the frequency domain solutions, the time response can be evaluated from an inverse Laplace transform. The authors have analyzed a piezoceramic disc operating in both the transmit or receive mode. The loading at the mechanical ports is not required to be symmetric but is assumed to be resistive. The analysis becomes cumbersome with intervening mechanical sections of arbitrary length. This process of Kasai et al. will lead to the same solutions as developed by Redwood and Onoe.

Kittinger and Rehwald [29] have adopted classical transmission line techniques for analyzing the transducer time response. Their fundamental assumption is that the effects of the electrical components

on the mechanical transmission line are small. Under this condition, it is assumed that most of the energy leaves the transducer system through one of the mechanical ports. The accuracy of that assumption is dependent upon the lumped elements at the electrical port and the amount of mismatch at the mechanical ports. Their objective is to improve the received tone-burst pulse shape during echo imaging by means of a front-side quarter-wave plate. The previously discussed matching schemes of Goll and Auld for matching high impedance transducer materials operating into low impedance media, such as water, suggest that the impedance of a single matching layer should be near the geometric mean of the transducer and medium impedances. However, Kittinger and Rehwald show the advantages of selecting the impedance of the matching layer to be greater than the impedance of the ceramic element for single-frequency operation.

Stepanishen [48] has analyzed the transient response of planar piezoelectric arrays. His results are directed toward the use of a pulsed sinusoidal electrical excitation. Individual array elements are piezoceramic bar transducers. The analysis is performed by modeling each element with its Mason equivalent circuit. Since the array elements are close to each other, the effective acoustical load impedance is not only a function of the load medium, but also of the mutual coupling between elements. Time domain solutions are calculated with the use of z-forms. The method of z-forms is a numerical approximation for determining the inverse z-transform and is described in Chapter III. Although Stepanishen has demonstrated the accuracy of z-forms for his particular application, the use of z-forms for the generalized disc transducer is very tedious. The aforementioned chapter

indicates that even for a simple disc configuration, the method requires considerable algebraic manipulation. Dvorak [13] has proved that the method of characteristics [6] and the z-transform method for calculating the time domain response are, in fact, mathematically equivalent.

CHAPTER III

DEVELOPMENT OF THE THEORY

3.1 The Transducer's Equivalent Circuit

Throughout this dissertation, calculations regarding the behavior of a piezoceramic disc are based upon the equivalent circuit originally described by Mason [34]. The equivalent circuit is developed from the laws of motion and piezoelectric equations governing a thin disc. The development presented here follows that as outlined by Berlincourt, Curran, and Jaffe[3], but additionally includes the detailed steps that directly link the equations to the final circuit.

The piezoelectric equations relate the mechanical and electrical conditions of a piezoelectric device. The mechanical properties are the stress T and strain S; and the electrical quantities are the electric field E and electric displacement D. Since the details of deriving those equations are provided by Berlincourt et al., they need not be repeated here. The one-dimensional form of the piezoelectric equations to be used in developing the equivalent circuit of a piezoceramic disc is as follows:

$$T = cS - hD \tag{3.1a}$$

and

$$E = -hS + bD \quad , \tag{3.1b}$$

where c = elastic stiffness determined at constant D

h = piezoelectric coefficient $= -\left.\frac{\partial T}{\partial D}\right|_S = -\left.\frac{\partial E}{\partial S}\right|_D$, and

b = dielectric impermeability for constant strain.

It is seen that Equations (3.1a) and (3.1b) reduce to the expected results relating stress, strain, electric field, and electric displacement for a nonpiezoelectric device (h=0). All of the parameters in Equation (3.1) refer to the thickness direction and assume that the piezoelectric material is anisotropic, but poled in the thickness direction. It is assumed that there is no leakage flux, so that the only D component is in the thickness direction. Moreover, D is assumed to be uniform. These assumptions on D are generally valid since the relative dielectric constant of most piezoceramic materials is greater than 100 and the two flat surfaces are coated with a conductive layer. For lateral dimensions much larger than the thickness dimensions, the ceramic can be considered constrained in all directions except the thickness direction. This is consistent with the assumption that the wave propagation can be described by a plane wave in the thickness direction. The equivalent circuit to be developed is appropriate for an arbitrarily shaped transducer face (i.e., round, polygonal, etc.) provided that the above conditions are satisfied. Reference is made to a thin disc transducer since that is the shape which is ultimately considered.

The final equation required for describing the motion of a piezoelectric transducer is the one-dimensional plane wave equation. For plane wave propagation, it is assumed that all of the particles in a plane parallel to the transducer surfaces have equal velocity. Therefore, by Newton's second law, the particle displacement ξ is given

by.

$$\rho\frac{\partial^2\xi}{\partial t^2} = \frac{\partial T}{\partial x} \quad , \tag{3.2}$$

where ρ is the density of the material and x is in the direction of wave propagation. Substitution of Equation (3.1a) into Equation (3.2) yields.

$$\rho\frac{\partial^2\xi}{\partial t^2} = c\frac{\partial S}{\partial x} - h\frac{\partial D}{\partial x} \quad . \tag{3.3}$$

By definition, $S = \frac{\partial\xi}{\partial x}$, so Equation (3.3) can be rewritten as:

$$\rho\frac{\partial^2\xi}{\partial t^2} = c\frac{\partial^2\xi}{\partial x^2} - h\frac{\partial D}{\partial x} \quad . \tag{3.4}$$

As previously mentioned, it is reasonable to assume that D is uniform in the piezoelectric element and the one-dimensional wave equation is simply:

$$\rho\frac{\partial^2\xi}{\partial t^2} = c\frac{\partial^2\xi}{\partial x^2} \quad . \tag{3.5}$$

By manipulating and applying the appropriate boundary conditions to Equations (3.1) and (3.5), the equivalent circuit for the piezoelectric disc can be developed. Figure 3.1a illustrates the disc showing the convention assumed for the direction of force F_i and particle velocity U_i at each face. Figure 3.1b shows the convention for representing the force and velocity in an equivalent circuit. The sign convention shown is consistent with that used for describing a network in terms of its

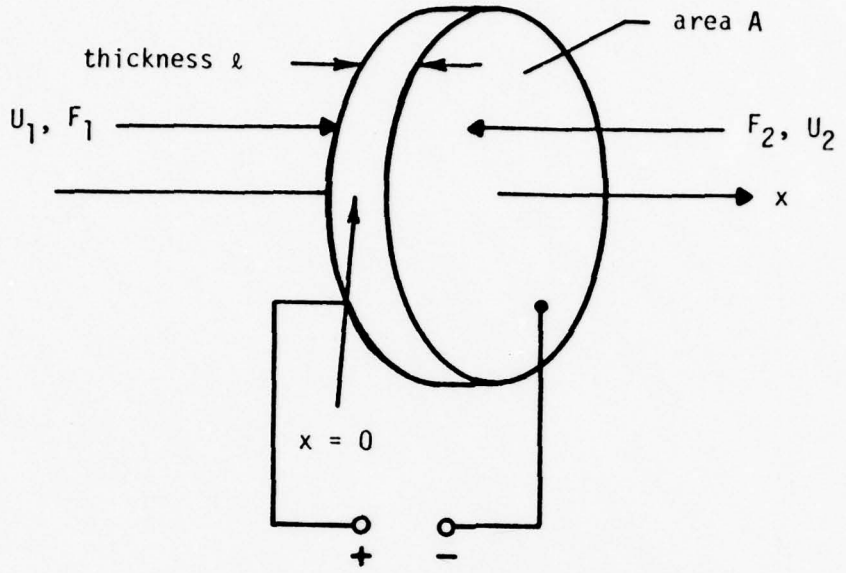

(a)

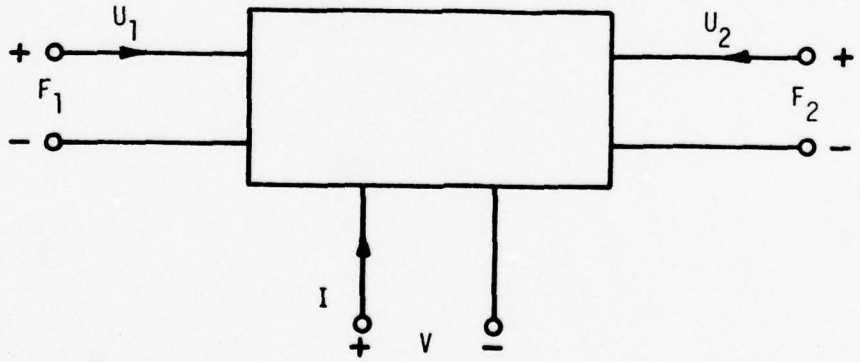

(b)

Figure 3.1. The mechanics for describing a planar disc
a. The actual disc
b. Its schematic representation

impedance matrix.

The general solution to the wave equation, assuming that the time variation is e^{jwt}, is given by:

$$\xi = [B_1 \sin\frac{wx}{v} + B_2 \cos\frac{wx}{v}] e^{jwt} \quad , \tag{3.6}$$

where B_1 and B_2 are constants to be determined by the boundary conditions, and v is the velocity of the plane wave. The constants B_1 and B_2 can be evaluated in terms of the face velocities by noting that:

$$U_1 = \frac{\partial \xi}{\partial t}\Big|_{x=\frac{-l}{2}} = jw(-B_1 \sin\frac{wl}{2v} + B_2 \cos\frac{wl}{2v}) \tag{3.7a}$$

and

$$U_2 = -\frac{\partial \xi}{\partial t}\Big|_{x=\frac{l}{2}} = -jw(B_1 \sin\frac{wl}{2v} + B_2 \cos\frac{wl}{2v}) \quad , \tag{3.7b}$$

where the time factor is implicitly assumed. Solving for B_1 and B_2 yields:

$$B_1 = -(U_1 + U_2)/2jw\sin\frac{wl}{2v} \tag{3.8a}$$

and

$$B_2 = (U_1 - U_2)/2jw\cos\frac{wl}{2v} \quad . \tag{3.8b}$$

Substituting Equation (3.8) into Equation (3.6) gives:

$$\xi = \frac{U_1 + U_2}{2jw\sin\frac{wl}{2v}} \sin\frac{wx}{v} + \frac{U_1 - U_2}{2jw\cos\frac{wl}{2v}} \cos\frac{wx}{v} \quad . \tag{3.9}$$

The force at each face can be calculated from Equation (3.1a) as follows:

$$F(-\tfrac{1}{2}) = F_1 = -AT(-\tfrac{1}{2}) \tag{3.10a}$$

and

$$F(\tfrac{1}{2}) = F_2 = -AT(\tfrac{1}{2}) \quad , \tag{3.10b}$$

where A is the area of each face as illustrated in Figure 3.1a. The stress, T, is evaluated in terms of the face velocities from Equation (3.1a) by recalling that:

$$S = \frac{\partial \xi}{\partial x} \quad . \tag{3.11}$$

The following expression is obtained by substituting Equation (3.9) into Equation (3.11):

$$S = -\frac{w}{v}\frac{U_1 + U_2}{2jw\sin\frac{wl}{2v}}\cos\frac{wx}{v} - \frac{w}{v}\frac{U_1 - U_2}{2jw\cos\frac{wl}{2v}}\sin\frac{wx}{v} \quad . \tag{3.12}$$

Performing substitutions to Equation (3.10) [from Equations (3.1a) and (3.12)] gives the following results:

$$F_1 = -A\{-\frac{c}{v}\frac{U_1 + U_2}{\sin\frac{wl}{2v}}\cos\frac{wl}{2v} + \frac{c}{v}\frac{U_1 - U_2}{\cos\frac{wl}{2v}}\sin\frac{wl}{2v} - hD\} \tag{3.13a}$$

and

$$F_2 = -A\{-\frac{c}{v}\frac{U_1 + U_2}{\sin\frac{wl}{2v}}\cos\frac{wl}{2v} - \frac{c}{v}\frac{U_1 - U_2}{\cos\frac{wl}{2v}}\sin\frac{wl}{2v} - hD\} \quad . \tag{3.13b}$$

It is well known that Equation (3.5) defines the velocity of plane wave propagation in the ceramic as:

$$v = \sqrt{\frac{c}{\rho}} \quad . \tag{3.14}$$

Using Equation (3.14) along with the following definitions:

$$I = jwAD \tag{3.15a}$$

and

$$Z_o = \rho vA = A\sqrt{c\rho} \quad , \tag{3.15b}$$

where I is the current supplied to the transducer and Z_o is the transducer's mechanical impedance. Equation (3.13) can be rewritten as follows:

$$F_1 = \frac{Z_o \cot\frac{wl}{2v}}{2j}(U_1 + U_2) - \frac{Z_o \tan\frac{wl}{2v}}{2j}(U_1 - U_2) + \frac{hI}{jw} \tag{3.16a}$$

and

$$F_2 = \frac{Z_o \cot\frac{wl}{2v}}{2j}(U_1 + U_2) + \frac{Z_o \tan\frac{wl}{2v}}{2j}(U_1 - U_2) + \frac{hI}{jw} \quad . \tag{3.16b}$$

The voltage V across the plate is obtained by substituting Equations (3.12) and (3.15a) into Equation (3.1b) and integrating:

$$V = \int_{-1/2}^{1/2} E dx = \int_{-1/2}^{1/2} -h\left[-\frac{w}{v}\frac{(U_1 + U_2)\cos\frac{wx}{v}}{2jw\sin\frac{wl}{2v}} - \frac{w}{v}\frac{(U_1 - U_2)\sin\frac{wx}{v}}{2jw\cos\frac{wl}{2v}} + b\frac{I}{jwA}\right]dz$$

$$= \frac{h(U_1 + U_2)}{jw} + \frac{I}{jwC_o} \quad , \tag{3.17}$$

where $C_o = \frac{A}{bl}$. (3.18)

Equations (3.16) and (3.17) can be arranged into a matrix formalism as follows:

$$\begin{bmatrix} F_1 \\ F_2 \\ V \end{bmatrix} = \begin{bmatrix} \frac{Z_o(\cot\frac{wl}{2v} - \tan\frac{wl}{2v})}{2j} & \frac{Z_o(\cot\frac{wl}{2v} + \tan\frac{wl}{2v})}{2j} & \frac{h}{jw} \\ \frac{Z_o(\cot\frac{wl}{2v} + \tan\frac{wl}{2v})}{2j} & \frac{Z_o(\cot\frac{wl}{2v} - \tan\frac{wl}{2v})}{2j} & \frac{h}{jw} \\ \frac{h}{jw} & \frac{h}{jw} & \frac{1}{jwC_o} \end{bmatrix} \begin{bmatrix} U_1 \\ U_2 \\ I \end{bmatrix} . \quad (3.19)$$

The most direct way of finding the equivalent circuit corresponding to Equation (3.19), is by starting with the generalized form of the known solution. Then, by calculating the impedance matrix of the generalized circuit and by equating the elements to the values in Equation (3.19), the equivalence between the two can be established. Figure 3.2 shows the general form of the equivalent circuit of a piezoelectric disc transducer. With all ports open circuited, the following relations can be obtained from Figure 3.2 by inspection:

$$F_1 = (Z_s + Z_p)U_1 + Z_pU_2 + (U_1 + U_2)(Z_a + Z_b)\phi^2 + IZ_a \quad ,$$

$$F_2 = Z_pU_1 + (Z_s + Z_p)U_2 + (U_1 + U_2)(Z_a + z_b)\phi^2 + IZ_a \quad , \quad (3.20)$$

and

$$V = \phi Z_aU_1 + \phi Z_aU_2 + IZ_a \quad .$$

Collecting similar terms in Equations (3.20), they can be rearranged into the following matrix format:

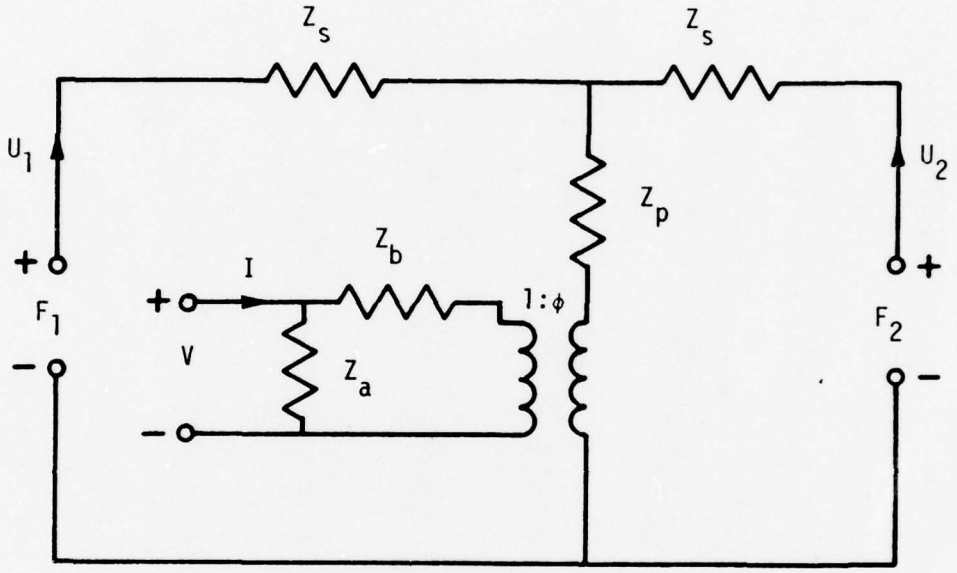

Figure 3.2. Generalized equivalent circuit of a piezoelectric element

$$\begin{bmatrix} F_1 \\ F_2 \\ E \end{bmatrix} = \begin{bmatrix} Z_p+Z_s+\phi^2(Z_a+Z_b) & Z_p+\phi^2(Z_a+Z_b) & \phi Z_a \\ Z_p+\phi^2(Z_a+Z_b) & Z_p+Z_s+\phi^2(Z_a+Z_b) & \phi Z_a \\ \phi Z_a & \phi Z_a & Z_a \end{bmatrix} \begin{bmatrix} U_1 \\ U_2 \\ I \end{bmatrix} \quad . \qquad (3.21)$$

By equating the matrix elements of Equation 3.19 with the matrix elements of Equation (3.21), the following results are obtained:

$$Z_a = \frac{1}{jwC_o} \qquad (3.22a)$$

and

$$\phi = \frac{h}{jwZ_a} = hC_o \quad . \qquad (3.22b)$$

However, Z_p, Z_s, and Z_b are not uniquely determined by Equations (3.19) and (3.21). By selecting

$$Z_b = - Z_a \quad , \qquad (3.23)$$

Z_p and Z_s are then given by:

$$Z_s = jZ_o \tan\frac{wl}{2v} \qquad (3.24a)$$

and

$$Z_p = -jZ_o / \sin\frac{wl}{v} \quad , \qquad (3.24b)$$

which is consistent with the definitions of Z_p and Z_s for the case where the electric field is perpendicular to the direction of poling. Under

the condition of Equation (3.23), Z_b has the frequency response of a negative capacitor, C_o, where C_o represents the clamped capacitance of the disc. The complete equivalent circuit of a piezoelectric disc operating in thickness mode is shown in Figure 3.3. The impedances Z_L and Z_B represent arbitrary mechanical loading at the front and back ports, respectively. Acoustic load impedances are transformed to mechanical impedances by multiplying their specific acoustic impedances (density - sound speed product) by the area A. Losses and attenuation through the ceramic are typically modeled by including an imaginary velocity component. The loss is analogous to the attenuation constant of a transmission line. Mathematically, that loss is included as follows:

$$v = v_o(1 + \gamma j) \quad , \tag{3.25}$$

where v_o is the real component, and γ is the loss factor.

For nonpiezoelectric materials, ϕ is equal to zero and the circuit of Figure 3.3 can be simplified to the form shown in Figure 3.4. A little algebra quickly shows that the mechanical section represented by Figure 3.4 is exactly equivalent to the transmission line transformation of Equation (2.6). Cascading the circuit of Figure 3.4 to either of the mechanical ports in the circuit of Figure 3.3 corresponds to including a mechanical layer at that face of the transducer. The process can be continued to account for all subsequent layers. In this work, the terminating front- and back-side acoustical loads are modeled resistively. This is justified at frequencies where the characteristic dimension of the transducer is substantially larger than the wavelength

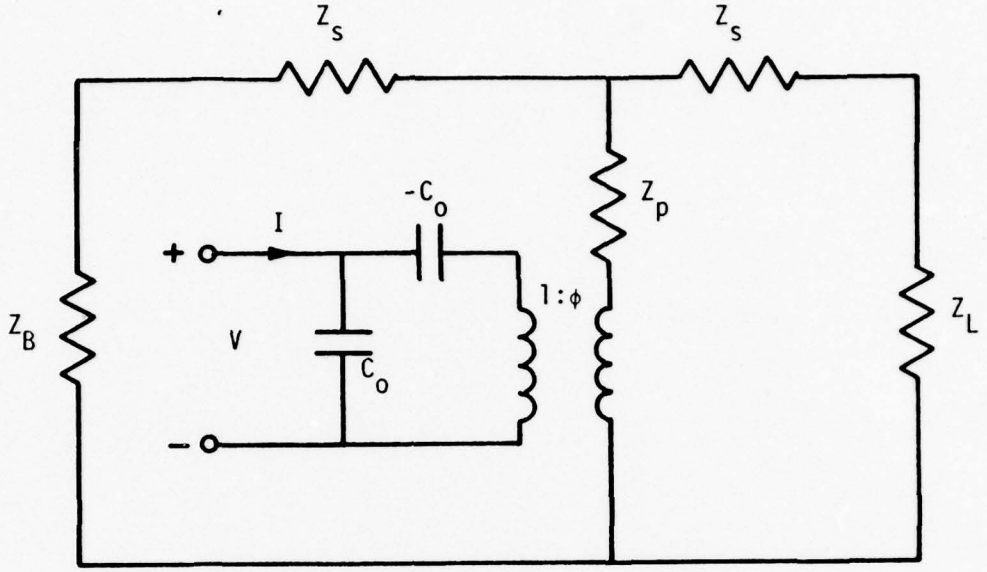

$$Z_s = jZ_o \tan\left(\frac{w\ell}{2v}\right)$$

$$Z_p = -jZ_o / \sin\left(\frac{w\ell}{v}\right)$$

$$Z_o = \rho VA$$

$$C_o = \frac{A}{b\ell}$$

$$\phi = hC_o$$

Z_B, Z_L = mechanical loads

Figure 3.3. Equivalent circuit for a planar disc operating in the thickness mode with poling and electric field in the thickness direction.

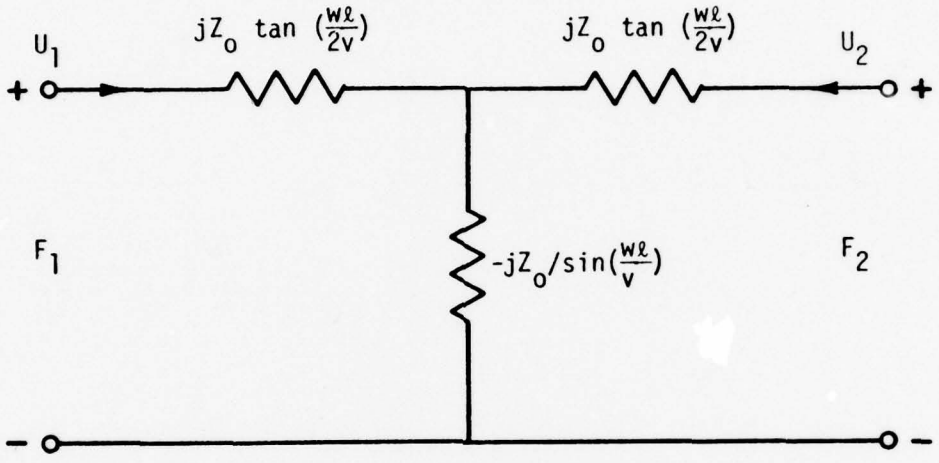

Figure 3.4. Equivalent circuit for a generalized nonpiezoelectric section

(in the load) and when there is no significant reflected wave in the load medium [28]. The restriction on the reflected wave is satisfied for infinitely long or highly lossy media. The boundary conditions require continuity of force and normal face velocity at each interface. Cascading two-ports automatically insures that requirement since voltage and current are continuous at port boundaries. Because the complete transducer model can be represented by an equivalent electrical circuit, all of the theorems and procedures that apply to circuit analysis can be utilized in the analysis of the transducers. Appendix A shows the mechanics of utilizing the equivalent circuit of Figure 3.3 for a low-frequency evaluation of the piezoelectric coupling coefficient.

The generalized equivalent circuit allowing for electrical and mechanical matching is illustrated in Figure 3.5. As drawn, it represents a transmitting element. By inserting a voltage source in series with the acoustic load Z_L, and replacing the original source with an impedance, the resulting circuit describes a receiving element. The emphasis of this work is to optimize the transmitting response. It should be pointed out, that optimizing a particular aspect of the transmitting response does not insure that it is optimized in the receiving mode. According to electrical reciprocity, the receiving response is identical to the transmitting response to the extent that the acoustical and electrical boundary conditions are maintained equal. Consequently, different strategies may need to be employed in the design of transducers operating as transceivers than for single mode applications.

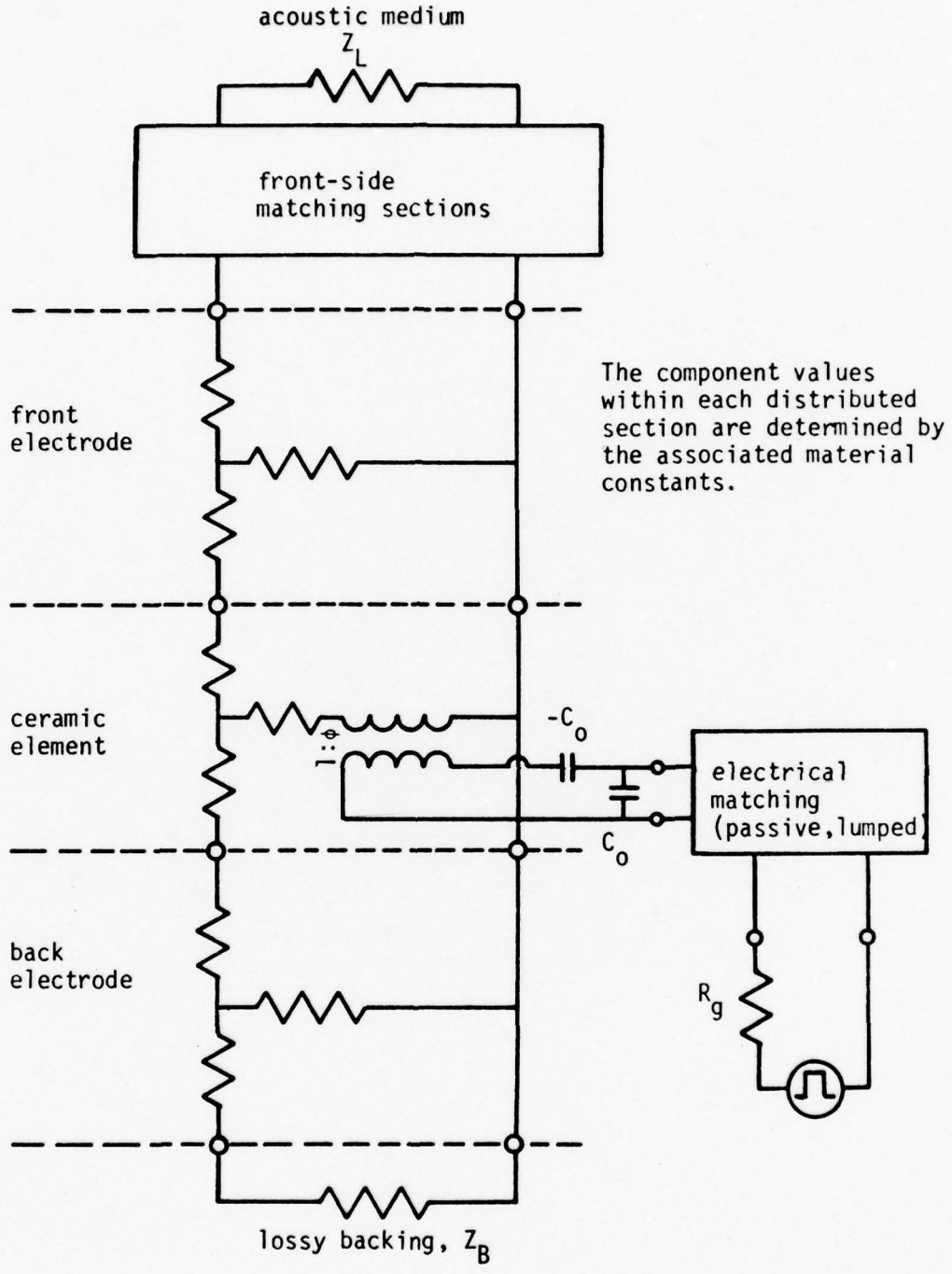

Figure 3.5. Equivalent circuit of the disc transducer and matching systems

3.2 Characterizing the Transducer's Frequency Domain Response

The objectives of this section are twofold. The first is to elaborate upon the power loss factor, P_L, that was mentioned in Chapter II. The second is to illustrate its use with specific examples. These examples are used later to demonstrate the theoretical improvements of optimization. A suitable choice of piezoelectric material can simultaneously provide numerical and experimental examples. Throughout the remainder of this work, lead metaniobate is used exclusively as the active piezoceramic element. Although the optimization procedures of Chapter IV are not dependent upon the type of piezoceramic material selected, lead metaniobate has the advantage of reducing complications from radial mode contributions due to low coupling between the radial and thickness modes. Appendix B describes the experimental procedure for measuring the material constants necessary for modeling lead metaniobate. The numerical values to be used are those listed in Appendix Table B.2 with set to 0.018 to account for additional losses as described in the text of Appendix B.

As mentioned in Chapter II, the power loss factor is often used as a frequency domain descriptor in matching theory. In the time domain, the velocity response at the transducer- medium interface provides an appropriate descriptor of the system's behavior. For a resistively loaded disc, this velocity is proportional to the time differential of on-axis pressure. Using the notation of the equivalent circuit, the face velocity is equal to the current U_L through the load Z_L in Figure 3.5. The average output power, P_{out}, is calculated by:

$$P_{out} = |U_L(w)|^2 Re[Z_L(w)] \quad , \tag{3.26}$$

where $U_L(w)$ represents the rms sinusoidal face velocity. Standard circuit analysis techniques can be utilized in calculating the frequency response of the face velocity per unit volt drive, denoted by $U_F(w)$. It is assumed that the transducers are to be driven by a voltage generator with a constant and real input impedance, R_g. The maximum average power available from a voltage source V(w) in series with R_g occurs for conjugate matching and is given by [10]:

$$P_{avail}(w) = \frac{|V(w)|^2}{4R_g} \quad , \tag{3.27}$$

where V(w) also represents the rms value. The power loss factor is given by substituting Equations (3.26) and (3.27) into Equation (2.4) and is equal to

$$P_L(w) = \frac{|U_L(w)|^2 Re[Z_L(w)]}{|V(w)|^2/(4R_g)} \quad . \tag{3.28}$$

Unless specifically stated otherwise, references to the frequency domain response refer to the power loss ratio.

A program for a digital computer has been written to evaluate the transducer input impedance, the power loss factor $P_L(w)$, and velocity response $U_F(w)$. The program is sufficiently versatile to specify several layers surrounding the transducer and to allow for arbitrary acoustical loading (Z_B and Z_L). Appendix B demonstrates an application for utilizing the input impedance. The following section examines various methods of calculating the time domain response of the face velocity, $u_F(t)$, from its frequency domain representation, $U_F(w)$. This

section concludes by presenting a few simple systems to be used as examples in the next section.

An interesting test case is to examine the effect of the silver electrodes on the transducer faces. As described by Heuter and Bolt [21], one would expect that the mass loading caused by the thin silver layers to decrease the resonance frequency. Figure 3.6 compares the frequency response of the lead metaniobate disc in Appendix Table B.2 with and without the silver layers. In each case, the transducer is acoustically loaded by water on one face. For zero thickness and massless electrodes, the resonance frequency would shift from 2.8 MHz to 3.5 MHz. For future referencing, the system with no electrodes is denoted as system A. The solid curves in the figure show the amplitude response and the dashed curves the phase response. The same representation is used throughout this work.

As described in Chapter II, transmission line theory suggests the use of a quarter-wave matching section between the transducer and water load to improve bandwidth. With infinite length transmission lines, a perfect match at resonance is achieved by selecting the impedance as the geometric mean of the load and generator impedances. For later comparison, the matching section for this next example is set to the geometric mean of the impedances of the ceramic and water. For the sake of simplicity, the silver is assumed massless, so the length of the section must be quarter-wave at 3.5 MHz (the frequency at which the ceramic is half-wave resonant). Future references to "quarter-wave" length sections always refer to the frequency at which the ceramic is one half-wave long. Table 3.1 lists the properties of the matching section. Its speed of sound is near the value for quartz, but the

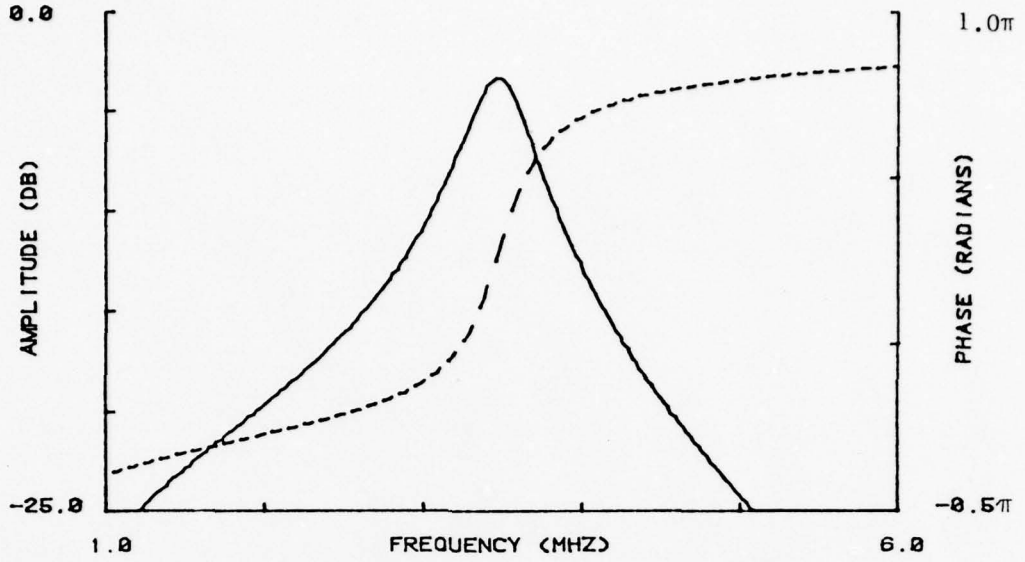

(a)

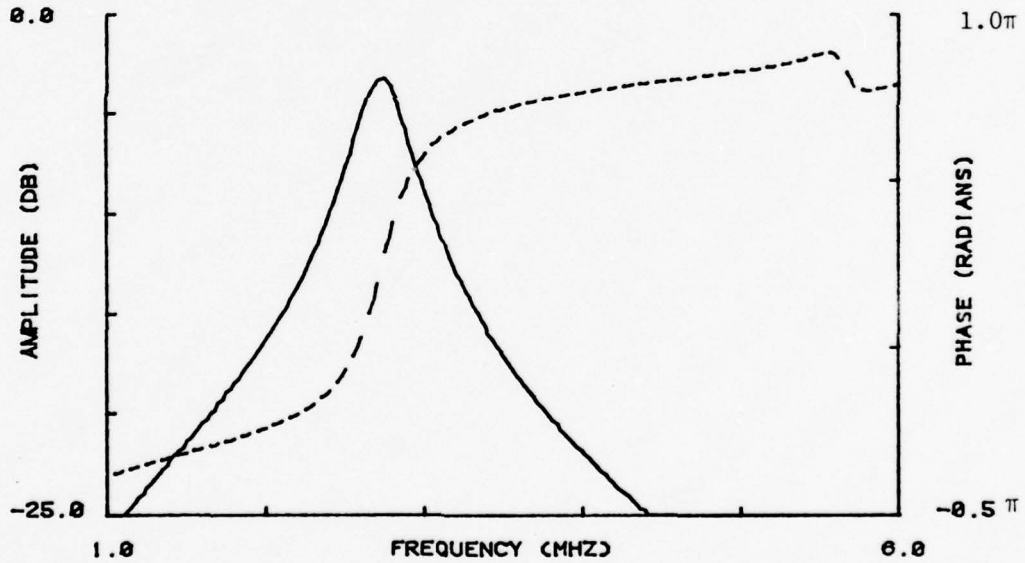

(b)

Figure 3.6: Effect of silver electrodes on frequency response
a. Without silver
b. With silver

TABLE 3.1
PARAMETERS OF THE QUARTER-WAVE MATCHING
SECTION FOR SYSTEM B

Parameter	Value
Density	1.19×10^{3} kg/m^{3}
Speed of sound	4.94×10^{3} m/sec
Thickness	3.512×10^{-3} m
Loss factor	0.0

density of the section is greater to give the desired impedance. The frequency response of this system, denoted as system B, is shown in Figure 3.7.

Due to the distributed element representation of the Mason equivalent circuit, the frequency response above the second harmonic is still meaningful. (For lumped circuit approximations, the equivalence is only valid near the fundamental resonance.) Figure 3.8 shows the full frequency response of systems A and B up to the tenth harmonic.

3.3 Calculation of the Time Response

In the previous section, the frequency domain velocity response at the transducer-water interface, $U_F(w)$, is calculated by applying standard circuit analysis procedures to the Mason equivalent circuit. The response in the complex frequency plane is found by substituting the complex variable s for jw. This s-plane representation is the Laplace transform of the impulse response. Throughout this work, the time response of the transducer system is characterized by various qualities of the velocity impulse response at the system-water interface. The

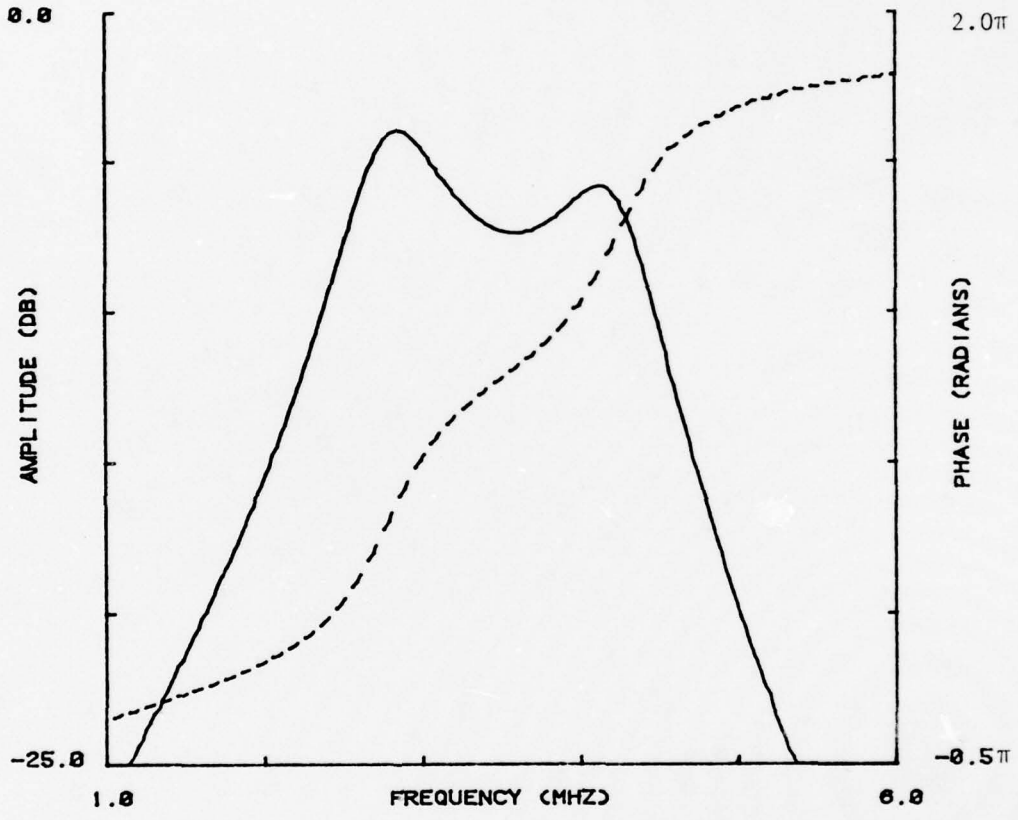

Figure 3.7. Frequency response of system B with the quartz matching section of Table 3.1.

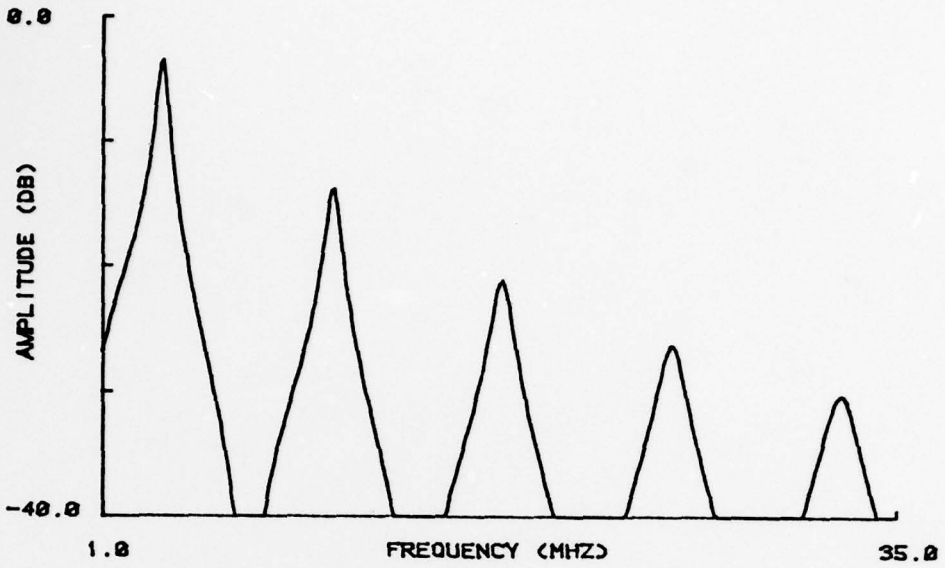

(a)

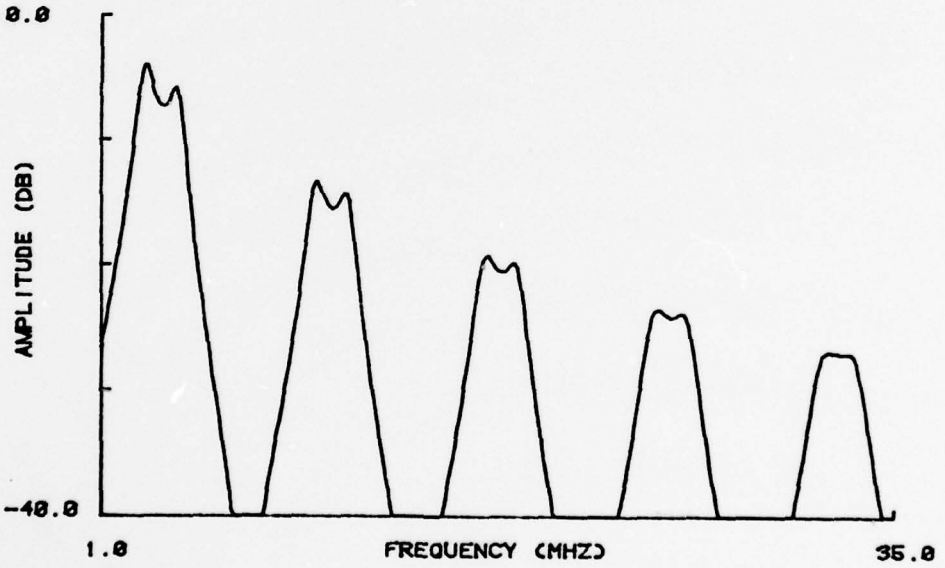

(b)

Figure 3.8. Frequency response of systems A and B up to tenth harmonic
a. Amplitude response of system A
b. Amplitude response of system B

Laplace transform of $U_F(s)$ and its inverse are given, respectively, by:

$$U_F(s) = \int_0^\infty e^{-st} u_F(t)\,dt \tag{3.29a}$$

and

$$u_F(t) = \frac{1}{2\pi j} \int_{C-j\infty}^{C+j\infty} e^{st} U_F(s)\,ds \quad , \tag{3.29b}$$

where $u_F(t)$ represents the impulse response, and $U_F(s)$ is required to be analytic for the real part of s greater than C. Since $U_F(s)$ is the system function of a passive, realizable circuit that includes at least some resistive loss, all of its poles are within the left half-plane. Therefore, the parameter C in Equation (3.29b) can be set to zero.

For transducer networks, Equation (3.29b) will not, in general, have a closed form solution for arbitrary $U_F(s)$. Consequently, numerical methods must be utilized for obtaining the time response. Three possible techniques are to be described in this section. Two of them, the z-form technique and the Pade approximation, are direct numerical evaluations of Equation (3.29b). The third procedure uses the discrete Fourier transform.

3.3.1 Discrete Fourier Transform. A possible approach for obtaining the impulse response is to consider the use of the inverse discrete Fourier transform. It is well known that a band-limited signal can be uniquely defined by its digital representation. An N-point discrete Fourier transform (DFT) and its inverse (IDFT) are defined by the following:

$$U(k) = \sum_{n=0}^{N-1} u(n) W_N^{kn} \qquad 0 \leq k \leq N-1 \tag{3.30a}$$

and

$$u(n) = \frac{1}{N}\sum_{k=0}^{N-1} U(k)W_N^{-kn} \qquad 0 \leq n \leq N-1 \quad , \tag{3.30b}$$

where $W_N = e^{-j(2\pi/N)}$; u(n) represents the time series, and U(k) represents the frequency domain series. The finite duration sequences represent one period of a periodic sequence. The implied frequency and time domain analog periods are f_s and T, respectively. The time and frequency increments ΔT and Δf are therefore related by:

$$\Delta T = \frac{1}{f_s} \tag{3.31a}$$

and

$$\Delta f = \frac{1}{T} \quad . \tag{3.31b}$$

From Equations (3.30a) and (3.31b) it is readily seen that the frequency components used for reconstructing the signal are the fundamental and harmonics of the time domain repetition rate. This is similar to the continuous Fourier series except that only a finite number of harmonics are considered. In practice, the DFT and IDFT are calculated by a fast Fourier transform algorithm [38].

Since the time response is a real sequence, certain symmetry properties of the frequency response can be utilized:

1. The real part of the frequency response is symmetric about a reference point.
2. The imaginary part of the frequency response is antisymmetric about the same reference.

For even transform sizes, these are most readily interpreted by considering the N/2 point as the symmetry point, starting the denumerating from point zero. Under those conditions, U(0) is not

symmetric with any other point in the series. From Equation (3.30b) it is easily seen that the imaginary components of U(0) and U(N/2) must be zero. Because of the symmetry, it is only necessary to calculate the frequency domain points up to U(N/2), the others being defined by symmetry. The situation is illustrated in Figure 3.9. From the sampling theorem, it is recalled that the $f_s/2$ (or N/2) frequency component is actually the highest that can be represented without aliasing.

Using the DFT to obtain the time response requires that a transform size and sampling rate be selected. Selection of any two of transform size, sampling rate, and maximum frequency component will obviously determine the third. It must also be remembered that a sampling rate which marginally satisfies the Nyquist criteria may not necessarily insure good interpolation.

To achieve a greater sampling rate in the time domain, Equation (3.31a) dictates that f_s must be increased. For most practical cases, f_s is selected to be greater than twice the actual band-limiting frequency, denoted henceforth as f_c. This practice improves interpolation in the time domain. Figure 3.10 illustrates an operational interpretation of f_c. At frequencies above f_c, zeros can be substituted for the true frequency response without any serious distortion occurring in the time domain. If this condition is not met, then the choice of f_c is too low for the IDFT calculation.

The frequency responses of Figure 3.8 show that there is not an obvious point at which the piezoceramic transducer can be considered band-limited. As a matter of fact, under certain conditions, the Mason equivalent circuit does not present a band-limited representation.

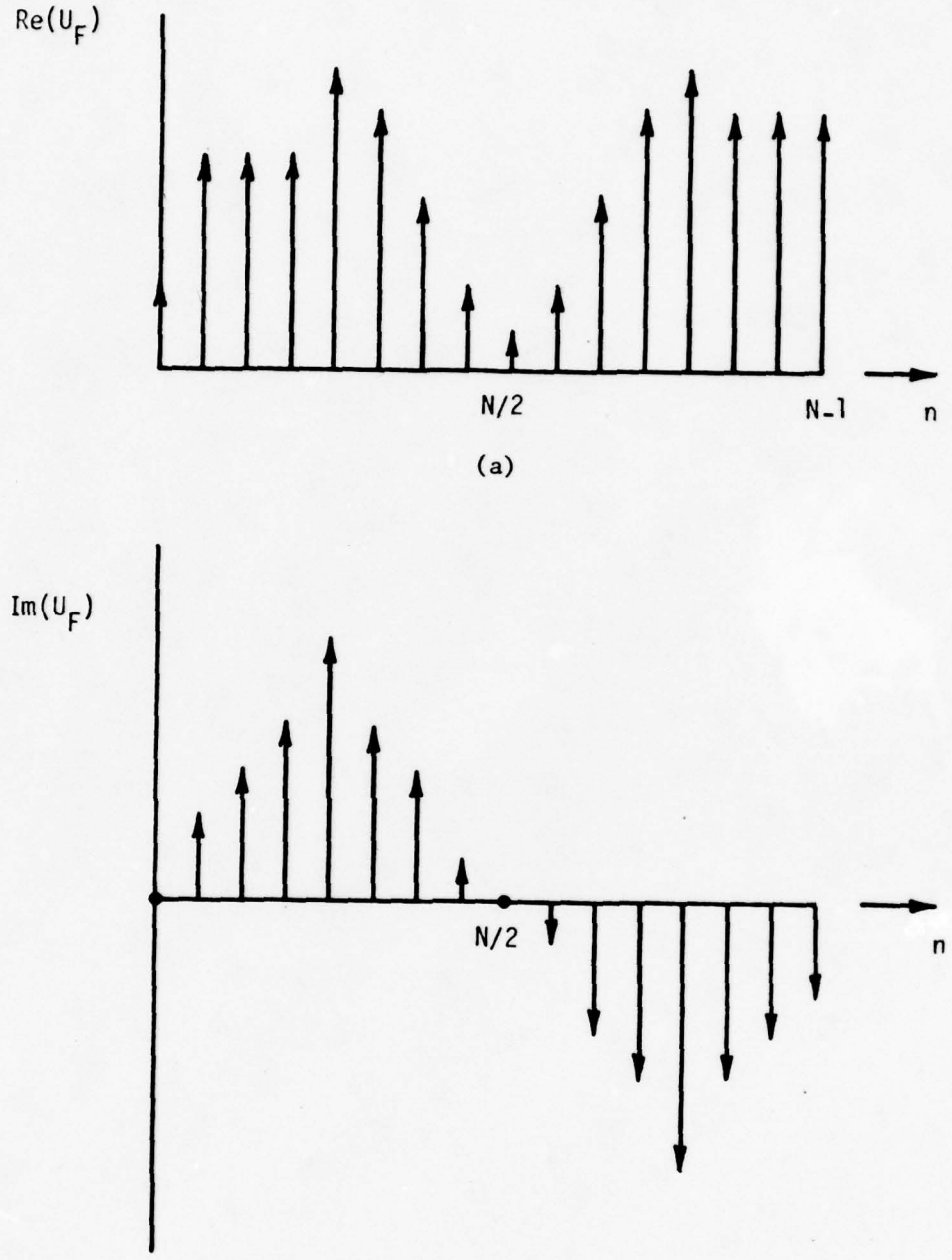

Figure 3.9. Frequency domain symmetry for IDFT time response
a. Symmetry of the real part
b. Symmetry of the imaginary part

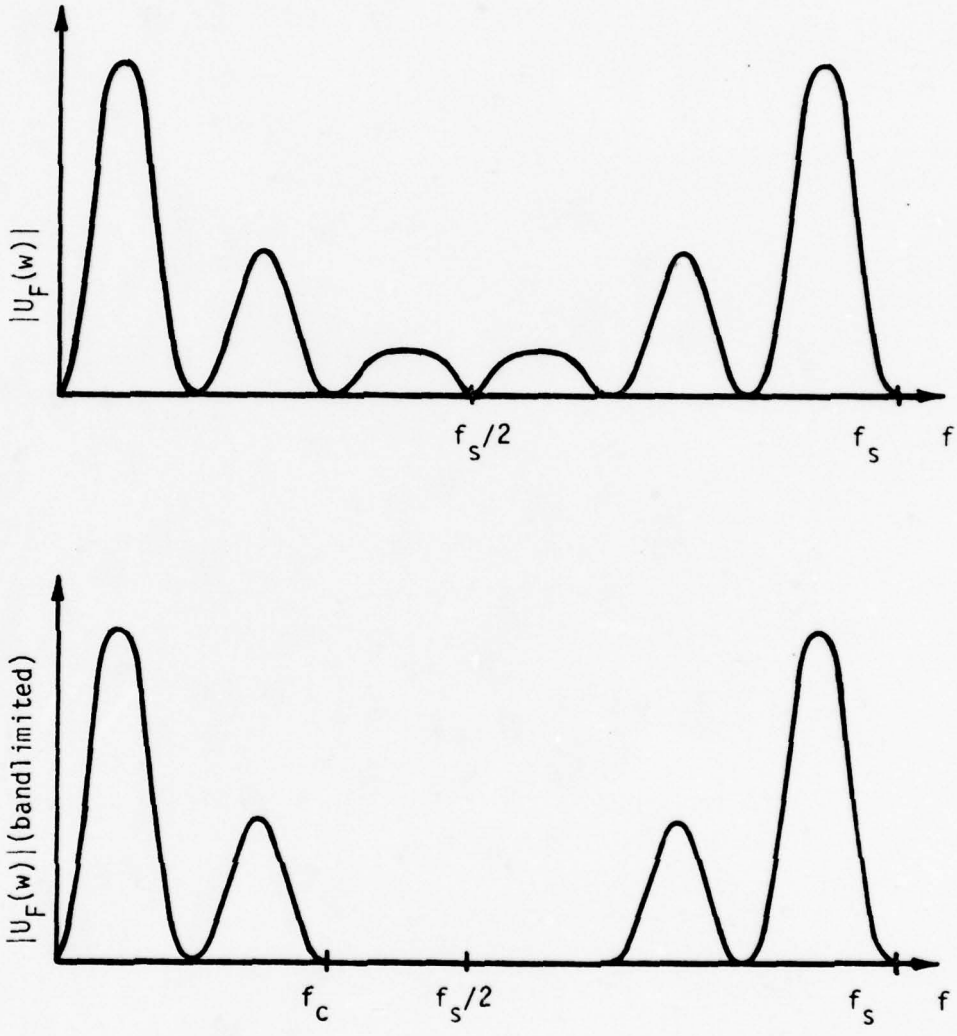

Figure 3.10. Demonstration of band-limiting at frequency f_c.

This is most readily demonstrated for a disc transducer with arbitrary resistive, mechanical loading. From Figure 3.4, the face velocity per volt drive, $U_F(w)$, is given by:

$$U_F(w) = \frac{jwC_o\phi Z_L}{-w^2C_o^2Z_mR_g + jwC_oZ_m - \phi^2} \quad , \tag{3.32}$$

where Z_m is the net impedance presented on the mechanical side of the transformer. If γ is zero, Z_m is truly periodic with no high frequency limit. The high frequency resonance peaks are therefore very dependent upon γ, R_g, and C_o as seen by Equation (3.32). For the limiting case of $R_g=0$ and $\gamma=0$, $U_F(w)$ is not band-limited.

It is tempting to suggest that the IDFT be used on the transducer configurations that are, in theory, band-limited. However, when so doing, the resulting impulse response does not accurately depict the observed (experimental) response. The difficulties appear to be from the inclusion of the higher harmonics. Although the value of does influence the amplitudes of those harmonics, the model seems to over predict their importance. Input impedance measurements of the transducers suggest that there are other high frequency losses not considered by the model. As a result, explicit inclusion of the predicted harmonics tends to overemphasize their importance. At the other extreme, excluding all of the predicted harmonics does not accurately portray the transducer operation. Figure 3.11 demonstrates the point using system B as an example. In that figure, the impulse response has been calculated for two different choices of f_c: at the second and sixth harmonics. The responses are normalized to the peak velocity of system A band-limited at the second harmonic. Harmonics

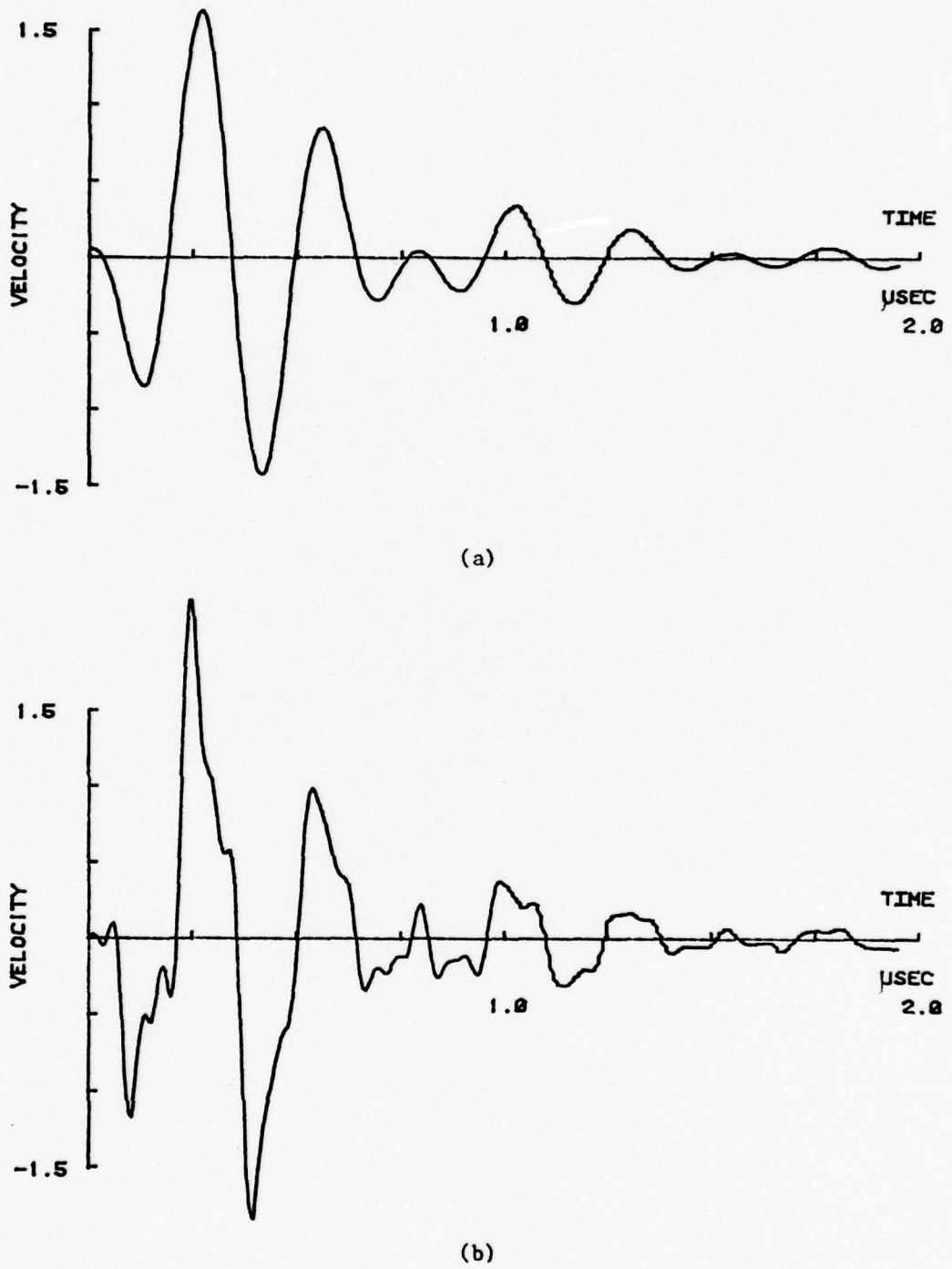

Figure 3.11. Evaluating the time response of system B using a 2048 IDFT with Δf=50 KHz, including components up to
a. Second harmonic
b. Sixth harmonic

above the sixth harmonic are found to effect only minor changes to the impulse response. The difficulties with the IDFT technique arise from the inaccuracies of the Mason model and are not caused by the approximations associated with the IDFT.

3.3.2 Z-Forms. The method of z-forms applies techniques from z-transform theory to the analysis of nonsampled systems. By changing the s-plane representation of the Laplace transform integral to its equivalent z-plane representation, the form of the inversion integral is similar to the inverse z-transform integral. The inversion process is completed by recalling that the z-transform inversion of the ratio of two polynomials can be calculated through synthetic division. Z-form approximations are used to transform the z-plane representation into a ratio of polynomials. The development of this transformation is detailed by Boxer and Thaler [5], and its applicability to the Mason circuit has been demonstrated by Stepanishen [48].

Boxer and Thaler have used four steps to summarize the entire procedure for obtaining the approximate z-form time domain response. They are:

1. Express the function $U_F(s)$ as a rational function of s^{-1}. The numerator and denomicator are polynomials of s^{-1} and possibly include a constant term.
2. Substitute for s^{-1}, s^{-2}, etc., the corresponding z-form in powers of z^{-1} and rearrange $U_F(s)$ as a rational fraction in powers of z^{-1}.
3. Divide the resulting expression by ΔT, where ΔT is the time interval between points at which the solution is desired.
4. Expand the fraction by synthetic division. The quotient is

a polynomial in powers of z^{-1}, and the coefficient corresponding to z^{-n} is the approximate value of the time response at $t=n\Delta T$.

The z-forms corresponding to s^{-N} have been tabulated up to N equal 5 by Boxer and Thaler. A more complete table is offered by Jury [25]. To better appreciate the possible complications with z-forms, a few simple transform pairs are listed in Table 3.2.

The utilitity of z-forms for calculating the transient response of bar transducers operating with electric field perpendicular to the stress has been demonstrated by Stepanishen. In that mode, there is no negative capacitor in the equivalent circuit [3]. Therefore, the transfer function defining the face velocity per volt drive can be represented by distributed elements only. By expressing the distributed elements in terms of complex exponentials, the overall transfer function consists exclusively of sums, products, and quotients of exponentials. As Table 3.2 indicates, s-plane exponentials have a simple (and exact) z-form. Consequently, the algebra required by Step 2 is fairly manageable.

Introduction of the negative capacitor (required for transducers operating with the electric field parallel to the stress) or other elements that are not in parallel with C_o requires that the transfer function be described by both distributed and lumped elements. In addition to the lumped elements, the introduction of intervening layers on the front face and resistive backing adds considerable complexity to the circuit transfer function. The combination of these two complications makes Step 2 difficult to implement in a dynamic fashion on a digital computer. Considerable algebraic manipulation is required

Table 3.2
AN ABBREVIATED TABLE OF Z-FORM PAIRS

S-plane	Z-form
$e^{-\Delta Ts}$	z^{-1}
s^{-1}	$\frac{\Delta T}{2} \frac{1 + z^{-1}}{1 - z^{-1}}$
s^{-2}	$\frac{(\Delta T)}{12}^2 \frac{1 + 10z^{-1} + z^{-2}}{(1 - z^{-1})^2}$
s^{-3}	$\frac{(\Delta T)}{2}^3 \frac{z^{-1} + z^{-2}}{(1 - z^{-1})^{-3}}$

to rearrange $U_F(s)$ as a rational fraction in powers of z^{-1}. Because of these drawbacks, the z-form technique is not readily adaptable to the present application and will not be considered further.

3.3.3 Pade Expansion. Under certain circumstances, the Laplace inversion integral of Equation (3.29b) can be evaluated by considering the residues of the integrand. If the limit of the integrand approaches s^{-n} (where $n>1$) as s increases to infinity, the path of the integral can be extended to enclose the appropriate half-plane. The integral can then be calculated as:

$$\frac{1}{2\pi j}\int U_F(s)e^{st}ds = \pm \Sigma(\text{residues of } U_F(s)e^{st} \text{ at poles inside the closed path}) \quad , (3.33)$$

where the positive sign applies when the path is closed with counterclockwise rotation, i.e., in the left half-plane, and the negative sign for the other case. Although the poles of $U_F(s)$ are not explicitly known, they must be in the left-half plane since $U_F(s)$ describes a stable circuit. Representing the exponential function, e^z, where $z=st$, in the complex plane with the Pade approximation, $\xi_{N,M}$ [45]:

$$\xi_{N,M}(z) = \frac{(M+N)! + (M+N-1)!\binom{N}{1}z + (M+N-2)!\binom{N}{2}z^2 + \ldots + M!\binom{N}{N}z^n}{(M+N)! - (M+N-1)!\binom{M}{1}z + (M+N-2)!\binom{M}{2}z^2 - \ldots + (-1)^M N!\binom{M}{M}z^m} \quad (3.34)$$

allows immediate identification of the integrand's right half-plane poles. All right half-plane poles are due to the poles of Equation (3.34) and can be found by using a standard polynomial root-finding

routine. The poles and corresponding residues have been tabulated to 16 decimal places, up to M=24, for M minus N differences up to 3 [45]. Appendix C lists a few sets of Pade coefficients and outlines a method for their calculation.

With the substitution of z=st and $\xi_{N,M}(z)$ for the exponential, the Laplace inversion of Equation (3.29b) becomes:

$$V_F(t) = -\frac{1}{2\pi jt}\int_{-j\infty}^{j\infty} V_F(\frac{z}{t})\,\xi_{N,M}(z)\,dz \quad . \tag{3.35}$$

For small differences between M and N, the poles of Equation (3.34) have been shown to be simple [45]. The Pade approximation can therefore be expressed in terms of its poles z_i and corresponding residues k_i as follows:

$$\xi_{N,M}(z) = \sum_{i=1}^{M} \frac{k_i}{z - z_i} \quad . \tag{3.36}$$

Upon substituting Equation (3.36) into Equation (3.35) and applying the results and conditions of Equation (3.33), the time response is approximated by:

$$u_F(t) = -\frac{1}{t}\sum_{i=1}^{M} k_i U_F(\frac{z_i}{t}) \tag{3.37}$$

The negative sign is included since the path of integration is clockwise around the right half-plane. For real time sequences, the computations of Equation (3.37) can be approximately halved from symmetry

consideration. In practice, Equation (3.37) is implemented by:

$$u_F(t) = -\frac{1}{t}\sum_{i=1}^{M/2} k_i U(\frac{\hat{z}_i}{t}) - \frac{1}{t}k_o U(\frac{\hat{z}_o}{t}) \quad , \tag{3.38}$$

where the $\hat{z}_i$ are the poles in the upper half-plane and $\hat{z}_o$ is the real pole for odd M, corresponding to the residue k_o.

Singhal and Vlach [45] have also examined the accuracy of the Pade inversion from an analytical and empirical viewpoint. The Pade expansion of Equation (3.34) has the first N+M+1 terms of its Taylor expansion equal to the Taylor expansion of e^z. Equation (3.37) reproduces the true time response to its first N+M+1 Taylor terms, so that the accuracy is good for those time sequences which can be represented by the initial terms of a Taylor expansion. From a theoretical standpoint, it is expected that accuracy should be high for small times. Singhal and Vlach have confirmed this by considering several poorly conditioned pulsed and stepped time responses that could be computed exactly and then compared with the approximation of Equation (3.37). Although increasing the order of the approximation generally improves the accuracy for later times, it also introduces the possibility of computer round-off error.

In a separate work, Vlach [49] suggests an approach for finding a suitable order of the Pade approximation. As might be expected, the approach is to increase the order of the approximation until any additional increase causes a large variation from the results of the previous order. This procedure has been applied to the transducer configurations A and B of Section 3.2, with selected results shown in Figures 3.12 and 3.13. From those figures, it is seen that round-off

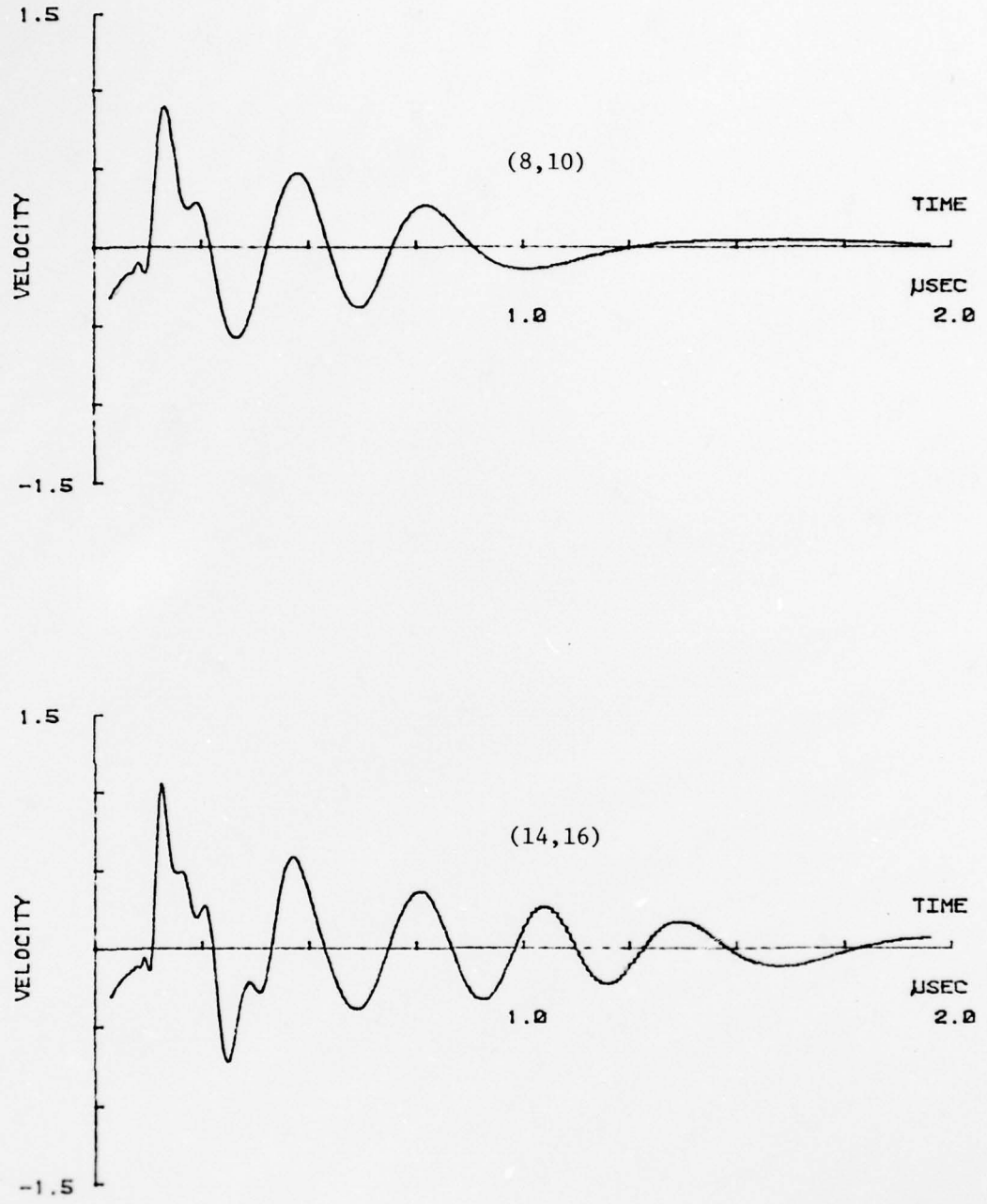

Figure 3.12. System A evaluated for different Pade orders

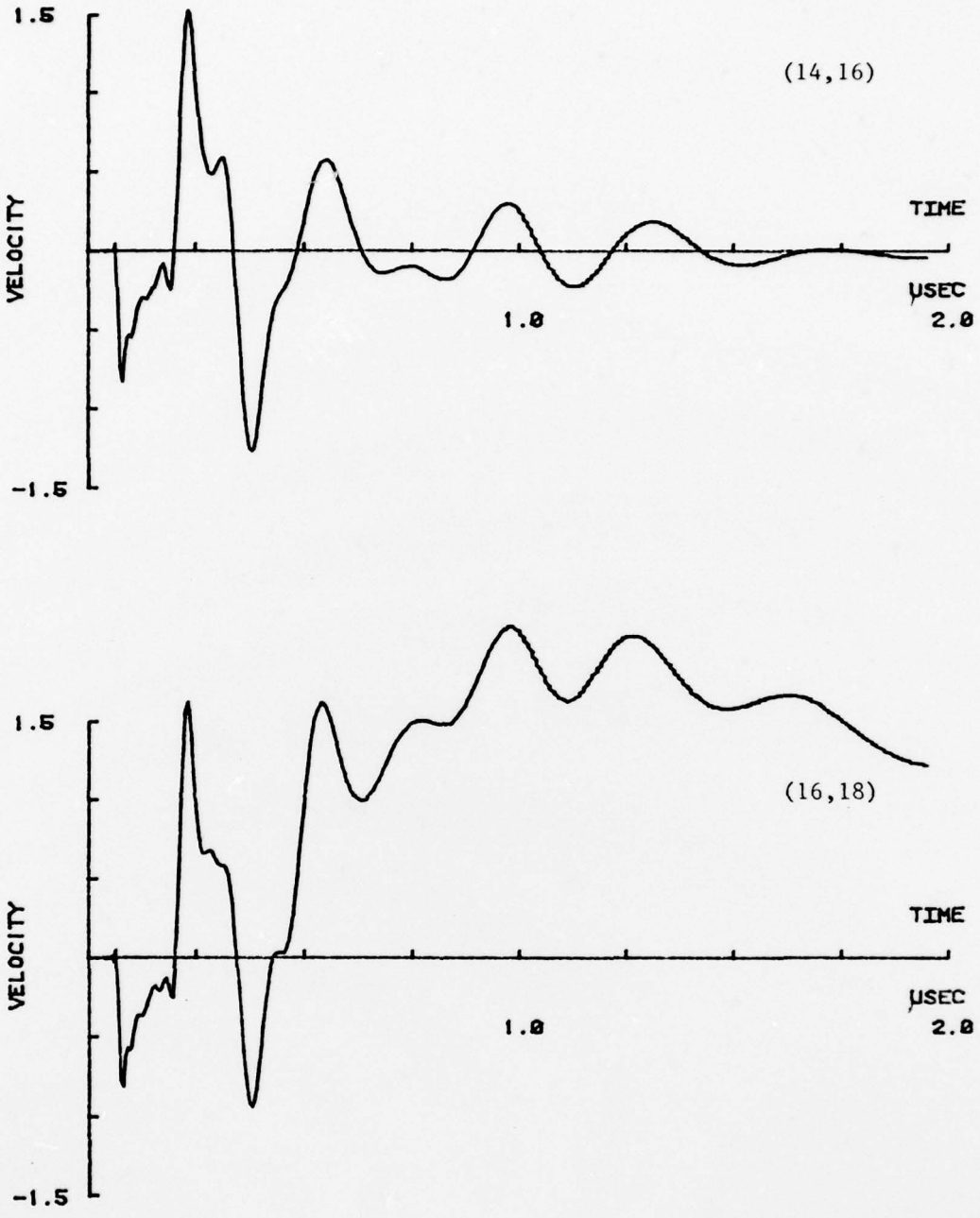

Figure 3.13. System B evaluated for different Pade orders

error begins to occur at N=16, M=18 (16,18). The approximations of (12,14) or (14,16) would therefore be suitable for evaluating the time responses of systems A and B. For situations which are similar but not equivalent to those cases, the (12,14) approximation has certain advantages over the (14,16) approximation. Such conservatism reduces the possibility of encountering a chance numerical situation causing round-off errors. In all cases, the difference between M and N is two which insures that the integrand of Equation (3.35) has the required $1/s^n$ (n>1) behavior at large s. For a stable transfer function with loss or driven by a resistive generator, it is well known that there can be no more zeros than poles. Therefore, two more poles in the Pade fraction are sufficient to provide that behavior at large s. The impulse responses of Figures 3.12 and 3.13, and all subsequent impulse responses, have been normalized to the peak velocity of system A for the (12,14) approximation. In the chapters that follow, the choice for this normalization becomes evident. It serves to emphasize the effects of matching schemes on relative output. The unnormalized peak velocity (to an impulse excitation) is $1.32X10^4$ m/sec.

For transfer functions with equal numbers of poles and zeros, it is not advantageous to increase the difference between M and N beyond two. In so doing, M would have to be increased to increase the order of the approximation. Increasing M has the undesirable effect of increasing the magnitudes of the residues and risking increased round-off [45]. Although permissible, odd values of M and N having a difference of two are not computationally efficient. For real time sequences, the (13,15) approximation is computationally equivalent to the (14,16) approximation

[see Equation (3.38)].

3.3.4 Summary of the Time Inversion Techniques. The Pade approximation to the time response has several advantages over the IDFT, the z-form, and the other techniques mentioned in the literature survey of Chapter II. As indicated by Equation (3.38), the calculation of the time response is straightforward and is readily implemented on a digital computer once the frequency response has been programmed. Use of the IDFT requires large array area on a digital computer, but the Pade method does not. Equation (3.38) shows that the Pade method requires M/2 circuit evaluations for each time domain point. For the IDFT, all points up to the band-limiting frequency, f_c, must be calculated. For the application at hand, there are modest computational savings with the IDFT method.

As mentioned in Section 3.3.1, the choice of f_c and γ in the IDFT calculation has a critical effect on the time response. Explicit inclusion of the higher order harmonics seems to overemphasize their theoretical contribution to the impulse response compared to the observed situation. On the other hand, the Pade method implicitly incorporates all of the harmonics in the calculations. High frequency components are indirectly neglected by the fact that the response is approximated by a Taylor series. Truncation of the Taylor series will cause the inaccuracies to become more significant at larger times. Comparing the time responses of system B as calculated by the Pade method (Figure 3.13) with the responses determined by the IDFT method (Figure 3.11), it is observed that the two are most similar when band-limiting the IDFT at the second harmonic. That comparison also reveals that the Pade time response does include frequency components

above the second harmonics as is evidenced by sharper time peaks than with the IDFT response (band-limited at the second harmonic). The presence of third and fifth harmonic components in the Pade time response has been confirmed by performing a DFT on the Pade time response. The inaccuracies that are incurred by the Pade approximation tend to compensate for the overemphasis of the harmonics by the Mason model. As a consequence, the Pade inversion is considered to be superior than the IDFT method.

Since the methods of Chapter II are not readily extendable to the generalized transducer configuration of Figure 3.5, they, too, are rejected for the present application in favor of the Pade approximation. The major disadvantage of the Pade inversion is its increased (but bounded) inaccuracy for large times. For impulse response evaluation where high accuracy is required for small times, the Pade response has been shown to be very accurate [45]. The Laplace inversion via the Pade approximation with N=12 and M=14 is used throughout this study for obtaining the impulse response immediately following excitation.

CHAPTER IV

OPTIMIZATION PROCEDURE

4.1 Effects of Matching at Each Port

A piezoelectric disc transducer has two mechanical ports and one electrical port. The transfer of energy to any one port is, in general, a function of the effective termination at all three ports. Since it is only desired to constrain the response at one of the ports, there should be considerable flexiblility in selecting the various port terminations for achieving that goal. This flexiblility is discussed later in this chapter and its utility is demonstrated in the next chapter. The purpose of this section is to demonstrate that the matching at each port has its own characteristic effect on the transient response which is dependent upon the particular port rather than the precise details of the matching scheme. With this premise accepted, there is justification for considering possible parameter subspaces during the optimization procedure and is discussed in detail later in this chapter.

To simplify the circumstances underlying energy trasnfer between the element and its loads, the ceramic and mechanical matching sections are assumed to be lossless (i.e., $\gamma=0$). Under this condition, energy loss can only occur by a resistive element at one of the ports. Lossless systems of this type are denoted by a tilde; e.g., $\tilde{A}$ and $\tilde{B}$ correspond to systems A and B of Chapter III. It is also emphasized that all of the theoretical and experimental conditions utilize an acoustic load of water and assume that the loading is purely resistive. In addition, any electrical excitation is applied with a voltage source

having a series resistance, R_g, of 50 ohms.

4.1.1 Loading at the Back Face. Upon examining the front face velocity transient under a voltage input for several conditions of back-side loading, one can gain a physical interpretation of the disc's mechanics. Figure 4.1 shows this impulse response of system $\tilde{A}$ for air backing, and for backings which are equal and double the specific acoustic impedance of the ceramic. As mentioned, these impedances are modeled resistively. (Subsequent references to the backing or front-side load impedances are typically normalized to the ceramic impedance.) From Figure 4.1 it is seen that the response up to approximately 0.14 microseconds is independent of the back-side load. Calculating the mechanical transit time, T_o, through the disc from the parameters of Table 3.2, it is also found to be about 0.14 microseconds. Hence, that first part of the response which includes the first velocity peak is caused by motion at the disc and water interface prior to any reflection. That part of the response is, therefore, unaffected by the backing.

The initial motion occurring at the back face can be considered 180^o out of phase with the front-face motion in the following sense: if the electrical excitation had a polarity causing the disc to expand, the water at the face would be compressed, but a rarified condition would simultaneously be propagated to the front face from the back face. The second pulse in Figures 4.1a to 4.1c results from the relaxation of the original front-face motion and is reinforced by the motion that originally occurred at the back face. This process continues as the thickness of the disc successively changes from thin to thick over each half-cycle.

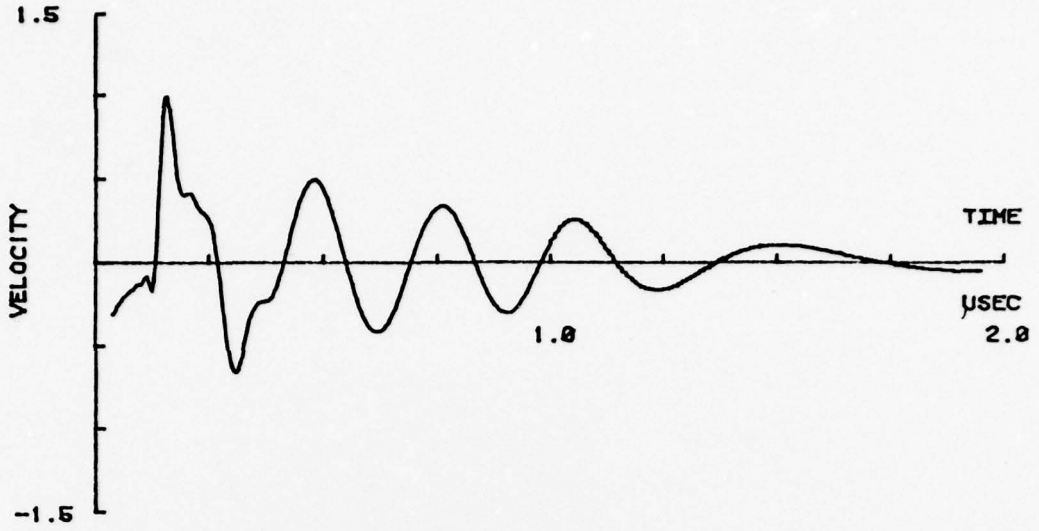

(a)

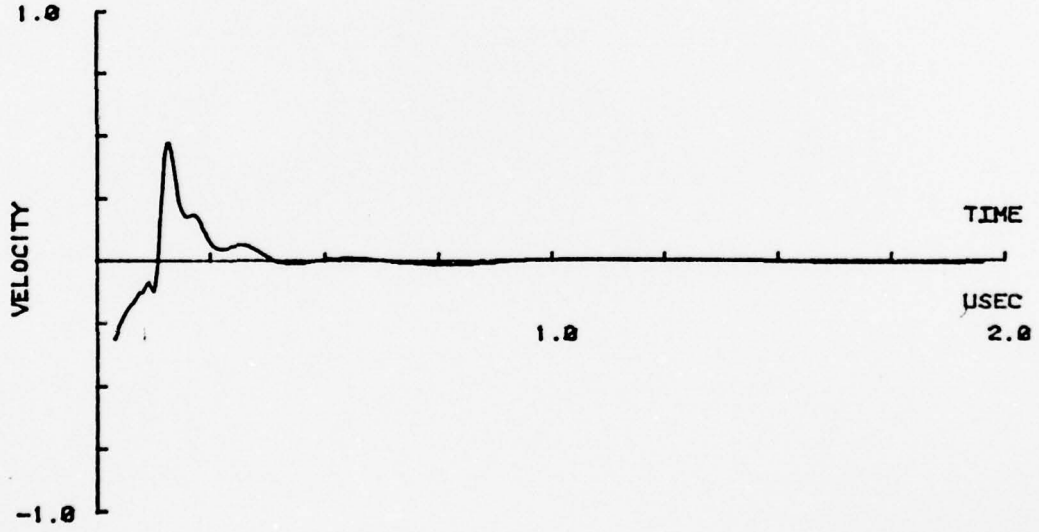

(b)

Figure 4.1. Comparison of the impulse response of System A with different backings
a. Air-backed
b. Matched backing, Z_B=1.0

Figure 4.1. (continued)
c. Backing set to Z_B=2.0

Peterson and Rosen [39] suggest that the transient response of an air-backed disc should appear more like a series of alternating positive- and negative-going impulses, separated in time by T_o seconds. However, there is an important difference between their case and the situation of Figure 4.1a. That difference is the short circuit boundary condition of Peterson and Rosen compared to the 50-ohm source impedance, R_g, included in the calculations for Figure 4.1a.

The reason for this difference is readily demonstrated in the frequency domain. As Peterson and Rosen describe, the successive impulses are reduced in amplitude depending upon the relative impedance mismatch between the ceramic and water. The Fourier transform of that time domain series of pulses is:

$$\sum_{n=0}^{\infty} A_n e^{-jnT_o} \quad ,$$

where the A_n is the amplitude of the n^{th} pulse, and T_o is the transit time through the ceramic. Qualitatively, the above series has a magnitude response with a maximum at $w=\pi/T_o$ and minima at d.c. and at $w=2\pi/T_o$. Moreover, the frequency response is periodic with period $1/T_o$. The periodicity is expected from the uniformly incremented discrete nature of the time response. The qualitative description of the frequency response corresponds to the calculated responses of Chapter III (up to the second harmonic). However, Equation (3.32) demonstrates that the frequency response of a disc driven by a resistive generator is <u>not</u> periodic. For the frequency response to be approximately periodic, that equation shows that the electrical termination must be short circuited. In practice, a short circuit condition still does not insure

a series of time domain impulses. Losses within the ceramic, i.e., $\gamma \neq 0$, have also been shown to reduce the amplitude of the higher harmonics. Reanalyzing the equivalent circuit for an air-backed, lossy disc with $R_g=0$ does, in fact, result in a time response more closely resembling a series of impulses (up to $3T_o$). After that time, the response is as depicted in Figure 4.1a. This discussion should serve to emphasize the potential importance of the electrical boundary conditions.

In Figure 4.1a, the decay of the response from one peak to the next is determined by the rate at which energy is removed from the transducer system. Improving the impedance match between the ceramic and front or back-side loads should generally increase this rate, as evidenced from Figure 4.1b. The response during 0.14 to 0.28 microseconds, corresponding to the second velocity pulse, primarily results from the original motion at the back face of the transducer. The peak velocity of the second pulse in Figure 4.1b is approximately half that of the corresponding pulse in the air-backed case. The situation is somewhat analogous to doubling the series resistance of a constant voltage (force) generator.

Additional increases to the backing impedance continues to augment the restriction of motion at the back face of the transducer. From the voltage source analogy, back-side loading with twice the impedance of the ceramic should reduce the peak height of the second pulse to approximately one-third the height of the air-backed case. This result is confirmed by Figure 4.1c. The velocity of the third pulse has changed sign since the reflection coefficient between the ceramic and backing changes sign upon increasing the impedance of the backing beyond the impedance of the ceramic [see Equation (2.8a)].

With these very simple examples in mind, it is possible to make some general observations about the utilization of back side loading for modifying the transient response. Using a backing impedance equal to the ceramic's impedance should approximately minimize the velocity peaks beyond the second pulse. It is expected that the third and subsequent pulses would be reduced since waves propagating through the ceramic toward the back face are mostly transmitted into the backing rather than reflected toward the front face. This configuration of matched backing achieves improvements to the transient response at the expense of reducing the peak power delivered to the water load by a factor of four compared to the air-backed case. Power, it is recalled, is proportional to the square of the face velocity (for a constant load impedance). Utilizing a back-side impedance greater than the ceramic's to further reduce the amplitude after the second pulse, results in increased energy beyond the second pulse due to the increased mismatch between the ceramic and backing.

4.1.2 Front-Side Matching. System B of Section 3.2 is an example of an air-backed transducer system with a quarter-wave matching plate between the front face and water load. In contrast to back-side loading, front-side matching can increase the amplitude of the first velocity pulse due to the reduced impedance mismatch between the ceramic and water load. That first pulse is still only caused by the initial motion at the front face of the ceramic. However, it is now delayed in reaching the water load by the transit time through any matching sections. Because of the quarter-wave section, the subsequent pulses are comprised of more than one component as illustrated in Figure 4.2. In the figure, wave propagation originating from the two faces of the

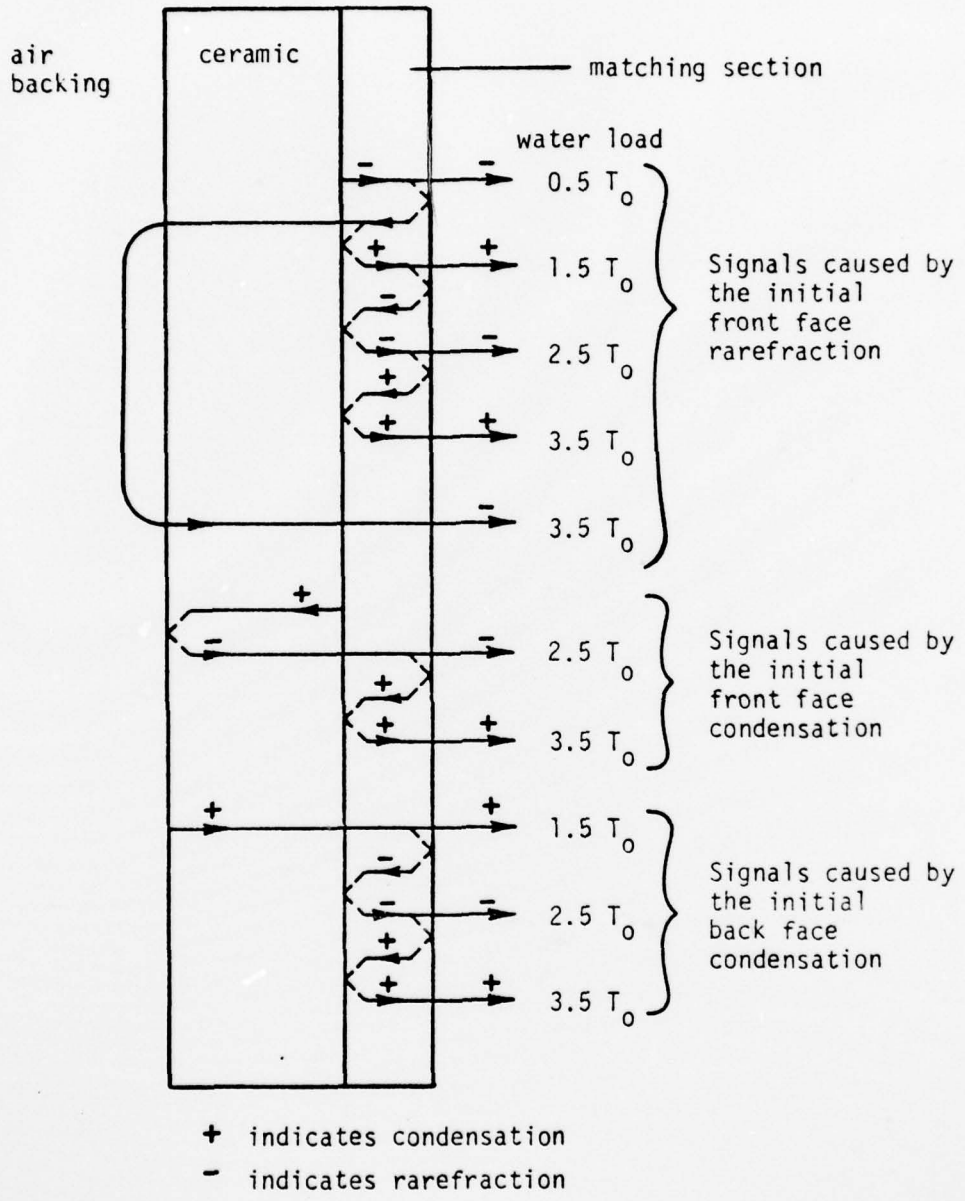

Figure 4.2. The paths of the acoustical signals in a system with a single quarter-wave matching section

disc is traced to the acoustic load. From the front surface, two distinct pressure waves are generated: one into the ceramic and one into the adjacent load. For an air-backed transducer, the air is assumed to provide a pressure release condition. As a consequence, motion at the back face only propagates a signal into the ceramic. No pressure waves are generated in the air, and waves reaching the air from the ceramic are assumed to be perfectly reflected with a sign change. The signals arriving at the acoustic load are labeled according to the time at which they arrive in terms of T_o, the travel time through the ceramic. As an example, the first signal reaching the load arrives after a delay of $0.5T_o$ through the matching section. Although the analysis incorrectly assumes a pulse-like response, it serves to demonstrate the relative signs of the components within each velocity pulse. For the case with a backing impedance less than the ceramic impedance, there are no out-of-phase components within a given pulse until $3.5T_o$, corresponding to the fourth pulse. This result is considered when establishing optimization criteria.

One can interpret front-side matching as a mechanism for increasing the removal rate of mechanical energy from the transducer system to the water load. It has the effect of increasing the peak power as well as the total energy delivered to the acoustical load. The specific example of system B has been illustrated in Figure 3.13a. The increase to peak power is due to the improved matching between the ceramic and water. As a consequence, the total energy (proportional to the square of the velocity response integrated over time) is increased. With the mechanical energy spending less time in the ceramic, the opportunity for dissipative and electrical losses is thereby reduced. An example is now

AD-A073 818 PENNSYLVANIA STATE UNIV UNIVERSITY PARK APPLIED RESE--ETC F/G 20/1
TRANSIENT RESPONSE OPTIMIZATION OF PIEZOELECTRIC DISC TRANSDUCE--ETC(U)
JUL 79 H A WOLF N00024-79-C-6043
UNCLASSIFIED ARL/PSU/TM-79-139 NL

2 OF 3
AD A073818

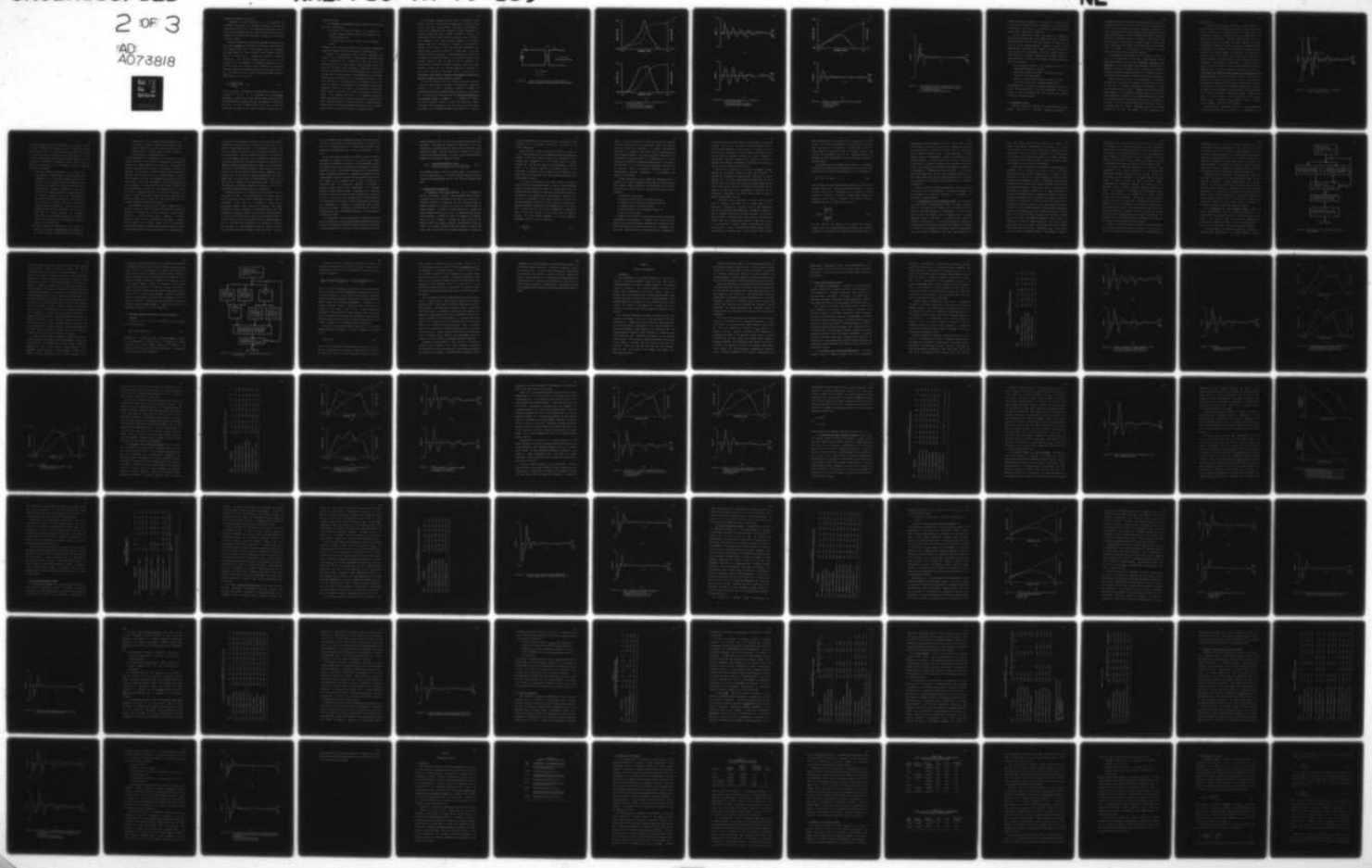

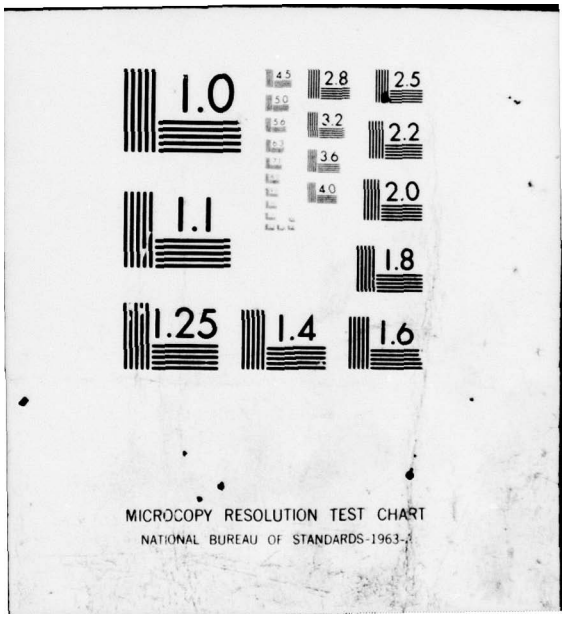
1.0
1.1
1.25
1.4
1.6
2.8
2.5
3.2
2.2
3.6
2.0
4.0
1.8
MICROCOPY RESOLUTION TEST CHART
NATIONAL BUREAU OF STANDARDS-1963-A

presented to demonstrate the point.

Considering the energy delivered up to 2.0 microseconds and normalizing with respect to the energy of system A, the energy for system B is found to be 1.90. For systems with considerable loss, such as those with substantial back-side loading, front-side matching is very important for preserving device efficiency. The point is to be explored in the next chapter.

The above findings about the delivered energies of systems A and B can also be estimated by considering the reflection coefficients along the mechanical delay line. Using Equation (2.8), the reflection coefficient between the ceramic and water, in the absensce of matching sections, is denoted as r_{cw}. Likewise, the reflection coefficient between the ceramic and the matching section, r_{cm}, can also be calculated. With the impedance of the matching section equal to the geometric mean of the ceramic and water impedances, the reflection coefficient between the matching section and the water, r_{mw}, is equal to r_{cm}. From Equation (2.2), the overall improvement in power transfer of system B over system A is given by:

$$\frac{[1 - r_{cm}^2].[1 - r_{mw}^2]}{[1-r_{cw}^2]} = 1.75 \quad , \tag{4.1}$$

where the reflection coefficients are calculated from parameters given in Tables 3.1 and B.1. It is conjectured that this estimated improvement is lower than the previously calculated improvement since the electromechanical coupling factor has been neglected in calculating the former. The rate of energy transfer to the load is greater for system B than for system A, and there is therefore less opportunity for

energy loss to R_g.

4.1.3 Matching at the Electrical Port. Matching at the electrical port has a twofold effect:

1. to increase the power delivered to the transducer by providing impedance matching between the transducer and resistive generator and
2. to broad-band the frequency response of the transducer system.

The impact of the electrical termination on the impulse response has already been observed and is further examined in this subsection.

Redwood's [42] observations about a stressed piezoceramic bar provide a clue to the performance of lumped element matching circuits with a piezoceramic disc. Redwood notes that his results are qualitatively correct for other transducer shapes and polarizations. He shows that the stored electrical energy is removed much more quickly than the mechanical energy for low shunting resistances. The initial discharge rate of electrical energy is approximated by an R-C discharge, where $C=C_{eff}$ (see Appendix A) and R is the generator resistance. Using system A driven by a 50-ohm generator as an example, the R-C time constant is about 2.6 times smaller than the mechanical transit time through the ceramic. It is reasonable to expect that the addition of lumped elements could store and prolong the release of electrical energy. In the examples that follow, it is shown that electrical matching can increase the total energy delivered to the acoustical load and in some ways improve the characteristics of the impulse response. However, there are certain complications which seem to result from the delayed release of the electrical energy at inopportune times.

The very simple matching circuit of Figure 4.3 demonstrates these effects. This type of circuit has been suggested by Goll [19], Desilets et al. [11], Kossoff [30], and others. The value of the inductance is selected to be resonant with the transducer's clamped capacitance at a frequency slightly less than the resonance frequency of system A. The transformer ratio also tends to match the real part of the transducer's input impedance to the 50-ohm generator impedance at frequencies somewhat removed from the transducer resonance. It is desirable to restrict the turns ratio to two since wide-band transformers with arbitrary turns ratios are difficult to construct [22]. As is then expected, the frequency response is broad-banded and the insertion loss is improved off resonance compared to the case with no matching. The resulting response is shown in Figure 4.4 and is compared to the response without matching. The impulse responses for the two systems are shown in Figure 4.5. The electrical matching has increased the total energy delivered to the water load by a factor of 1.73. Unfortunately, this increase is achieved at the expense of extending the duration of significant energy transfer to the load.

A time domain interpretation on the effects of electrical matching is that the network increases the width of the pulse that reaches the transducer. As a result, the energy is delayed in reaching the transducer and prolongs the ultimate release of energy to the acoustical load. This situation is demonstrated by using both matched backing and the electrical network of Figure 4.3. The frequency and impulse responses are presented in Figures 4.6a and 4.6b, respectively. Figure 4.7 replots that time response on the same axis as the time response with backing but no electrical matching (from Figure 4.1b). From the

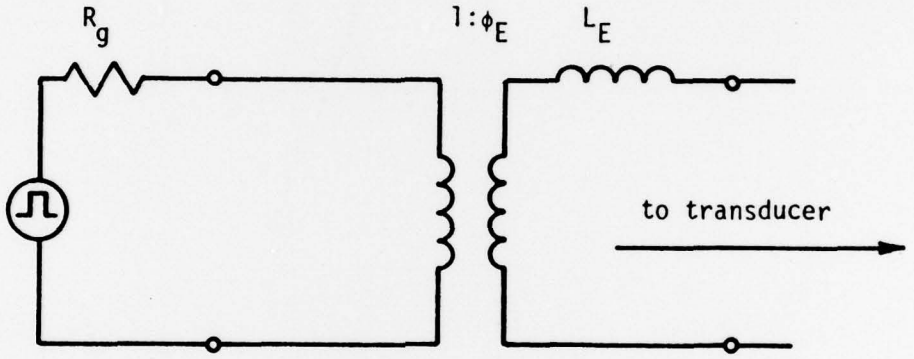

$L_E = 2.0\ \mu Hy$

$\phi_E = 0.5$

Figure 4.3. A simple matching network for broad-banding the amplitude response and linearizing the phase response

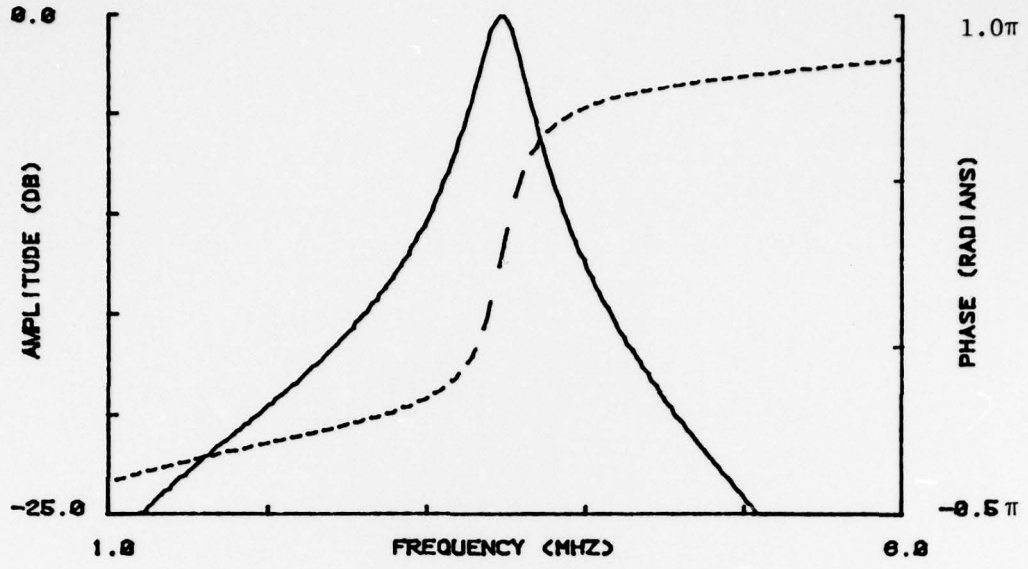

(a)

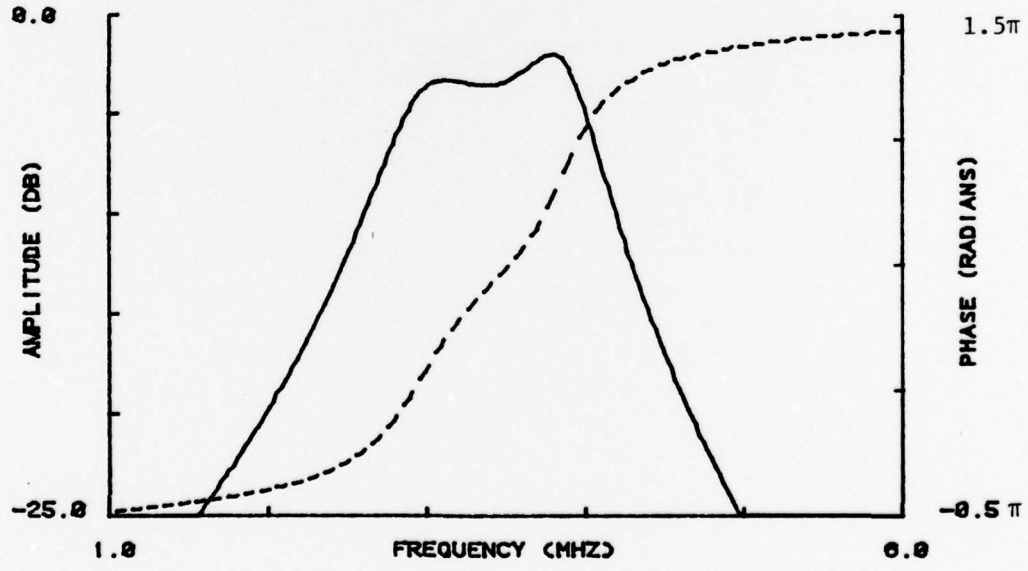

(b)

Figure 4.4. A frequency domain comparison of the effects of electrical matching
a. No matching network employed
b. With the network of Figure 4.3

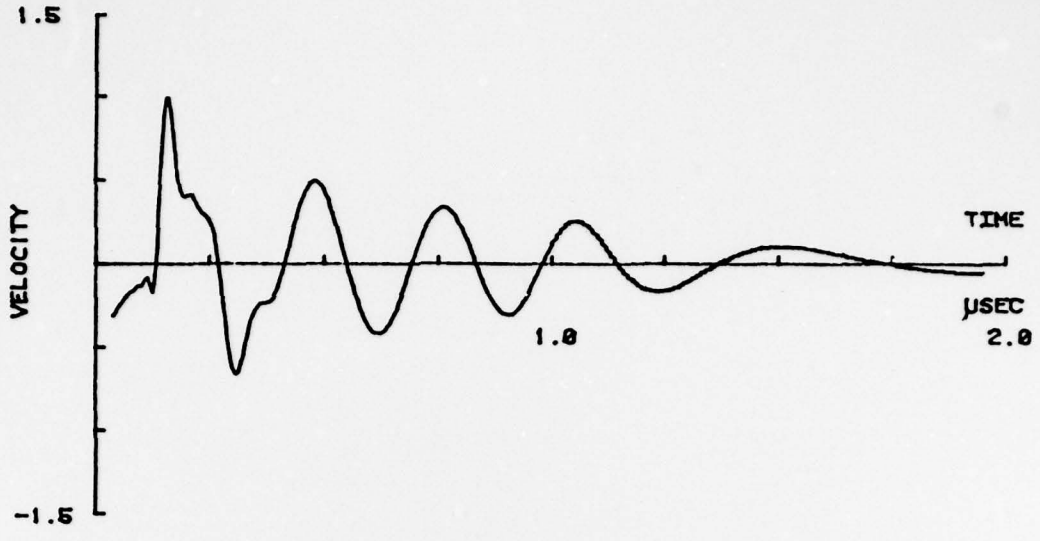

(a)

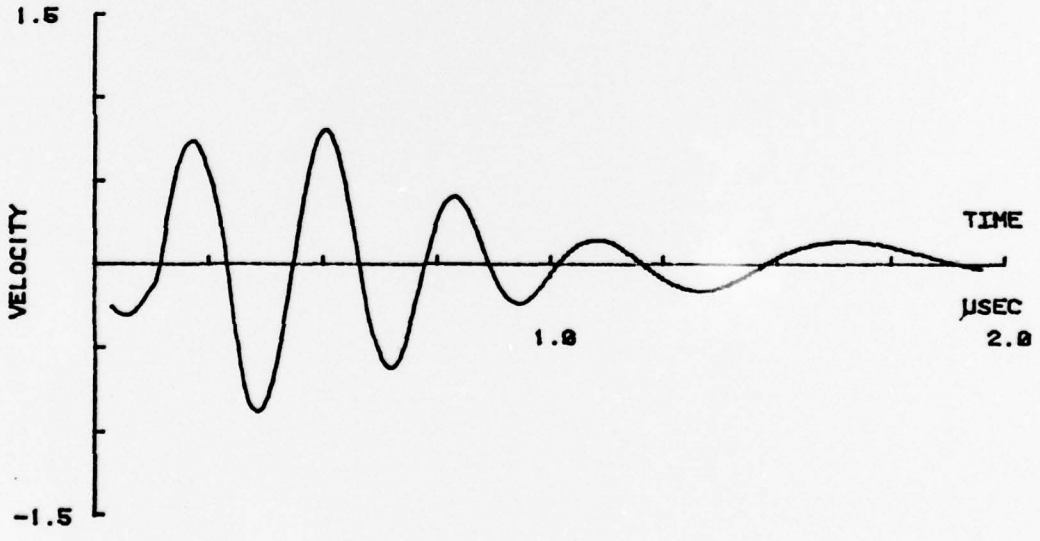

(b)

Figure 4.5. A time domain comparison of the effects of electrical matching
a. No matching network employed
b. With the network of Figure 4.3

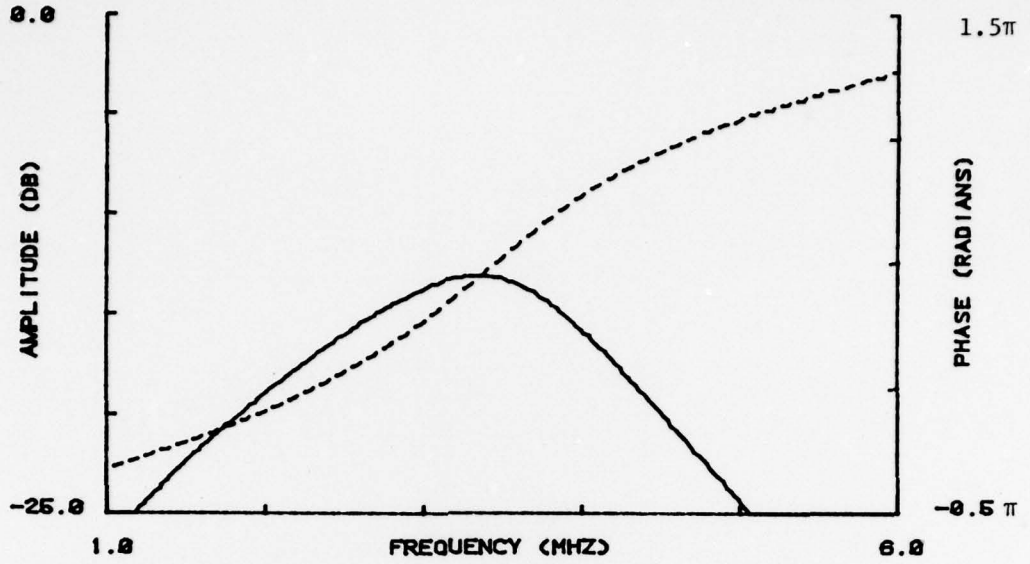

(a)

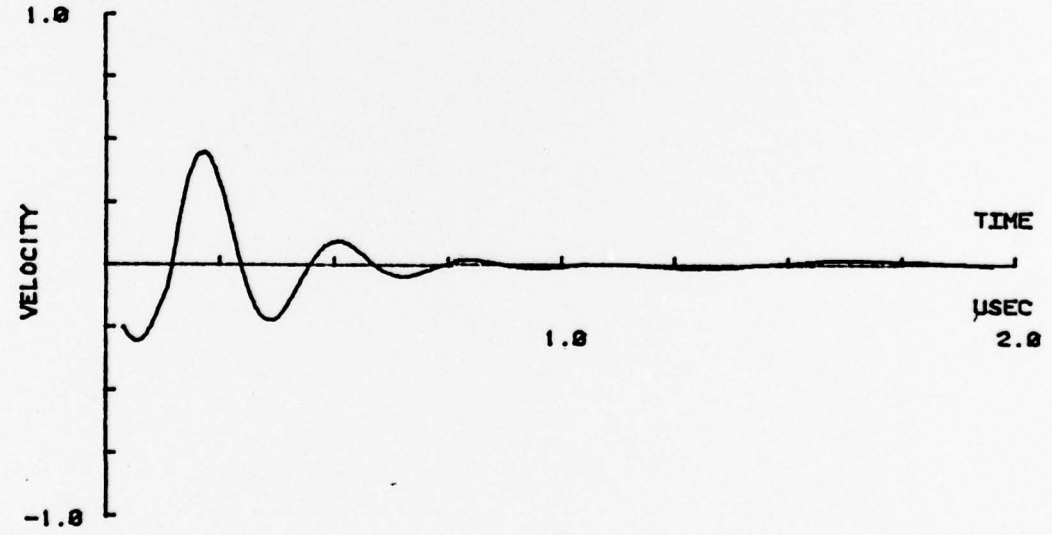

(b)

Figure 4.6. Response of backed transducer with the matching network of Figure 4.3
a. Frequency domain
b. Time domain

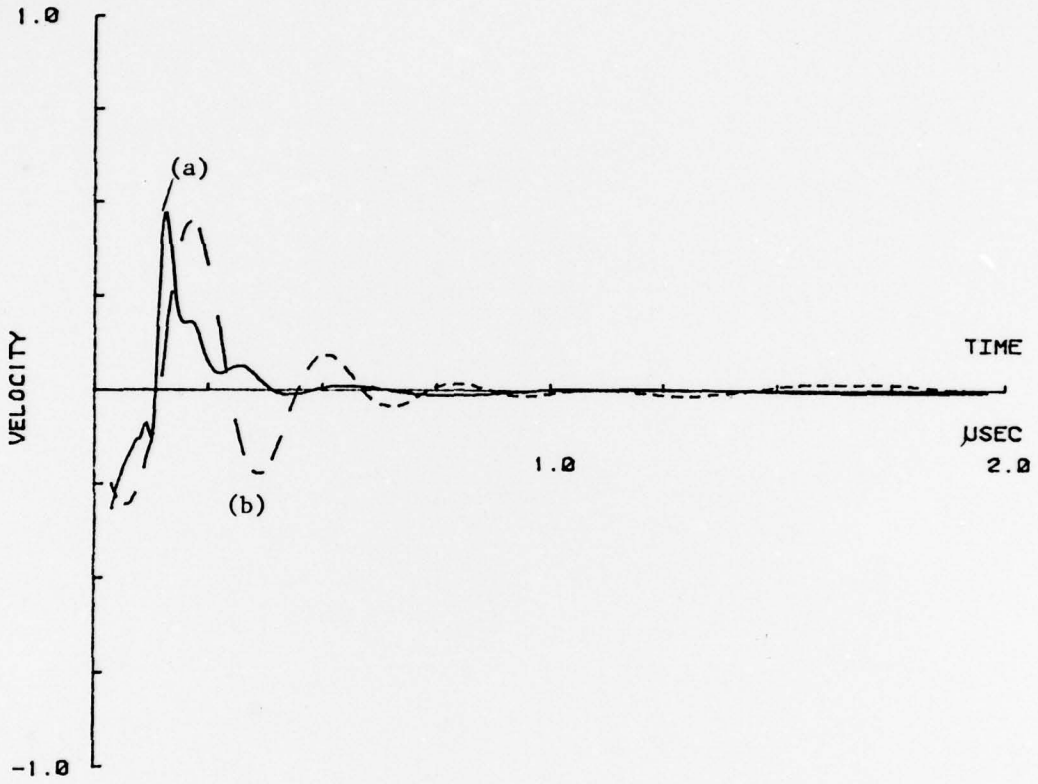

Figure 4.7. Time responses overlaid to demonstrate the effects of electrcial matching; backing fixed to Z_B=1.0
a. No electrical matching
b. Electrical matching of Figure 4.3

comparison presented in Figure 4.7, it becomes clear that significant velocity peaks now appear after the second pulse (i.e., later than 0.28 microseconds). They result from the condition of delayed electrical energy causing delayed motion at both faces.

It can be argued that certain pulse shapes (or equivalently, electrical matching networks) should improve the transient response by delivering energy to the transducer at precisely the right time and phase to cancel unwanted transients. However, a judicious design procedure must be employed if the network is to reduce ringing. It seems that Kossoff's warning about the use of lumped elements when concerned about the transient response cannot be treated lightly. A direct approach for the design of an electrical matching network would seem to be as follows:

1. By convolution, determine a time domain excitation for achieving the desired face velocity.
2. With Fourier transform techniques, calculate the frequency response of the required signal.
3. From the frequency response, network synthesis techniques can be used for devising a suitable matching circuit.

The development of such networks for use with piezoceramic elements will be left for future researchers. This work concentrates on the use of matching at the two mechanical ports for improving the transient response to an impulse excitation.

4.2 Optimization Criteria

In Section 1.2 goals for optimizing the impulse response have been offered. Selection of a particular optimization procedure is

necessarily dependent upon the intended application of the transducer. In medical situations, it is often desired to reduce the ring-down even at the expense of transducer efficiency. For other applications, the need for increased pulse penetration may sacrifice ring-down quality for higher peak velocities. It quickly becomes evident that the concept and definition of ring-down must also be clarified. Traditionally, ring-down or transient energy refers to the spurious energy after the major pulse. With slight modification, that interpretation is to be applied here. The purpose of this section is to discuss the various optimization criteria and the concept of ring-down.

The optimization goal emphasized in this work is to increase the ratio of the peak power to the peak ring-down power, without significantly reducing the peak power. This ratio is denoted as the peaks ratio. In pulse detection applications where high resolution is important, this type of response offers an improved signal-to-noise ratio and should enhance image reconstruction. In transceive operation, it reduces the time required for receiver recovery after transmitting.

Another optimization goal is to simply maximize the total energy delivered up to a specified time or event. Selecting that cutoff time so that most of the energy (approximately three-fourths or more) eventually delivered to the load is included in the calculations yields designs similar to that described by Desilets, Kino, and Fraser [11]. This confirmation of the Desilets et al. design (demonstrated in Section 5.2) is expected when it is recalled that their goal is to maximize the efficiency. It has also been found that if the cutoff time is chosen in a way which does not include a substantial portion of the energy delivered to the load, the results of that optimization are

unpredictable.

For the sake of consistency, the start of ring-down energy is defined in terms of an event rather than a specific time. Ring-down is defined to begin after a specified number of velocity pulses have occurred and is denoted as the separation time, $t_s(n)$, which defines the completion of the n^{th} pulse. The minor pulses which may precede the first major pulse are not included in the pulse numbering. The energy delivered up to time $t_s(n)$ is called early energy, and subsequent energy is referred to as late energy. The time response of system B is shown in Figure 4.8 with $t_s(3)$ included for illustration. The advantage of defining $t_s(n)$ in this manner is that the first few peaks of the transient response are relatively fixed in time location, approximately independent of the mechanical matching scheme. Any overall shift is caused by a change of time delay from the intervening layers between the ceramic and load. The relative amplitudes of the peaks can change, but their location and width are relatively fixed by the propagation delay through the ceramic. Although the results in Section 4.1.1 indicate the possibility of widening the second pulse by using backing impedances greater than the impedance of the ceramic, the implications with respect to the changes on $t_s(n)$ and on the optimization outcome are not serious. In Chapter V, it is demonstrated that the practical solutions generally do not result in significant second pulse distortion. Having defined $t_s(n)$, it is then possible to also illustrate the peak ring-down velocity, v_{ring}. In Figure 4.8, v_{ring} happens to occur for the first peak of ring-down. This is not true in general.

The rationale for selecting the value of n of $t_s(n)$ is understood by considering the discussion of Section 4.1. As explained in that

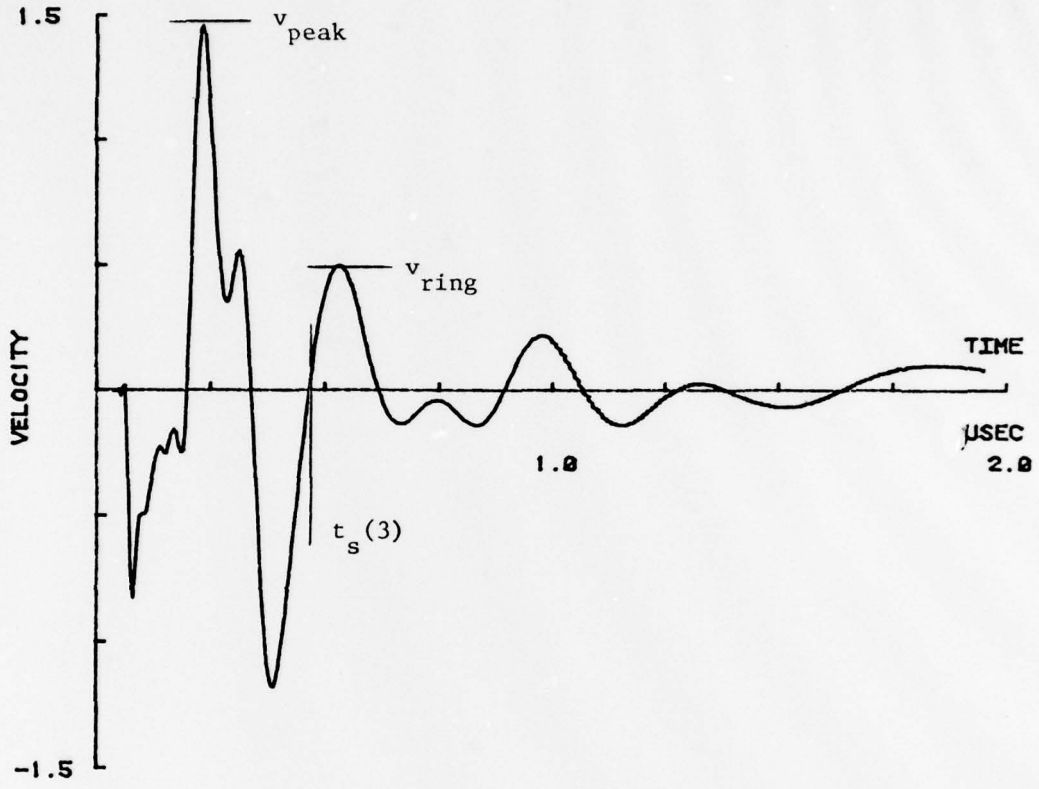

Figure 4.8. A typical time response for illustrating $t_s(n=3)$, v_{peak}, and v_{ring}

section, back-side loading reduces the height of the second pulse and can almost eliminate the third pulse. For an air-backed or lightly backed system, little can be done to moderate the height of the second or third pulse, and not increase velocity peaks after $t_s(3)$. On the contrary, improved front-side matching increases the height of the first three pulses, and reduces the amplitude of later pulses. Since two distinct situations exist, it is reasonable to apply the following criteria for selecting n:

1. For light backing, the minimum value of n is three. The most important elements available for optimization are the parameters of the front-side matching sections. From Section 4.1.2 it is observed that a front-side section has the effect of increasing the amplitudes of the first three velocity pulses. Although the discussion of that section is limited to a single quarter-wave matching transformer, the amplitude increase to the first three pulses is observed for multiple matching sections. The increase over the unmatched case is observed even if the section lengths deviate modestly from quarter-wave. After $t_s(3)$, there are components contributing to the response which are out of phase with the resulting response. It is therefore expected that these additional components can be adjusted to alter the post-$t_s(3)$ part of the response by varying the design of the front-side match.
2. For heavy backing, the minimum value for n is two. In Section 4.1.1 back-side loading matched to the impedance of the ceramic is shown to substantially reduce the transient

response after $t_s(2)$. Without electrical matching, it is not possible to achieve a unipolar impulse response. Even under the conditions of perfect acoustical matching at both mechanical faces, a bipolar impulse response is expected due to the motion at the back face [16].

For most applications, it is assumed that it is desirable to keep $t_s(n)$ as small as possible. This restriction is appropriate if the pulse-like quality of the impulse response is to be improved. The distinction of different separation times should not be considered as arbitrary or artificial. The two types of transducers would normally have different applications. One should not expect the transient response of a lightly backed transducr to have the same ring-down characteristics of a heavily backed system. Until later clarification, light backing implies an acoustic impedance less than about 25% of the ceramic's impedance and heavy backing greater than about 75%. The present discussion is limited to the use of resistive backings. No reflections from within the backing are taken into account, though this could readily be done. Generally, backing materials, when used, are sufficiently lossy to be considered echo-free for all practical purposes.

The optimization criterion for the backing impedance must be modified for cases that are to have light backing material. Without any modification, all peaks ratio criteria would drive a lightly backed solution to a heavily loaded situation. Therefore, a separate optimization goal is to be established for determining a suitable backing impedance in the lightly damped case. This alternative procedure must recognize a condition where additional increases in back-side loading deteriorate the pre-$t_s(3)$ response at an unacceptable rate.

In Chapter V, it is demonstrated that there is such a compromise between the reduction of peak power and the increase of the peaks ratio that is expected with increased backing. It is demonstrated that this rate change is modest for a one-layer match, but is quite considerable for the two-layer match. This can probably be attributed to the fact that the velocity response after $t_s(3)$ contains several more components from internal reflections for the two-layer case than for the one-layer case. Through the previously used ray-tracing procedure, it can be determined that several of these additional components are a function of back-side loading as well as the front-side matching scheme. Regardless of the precise details of the front-side matching configuration, the results indicate that the optimal amount of backing impedance is about two to three times the impedance presented by the water load. This result is consistent with the findings presented by Desilets et al. [11] when considering tradeoffs between efficiency and performance.

Although the peaks ratio is calculated by the division of only two time domain velocities, a considerable portion of the impulse response must be calculated in order to select those proper two points. With the availability of this data, it is reasonable to search for an optimization parameter that utilizes the additional time domain information to enhance the process of improving the peaks ratio. One disadvantage of applying the peaks ratio directly in the search routine is that very fine interpolation is required to insure that the values of the true peak is not being overstepped. Another possible drawback is that all other time domain characteristics are ignored with the peaks ratio criterion. For some applications, it may be desired to increase the early energy and accept a slightly poorer peaks ratio. In such a

case, it is possible that the supplemental energy would be manifested as an increase to the energy of an early pulse without affecting the peak power. It is therefore desirable to allow for some flexiblity in the optimization parameter beyond the criterion of improving the peaks ratio.

At the very least, an optimization parameter could be defined by calculating the energy in the vicinity of v_{peak} and v_{ring}. Although this approach would reduce the impact of poor interpolation that has been suggested above, it does not address the requirement of including a substantial portion of the available information into the optimization process. Beginning the search for an optimization parameter with fairly straightforward routines, it has been found that maximizing the ratio of early energy to peak ring-down power is quite successful as an optimization goal. It recognizes the importance of attempting to increase the peak power and early energy subject to the constraint imposed by the peak ring-down power. Concurrently, the optimization goal may be achieved by reducing the peak ring-down power. Maximizing the ratio of early energy to peak ring-down power has the disadvantage of not being specific as to which of those two mechanisms are dominant. As a consequence, the likelihood of encountering locally optimal solutions is increased. Although locally optimal solutions tend to be somewhat annoying, they are tolerable by pointing out the availability of alternative designs.

It is important that the early energy used to calculate that search function includes most of the significant energy ultimately delivered to the load. For cases with substantial back-side loading, the requirement is typically satisfied for $t_s(2)$, but is not necessarily met for lightly

loaded designs with $t_s(3)$. When the early energy does not satisfy this requirement, the optimization parameter has been found to lose some dependability. Excluding significant energy from the calculation of the optimization parameter does not allow for an increase to late energy resulting from improved matching. To account for this, the optimization parameter to be maximized is defined as follows:

$$\text{opt}(n) = \frac{\text{total energy delivered to load}}{\text{peak power delivered to the load after } t_s(n)} \quad . \quad (4.2)$$

For reasonable matching, most of the energy transfer occurs within the first ten transit times, T_o. The results presented in Chapters V and VI confirm that maximizing opt(n) does, in fact, lead to an improved peaks ratio.

4.3 Implementing the Optimization

4.3.1 Selection of the Search Procedure. Once the optimization goal has been defined, a suitable search technique must be devised. Considering that each mechanical section adds both a length and an impedance available for optimization, and that back-side loading is possibly available for adjustment, the need for an efficient search is quickly recognized. It would be an almost endless task to examine the entire parameter space even for the case of a single matching layer and back-side loading. Fortunately, in terms of minimizing the parameter space, it is not necessary to consider the sound velocity of the matching section as a separate parameter. From Equations (3.15b) and (3.24), it is readily determined that the product of density and velocity and ratio of velocity to length are sufficient to define the

relevant characteristics of the matching sections. Alternatively, these quantities can be independently controlled by the density and the length, respectively.

Having selected a suitable optimization criterion and defined the set of variable parameters, it is now feasible to begin the optimization process. As with most search procedures, the determination of the starting point parameters (i.e., the initial guess) can greatly influence the efficiency and outcome of the optimization. Realistic limits on the allowable range for each parameter should also be established in accordance with the physics of the situation. Such limits restrict the optimization from wandering into regions which have limited physical meaning.

In the case of transmission lines, there has been considerable effort and research documenting impedance matching and the broad-banding between a resistive generator and load. As has been noted and is to be further demonstrated, mechanical quarter-wave sections effect changes to the frequency domain characteristics of piezoelectric transducers that can result in improvements to the impulse response. Young [50] has tabulated transformer designs up to four sections for Butterworth or Tchebychev pass band characteristics for impedance ratios from 1.25 to 100. A possible starting point is then established by selecting the number of front-side sections and the desired type of frequency response. The tables include bandwidths, W, for the Tchebychev transformers from 0.1 to 1.2. W is defined as:

$$W = \frac{f_2 - f_1}{f_o} \quad , \tag{4.3}$$

where f_o is the center frequency at which all the sections are quarter-wave; and f_1 and f_2 specify the lower and upper limits of the Tchebychev pass band response. The bandwidth, W, is a means of specifying the scale factor, a_2, in Equation (2.3), with f_1 and f_2 corresponding to the points at which $\cos(kl)=a_2$. For notational purposes, the maximally flat configuration is denoted by W=MF. As a starting guess, it has been found to be reasonable to compromise bandwidth and pass band ripple by selecting W=0.6. It is stressed that the transmission line analogy is not exact with respect to a piezoceramic transducer because of the electromechanical coupling. Consequently, a true Tchebychev type response is not expected.

A search procedure can now be adopted for maximizing opt(n) of Equation (4.2). Search techniques of many varieties abound throughout the literature. When evaluating the appropriateness of the different techniques, the following factors of the optimization problem must be considered:

1. likelihood of local maxima,
2. accuracy and difficulty of calculating derivatives,
3. closeness of the initial guess to the final solution,
4. required accuracy of the final solution,
5. general qualities of the optimization function, and
6. speed of the convergence.

Although details of the opt(n) function are not known, some general characteristics are anticipated. For example, it is expected that the impedance of the matching sections should decrease monotonically away from the ceramic and be bounded at the low end by the impedance of the water load. Matching theory also dictates that section lengths would

not be idealized at values much longer than quarter-wave. Any increase in length tends to make a section more frequency sensitive which is typically counterproductive to broad-banding. At the very least, the lengths should not approach the half-wave value as half-wave sections are not useful for impedance matching. It is also reasonable to estimate that a back-side impedance in the vicinity of the ceramic's impedance should minimize the amplitude of the third velocity peak and therefore be a good starting guess for opt(2).

From the above discussion, it is seen that the parameter subspace defining the anticipated solutions is fairly well restricted. In addition, the starting point already provides a good, but not optimal solution. Due to the loose interpretation associated with the search function, opt(n), it is likely that more than a single optimum solution will be found. In fact, the search function has been designed with the intent of locating local maxima corresponding to physically different alternatives. Accordingly, the search routine should be able to identify locally optimal solutions.

At this point, it may be beneficial to recall that the actual device or system, not the model, is the ultimate target for any simulation and optimization. In Appendix B, it has been demonstrated that there are noticeable variations between the model of a simple disc with no matching sections and its physical counterpart. It is likely that the addition of matching layers, leads, housing, and backing will enhance, rather than diminish, these differences. Variations are also to be expected due to limited accuracy in measuring the physical constants of the sections. The construction process itself introduces the possibility of irregularities. Even if the model were a nearly

perfect representation of the physical device, calculation of the time response is by numerical approximation, necessarily introducing some error. The purpose of this discussion is to suggest that a locally or globally optimum solution need be found to only modest accuracy. The solutions and experimental cases in the subsequent chapters are calculated to within a percentage or two and are probably examples of over-calculation.

The gradient search (or steepest descent) method is a recommended procedure for well-behaved search functions when only the function value and its gradient are known at each iteration [7]. It is formalized by:

$$\underline{p}^{i+1} = \underline{p}^{i} + q^{i} \nabla^{i} \mathrm{opt}(n) \quad , \tag{4.4}$$

where the superscripts indicate the iteration number, $\underline{p}$ is the vector of parameters being varied, $\nabla^{i}\mathrm{opt}(n)$ is the gradient, and q^{i} is a scalar to control the step size. The gradient, it is recalled, is a vector defining the direction of a function's maximum positive change. The components of the vector are defined by the partial derivatives (sometimes referred to as sensitivities) of opt(n):

$$\nabla \mathrm{opt}(n) = \begin{bmatrix} \dfrac{\partial \mathrm{opt}(n)}{\partial p_1} \\ \vdots \\ \dfrac{\partial \mathrm{opt}(n)}{\partial p_n} \end{bmatrix} \tag{4.5}$$

Any small motion in the direction of the gradient will therefore increase opt(n). By judiciously selecting the starting point, different subspaces can be examined for the possibility of other local maxima. A

disadvantage is that convergence is, at best, linear. This is not a severe difficulty since the starting point is assumed to be good and only modest accuracy is required for the final solution. The gradient search suggested by Equation (4.5) is quite successful in finding improved transducer configurations. Its use is demonstrated in the following chapters. A variation on Equation (4.4) is to search in one direction until a maximum is found and then recalculate the gradient vector. Such a strategy should reduce the total number of computations. A possibility of improving the search direction is to utilize information obtained from all of the previous gradient vectors at each step. These modifications and the precise implementation of Equation (4.4), including the calculation of the gradient and q^i, are discussed in Section 4.4.

Because of the physical differences between the lightly and heavily backed cases, there are some differences in the search strategies. The two procedures are separately described in the following two subsections. matching sections.

4.3.2 Optimization with Light Back-Side Loading. For transducers with light backing, the optimization process is somewhat simplified since the actual value of the backing has very little effect on the finalized front-side configuration. Consequently, it has been found that the back side impedance can be optimized after a suitable front-side design has been found. As a matter of fact, results in Chapter V show that there is little difference between optimizing the front-side sections for either air loading or the optimal light backing. It turns out that the optimal light backing impedance is approximately 20% of the ceramic's impedance or about twice that presented by the

water load. These results are not surprising upon a review of the lightly backed system. By definition, the peak power of a lightly backed transducer system is not to be significantly impaired compared to the air-backed case. Restricting the impedance to the aforementioned level allows for only slight energy transfer to the backing. The impact of light backing on the impulse response is therefore secondary compared to the changes caused by the front-side matching.

It has already been suggested through physical arguments that the optimization may be conducted port by port, working in parameter subspaces rather than the entire parameter space. In practice, it has been found to be beneficial to further separate the front-side length variables from the impedance variables. In other words, the vector $\underline{p}$ of Equation (4.4) would contain either length or impedance variables during the front-side optimization. However, that separation does not preclude the possiblity of finding an optimal set of lengths, restarting the search on the impedances from those lengths, and continuing successively on lengths and impedances until no additional improvements are possible. The results to be presented in Chapter V justify that separation when considering the different effects of length and impedance optimization. It will be seen that length adjustments generally achieve improvements to opt(n) by decreasing v_{ring}. With changes to the lengths, the time delays of the separate velocity components are selected to minimize v_{ring}. On the other hand, impedance adjustments tend to improve the overall match (compared to length optimization) and thereby increase either peak power or total energy. From that process, energy is removed more quickly, with the possibility of depressing v_{ring}. Another reason for not combining the parameter subspaces is more directly related to

the gradient search technique and, more specifically, to the gradient. It is possible that the length sensitivities could be considerably different from the impedance sensitivities. Under such circumstances, the convergence of the gradient search is very slow. The possibility of large differences (in magnitude) between the maximum and minimum components of the gradient vector are reduced by not mixing the two sets of parameters and by keeping the number of variable parameters small.

One approach to beginning the search is to demand that major improvements to the impulse response are to be from impedance adjustments, reserving the length variations for small effects. Goll [19] suggests a similar technique in the frequency domain where small changes in length are shown to improve pass band symmetry. Implementation is achieved by beginning the optimization on the impedances and then alternately adjusting length and impedances as needed. The optimum set of impedances for quarter-wave matching sections has been found to be unimodal (i.e., no locally optimal solutions have been encountered). The foregoing claim is made after testing a variety of starting points. Continuing the optimization on lengths from that set of impedances yields only minor improvements to the peaks ratio and results in only small deviations from quarter-wave. Since this optimal set of lengths is near the quarter-wave starting point, very few successive iterations on lengths and impedances are required to reach a final solution which is presumably the best that can be achieved for approximately quarter-wave sections.

In addition to checking solution uniqueness by utilizing different starting points, another test has been incorporated. For the particular case of light backing, the same solution is usually achieved whether the

optimization process is begun with lengths or impedances. The only disadvantage of beginning with lengths is that a poor initial guess for the impedances may cause the first set of optimal lengths to stray more from quarter-wave than required by the final solution. With suboptimal impedances, length adjustments become more crucial. Deviations from quarter-wave are observed to become significant as the dependence upon length adjustment is increased. The result is that more successive iterations to lengths and impedances are required to reach the globally optimal solution than by starting the optimization on impedances.

Having determined a satisfactory front-side matching scheme, the next step in the procedure is to change the back-side loading. The most direct way of selecting a suitable backing impedance is a graphical approach. By plotting the peak power against the peaks ratio (for different values of backing), one immediately sees the tradeoff between improvements to the peaks ratio at the expense of losing the desirable energy. Results in Chapter V demonstrate that there is a maximum level of backing beyond which an increase to the peaks ratio is achieved at a considerable decrease to the peak power. Figure 4.9 summarizes the optimization procedure for the lightly backed transducer.

4.3.3 Optimization with Heavy Back-Side Loading. Unlike the lightly backed situation, there is considerable interaction in the heavily loaded case between the back-side loading adjustment and the design of the front-side match. The interaction complicates the optimization procedure and, though the general approach outlined in Section 4.3.2 is applied here, the results are somewhat different.

A successful method for starting the optimization procedure is by fixing back-side damping equal to the ceramic's impedance. However,

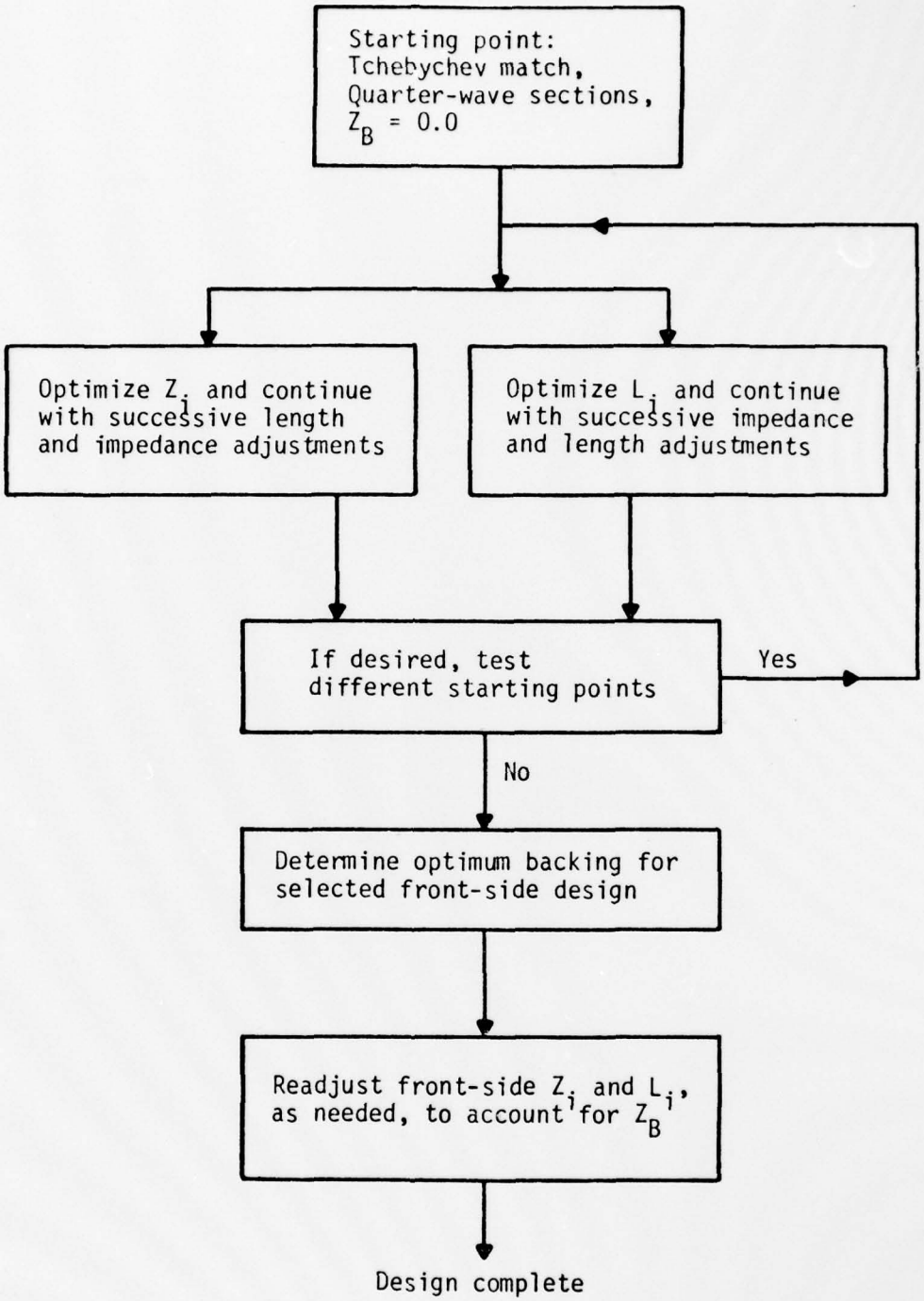

Figure 4.9. Flow chart of the optimization procedure for light backing

unlike the lightly damped case, two separate locally optimum solutions will typically be reached depending on whether the front-side optimization begins with length or impedance adjustments. If it is desired to maintain the front-side transformer sections approximately quarter-wave in length, impedances should first be optimized. Length adjustments then lead to only modest deviations from quarter-wave. However, a completely different set of lengths and impedances is sometimes found to be optimal by allowing more substantial departures from quarter-wave lengths. The consequences on the impulse response of one method compared to the other are examined in the next chapter. For the present discussion, the salient feature of these two procedures is that they aid in searching different sectors of the parameter subspaces for locally optimal solutions. Having determined an appropriate selection for the front-side match, the inital back-side impedance can now be modified. In general, once the front-side optimization is completed, only small changes to the backing impedance are required, and subsequent readjustments to the front-side match will be minor. This seems to be true whether length or impedance emphasis has been used for the front-side match. Several successive optimizations between the front-side match and backing can sometimes lead to more substantial changes to Z_B, but the process is slow and not conclusive.

The aforementioned approach substantially neglects most of the available subspace for optimizing the backing impedance. Consequently, the solution that is found might only be locally optimal. However, by beginning the search procedure with the backing impedance (and a nonoptimal front-side scheme), a greater emphasis is placed on the backing to achieve improvements to the impulse response. It is

consequently observed that Z_B undergoes larger changes when optimized in a configuration which does not possess an optimal front-side matching scheme. The utility of this approach for searching other subspaces for locally optimal solutions is examined in the next chapter. Although the presence of numerous locally optimal solutions is confusing, it allows a great deal of design flexibility. In Chapter V it is shown that a range of the backing impedance reduces the rigidity of the impedance specifications required for the front-side sections. The number of different solutions yielding very similar impulse responses will also be shown to be not as large as might be thought. There are significantly different characteristics between solutions emphasizing length over impedance optimization. Likewise, there are also certain drawbacks with using some ranges of backing impedances. Figure 4.10 flow charts the optimization procedure for the heavily backed case.

4.4 Additional Remarks and Limitations on the Gradient Search Procedure

To control and limit the step size during the search, Equation (4.5) is implemented by:

$$\underline{p}^{i+1} = \underline{p}^{i}[\underline{1} + q^{i}\underline{\nabla}^{i}\mathrm{opt}'(n)] \quad , \tag{4.6}$$

where $\underline{\nabla}^{i}\mathrm{opt}'(n)$ is normalized so that its maximum component is unity. By the representation of Equation (4.6), q^{i} represents the maximum fractional change of any parameter during the i^{th} iteration. The purpose of this section is to describe the calculation of the gradient and the determination of a suitable q^{i}.

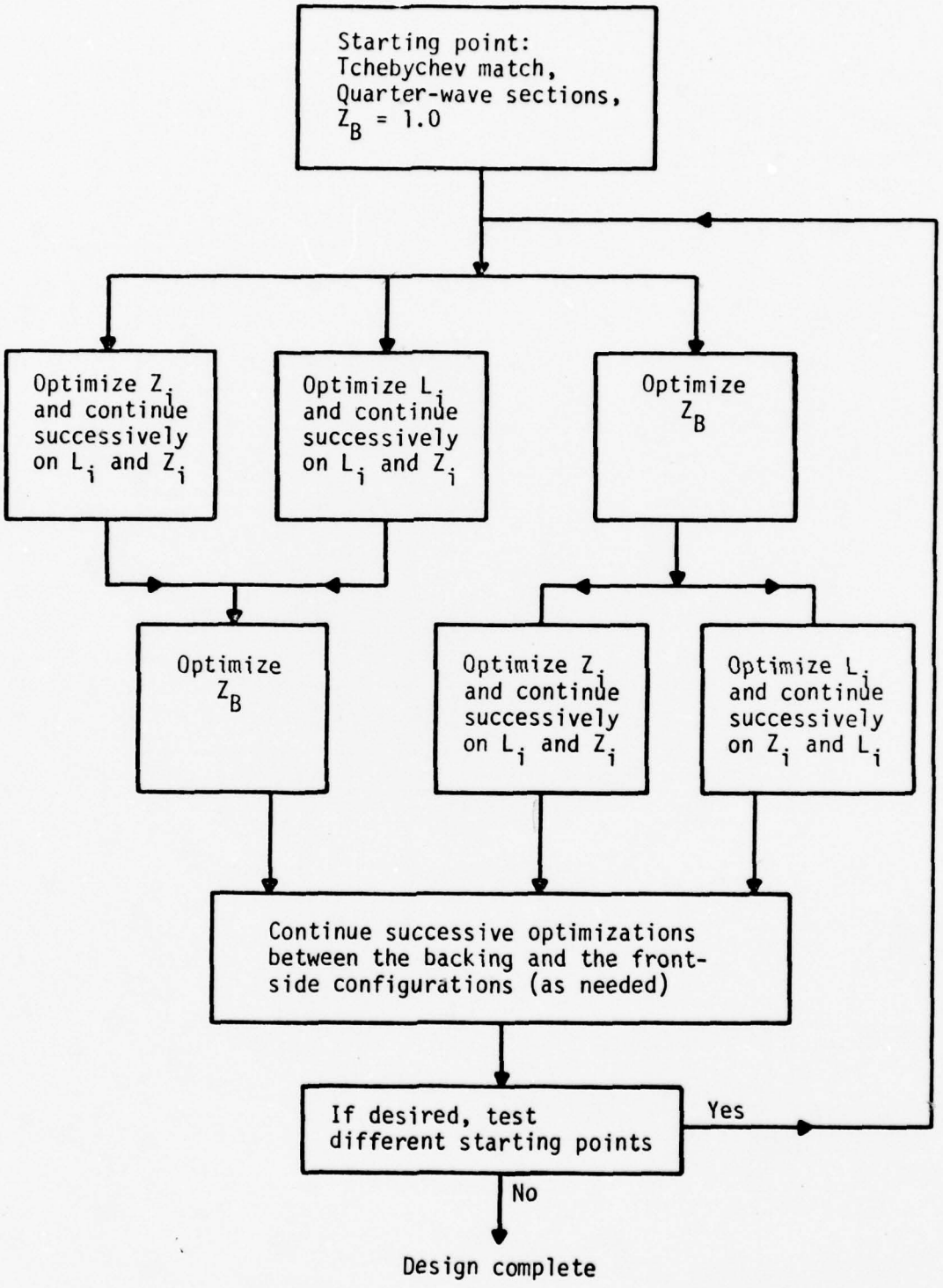

Figure 4.10. A flow chart of the optimization procedure for heavy backing

There are two typical methods for calculating the gradient: by parameter perturbation or by the method of adjoint network analysis. Perturbation is a direct means for determining the partial derivatives. They are calculated by:

$$\frac{\partial \text{opt}(n,p_j)}{\partial p_j} = \frac{\text{opt}(n,p_j+\Delta p_j)-\text{opt}(n,p_j)}{\Delta p_j} = \frac{\text{opt}[n,p_j(1+\alpha)]-\text{opt}(n,p_j)}{\Delta p_j} \quad (4.7)$$

where p_j is one of the parameters being varied, and α is the fractional amount of variation. The major disadvantage of perturbation is that for n variable parameters, a total of n+1 circuit analyses are required. With the the method of adjoints [7,12,24], only two network analyses are needed; however, more incidental "bookkeeping" is required. In the present application, where the sensitivity vector is limited to a maximum of three elements, there is only a modest computational advantage for using the method of adjoint analysis. This is especially true if the gradient does not need to be recalculated at each iteration. Parameter perturbation has been used to calculate sensitivities in this research. Selection of α is described in the next paragraph.

The scheme for selecting the search step size, q^i, is based upon successive gradient calculations. A necessary condition at an extremum is that:

$$\nabla^i \text{opt}(n) = \underline{0} \quad . \quad (4.8)$$

When all of the components of $\underline{\nabla}^i \text{opt}(n)$ change sign from one iteration to the next, indicating that the condition of Equation (4.8) has been met, the value of q^i is halved to improve the solution accuracy. Due to the

linear nature of the search process, the maximum relative error in locating a locally optimal solution is $q^i/2$ in the immediate vicintity of a solution. In the examples of Chapters V and VI, q^i is set to 0.02 and is reduced to 0.01 when all of the components of the gradient change sign from one iteration to the next. No attempt has been made to speed up the search by increasing q^i during regions of no sign changes to the components of the sensitivity vector. In all cases, α in the sensitivity calculation has been set equal to q^i. The parameter changes are therefore restricted to regions where there is a direct knowledge of the gradient.

For any reasonable front-side matching scheme up to three sections, there is a unique value of (heavy) backing impedance which globally maximizes opt(2). On the contrary, with heavy backing the likelihood of local optima for front-side designs is found to increase as the number of matching sections is increased. As has already been suggested, the impedance or length starting points must be supplemented with others to insure an adequate search of the subspaces. In performing that forced search of the front-side subspaces, it has been found that the section adjacent to the ceramic has the greatest overall effect. A successful approach in the search for other length solutions has been to start with that section length reduced to between 50% and 70% of its quarter-wave value. A reasonable search range for the corresponding impedance is defined by its value for W=0.6 to approximately one-half that value.

Although the search procedure in this work does recalculate the gradient vector by Equation (4.7), at each iteration, considerable efficiency can be gained by the adoption of a more liberalized approach. One possibilty is to perform a recalculation once a maximum is reached.

A somewhat more conservative system is to recalculate the gradient after a prescribed number of iterations. The point to be made is that the search function seems to be sufficiently well-behaved to not warrant a recalculation at each iteration. In light of the above comments, the method of Fletcher and Powell [7], which utilizes previous gradients for modifying the search direction, would probably be of only marginal use within a length or impedance optimization set. That modification would not be meaningful when switching from optimizing one parameter subset to another.

CHAPTER V

RESULTS OF OPTIMIZATION

5.1 Introduction

Upon implementing the optimization procedures of Chapter IV, a variety of satisfactory transducer designs are found. These designs offer improvements to the impulse response compared to the techniques outlined in Chapter II. Some solutions maximize the peaks ratio, whereas other configurations yield locally optimal results. In addition, there are suboptimal designs offering good performance. When material availability and space limitations impose constraints on the parameter ranges, the requirement for such suboptimal solutions becomes germane. The purpose of this chapter is to present the various solutions in a way which contrasts the advantages and tradeoffs that are possible.

The theoretical improvements achieved by optimization are most meaningful by examining the lossless, nonsilvered model of the lead metaniobate disc combined with lossless front-side matching sections. With those restrictions, improvements to the transient response are directly attributable to energy transfer to the acoustical loads. The backing and water loading are included resistively. A maximum of three front-side sections, with impedances Z_i and lengths L_i, are considered in these results. The sections are numbered consecutively starting with the one closest to the water load. The utility of more than three sections is doubtful from both the theoretical [40] and availability point of view. The results in this chapter also support those theoretical conclusions.

Rather than attempting to meet a set of design specifications, the optimization procedure is devised to find a locally or globally optimal solution for a specified number of front-side sections. Consequently, the question of selecting the number of front-side sections is not directly addressed. A separate comparison is therefore presented which allows the effectiveness of increased matching sections to be evaluated.

The two broad categories of lightly and heavily backed transducers are treated distinctly. Within each category, results are presented for one, two, and three front-side sections. Since light backing has only a small influence on the design of the front-side matching system, the optimization of the backing is presented independently of the front-side adjustments. However, the particular value of heavy backing does influence the front-side match, rendering that separation approach inoperative. The results demonstrate the interaction between the backing impedance and front-side designs for one-, two-, and three-stage transformers.

To facilitate the comparison with the unmatched case, the impulse responses in this chapter are all normalized with respect to the peak face velocity of the air-backed disc loaded directly by water (system A). Under that normalization, system A has v_{peak} equal to one. Similarly, the total energy, E_t, delivered up to 2 microseconds is normalized with respect to the energy of system A. When it is useful for illustration of certain points, the complete impulse response is presented graphically. For demonstrating small changes in the response, it is often more appropriate to tabulate the important characteristics of the response. The tabular and graphic techniques are combined to present a thorough explanation of the potential advantages of time

domain design. Impedances and lengths are reported normalized to the ceramic impedance and to the section's quarter-wave length at resonance, respectively. In certain cases, plots of frequency domain responses are also included.

5.2 Lightly Backed Transducer Systems

5.2.1 Preview of the Results. To emphasize the possible impulse response improvements by front-side matching, the optimizations are first performed for air-backed transducers. Upon selection of a front-side match, light backing is increased to an optimal value. A subsequent readjustment of front-side sections demonstrates that only small changes are required to maintain optimum transducer performance.

With at least one matching section, peak power is found to be almost independent of the design of the front-side transformer. This insensitivity extends to reasonable variations in length, impedances, and number of front transformer sections. Any improvement to the peaks ratio must be made by decreasing v_{ring}. The results show that v_{ring} can be reduced by increasing the number of matching sections, with the most substantial decrease occurring by changing from a single-layer match to a two-layer match. With the number of matching sections fixed, length adjustments can usually effect a considerable improvement to the peaks ratio when materials having optimal impedances are not available. If the best set of matching impedances are selected, length adjustments can provide only a small improvement to the peaks ratio and are close to the quarter-wave solution.

5.2.2 Air Backing with a Single Front-Side Section. For a single matching section, a possible starting point in the optimization

procedure is from system B: a quarter-wave plate having an impedance equal to the geometric mean of the water and ceramic impedances. The impulse response for such a system has been shown in Figure 4.9. The details of the matching scheme and impulse response characteristics are listed in Table 5.1. Subsequent references to this entry are made as case "5.1:1". That notation is used throughout the chapter. The results of maximizing opt(3) by either length (case 5.1:2) or impedance (case 5.1:3) adjustments are shown in Figures 5.1a and 5.1b. As a contrast, Figure 5.1c shows the results of maximizing the total energy delivered to the water during the first two microseconds (case 5.1:4) with the section length fixed at quarter-wave.

Although Figure 5.1 demonstrates that there is a considerable difference in the impulse response after $t_s(3)$ between the length and impedance optimized cases, their pre-$t_s(3)$ responses and peaks ratios are approximately the same. On the contrary, energy maximization, case 5.1:4, causes some loss in peak power and a considerable reduction of the peaks ratio. It is interesting to note that the procedure of Desilets et al. [11] would recommend an impedance of 0.16 for maximizing transducer efficiency. That calculation is accomplished directly from Equation (2.5) and confirms the findings of case 5.1:4, which suggests an impedance of 0.17.

Figure 5.2 presents the frequency responses of cases 5.1:2, 5.1:3, and 5.1:4. It demonstrates that there is no obvious correlation between the compromises of bandwidth, phase linearity, the allowed ripple in each, and the resulting impulse response. Case 5.1:4, which offers an approximately gaussian response and a very linear phase in the pass band, has the worst peaks ratio with respect to $t_s(3)$. Yet after its

TABLE 5.1
AIR-BACKED SYSTEMS WITH ONE FRONT-SIDE SECTION

Case	Description	Z_1	L_1	V_p	V_r	PR	E%	E_t
5.1:1	Quarter-wave; geometric mean	.254	1.00	1.47	.500	9.3	.86	1.85
5.1:2	Impedance fixed; length optimized	.254	.769	1.34	.343	11.8	.83	1.56
5.1:3	Optimized impedance; length fixed	.327	1.00	1.43	.349	12.3	.88	1.72
5.1:4	Impedance to maximize energy	.170	1.00	1.37	.616	7.0	.79	1.93

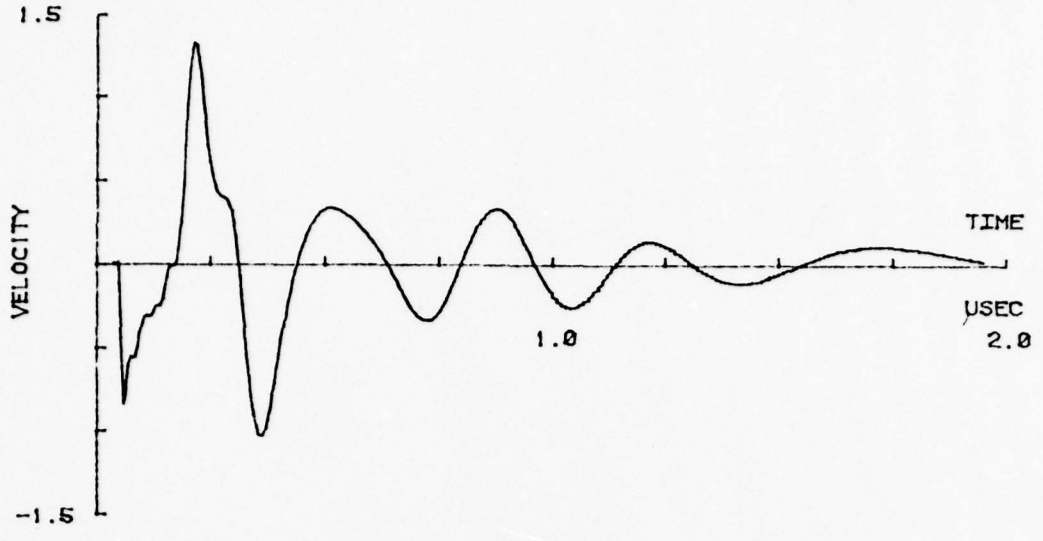

(a)

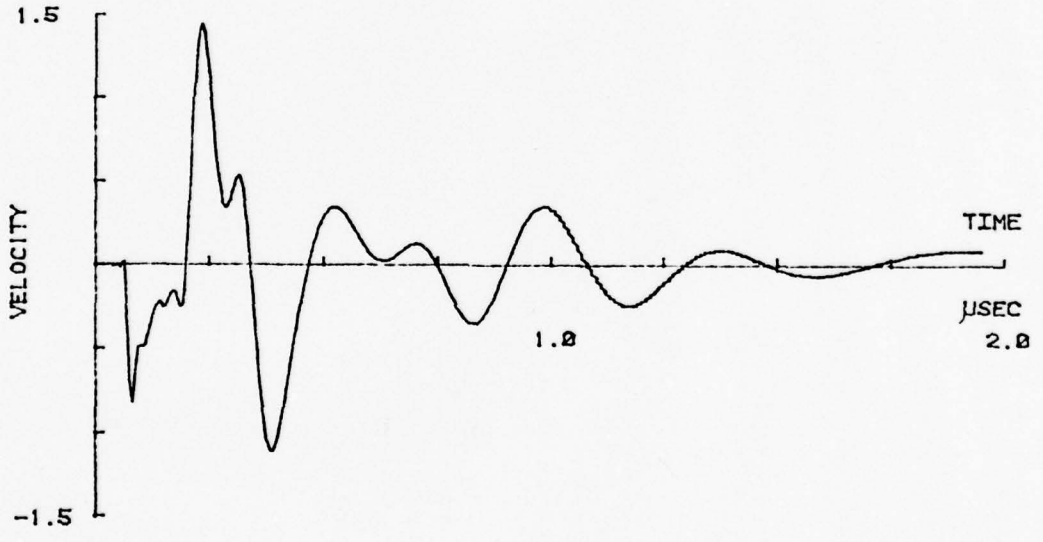

(b)

Figure 5.1. Impulse response with a single matching section
a. Length optimized to maximize opt(3)
b. Impedance optimized to maximize opt(3)

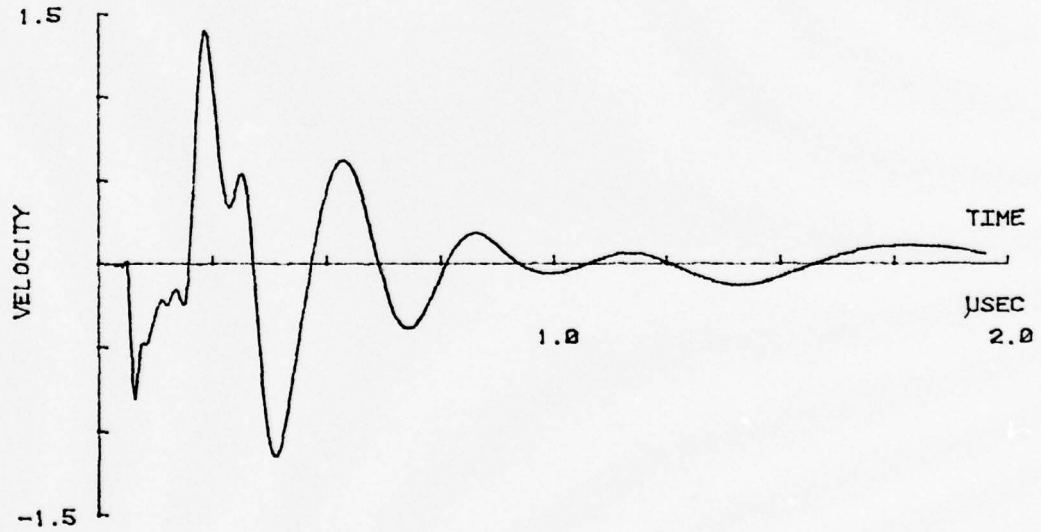

Figure 5.1. continued
c. Impedance optimized to maximize energy delivered to the load

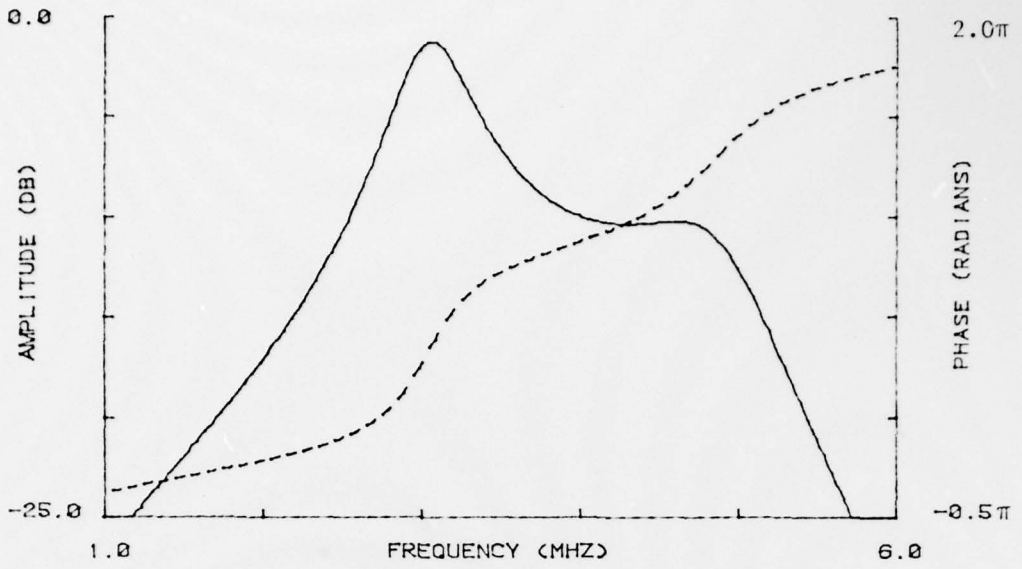

(a)

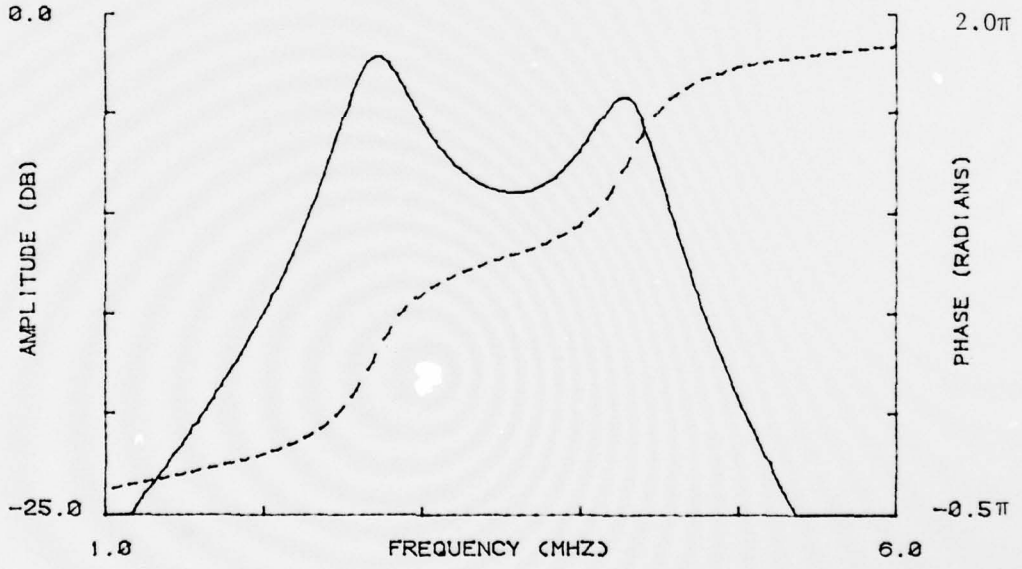

(b)

Figure 5.2. Frequency response with a single matching section
a. Length optimized to maximize opt(3)
b. Impedance optimized to maximize opt(3)

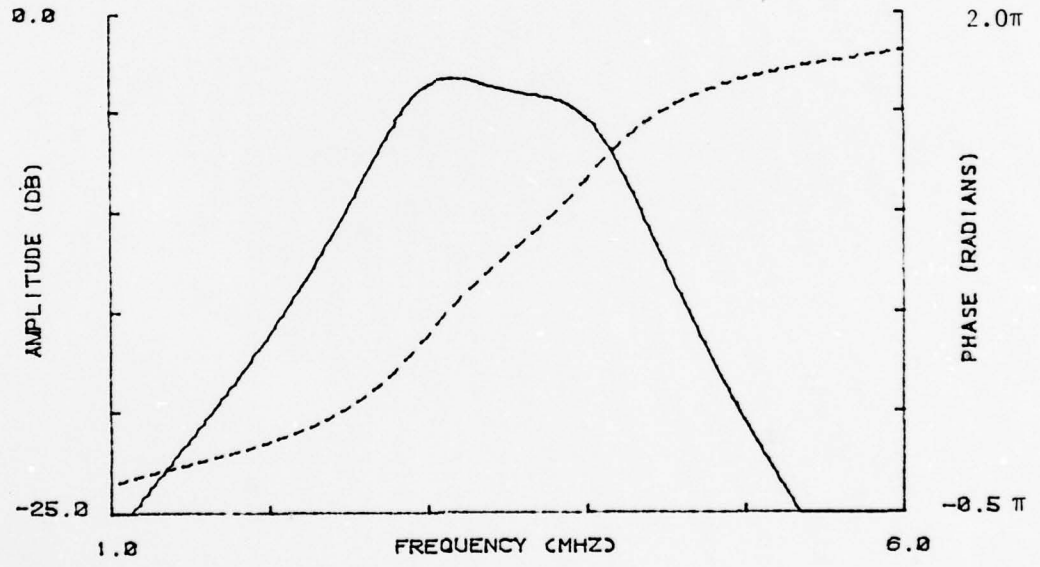

Figure 5.2: continued
c. Impedance optimized to maximize energy delivered to the load

fourth velocity pulse, its response decays more rapidly than the two optimized designs. By tolerating more ripple in the amplitude response, case 5.1:2 can be considered more broad-band than case 5.1:4. Likewise, case 5.1:3 has a larger region of linear phase.

The case of the simple one-layer matching system is also useful for demonstrating another utility of the optimization procedure. The results in Table 5.1 suggest that there is a considerable range of impedance and length combinations that might yield similar peaks ratios. A few checks within the implied limits of cases 5.1:2 and 5.1:3 have confirmed that property. The impedance optimized case of 5.1:3 is, in fact, the global maximum for the single-section system. That property has been verified by utilizing several other starting points. It also happens that the length optimized case, 5.1:2, is a local optimum; for small step sizes, the solution of 5.1:3 cannot be found from 5.1:2. Another point to be made is that the global maximum occurs by emphasizing impedance adjustments which is similar to lightly backed systems with two- and three-section transformers.

5.2.3 Air Backing with Two Front-Side Sections. All of the cases to be described in this subsection are summarized in Table 5.2. The first three entries, cases 5.2:1 to 5.2:3, represent the maximally flat case and the Tchebychev W=0.6 and W=1.0 cases, respectively. For notational purposes, the maximally flat case is represented as W=MF. With respect to the peaks ratio, the performance of all three systems is very similar. Figures 5.3 and 5.4 show the frequency and time domain responses for the W=MF and W=1.0 systems. Comparing the differences between the frequency amplitude responses, the tradeoffs between bandwidth and flatness are as would be expected. However, the phase

TABLE 5.2
AIR-BACKED SYSTEMS WITH TWO FRONT-SIDE SECTIONS

Case	Description	Z_1	Z_2	L_1	L_2	V_p	V_r	PR	E%	E_t
5.2:1	W=MF; lengths quarter-wave	.128	.503	1.00	1.00	1.49	.285	14.4	.88	1.87
5.2:2	W=0.6; lengths quarter-wave	.142	.453	1.00	1.00	1.52	.250	15.7	.92	1.89
5.2:3	W=1.0; lengths quarter-wave	.171	.377	1.00	1.00	1.49	.260	15.2	.90	1.81
5.2:4	Optimized impedances; quarter-wave	.154	.495	1.00	1.00	1.52	.209	17.2	.91	1.87
5.2:5	Optimized impedances and lengths	.154	.495	1.00	0.98	1.51	.204	17.4	.91	1.87
5.2:6	W=1.0; lengths optimized	.171	.377	1.28	0.89	1.34	.188	17.1	.91	1.60
5.2:7	Impedances to maximize energy	.089	.241	1.00	1.00	1.42	.562	8.1	.87	1.90

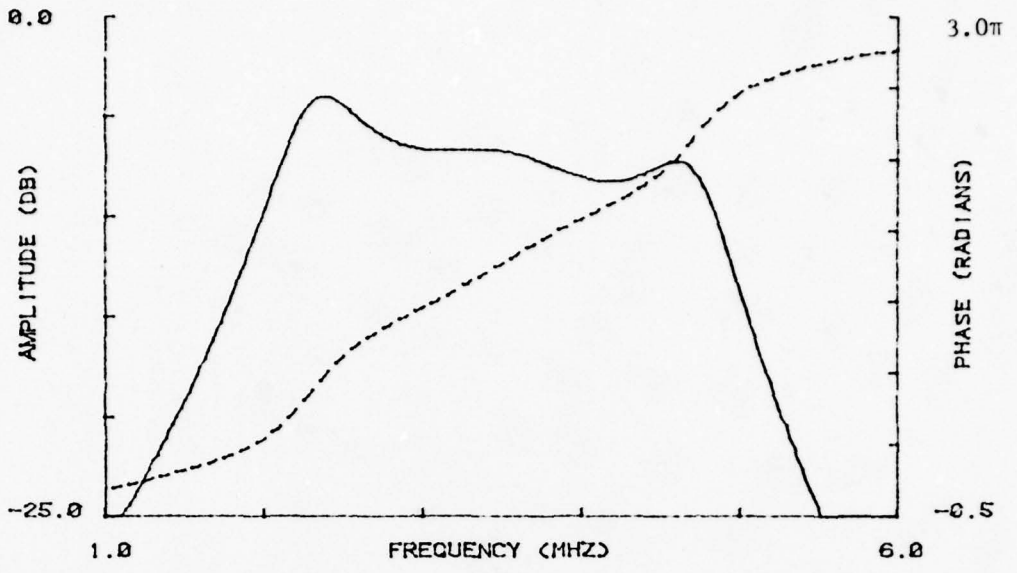

(a)

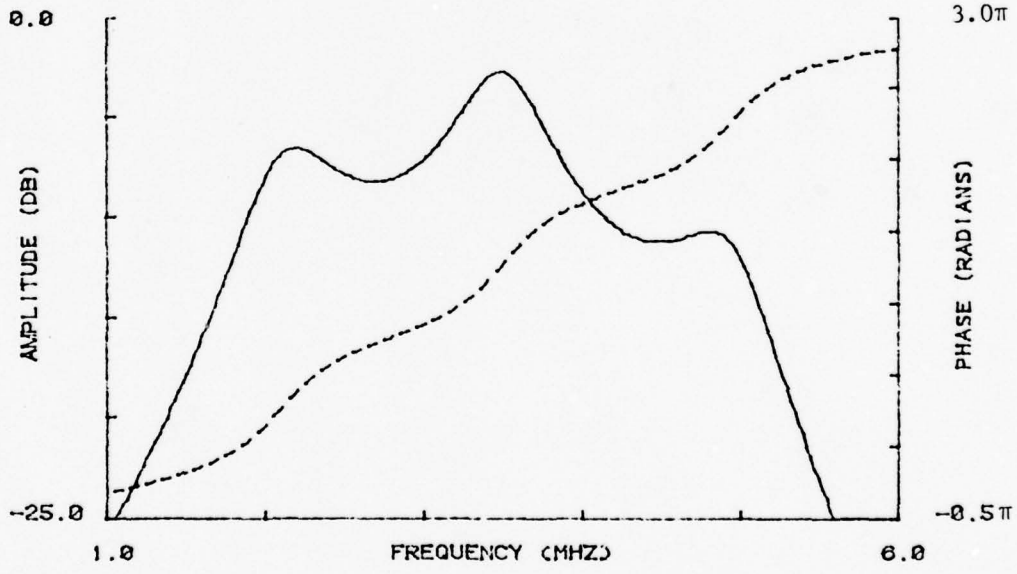

(b)

Figure 5.3. Frequency response of a two-section system
a. Maximally flat bandwidth
b. Bandwidth, W, equal to 1.0

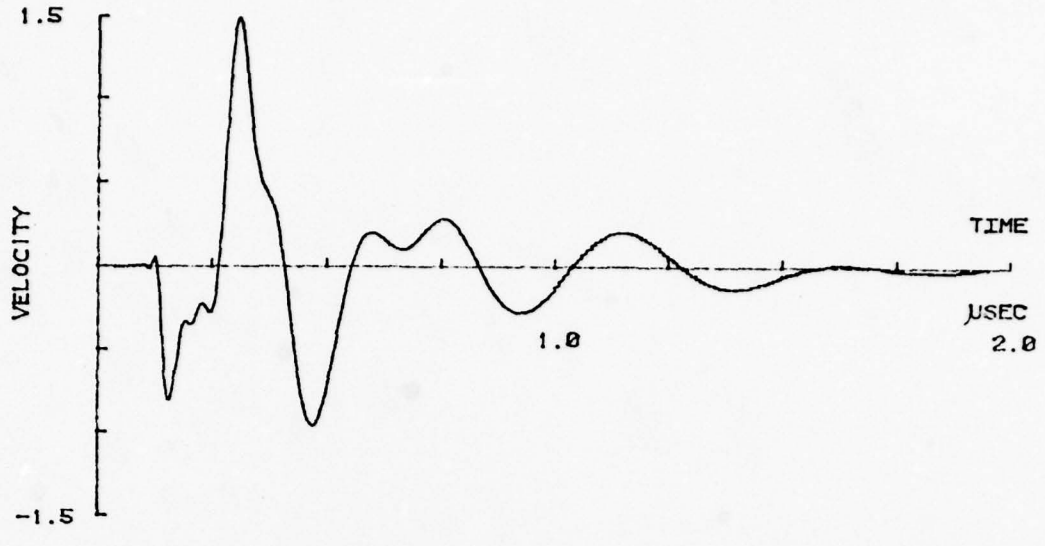

(a)

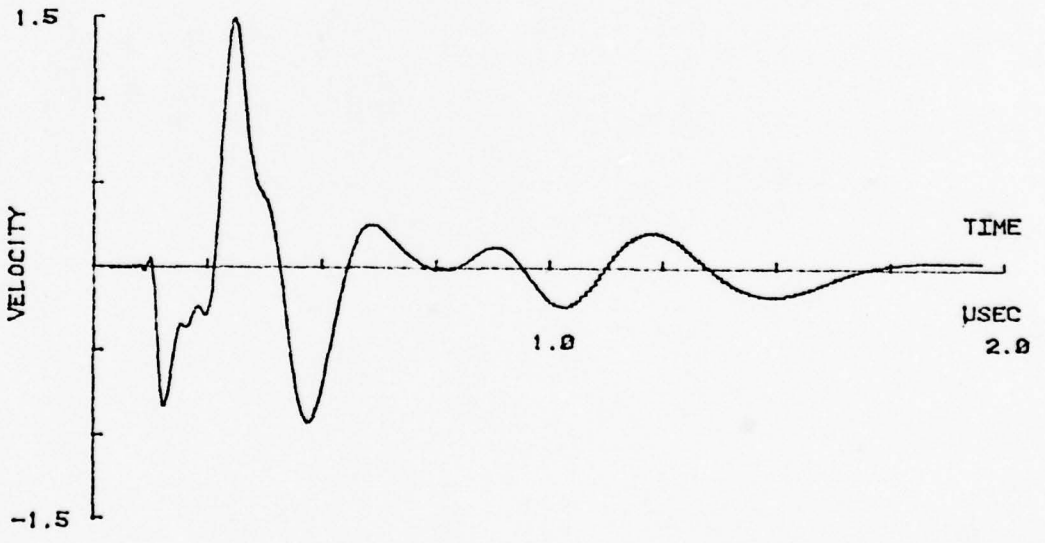

(b)

Figure 5.4. Impulse response of a two-section system
a. Maximally flat bandwidth
b. Bandwidth, W, equal to 1.0

responses do not differ drastically which supports the possibility of similar peaks ratio data in the time domain.

System 5.2:4 is devised by employing the opt(3) criterion on the impedances with any of the above cases as the starting point. Other starting points have also confirmed that the results of case 5.2:4 are indeed optimum for quarter-wave lengths. A slight improvement over case 5.2:4 can be accomplished by subjecting the section lengths to the optimization process. The results of performing successive length and impedance adjustments from case 5.2:4 are listed as case 5.2:5 and are displayed in Figure 5.5. No other locally maximum solutions have been found over the impedance and length subspace even when searching far from the solution of case 5.2:5. Furthermore, starting the complete optimization process on lengths rather than impedances ultimately leads to the solution of case 5.2:5. However, the convergence is somewhat slower. It is therefore surmised that case 5.2:5 is indeed a globally optimal solution.

Comparing cases 5.2:4 and 5.2:5, it is observed that only a very slight improvement is gained by length adjustments from a situation with optimal impedances. With impedances somewhat removed from the optimal set, the impact of length adjustments becomes more significant. As an example of length optimization, case 5.2:6 shows the possible improvement by using the opt(3) criterion to adjust the lengths from the W=1.0 system (case 5.2:3).

The final situation considered in this subsection is case 5.2:7 whose frequency and time domain responses are shown in Figure 5.6. With lengths fixed at quarter-wave, the impedances are adjusted to maximize the total energy during the first two microseconds. A qualitative

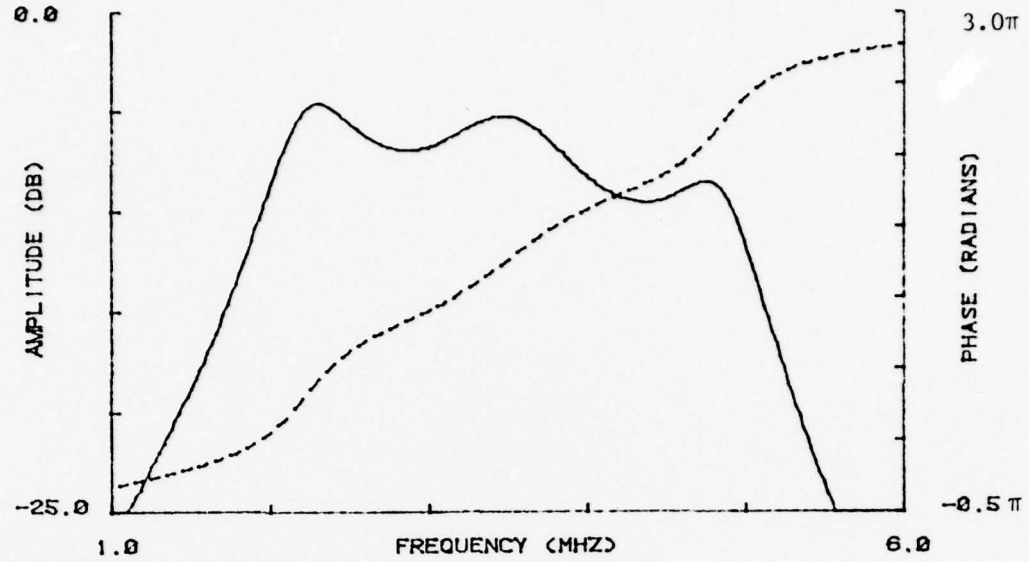

(a)

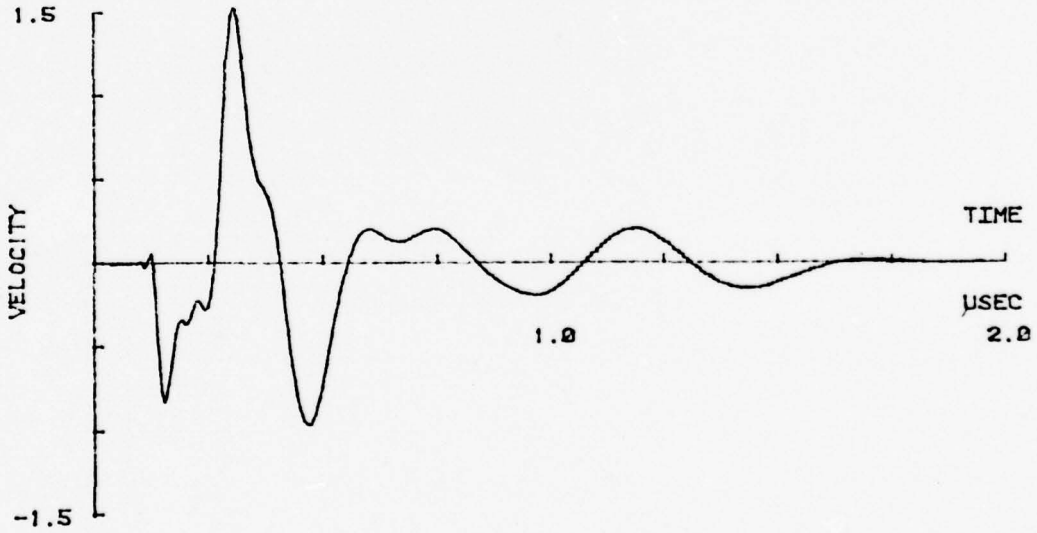

(b)

Figure 5.5. Response of as a result of optimizing both the impedances and lengths of a two-section transformer
a. Frequency domain
b. Time domain

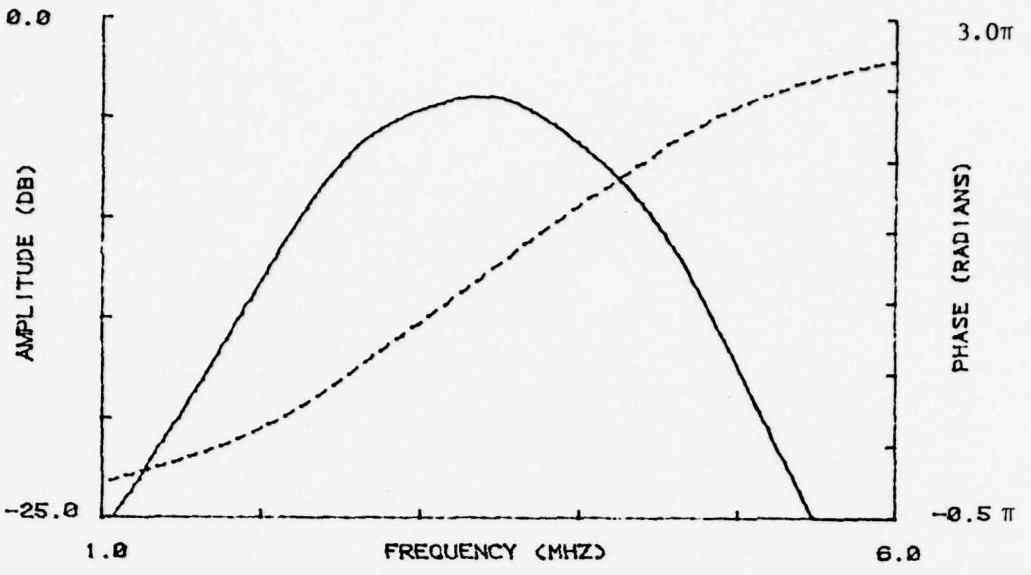

(a)

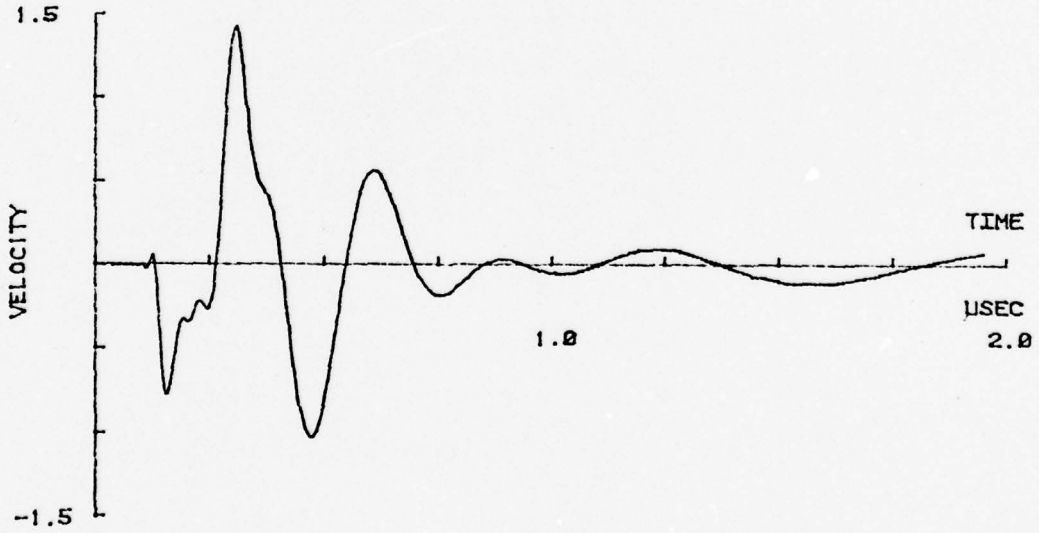

(b)

Figure 5.6. Response of a two-section system with the impedance adjusted to maximize the total energy
a. Frequency domain
b. Time domain

comparison with Figure 5.5 shows that the energy is maximized at the expense of significantly increasing the amplitude of the fourth peak. In effect, energy that had lingered in the system is now mostly removed during that fourth velocity pulse. The narrower bandwidth and smaller region of phase linearity also suggest that case 5.2:7 should result in more pulse distortion than case 5.2:5. Calculations from Equation (2.5) show that the impedances recommended by Desilets et al. for maximizing transducer efficiency are:

$$Z_1 = 0.100$$

and

$$Z_2 = 0.220$$

which approximate the impedances (Z_1=0.089, Z_2=.241) of case 5.2:7.

5.2.4 Air Backing with Three Front-Side Sections. Table 5.3 lists the transducer systems described in this section. Entries 5.3:1 to 5.3:3 have sections with quarter-wave lengths and impedances providing W=MF, W=0.6, and W=1.0 responses. The maximum peaks ratio and maximum v_{peak} are achieved for W=1.0. Applying the optimization criterion of opt(3) to the lengths of those systems yields the results summarized as cases 5.3:4 to 5.3:6. A wide variety of different nonquarter-wave starting points have confirmed that these length optimized solutions do represent global maxima for each respective impedance set. For these length optimized cases, impedances with W=1.0 still provides the greatest peaks ratio. The results show that most of the improvement to the peaks ratio is achieved by reducing v_{ring} for each system with only minor attenuation to v_{peak}.

TABLE 5.3
AIR-BACKED SYSTEMS WITH THREE FRONT-SIDE SECTIONS

Case	Description	Z_1	Z_2	Z_3	L_1	L_2	L_3	V_p	V_r	PR	E%	E_t
5.3:1	W=MF; lengths quarter-wave	.092	.254	.700	1.00	1.00	1.00	1.44	.277	14.3	.90	1.84
5.3:2	W=0.6; lengths quarter-wave	.099	.254	.654	1.00	1.00	1.00	1.46	.244	15.5	.92	1.86
5.3:3	W=1.0; lengths quarter-wave	.118	.254	.550	1.00	1.00	1.00	1.49	.147	20.1	.95	1.84
5.3:4	W=MF; lengths optimized	.092	.254	.700	1.28	1.05	.870	1.35	.208	16.2	.93	1.73
5.3:5	W=0.6; lengths optimized	.099	.254	.654	1.30	1.09	.900	1.38	.162	18.5	.95	1.74
5.3:6	W=1.0; lengths optimized	.118	.254	.550	1.14	.957	.844	1.47	.119	21.8	.96	1.79
5.3.7	Impedances optimized and lengths quarter-wave	.111	.188	.462	1.00	1.00	1.00	1.46	1.37	20.5	.96	1.81

Similarly, fixing the lengths to quarter-wave and applying the opt(3) criterion to the front-side impedances also achieves an increase in the peaks ratio by causing a reduction to v_{ring}. The result is listed as case 5.3:7 and its impulse response is shown in Figure 5.7. Incorporating length optimization to the result of case 5.3:7 only offers a slight improvement. The data of cases 5.3:6 and 5.3:7 suggest the possibility of a modest range of length and impedance combinations providing a good peaks ratio. The gradient search technique applied to the opt(3) criterion is not sufficiently sensitive to find the true global maximum over the length and impedance spaces for the three-section case. However, it is presumed to be near the ranges indicated from systems 5.3:6 and 5.3:7. The impulse response of case 5.3:7 shows that the post-t_s(3) ring-down peaks have been fairly well equalized. This characteristic has been noticed for the optimal one- and two-section transformer systems. Coupling this observation with the fact that situation 5.3:6 offers a slight peaks ratio improvement over case 5.3:7 at the expense of a modest decrease in v_{peak}, supports the hypothesis that these two cases should approximately define the limits of a globally maximum peaks ratio.

5.2.5 The Use of Light, but Non-Zero Backing. The purpose of adding light backing to a transducer is to improve the transient response without significantly degrading the device efficiency. Several possibilities have been considered to quantify the efficiency versus ring-down tradeoffs. One logical approach is to directly involve the important quantities of interest: peak power and peaks ratio. The relationship between these quantities is most readily understood by plotting peak power as a function of the peaks ratio for various backing

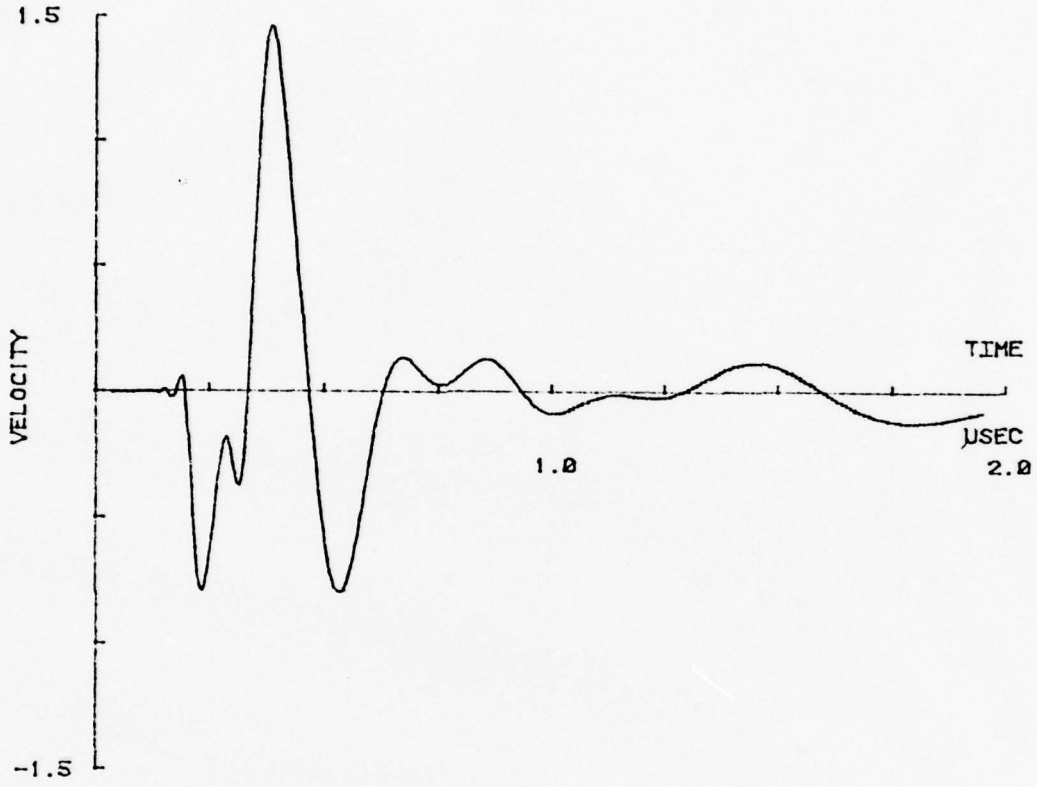

Figure 5.7. Impulse response with three quarter-wave sections with optimized impedances

impedances and fixed front-side matching. The results in this subsection utilize that particular relationship for selecting an optimal backing impedance. However, substitutions can be made if other quantities are deemed more important. For example, it might be desired to emphasize early energy rather than peak power. For that particular substitution, it has been observed that there is no significant change from the results about to be described.

Since the present measure of efficiency is linked to peak power, a performance limit on allowable loss must be established. It will be demonstrated that a natural break often occurs for approximately 1-dB loss of peak power as compared to a 5- or 6-dB loss with heavy backing. However, the effectiveness of light backing is dependent upon the design of the front-side match, and for some configurations, the break is less apparent.

The potential benefit offered by light backing seems to be related to the value of the peaks ratio of the air-backed systems. The three-section systems and optimized two-section systems do not show the amount of improvement that can be achieved with other front-side designs. As an example, Figure 5.8 presents plots of the peak power as a function of the peaks ratio with backing impedance as an implied parameter. Curve a is of case 5.1:3, a single-section optimized design, and curve b is of case 5.2:2, front-side impedances set to W=0.6 and lengths quarter-wave. The importance and meaning of the break point are best illustrated from Figure 5.8b. It shows that by sacrificing 1 dB of peak power, the peaks ratio can be improved by 3 dB. However, to achieve another 3 dB improvement in the peaks ratio, an additional 3 dB of peak power must be sacrificed. The break point is observed to be

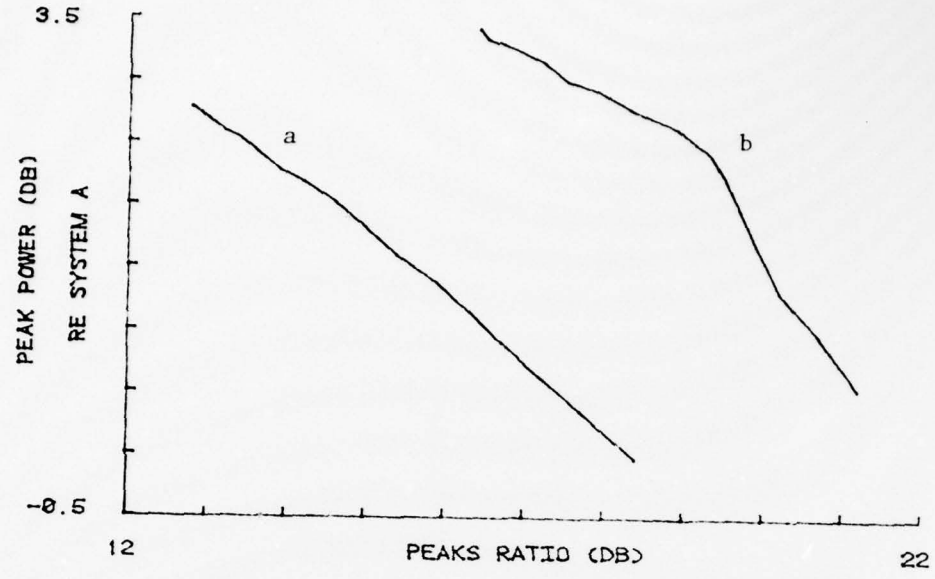

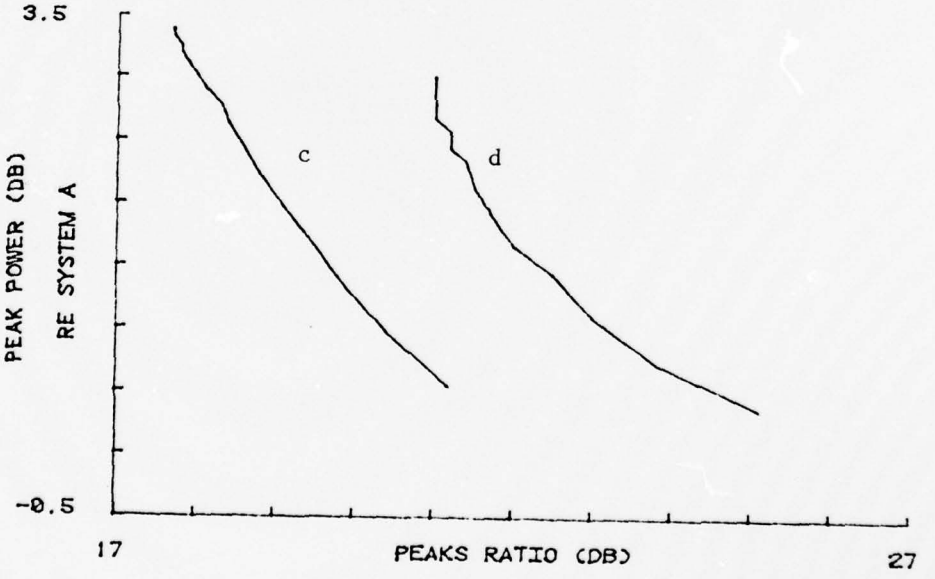

Figure 5.8. Peak power and peaks ratio as a funtion of Z_B with the following front-side designs
a. One-section impedance optimized (case 5.1:3)
b. Two-section W=0.6 (case 5.2:2)
c. Two-section impedance optimized (case 5.2:4)
d. Three-section impedance optimized (case 5.3:7)

better defined for the two section case rather than the single section case. This is attributed to the fact that the additional internal reflections caused by a second layer produces a greater variety of face velocity components that are a function of backing impedance.

Figures 5.8c and 5.8d show similar type curves for a two-section transformer (case 5.2:4) and a three-section transformer (case 5.3:7). Each has its front-side impedances optimized with lengths set at quarter-wave. The curves have no definitive break point that would optimize the efficiency and performance compromises. A 1-dB improvement in the peaks ratio is achieved with a 1-dB loss to the peak power. The results in Figure 5.8 quantify the back-side loading and efficiency compromises suggested by Desilets et al.

There remains the question about the quality of the front-side matching scheme having added the back-side loading. Selecting a backing impedance of 0.17, the results of reoptimizing the front-side impedances under the criterion of opt(3) are listed in Table 5.4. Upon comparing the results in Table 5.4 with the original air-backed cases, it is observed that only minor impedance changes are required to maintain an optimum configuration with respect to the peaks ratio. Front-side lengths are also found to require only slight readjustment as a result of light backing.

5.3 Heavily Backed Transducer Systems

5.3.1 Preview of the Results. As with the lightly backed systems, these results are separated according to the number of front-side matching sections. This approach allows a detailed study and comparison of different systems that can be devised with a fixed number of

TABLE 5.4
AIR-BACKED SYSTEMS RE-OPTIMIZED TO
ACCOUNT FOR LIGHT BACKING

Case	Description[1]	Z_1	Z_2	Z_3	V_p	V_r	PR	E%	E_t
5.1:3	Optimized front impedance for ZYB=0.0	.327	-	-	1.43	.349	12.3	.88	1.72
	Case 5.1:3 with Z_B=0.17	.327	-	-	1.24	.227	14.7	.91	1.18
	Re-optimized front impedance for Z_B=0.17	.340	-	-	1.23	.212	15.3	.90	1.16
5.2:4	Optimized front impedances for Z_B=0.0	.154	.495	-	1.52	.209	17.2	.91	1.87
	Case 5.2:4 with Z_B=0.17	.154	.495	-	1.32	.156	18.6	.94	1.30
	Re-optimized front impedances for Z_B=0.17	.160	.456	-	1.33	.125	20.5	.95	1.30
5.3:7	Optimized front impedances for Z_B=0.0	.111	.188	.462	1.46	.137	20.5	.96	1.89
	Case 5.3:7 with Z_B=0.17	.111	.188	.462	1.28	.107	21.5	.97	1.36
	Re-optimized front impedances for Z_B=0.17	The system with backing requires no changes from Z_B=0.0.							

[1]All of the above systems have matching sections with quarter-wave lengths.

sections. It serves to emphasize the flexibility and tradeoffs available through front-side and back-side adjustments. Unless stated otherwise, all of the optimizations in this section are carried out under the criteria of opt(2). After thoroughly examining systems with up to three front-side sections, a summary discussion details the considerations for selecting the number of sections to be used.

Since the backing now interacts with the selection of the front-side matching scheme, it must be treated actively during the optimization procedure. Its active role adds a new complication to the optimization process, but it provides considerable flexibility in selecting different front-side matching schemes which yield approximately similar impulse responses. To alleviate some of the potential confusion, the results are further subdivided according to the amount of backing required to achieve an optimization. Fortunately, only a few values of backing impedance are required to demonstrate the utility and flexibility of the optimization scheme. The lower limit of optimal backing is approximately equal to the impedance of the ceramic. Depending upon the details of the front-side match, a larger impedance may also be acceptable. An additional complication caused by the backing is that there are some situations where more than one locally optimal solution can be found for a fixed backing and a fixed set of front-side impedances or lengths. These cases are specifically noted and examined.

5.3.2 With a Single Front-Side Section. The results in this subsection demonstrate the considerable flexibility available when designing heavily backed transducers. As initiating values, it is reasonable to begin with backing equal in impedance to that of the

ceramic (i.e., Z_B=1) and a quarter-wave, geometric mean front-side section. For such a system, the results are listed as case 5.5:1 in Table 5.5 with the response shown in Figure 5.9. Applying the opt(2) criterion to Z_B leads to the solution of case 5.5:2. The 4.9-dB reduction in v_{ring} is accomplished at no loss to v_{peak}. Although length adjustments to the front section of 5.5:2 are not too helpful, some improvement in the peaks ratio can be gained by successive adjustments of the backing and front-side impedances. The general trend is to reduce both. For example, case 5.5:3 provides a locally optimal solution over the impedance space with the front-section length fixed.

The above results suggest the possibility of using less back-side loading in an attempt to reduce the loss that occurs to v_{peak}. To examine that approach, the front-side rather than the backing impedance of case 5.5:1 is first subjected to optimization with the results entered as case 5.5:4. Its complete impulse response is shown in Figure 5.10a. Unfortunately, the poorer front-side match dispels any chance of increasing v_{peak} even with the substantially reduced backing impedance. Figure 5.10b and case 5.5:5 display the results of accomplishing the optimization from case 5.5:1 by deviations from the quarter-wave front-section length. Although the length adjustment is helpful, it is not as powerful as the changes to the front-side impedance. Utilizing successive optimizations on length, impedance, and backing from case 5.5:5, the solution of case 5.5:6 is found. The system described by case 5.5:6 seems to globally maximize the peaks ratio. By presetting the backing impedance at other values, no optimization of the front-side match could improve the peaks ratio beyond its value for case 5.5:6.

The figures and results in this subsection do demonstrate that

TABLE 5.5
HEAVILY BACKED SYSTEMS WITH A SINGLE FRONT-SIDE MATCHING SECTION

Case	Description	Z_B	Z_1	L_1	V_p	V_r	PR	E_t
5.5:1	Geometric mean; quarter-wave	1.00	.254	1.00	.827	.217	11.6	.433
5.5:2	Case 5.5:1 with optimized backing	1.37	.254	1.00	.827	.070	21.5	.362
5.5:3	Optimized impedance for backing	1.26	.150	1.00	.669	.046	23.2	.292
5.5:4	Optimized impedance; length fixed	1.00	.091	1.00	.702	.039	25.0	.243
5.5:5	Geometric mean; optimized length	1.00	.254	.609	.878	.067	22.2	.292
5.5:6	Optimum impedance and length	1.00	.091	.854	.699	.034	26.4	.230

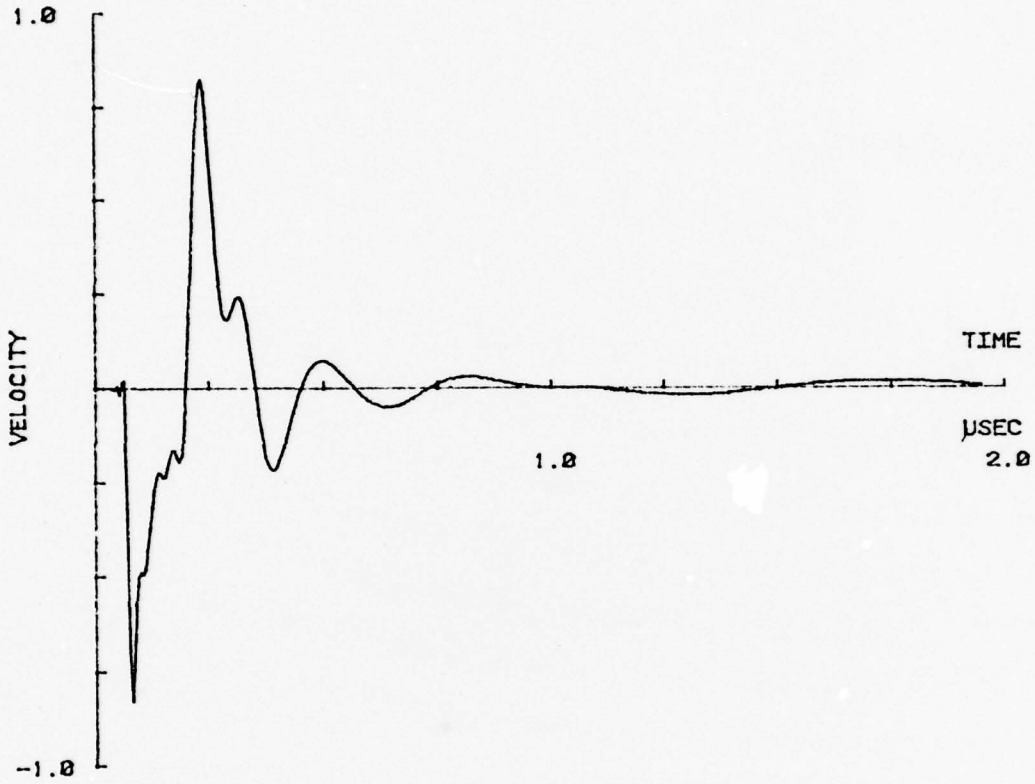

Figure 5.9. Impulse response using a single, quarter-wave matching section with no optimization and $Z_B = 1.0$

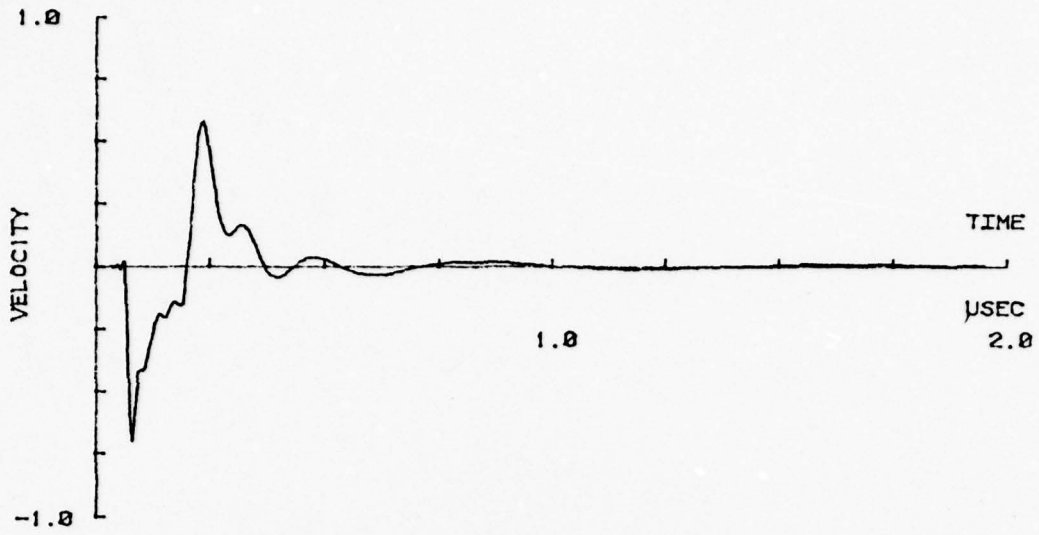

(a)

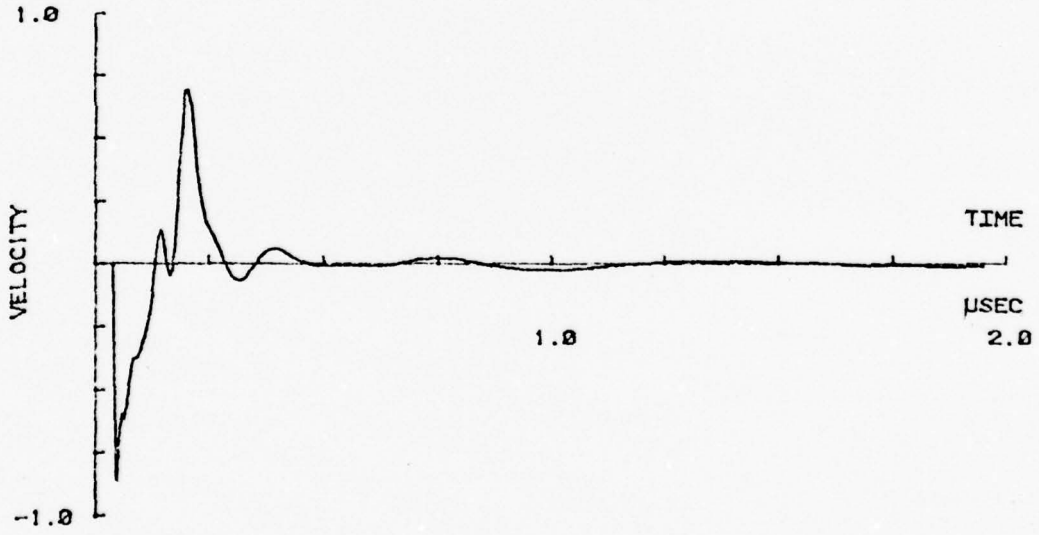

(b)

Figure 5.10. Impulse responses with either impedance or length optimization (Z_B=1.0)
a. Impedance optimized (case 5.5:4)
b. Length optimized (case 5.5:5)

systems with vastly different parameters can be designed to provide very similar impulse responses. There are, of course, some variations which should be considered depending upon the particular application. In addition to the characteristics listed in Table 5.5, the width of the second pulse and the total energy may also be important.

5.3.3 With Two Front-Side Sections. To appreciate the flexibility and improvements possible with time domain optimization, Tchebychev front matching and matched backing are selected as a starting point. Systems 5.6:1 and 5.6:2 in Table 5.6 list the parameters and characteristics for W=MF and W=1.0, respectively. Performing opt(2) on the backing impedance leads to the designs of cases 5.6:3 and 5.6:4. The requirement for greater backing in conjunction with the maximally flat match can be anticipated from frequency domain arguments. Since removal of high frequency energy is more neglected by the maximally flat match, additional resistive backing is required to suppress the high frequency components. The results of cases 5.6:3 and 5.6:4 also demonstrate that there is a considerable range of backing impedance (Z_B=0.98 to 1.63) for maximizing the peaks ratio. By selecting a few representative values from this range, the utility of incorporating a front-side optimization scheme is readily demonstrated. Three values of backing are specifically chosen: 0.98, 1.19,and 1.40. The upper range of Z_B is limited due to the considerable widening of the second pulse that occurs for Z_B=1.63. Therefore, Z_B=1.40 is selected since it represents the optimal value for maximizing the peaks ratio with a front-side W=0.6 configuration, and it does not significantly compromise the W=MF peaks ratio.

With Z_B=0.98, the front-side lengths and impedances are

TABLE 5.6
HEAVILY BACKED SYSTEMS FOR TWO FRONT-SIDE MATCHING SECTIONS

Case	Description	Z_B	Z_1	Z_2	L_1	L_2	V_p	V_r	PR	E_t
5.6:1	W=MF,lengths quarter-wave	1.00	.128	.503	1.00	1.00	.827	.159	14.3	.502
5.6:2	W=1.0, lengths quarter-wave	1.00	.171	.377	1.00	1.00	.812	.096	18.4	.510
5.6:3	W=MF, backing optimized	1.63	.128	.503	1.00	1.00	.721	.050	23.2	.405
5.6:4	W=1.0; backing optimized	.983	.171	.377	1.00	1.00	.827	.096	18.7	.513
5.6:5	Impedances and lengths optimized	.983	.073	.157	.677	.661	.759	.036	26.4	.310
5.6:6	Impedances and lengths optimized	.983	.069	.430	.991	.706	.698	.029	27.7	.292
5.6:7	Impedances and lengths optimized	1.19	.102	.255	1.26	1.02	.782	.053	23.4	.426
5.6:8	Impedances and lengths optimized	1.19	.102	.255	.885	.600	.837	.046	25.3	.354
5.6:9	Impedances and lengths optimized	1.19	.0798	.472	.99	.706	.737	.027	28.8	.331
5.6:10	W=1.0; lengths optimized	1.19	.171	.377	.768	.635	.896	.066	22.6	.431
5.6:11	Impedances and lengths optimized	1.40	.0931	.370	1.09	.900	.722	.025	29.1	.390

successively optimized to the outcome listed as case 5.6:5. That solution is found by either:

1. proceeding directly from a front-side configuration of W=1.0 or

2. using a starting point with lengths approximately 0.7.

The first method is somewhat slower since the Tchebychev impedances are approximately a local optimum for quarter-wave sections. Similar impulse response characteristics can be obtained for a wide range of Z_2 values. As an example, starting the optimizing process from W=MF, either of the above procedures lead to the design of case 5.6:6 which has a Z_2 value more than three times that of the 5.6:5 case. The design of case 5.6:6 is locally optimal over the subspace of front-side parameters. The similarity of the frequency responses of cases 5.6:5 and 5.6:6, as shown in Figure 5.11, confirms the time domain similarity of the solutions. With the large range for different solutions, the opt(2) criterion is not adequate for finding a globally optimal configuration, even with fixed backing. However, there are certain tradeoffs and considerations for selecting one system over another. These are to be illustrated with Z_B=1.19, where the special case of a matched backing is avoided.

Restricting Z_B to 1.19 and starting with the optimization of the front-side impedances, the front-side design of case 5.6:7 is found. That solution is determined by strating with an impedance optimization trom either the W=MF or W=1.0 systems. The peaks ratio of case 5.6:7 can be improved by permitting more significant deviations from quarter-wave. The point is demonstrated by the locally optimal solution of case 5.6:8 which has its impedances fixed to the values of case 5.6:7

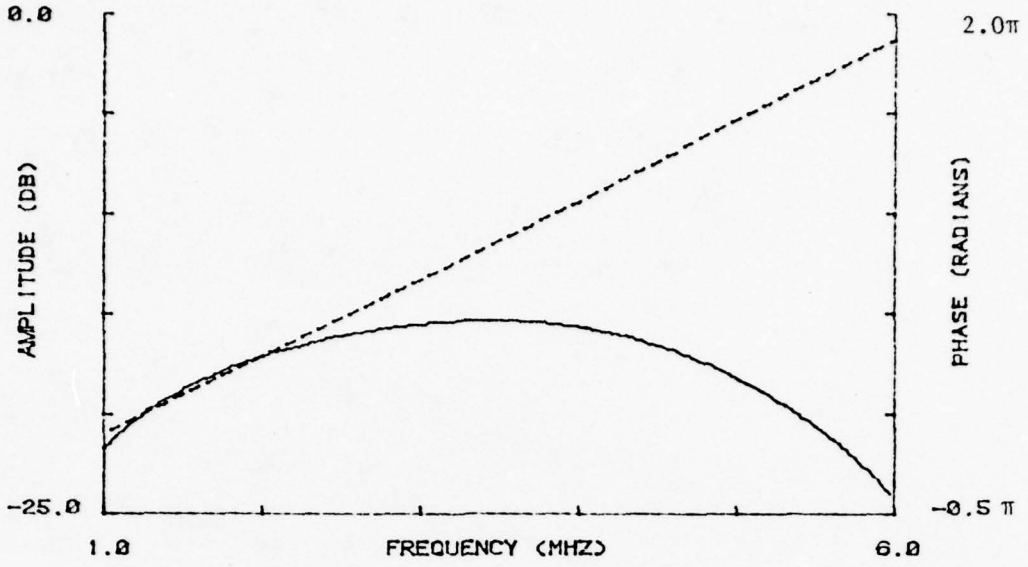

(a)

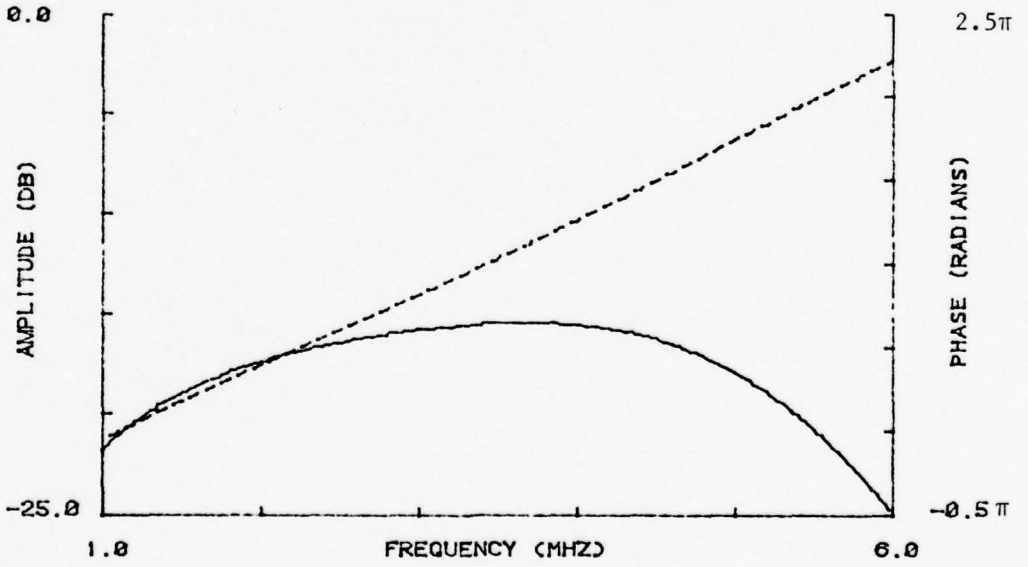

(b)

Figure 5.11. A frequency domain comparison between two locally optimal time domain solutions
a. Case 5.6:5
b. Case 5.6:6

but utilizes considerably different section lengths. System 5.6:8 is found by starting a length optimization from system 5.6:7 with L_2 first changed to approximately 0.7. These two impulse responses are illustrated in Figure 5.12 which shows that system 5.6:8 has the added advantage of reduced second pulse width. The maximum value for opt(2) with Z_B fixed at 1.19 occurs for the configuration of case 5.6:9 shown in Figure 5.13. That solution is reached by beginning with length optimization from the quarter-wave, maximally flat starting point. Numerous other starting points seem to confirm that this front-side configuration is globally optimal for the set value of backing.

Comparing cases 5.6:8 and 5.6:9 suggests that there is a wide range of impedances that will yield good results. The flexibility aspect of the design and optimization procedure is again demonstrated by considering the midrange situation of case 5.6:10. With the impedances fixed to prescribe a W=1.0 match, a reasonably satisfactory peaks ratio can be achieved by length adjustment. The improvement to the peaks ratio over the quarter-wave configuration with matched backing (case 5.6:2) is greater than 4 dB.

The design of case 5.6:11 represents the globally optimal design for Z_B=1.40. That solution is found directly from either the W=MF or W=1.0 systems and starting with either length or impedance optimization. Several other starting points have been examined and seem to confirm that system 5.6:11 is, in fact, the only solution for Z_B=1.40. Although the possibility of other solutions has been found for considerably reduced front-side impedances, they have been rejected due to their very low peak face velocities. Figure 5.14 illustrates the response of system 5.6:11 and the fact that there is some widening of the second

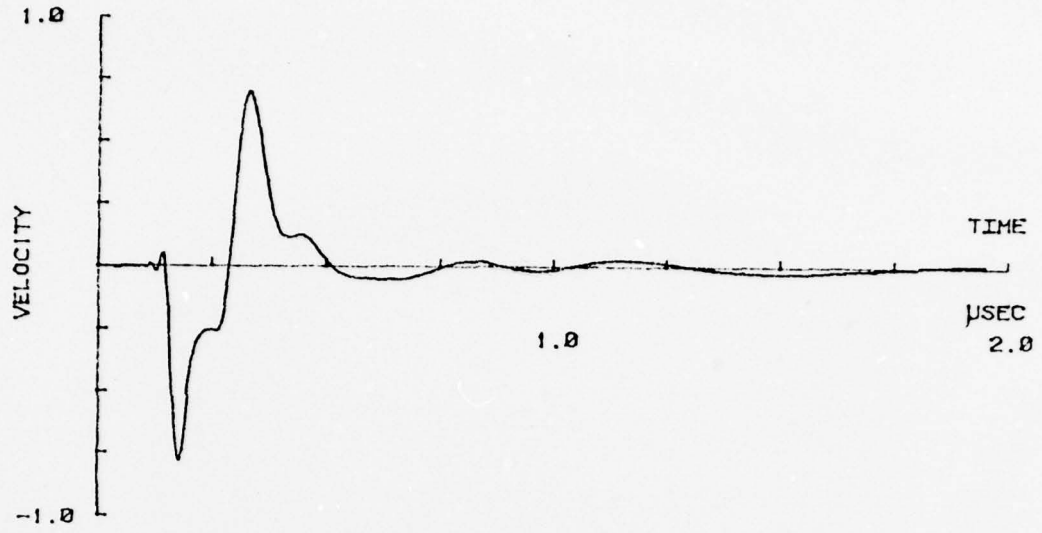

(a)

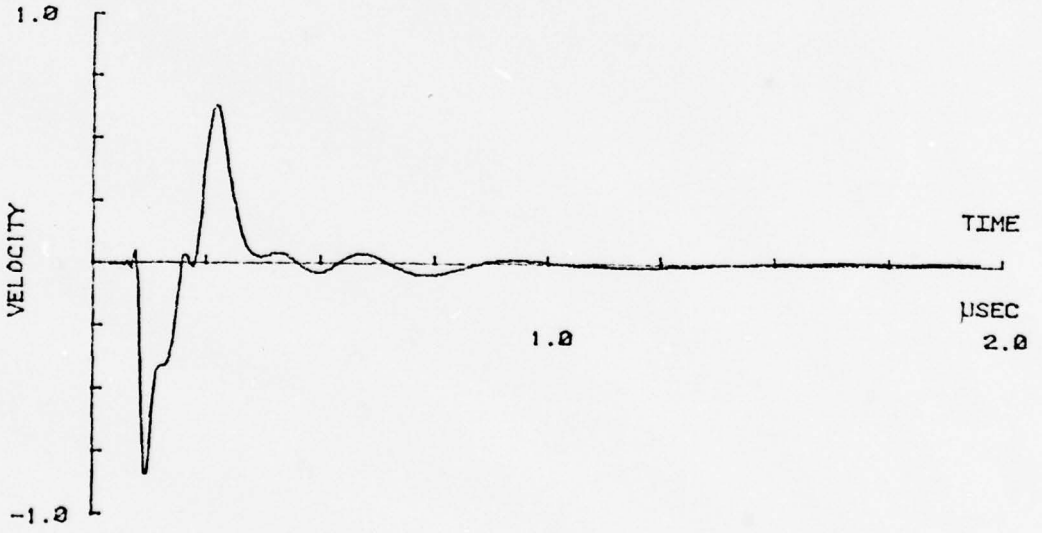

(b)

Figure 5.12. A time domain comparison between two locally optimal solutions
a. Case 5.6:7
b. Case 5.6:8

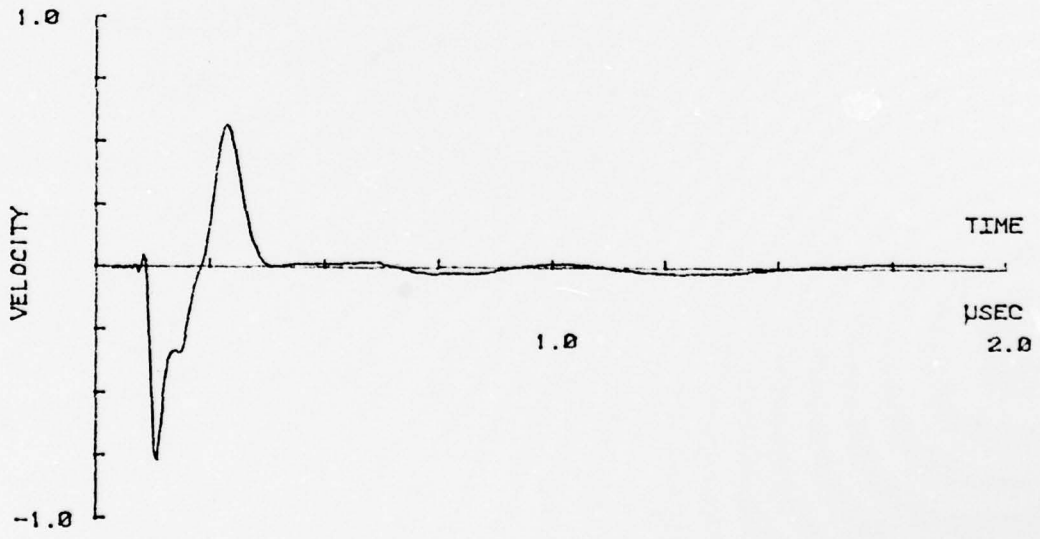

Figure 5.13. Impulse response of case 5.6:9 utilizing optimized impedances and lengths with Z_B fixed at 1.19

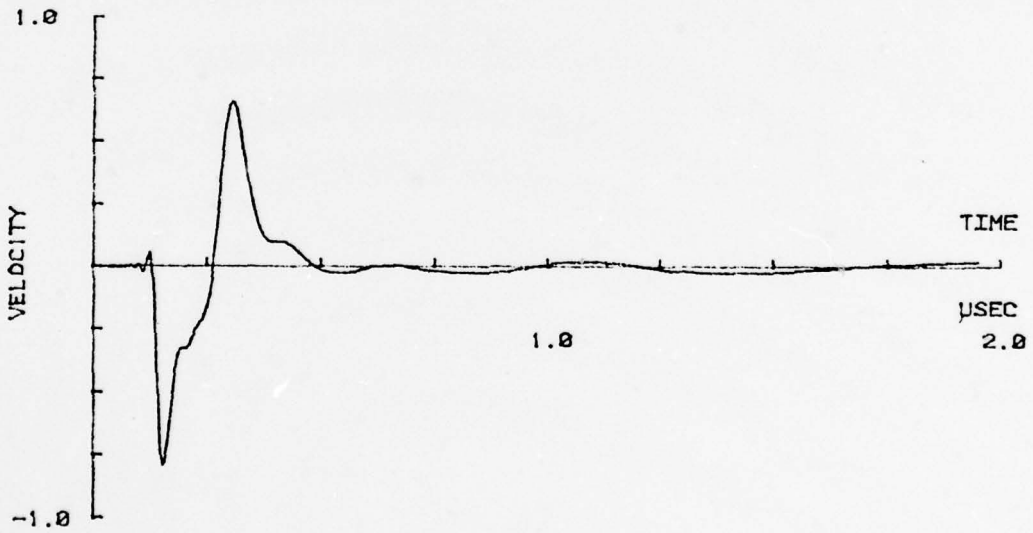

Figure 5.14. Optimized impulse response using two front-side sections and with Z_B fixed at 1.40.

pulse.

5.3.4 With Three Front-Side Sections. With three matching sections, the problems of local maxima are as severe as with the two-section transformers. It is therefore difficult to demonstrate whether or not a solution represents a globally optimal design. Consequently, the results in this subsection only serve to demonstrate that:

1. The procedures described in Chapter IV can realize significant improvements in the peaks ratios over the classical designs.
2. A three-section transformer has certain benefits and certain drawbacks over the one- and two-section arrangements.

The transducer systems in this subsection are all described in Table 5.7. *Entries* 5.7:1, 5.7:2, *and* 5.7:3, respectively, list the results of incorporating matched backing with front-side W=MF, W=0.6, and W=1.0 quarter-wave matching schemes. The subsequent three cases demonstrate the improvements possible by adjusting the backing impedance. It is observed that an increased bandwidth requires a reduced backing impedance, which is reminiscent of the two-section situation.

For demonstrating the effects of front-side matching, fixed backing impedances of Z_B=0.82 and 1.07 are selected. These two values correspond to the implied range defined by the values of Z_B for cases 5.7:4, 5.7:5, and 5.7:6. With Z_B=0.82 and with quarter-wave section lengths, case 5.7:7 shows the result of optimizing the front-side impedances. That same solution is reached from a wide range of starting

TABLE 5.7
HEAVILY BACKED SYSTEMS WITH THREE FRONT-SIDE MATCHING SECTIONS

Case	Description	Z_B	Z_1	Z_2	Z_3	L_1	L_2	L_3	V_p	V_r	PR	E_t
5.7:1	W=MF, lengths quarter-wave	1.00	.092	.254	.700	1.00	1.00	1.00	.850	.080	20.5	.569
5.7:2	W=0.6; lengths quarter-wave	1.00	.099	.254	.654	1.00	1.00	1.00	.867	.081	20.6	.587
5.7:3	W=1.0; lengths quarter-wave	1.00	.118	.254	.550	1.00	1.00	1.00	.865	.096	19.1	.600
5.7:4	W=MF; lengths fixed; Z_B opt.	1.07	.092	.254	.700	1.00	1.00	1.00	.827	.062	22.5	.549
5.7:5	W=0.6; lengths fixed; Z_B opt.	.960	.099	.254	.654	1.00	1.00	1.00	.870	.0789	20.9	.600
5.7:6	W=1.0; lengths fixed; Z_B	.820	.118	.254	.550	1.00	1.00	1.00	.922	.0917	20.1	.662
5.7:7	Impedances optimized	.820	.132	.168	.385	1.00	1.00	1.00	.835	.041	26.2	.569
5.7:8	W=1.0; lengths optimized	.820	.118	.254	.550	1.21	1.12	.684	.850	.0549	23.8	.592
5.7:9	Impedances optimized	1.07	.089	.113	.355	1.00	1.00	1.00	.767	.038	26.1	.490
5.7:10	W=MF; lengths optimized	1.07	.092	.254	.700	1.28	1.03	.587	.756	.038	26.7	.492

impedances. The major factor contributing to slowing the convergence is that Z_2 is not very critical to the final result. With the impedances of case 5.7:7, the quarter-wave lengths provide at least a locally optimal situation. Several nonquarter-wave starting points suggest that system 5.7:7 represents a unimodal maximum over the length subspace (for fixed impedances). On the other hand, the W=1.0 system of 5.7:6 has at least two locally optimal solutions over the length subspace: one found at quarter-wave (case 5.7:6), and the other by starting the search for L_3 near 0.7. The latter solution is listed as system 5.7:8.

The following cases serve to demonstrate that there are locally optimal solutions within the subspaces of either front-side lengths or front-side impedances. The backing impedance, Z_B, is fixed at 1.07. With the lengths fixed at quarter-wave, the impedances of case 5.7:9 maximize the peaks ratio. Testing a variety of starting lengths, the quarter-wave lengths of system 5.7:9 also seem to be the best selection for maximizing the peaks ratio for that set of impedances. Therefore, case 5.7:9 is locally optimal over the subspace of all front-side parameters. Another quarter-wave solution, 5.7:4, is also confirmed to be locally optimal with respect to the front-side parameters. Also, for the impedances of system 5.7:4, a superior solution (case 5.7:10) is located by starting the search with L_3 short.

Although the complete versatility afforded by the optimization of a three-section transformer has not been fully demonstrated, the results show the potential for selecting a wide variety of good designs. In addition to flexibility, there are other features of the design that are worth mentioning. Figure 5.15 illustrates the impulse response of case 5.7:7 which has optimized impedances for quarter-wave lengths.

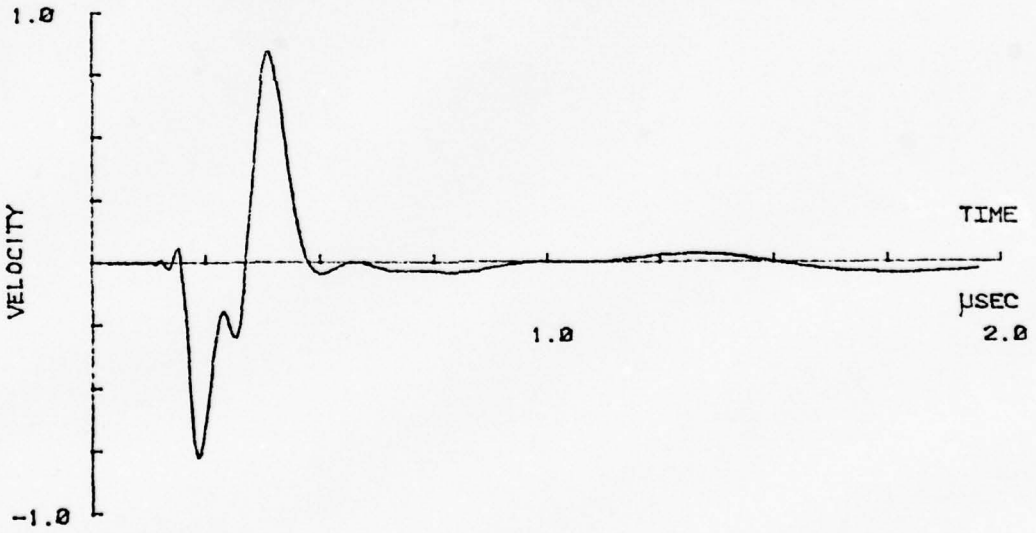

Figure 5.15. Impulse response with a three-section quarter-wave transformer with optimized impedances (case 5.7:7)

Contrasting its response with a one- (case 5.5:4) or two-section (case 5.6:7) case that have been impedance optimized using nearly quarter-wave lengths reveals the following:

1. The peak ring-down velocity, v_{ring}, occurs significantly beyond the second pulse for the three-section transformer.
2. Although v_{peak} is not significantly increased, the second pulse is heightened to an amplitude approximately equal to the first pulse.

On account of the additional layer, there is increased possibility for energy storage within the mechanical sections. As a consequence, the peak ring-down power can occur significantly after the peak power has occurred. (In practice, this effect may not be observed due to the mechanical losses that have not been considered in the model.) It is also expected that additional sections should improve the quality of the match and thereby increase the total energy delivered to the water. This conclusion is confirmed by reviewing the results of the three aforementioned cases which are repeated for convenience in Table 5.8.

5.4 Parameter Sensitivity

The consequences of parameter sensitivity during the optimization procedure have been mentioned in the previous section. Although parameters imposing only minor effects on the search function complicate and slow the convergence process during optimization, they can be beneficial to the finalized design. In practical situations where quality control becomes a factor, it is desirable for the most sensitive parameters to correspond to the most accurately controllable physical quantities, and vice versa. It may even be desirable to trade some

TABLE 5.8
A COMPARISON OF HEAVILY BACKED SYSTEMS
WITH ONE-, TWO-, AND THREE-SECTION TRANSFORMERS

Case	Description	Z_B	Z_1	Z_2	Z_3	L_1	L_2	L_3	V_p	V_r	PR	E_t
5.5:4	Each case has a locally	1.00	.0911	-	-	1.00	-	-	.702	.039	25.0	.243
5.6:7	optimal front-side design for	1.19	.102	.255	-	1.26	1.02	-	.782	.053	23.4	.426
5.7:7	its respective value of Z_B.	.820	.123	.168	.385	1.00	1.00	1.00	.835	.041	26.2	.569

performance for achieving a more favorable distribution of parameter sensitivities.

This section is devoted to examining the impact of parameter variability on the peaks ratio. By selecting and perturbing representative solutions from Section 5.3, the element sensitivities can be estimated. The ramifications of different optimization schemes and transformer complexity can also be evaluated with respect to sensitivity. A fixed deviation of +5.0% is used (although the first derivative may not be quite constant over that large a range). From a practical standpoint, most quantities can be readily measured and maintained to that accuracy. Perturbation is limited to one parameter at a time to allow for a direct analysis of each. Although a nonlinear composite effect may occur with more than a single variation, the number of possibilities are too numerous to consider separately. Several test cases have generally shown that the total deviation is approximately represented by the sum of the individual perturbations. As with the presentation of the performance characteristics, the perturbation results are reported separately for air and heavy backing.

5.4.1 Air Loading. The results of Table 5.9 show that it is not possible to generalize whether optimization of a parameter will increase or decrease its sensitivity. For the the single matching section, either length or impedance optimizaton increases the sensitivity of the respective parameter. Conversely, impedance optimization on the two-section case of 5.2:1 (leading to case 5.2:4) significantly decreases the sensitivity of Z_1. By contrasting cases 5.2:1 and 5.2:3 with cases 5.3:1 and 5.3:3, it is observed that the deviations as a function of bandwidth are not consistent when changing from a two- to

TABLE 5.9
EXAMPLES FOR SENSITIVITY ANALYSIS: AIR-BACKED

Case	Description	NOM[1]	Change caused to PR by a 5% perturbation Z_1	Z_2	Z_3	L_1	L_2	L_3
5.1:1	Geometric mean; quarter-wave	9.28	+0.44	-	-	-0.27	-	-
5.1:2	Geometric mean; length optimized	11.81	-.013	-	-	-0.71	-	-
5.1:3	Impedance optimized; quarter-wave	12.25	-0.80	-	-	-0.38	-	-
5.2:1	W=MF; quarter-wave	14.34	+0.62	-1.04	-	-0.19	-0.23	-
5.2:3	W=1.0; quarter-wave	15.17	+0.28	+0.32	-	+0.11	-0.29	-
5.2:6	W=1.0; lengths optimized	17.07	-0.90	+0.19	-	-0.12	-0.31	-
5.2:4	Impedances optimized; lengths quarter-wave	17.24	-0.16	-1.11	-	-0.17	-0.62	-
5.2:5	Impedances and lengths optimized	17.37	-0.19	-1.28	-	-0.48	-0.50	-
5.3:1	W=MF; quarter-wave	14.35	-0.41	+0.88	-0.98	-0.12	+0.36	-0.36
5.3:3	W=1.0; quarter-wave	20.09	+0.12	-0.63	-1.77	-0.10	-0.15	-0.76
5.3:6	W=1.0; lengths optimized	21.84	-0.38	-0.75	-2.32	-0.34	-0.59	-0.58
5.3:7	Impedances optimized; lengths quarter-wave	20.53	+0.16	-0.52	-2.16	-0.25	-0.37	-0.85

[1]NOM: the nominal, unpreturbed value of the peaks ratio (PR)

three- stage transformer. However, one generalization can be noted: the largest sensitivities are associated with the matching section adjacent to the ceramic, with the impedance parameter being dominant. Although the length sensitivity of this section is not as large as the corresponding impedance sensitivity, its length sensitivity is typically greater than the length sensitivities of other sections.

5.4.2 Heavy Backing. For all of the quarter-wave Tchebychev situations listed in Table 5.10, the sensitivities of the front-side parameters are increased as the backing impedance deviates from the matched condition of Z_B=1.0. The case of backing equal to the ceramic's impedance tends to maximize the energy delivered to the backing and thereby diminishes the available energy that can reach the active face. The requirements of the front-side match for controlling the peaks ratio is consequently reduced.

A few examples are also listed which demonstrate the effects on sensitivities as a consequence of front-side matching. Upon optimizing the impedance of a single quarter-wave section, its length and impedance sensitivities are considerably increased (cases 5.5:1 and 5.5:4). On the other hand, the length optimized system of case 5.5:5 is very stable with respect to impedance variations, but length deviations inflict a substantial effect. The globally optimal system of case 5.5:6 offers good performance as well as a good compromise of sensitivities. The examples of cases 5.6:5 and 5.6:6, which have additional flexibility afforded by a second matching section, demonstrate another point of interest. Tolerating only minor differences in performance offers the choice of assigning a low sensitivity to either Z_2 or Z_B with the remaining sensitivities approximately unchanged. The effects of

TABLE 5.10
EXAMPLES FOR SENSITIVITY ANALYSIS: HEAVILY BACKED

Case	Description	NOM	Change from the NOM peaks ratio by a +5% perturbation						
			Z_1	Z_2	Z_3	L_1	L_2	L_3	Z_B
5.5:1	Geo. mean; quarter-wave; Z_B matched	11.63	0.0	-	-	-0.19	-	-	+1.01
5.5:2	Geo. mean; quarter-wave; Z_B optimized	21.49	-0.22	-	-	-1.36	-	-	-0.55
5.5:3	Impedance opt.; q-wave; Z_B matched	25.03	-2.01	-	-	-0.81	-	-	-0.35
5.5:5	Geo. mean; length opt.; Z_B matched	22.21	-0.01	-	-	-1.37	-	-	-0.97
5.5:6	All parameters optimized	26.34	-1.27	-	-	-0.70	-	-	-0.83
5.6:1	W=MF; quarter-wave; Z_B matched	14.30	+0.12	-0.10	-	+0.05	-0.02	-	+0.79
5.6:3	W=MF; quarter-wave; Z_B optimized	24.25	-0.24	+0.02	-	-0.86	-1.72	-	-0.64
5.6:5	Front-side is locally opt.; Z_B=.98	26.79	-0.91	-1.62	-	-0.21	-2.30	-	-0.05
5.6:6	Front-side is locally opt.; Z_B=.98	28.00	-0.72	-0.23	-	-0.38	-2.85	-	+1.01
5.6:2	W=1.0;quarter-wave; Z_B matched	18.60	-0.74	+0.04	-	+0.27	+0.29	-	-0.29

The abbreviations used in this table are as follows:
geo. mean: geometric mean
NOM: the unpreturbed value of the peaks ratio
opt.: optimized values
q-wave: quarter-wave

TABLE 5.10 continued

Case	Description	NOM	Change from the NOM peaks ratio by a +5% perturbation Z_1	Z_2	Z_3	L_1	L_2	L_3	Z_B
5.7:1	W=MF; quarter-wave; Z_B matched	20.55	+0.56	+0.04	-0.52	-0.57	+0.14	-0.59	+1.47
5.7:4	W=MF; quarter-wave; opt. backing	22.46	-0.71	-0.12	-0.56	-0.55	+0.13	-0.56	-0.66
5.7:3	W=1.0; quarter-wave;Z_B matched	19.10	+0.02	-0.04	+0.03	+0.20	-0.07	+0.02	-0.25
5.7:6	W=1.0; quarter-wave; opt backing	20.20	-0.01	+0.02	-0.41	-0.53	-0.85	-0.53	-0.25
5.7:7	Impedances opt.; quarter-wave; Z_b=.82	25.89	-1.00	-0.26	-0.60	-2.13	-2.52	+0.26	-0.30

sensitivity as a function of the Tchebychev bandwidth are reversed from the lightly backed case. With matched backing, generally decreased sensitivities are associated with decreased bandwidth for two matching sections and increased bandwidth for three matching sections.

5.5 Effects of Including the Electrodes in the Model

In Chapter III it has been demonstrated that the electrodes can have a significant impact on the frequency response. Changes in the time domain must also be anticipated. The purpose of this section is to examine these effects on the impulse response. By adding sections simulating silver electrodes to a few of the optimized systems of Sections 5.2 and 5.3, a deterioration of the peaks ratio is seen to result. The finding emphasizes the need for including electrode characteristics in the analysis during the optimization. Table 5.11 lists the cases considered and the changes caused by the electrodes. In addition to degrading the response, it is also shown that the previously calculated solutions are no longer optimal when the electrodes are appended to the model. The results in Table 5.11 establish that these peaks ratios can be improved by subjecting the complete system to the optimization process. One and two front-section systems with both air and heavy backing are included in the examples that follow. The parameters describing the silver layer are listed in Appendix Table B.2.

Figure 5.16a plots the impulse response of the air-backed single-section system of case 5.1:3 on the same set of axis as system 5.1:3s, where the s denotes that silvered electrodes have been included. Figure 5.16b presents a similar plot for the air-backed two-section system of cases 5.2:5 and 5.2:5s. The responses of the heavily backed

TABLE 5.11
EFFECTS OF INCLUDING SILVER ELECTRODES

Case	Description	Z_B	Z_1	Z_2	L_1	L_2	V_p	V_r	PR	E_t
5.1:3	Optimum impedances and lengths	0.0	.33	-	1.00	-	1.43	.349	12.3	1.72
5.1:3S	Silver electrodes added to 5.1:3	0.0	.33	-	1.00	-	.994	.377	8.5	1.45
5.1:3SO	Optimizing impedances of 5.1:3S	0.0	.246	-	1.00	-	1.00	.287	11.0	1.44
5.2:5	Optimum impedances and lengths	0.0	.154	.495	.997	.982	1.51	.204	17.4	1.87
5.2:5S	Silver electrodes added to 5.2:5	0.0	.154	.495	.997	.982	1.16	.307	11.6	1.65
5.2:5SO	Optimizing lengths of 5.2:5S	0.0	.154	.495	.725	.663	1.15	.222	14.3	1.61
5.5:6	Optimized impedances and lengths	1.00	.091	-	.854	-	.699	.034	26.4	0.23
5.5:6S	Silver electrodes added to 5.5:6	1.00	.091	-	.854	-	.426	.021	26.0	0.17
5.5:6SO	Optimizing impedances of 5.5:6S	1.00	.136	-	.854	-	.482	.021	26.8	0.23
5.6:11	Optimized impedances and lengths	1.40	.093	.370	1.09	.900	.722	.025	29.1	0.39
5.6:11S	Silver electrodes added to 5.6:11	1.40	.093	.370	1.09	.900	.683	.065	20.5	0.35
5.6:11SL	Optimizing lengths of 5.6:11S	1.40	.093	.370	1.02	.974	.683	.035	25.7	0.36
5.6:11SI	Optimizing impedances of 5.6:11S	1.40	.125	.586	1.09	.900	.704	.037	25.7	0.35

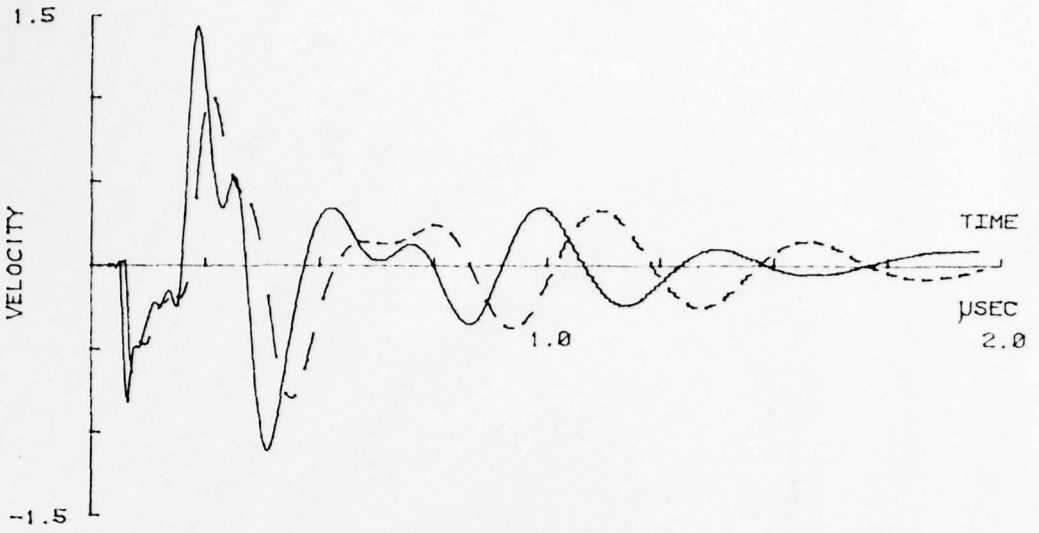

(a)

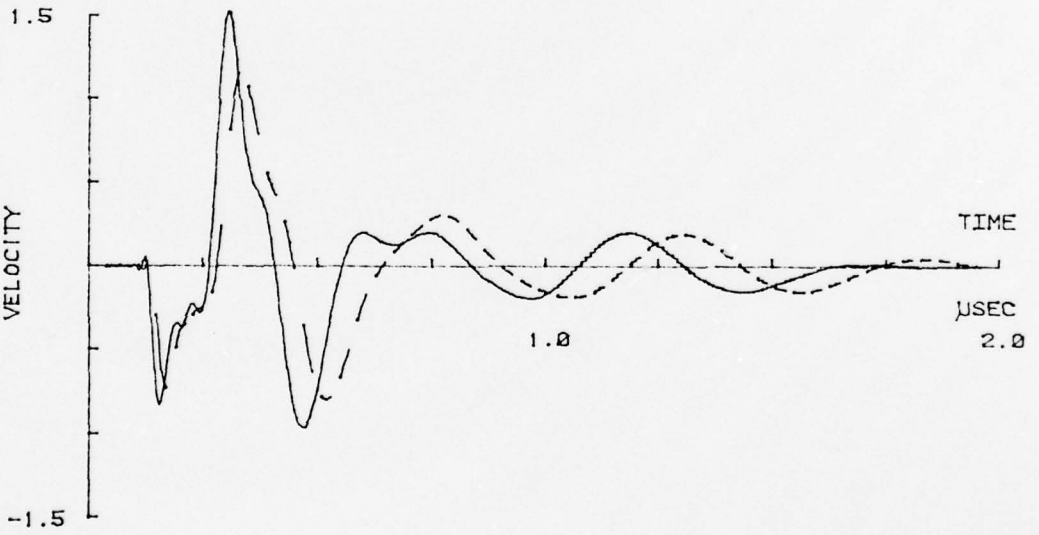

(b)

Figure 5.16. The effects of the electrodes on the impulse response of air-backed systems (solid curves represent the nonsilvered)
a. With one front-side section
b. With two front-side sections

designs of cases 5.5:6 and 5.6:11 are plotted together with their silvered counterparts in Figure 5.17. The two figures and data of Table 5.11 establish the following consequences on the impulse response attributable to the electrodes:

1. v_{peak} is reduced,
2. the peaks ratio is increased,
3. the width of the second pulse is increased (for the heavily backed systems), and
4. the post-$t_s(3)$ response of the lightly backed systems is somewhat modified.

Due to problems with locally optimal solutions and changes to the waveform, it would be difficult to present a meaningful comparison between the truly optimal silvered and nonsilvered solutions. On the contrary, a direct review of adjustments to either the section lengths or impedances is more effective for proving that the nonsilvered solutions, with electrodes subsequently included, are no longer optimal. The proper design procedure must be to subject the complete model, including the elctrodes, optimization.

The theoretical impact of excluding the electrodes during the optimization process is illustrated by examining a few such re-optimizations. For the air-backed systems, impedance re-optimization is applied to the single-transformer system (case 5.1:3SO) and length optimization to the two-transformer system (case 5.2:5SO). Each solution is unimodal for all the other parameters fixed. The improvements to the single-section heavily backed system are slight for either length or impedance (case 5.5:6SO) adjustment. With two front-side sections, length (case 5.6:11SO) or impedance (case 5.6:11SI)

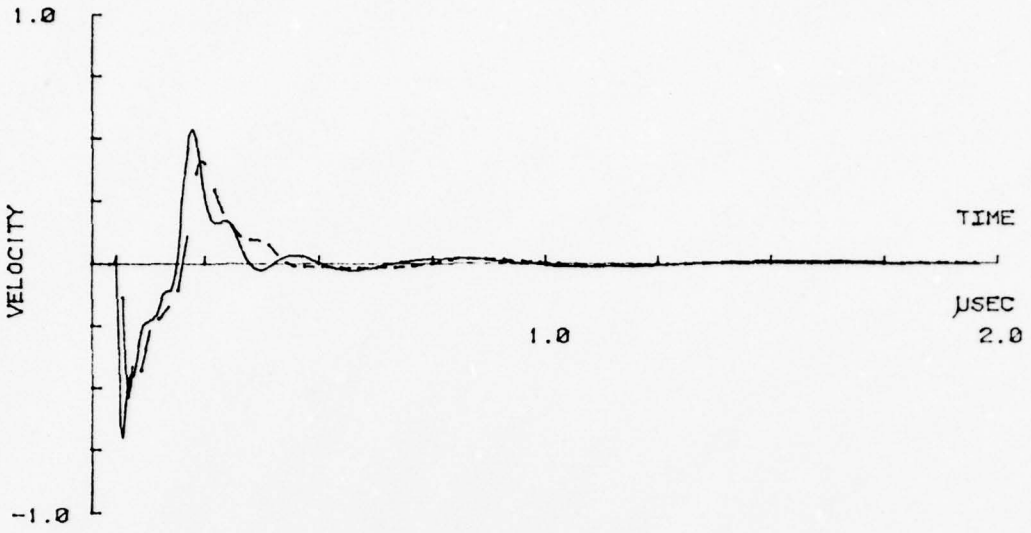

(a)

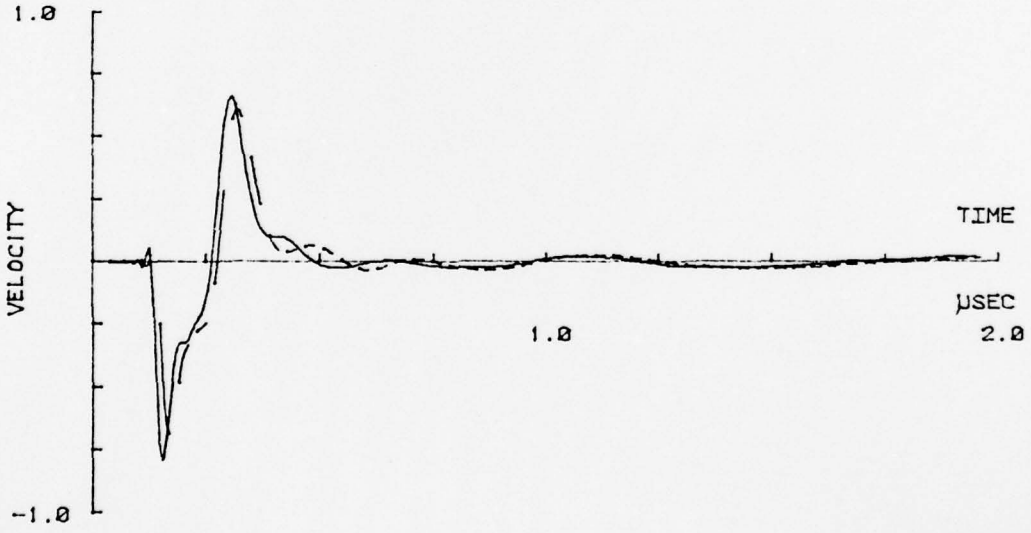

(b)

Figure 5.17. The effects of the electrodes on the impulse response of heavily backed systems (solid curves represent the nonsilvered)
a. With one front-side section
b. With two front-side sections

readjustments show a more dramatic improvement. Although not explicitly demonstrated, the optimal backing impedance is not significantly changed by the inclusion of the electrodes.

CHAPTER VI

EXPERIMENTAL RESULTS

6.1 Objectives

The purpose of this chapter is to provide experimental verification that the procedures described in the previous chapters can be reduced to practice. To achieve that goal, an assortment of transducer systems, summarized in Table 6.1, have been constructed and tested. Half of those systems represent a control group employing nonoptimized, quarter-wave matching schemes. With those systems, the matching sections are quarter-wave at the fundamental resonance of the ceramic. The corresponding optimized systems have been designed by allowing length variations to the front-side sections. For light and heavy backing, both one and two front-side sections have been tested. Frequency and time domain measurements are carried out on each system and are contrasted with the predicted results.

In additon to comparing the measured and predicted results, there are complete discussions of the construction and experimental procedures. By evaluating the results with an understanding of the construction and measurement processes, it is possible to account for some of the discrepancies between the theoretical and observed findings. Identifying the critical areas of design and construction should increase the likelihood of improving transducer performance. Although there are numerous potential sources for error, the results in this chapter show generally good agreement between the experimental and predicted results and, therefore, demonstrate the applicability of the optimization processes.

TABLE 6.1
SUMMARY OF THE EXPERIMENTAL CASES

Code	Description of the Transducer System
L-1	Lightly backed; quarter-wave section of quartz on front side
L-1-O	Length optimized version of L-1
L-2	Lightly backed; quarter-wave sections of quartz and lucite on front side
L-2-O	Length optimized version of L-2
H-1	Heavily backed; quarter-wave section of quartz on front side
H-1-O	Length optimized version of H-1
H-2	Heavily backed; quarter-wave sections of quartz and lucite on front side
H-2-O	Length optimized version of H-2

6.2 Designing the Test Examples

Due to a limited number of commercially available materials having suitable impedances for front-side sections, demonstration of the optimization process is limited to adjusting the section lengths. Although it is possible to synthesize composite materials with proper impedances, their use introduces new questions concerning uniformity and repeatability. The secondary changes to the ring-down that are being examined could be masked by such variations. Using commercial quartz and lucite reduces the possibility of material variability. Lucite and quartz have been selected since their impedances are in the proper range for providing a good impedance match between ceramic and water. Also, others [19, 20] have specifically demonstrated impedance matching with a two-section (quartz and lucite) transformer. The backing impedance is a fabricated material. Since the desired acoustic signal does not pass through the back-side loading, a high degree of quality control is not required. It is sufficient to know the material's impedance and that the backing is very lossy.

The required physical constants for the matching sections and backing impedances are listed in Table 6.2. The quartz is General Electric fused quartz, and the lucite is marketed as Plexiglas. The backing material is fabricated by suspending tungsten particles in Abson using a hot molding process [32]. The densities of the materials are measured directly by standard weight-volumetric techniques. The speed of sound in lucite is easily obtained by measuring the round-trip travel time of an acoustic pulse in a 0.64-cm (1/4-inch) thick sample. Due to the high attenuation of the backing materials, a one-way travel time is measured by using a transducer at each end of the sample. For both

TABLE 6.2
PHYSICAL PROPERTIES OF THE BACKING
AND FRONT-SIDE MATCHING SECTIONS

Material	Density (kg/m^3)	Speed of sound (m/sec)	Impedance normalized to ceramic	Loss (dB/cm)
Lucite	$1.17X10^3$	$2.80X10^3$	0.141	0
Quartz	$2.15X10^3$	$5.90X10^3$	0.545	0
Light backing	$2.00X10^3$	$1.46X10^3$	0.126	>30
Heavy backing	$12.46X10^3$	$1.27X10^3$	0.680	>30

processes, times are measured on a delayed-sweep oscilloscope. The sound speed in quartz listed in Table 6.2 is from published data provided by the manufacturer. The attenuation through the 1-cm long backing materials is greater than 30 dB. This attenuation rate and length insure that there is negligible reflected energy available to reenter the ceramic (from the backing) during the first several microseconds of the impulse response. Losses in the thin quartz and lucite sections are assumed to be small and are neglected.

The determination of optimal front-side lengths proceeds as described in Chapter IV. The process is considerably simplified since the back-side loading and front-side impedances are assumed to be fixed. The light backing is selected to be approximately twice the impedance of the water load. The impedance of the heavy backing is deliberately chosen to be considerably less than the optimum value (which would approximate the ceramic's impedance). In that situation, it is possible to emphasize the improvements that can be achieved through adjustments to the lengths of the front-side sections. Since the silver electrodes

have a considerable influence on the performance of the transducer, they are now included in the model with the parameters listed in Appendix B. Table 6.3a summarizes the required lengths and performance characteristics of the different transducer systems.

From that table, it is observed that the optimized length of the quartz section does not change appreciably from the one-section to the two-section case. Selecting the same quartz length for each simplifies the construction process. Upon building and testing any one-section system, the corresponding two-section system is simply fabricated by adding a layer of lucite. Therefore, only four distinct assemblies of backing, ceramic, and quartz need to be constructed. The two-layer systems are then easily built from the corresponding one-layer cases. The single section designs are built with the quartz lengths listed in Table 6.3a. Since the "optimized" two-section transducers also use those lengths, there must be a performance loss compared to the truly optimal solutions of Table 6.3a (caused by the use of nonoptimal quartz lengths). That degradation can be minimized by reoptimizing the lucite lengths for the specified quartz lengths. Table 6.3b summarizes the results for those two suboptimal solutions, denoted by the suffix SO.

6.3 Assembly of the Transducer Systems

The construction process is aptly summarized as a series of cleanings and epoxy curings. The front sections, ceramic disc, and backing are attached to each other with Hysol epoxy (R9-2039 with hardener H2-3561, degassed in an evacuated environment). The leads are connected to the silver electrodes with conductive Ablestik adhesive. To insure good adhesion, reliability, and repeatability, all surfaces

TABLE 6.3a
SECTION LENGTHS AND IMPULSE RESPONSE CHARACTERISTICS
OF THE VARIOUS TRANSDUCER SYSTEMS

System code	Lucite length (m)	Quartz length(m)	V_{peak}	V_{ring}	Peaks ratio (dB)
L-1	-	$4.19X10^{-4}$	0.83	0.33	8.1
L-1-O	-	$5.31X10^{-4}$	0.87	0.27	10.2
L-2	$1.99X10^{-4}$	$4.19X10^{-4}$	1.05	0.20	14.2
L-2-O	$2.01X10^{-4}$	$4.91X10^{-4}$	1.09	0.16	16.5
H-1	-	$4.19X10^{-4}$	0.66	0.18	11.3
H-1-O	-	$3.02X10^{-4}$	0.67	0.08	18.3
H-2	$1.99X10^{-4}$	$4.19X10^{-4}$	0.83	0.26	10.0
H-2-O	$1.27X10^{-4}$	$2.85X10^{-4}$	0.74	0.12	16.0

TABLE 6.3b
SECTION LENGTHS AND IMPULSE RESPONSE CHARACTERISTICS
OF THE SUBOPTIMAL TWO-SECTION SYSTEMS

System code	Lucite length(m)	Quartz length (m)	V_{peak}	V_{ring}	Peaks ratio (dB)
L-2-SO	$2.13X10^{-4}$	$5.31X10^{-4}$	1.09	0.16	16.4
H-2-SO	$1.21X10^{-4}$	$3.02X10^{-4}$	0.74	0.12	15.7

must be thoroughly cleaned prior to bonding. This section outlines the steps in building any of the one- or two-layer transducer systems mentioned in the previous section.

The cleaning process consists of applying organic solvents for removing any oil or grease. Toluene, acetone, and ethanol are used on the ceramic, quartz, and the leads. To prevent possible damage to the plastic materials, only ethanol is used to clean the lucite and backing. After each cleaning, the pieces are heated for two hours at $70^{o}C$ to remove any absorbed solvent. Cleaning and heating are done at each step of the assembly, immediately prior to bonding.

The first step in the construction process is to bond a pair of leads to each electrode. The leads, about 2 cm long and about $7X10^{-3}$ cm in diameter, are attached to the electrodes on the edge of the disc. In this way, the front and back surfaces are maintained flat to allow for the attachment of backing and matching sections. The Ablestik conductive epoxy must cure at $150^{o}C$ for approximately one-half hour. This temperature is well below the $400^{o}C$ Curie temperature of lead metaniobate. An ohmmeter was used to confirm that there was no dc short between the electrodes and that the resistance through the bond was less than 0.5 ohm. As a final check, a Hewlett Packard Vector Impedance Meter confirmed an input impedance similar to that of Figure B.1 (in Appendix B). Although the discs are presumed to be from the same production lots, some small (input) impedance differences can be noticed from disc to disc.

The next steps in the process are to bond the backing and quartz to ceramic. It is advisable to perform these in two separate operations. The disadvantage in so doing is that an extra delay is introduced

waiting for epoxy curing, but the advantages are as follows:

1. independent evaluation of the bond by measuring the input impedance at each step and
2. allowing additional force to be provided during the backing-ceramic curing without the risk of damage to the fragile quartz.

Bond thicknesses were estimated by measuring the individual sections before bonding and measuring the composite structure after bonding. The backing-ceramic bond is less than 2.54×10^{-4} cm (0.0001 inch) thick. To some extent, the two materials are actually in contact. Contact is confirmed by noting that there is a finite electrical resistance between the backing and silver electrode. This measurement is possible since the tungsten particles cause the backing to be conductive. The front-side bonds are from 7.6×10^{-4} to 12.7×10^{-4} cm (0.0003 to 0.0005 inch) thick. For repeatability, curing was conducted at room temperature (approximately $21^{\circ}C$) with relative humidity less than 50%. It was observed that elevating the temperature or the humidity reduces the reliability of the bond.

At this point, construction of a transducer system with a single matching section is complete. Waterproofing is accomplished by using the type of housing described in Appendix B. Fifty-ohm coaxial cable (RG-174), approximately 0.75 meter long, is soldered to the leads of the ceramic prior to sealing the housing.

6.4 The Experimental Procedure

6.4.1 Frequency Domain. In practice, the frequency response of a transducer is not measured in terms of its power loss ratio. The disadvantage of the power loss ratio is that it is not uniquely dependent upon the transducer; it is also a function of the particular voltage generator. For cases where the precise characteristics of the generator are not known and may be more complicated than a resistor in series with an ideal voltage source, power loss calculations may be impossible. Therefore, the transducer's voltage (short-circuit) or current (open-circuit) transmitting responses are typically the quantity of interest. The voltage transmitting response is defined as:

$$S_s(w,r_o) = \left.\frac{p_o(w,r_o)}{V}\right|_{V=1} , \qquad (6.1)$$

where $p_o(w,r_o)$ is the on-axis rms pressure at distance, r_o and frequency w, for one volt, V, across the transducer. As a frequency domain check on the accuracy of the Mason model, $S_s(w,r_o)$ is used as the basis for determining the experimental rms power delivered to the water per rms volt of excitation. The open-circuit response, $S_o(w,r_o)$, is similarly defined for a current drive situation.

The total rms power, P_D, delivered to the water medium by a planar disc transducer in an infinite baffle is given by [28]:

$$P_D = \frac{4\pi r_o^2 I_o}{(ka)^2}\left[1 - \frac{2J_1(2ka)}{2ka}\right] , \qquad (6.2)$$

where k is the wave number in water, a is the radius of the transducer,

and J_1 is the Bessel function of the first kind of order one. The on-axis rms intensity, I_o is:

$$I_o = \frac{p_o^2}{(\rho v)_{water}} \quad . \tag{6.3}$$

For ka>4, $J_1(2ka)$ is approximately zero and the requirement for an infinite baffle can be removed without appreciably changing the directivity function. With water loading at 1 MHz, the 1.27-cm diameter transducers have ka=26.6. Equation (6.3) can be substituted into Equation (6.2) yielding:

$$P_D = \frac{4\pi r_o^2 p_o^2}{(ka)^2 (\rho v)_{water}} \quad , \tag{6.4}$$

where the Bessel function has been neglected. The above derivation assumes that the front-side matching sections do not affect the directivity pattern of the disc transducer. Measurements on the transducer systems of Section 6.2 have confirmed that assumption. At worst, deviations are second order and can be contributed to experimental error. Therefore, Equation (6.4) allows for a direct frequency domain comparison between experimental and theoretical results. The theoretical rms power is calculated as the rms power delivered to Z_L (with generator resistance, R_g=0) in the model of Figure 3.5.

Measurements of p_o have been conducted in a Plexiglas tank, 1.8 meter long, 0.6 meter wide, and 0.5 meter deep. A tone-burst signal provides the transducer excitation. The pulse duration is short enough

AD-A073 818 PENNSYLVANIA STATE UNIV UNIVERSITY PARK APPLIED RESE--ETC F/G 20/1
TRANSIENT RESPONSE OPTIMIZATION OF PIEZOELECTRIC DISC TRANSDUCE--ETC(U)
JUL 79 H A WOLF N00024-79-C-6043
UNCLASSIFIED ARL/PSU/TM-79-139 NL

3 OF 3
AD A073818

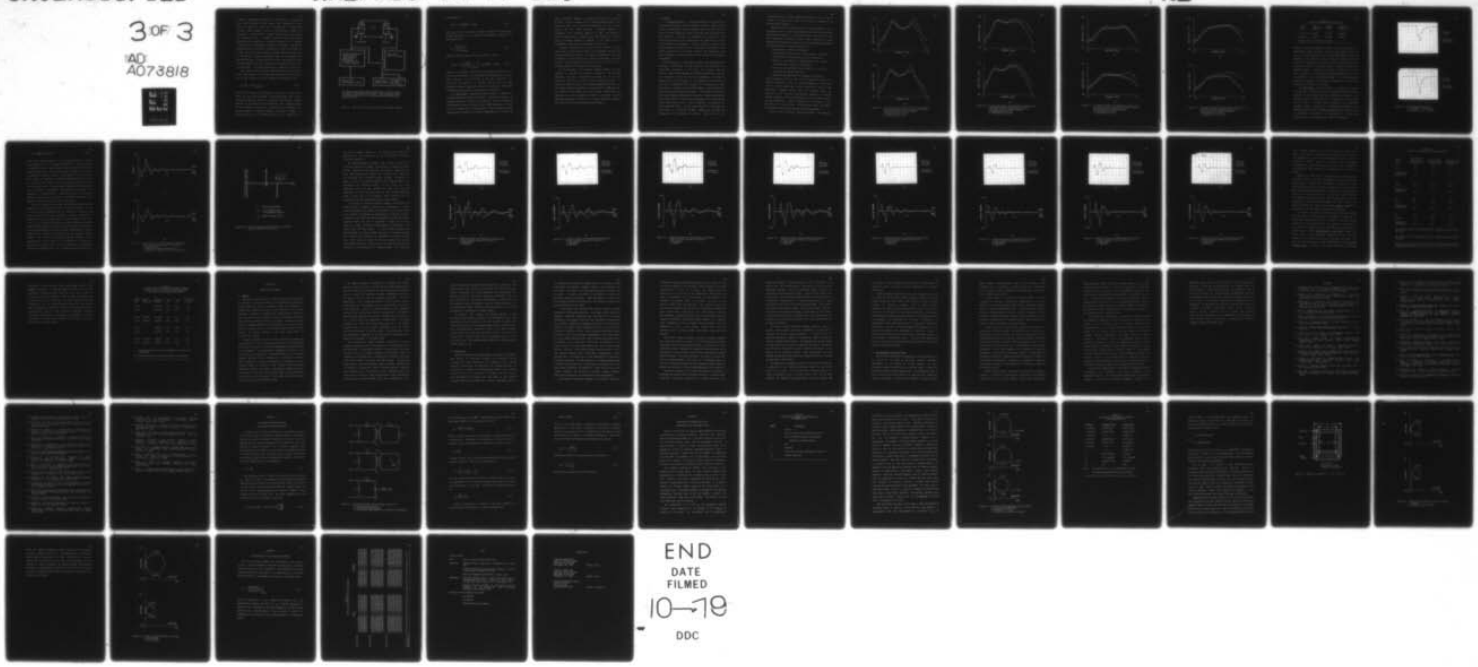

END
DATE FILMED
10-79
DDC

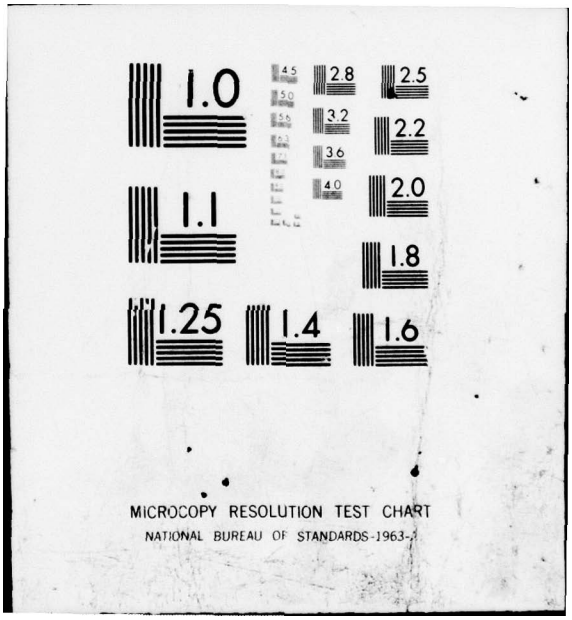
1.0
1.1
1.25
1.4
1.6
1.8
2.0
2.2
2.5
2.8
3.2
3.6
4.0
4.5
5.0
MICROCOPY RESOLUTION TEST CHART
NATIONAL BUREAU OF STANDARDS-1963-A

to prevent interfering reflections from the walls but is sufficiently long to allow signals to reach steady state. Approximately twenty cycles of signal were found to be satisfactory. A commercially available 10-MHz transducer serves as the receiving transducer for measuring p_o. Its open circuit receiving sensitivity, M_o, was measured by substitution with a 2.25-MHz transducer whose open-circuit sensitivity was determined by reciprocity calibration [15]. Repeated calibrations with interchanged and different transducers confirmed the repeatability of the reciprocity calibration to within 0.5 dB from 1 to 4.5 MHz. The drive voltage and receiver output voltage were measured on an oscilloscope. Voltage measurements from the oscilloscope were obtained by matching the amplitudes of a steady sinusoidal signal with the pulsed amplitude and then measuring the sinusoidal voltage directly on a RF voltmeter. The experimental setup is illustrated in Figure 6.1.

The separation distance between transducers has been maintained at 40 cm. This distance is well beyond the last maximum of the Fresnel zone for disc transducers in their fundamental operating band [28]:

$$d_f = \frac{a^2}{\lambda} = 12 \text{ cm}\Big|_{f=4.5\text{MHz}} , \qquad (6.5)$$

where a is the radius of the transducer and λ is the wavelegth in the water. The free field is assumed to be achieved beyond $2d_f$. On-axis intensity measurements beyond 40 cm confirmed that distance as being adequate for insuring free field conditions. Axial alignment between the two transducers was achieved by positioning the transducers for maximum output at the highest frequency of interest (4.5 MHz). By expressing M_o in dB re 1 volt/(N/m^2) and S_s in dB re 1 (N/m^2)/volt, S_s

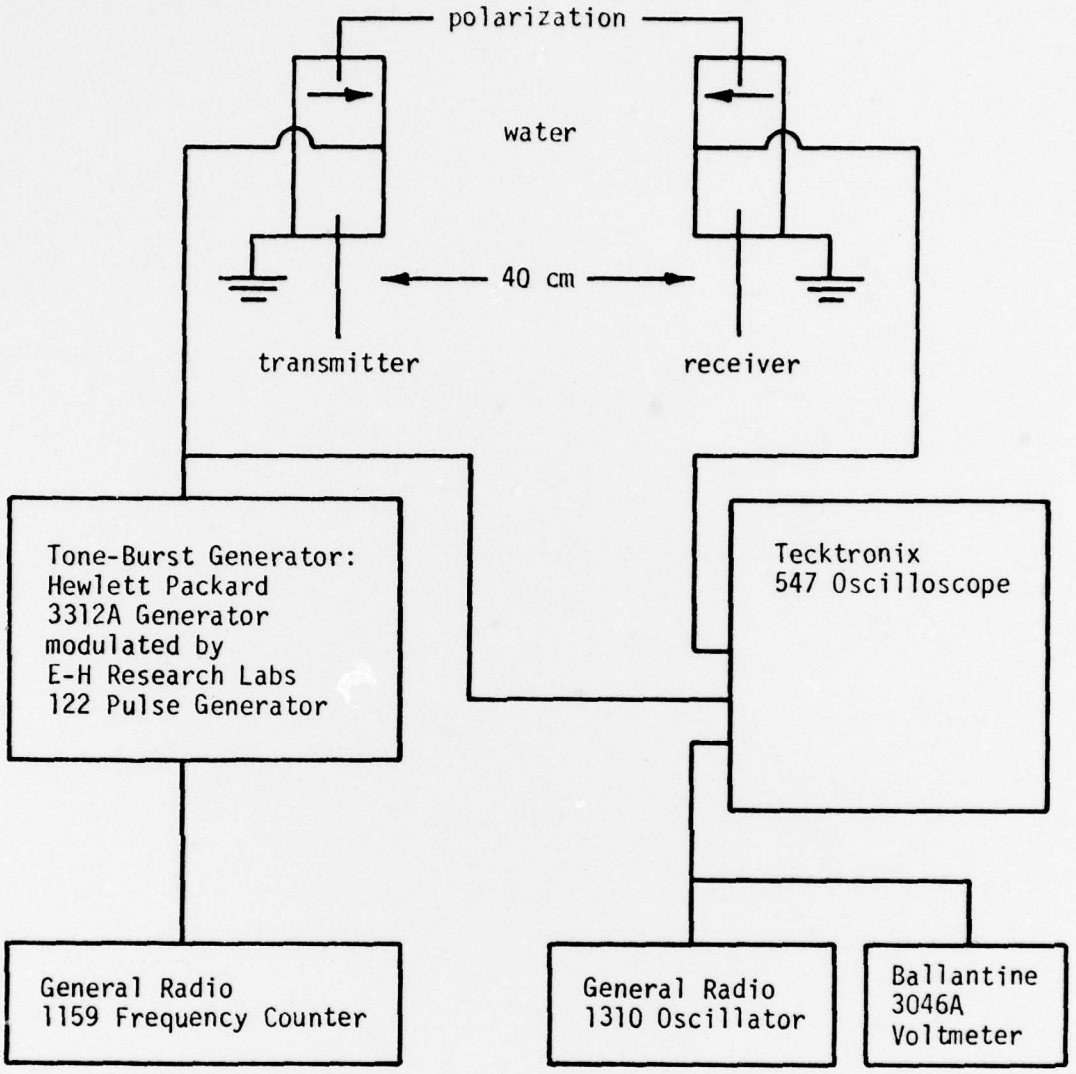

All voltage measurements have been made using a single voltmeter to measure a free-running sine signal. The free-running signal has been adjusted to have the same amplitude as the tone-burst signal under test.

Figure 6.1. Experimental setup for measuring the frequency response

is determined as:

$$S_s(dB) = 20\log\left(\frac{E_{out}}{V}\right) - M_o(dB) \quad , \tag{6.6}$$

where E_{out} is the receiver output voltage. Calculation of rms power per rms volt of drive, P_v, is accomplished by substituting Equation (6.1) into Equation (6.4):

$$P_v = \frac{4\pi r^2 S_s(f,r_o)}{(ka)^2(\rho v)_{water}} \quad . \tag{6.7}$$

Using the results of Equation (6.6), P_v in dB re 1 Watt is:

$$P_v(dB) = 10\log\left[\frac{4\pi r_o^2}{k^2a^2(\rho v)_{water}}\right] + 20\log\left(\frac{E_{out}}{V}\right) - M_o(dB) \quad . \tag{6.8}$$

Equation (6.8) together with the general procedure outlined in this section, form the basis for the experimental determination of acoustical power delivered to the water load by the disc transducers. The theoretical calculation of P_v procedes directly from the Mason equivalent circuit with R_g=0 and a 1-rms volt excitation. The measured and predicted power responses are presented in Section 6.5.

6.4.2 Time Domain. Measuring the impulse response is somewhat more straightforward than measuring the frequency domain power response. An electrical impulse is applied to the transducer, and the resulting far field pressure response is measured by the 10-MHz hydrophone of Section 6.4.1. The open-circuit receiving response of that transducer has been experimentally verified to be frequency independent up to 4.5 MHz, and

since it is heavily damped, it is presumed to be flat up to at least 7 or 8 MHz. Its flat response over the primary operating range of the transducers under test should allow reproduction of the far-field pressure with only minor distortion. Transducer alignment is accomplished in the frequency domain at 4.5 MHz. By providing an electrical impulse with a repetition rate in the vicinity of 30 KHz, a stable oscilloscope display is obtained at the receiver and is photographed. These results are presented in Section 6.5.

A special pulsing circuit has been built to provide a -40-volt pulse across a 50-ohm resistive load. With no transducer connected, the 20-dB time-width of the pulse is less than 0.1 microsecond. Connecting a transducer increases this time to about 0.2 microsecond. The exact details of this experimental excitation as well as its effect on the transient response are detailed in the next section.

For the measurement of the transient pressure response it was also important to ascertain the relative polarity of the receiving transducer. This was accomplished by driving one of the test transducers from Table 6.1 with a fixed electrical excitation. To receive the acoustical signal, two separate measuremets were made: one with another transducer from Table 6.1 and one with the 10-MHz receiver. The polarity of the 10-MHz receiver can then be inferred since the polarities of the test transducers in Table 6.1 are known. With the polarities arranged as in Figure 6.1, a negative electrical excitation will result in the first received pulse being negative.

6.5 Results

6.5.1 Frequency Domain. A comparison between the theoretical and measured power responses for the transducer systems of Table 6.3 would reveal an approximately constant frequency shift. For each case, the observed resonance peaks were as much as 0.5 MHz lower in frequency than were predicted. By testing the transducers at each phase of the construction process, it was determined that the addition of the quartz layer induced the discrepancy. The first attempt to explain these differences was to attribute them to an inaccurate determination of the physical properties of the quartz. However, 20% variations to the model's densities and sound velocities did not account for the observed discrepancies.

The next approach to resolving this problem was considerably more successful. By including the epoxy bonds (at the silver-quartz and quartz-lucite boundaries) to the model, the necessary shift was achieved. Since the bond between the backing and ceramic has virtually zero thickness, it does not need to be considered. The amount of frequency shift is very sensitive to the thickness of the silver-quartz bond and is comparatively less sensitive to the quartz-lucite bond. This result is expected due to the high impedance mismatch between the epoxy and the adjacent quartz and ceramic. On the other hand, there is only a small mismatch between epoxy and lucite. Using the approxmately known bond thickness as a guide, small adjustments to the bond thickness in the model quickly lead to a good alignment of the predicted and observed resonance peaks. Even by restricting the two bond lengths to being equal, a satisfactory alignment between the predicted and experimental power responses was achieved. Table 6.4 lists the

characteristics of the epoxy bonds, and Figures 6.2 to 6.5 show the results of including those bonds in the model as compared to the measured power responses, P_v.

Having included the correction for the bonds, Figures 6.2 to 6.5 demonstrates that the greatest discrepancy between the the theoretical and observed responses is a level shift, which is most severe at the high frequencies and resonance peaks. Losses which have not been considered in the model are assumed to be at least partially responsible for these differences. Possible causes include:

1. energy lost to radial mode components,
2. high frequency losses in the ceramic, quartz, and lucite which are not fully accounted for by the loss factor ,
3. effects of the capacitive loading caused by the coaxial cable between the transducer and generator,
4. electrical and mechanical losses incurred as a result of the conductive adhesive bond, and
5. mechanical coupling between the transducer and housing.

From an experimental point of view, it is also expected that there is an increased possibility of error at the high frequencies. The relative error is certainly greater due to lower signal level. Also, at high frequencies, alignment becomes much more critical. Since the directivity factor increases with increased frequency, an off-axis condition manifests itself by under-measuring the true on-axis response at high frequencies. However, because of the consistency of the differences, it is expected that the theoretical factors are probably more responsible for the discrepancies than the experimental.

A special note is necessary about system H-2-SO. The comparison

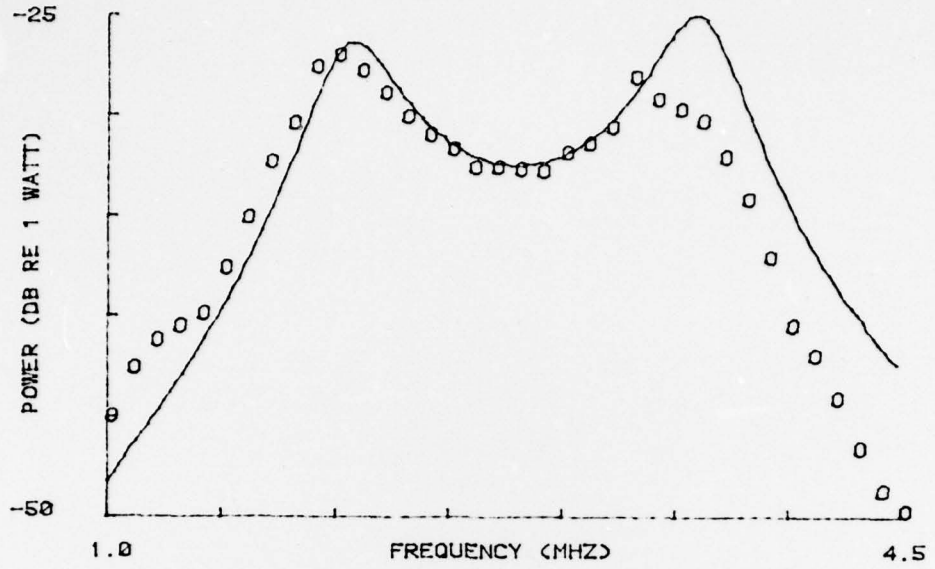

(a)

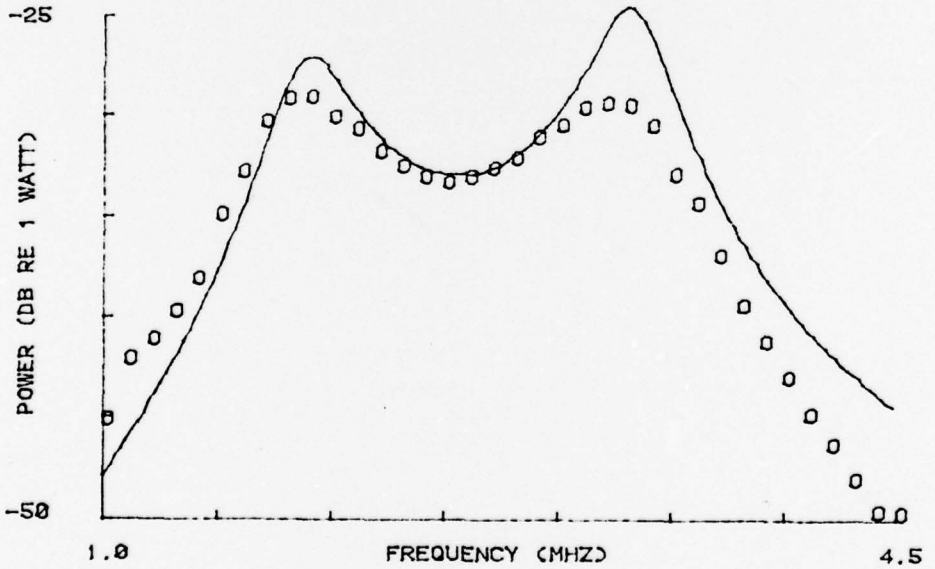

(b)

Figure 6.2. A comparison between the theoretical (solid curves) and measured power responses (P_V); with a single front-side section and light backing
a. Nonoptimized (case L-1)
b. Optimized (case L-1-O)

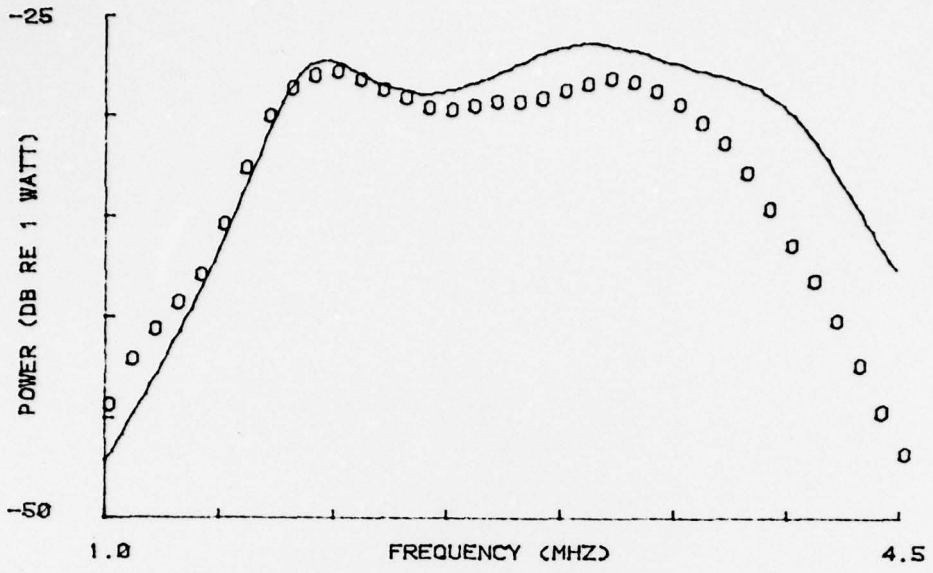

(a)

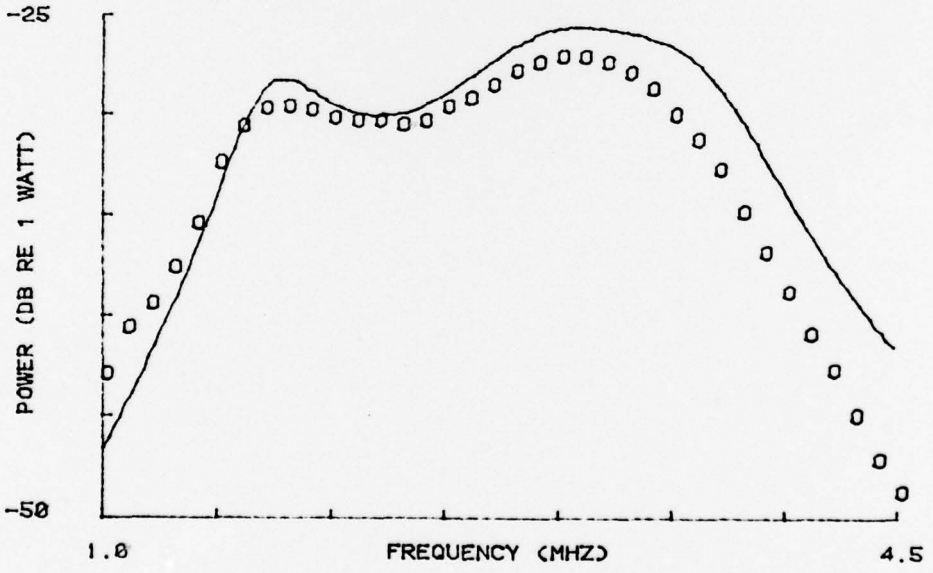

(b)

Figure 6.3. A comparison between the theoretical (solid curves) and measured power responses (P_V); with two front-side sections and light backing
a. Nonoptimized case (L-2)
b. Optimized case (L-2-SO)

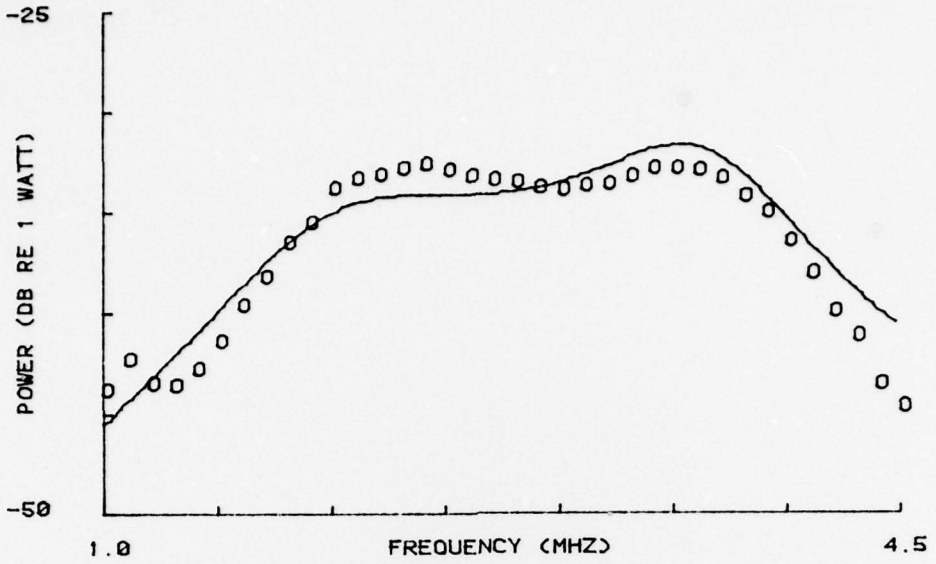

(a)

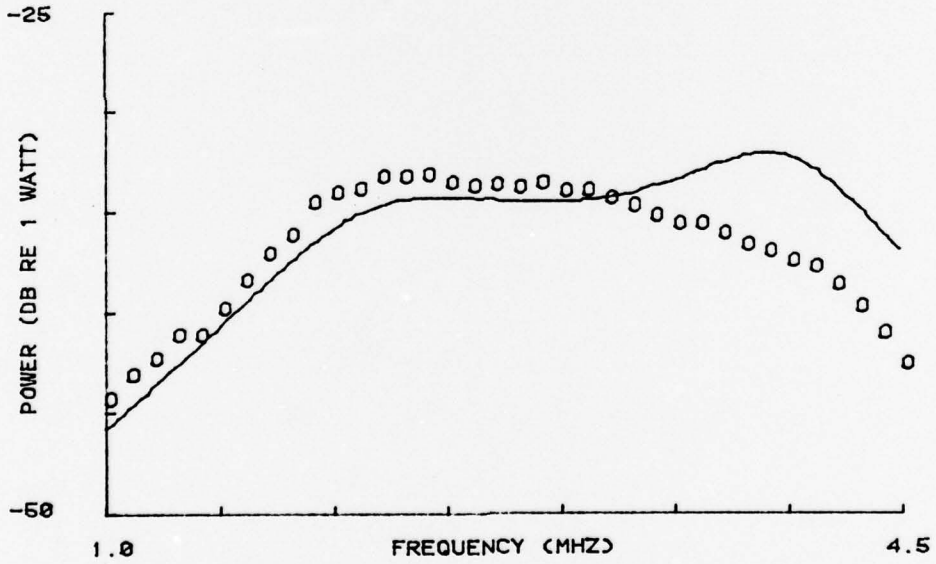

(b)

Figure 6.4. A comparison between the theoretical (solid curves) and measured power responses (P_V); with a single front-side section and heavy backing
a. Nonoptimized case (H-1)
b. Optimized case (H-1-O)

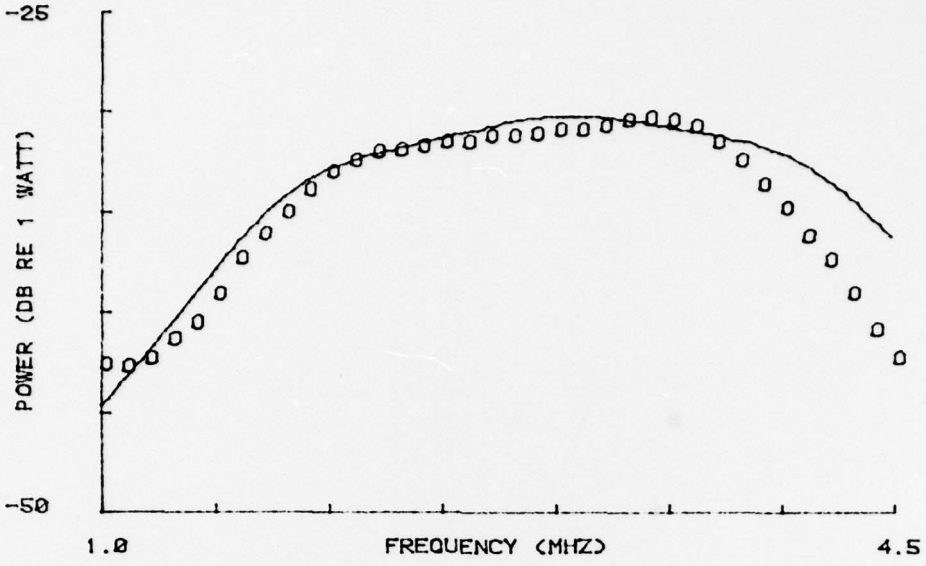

(a)

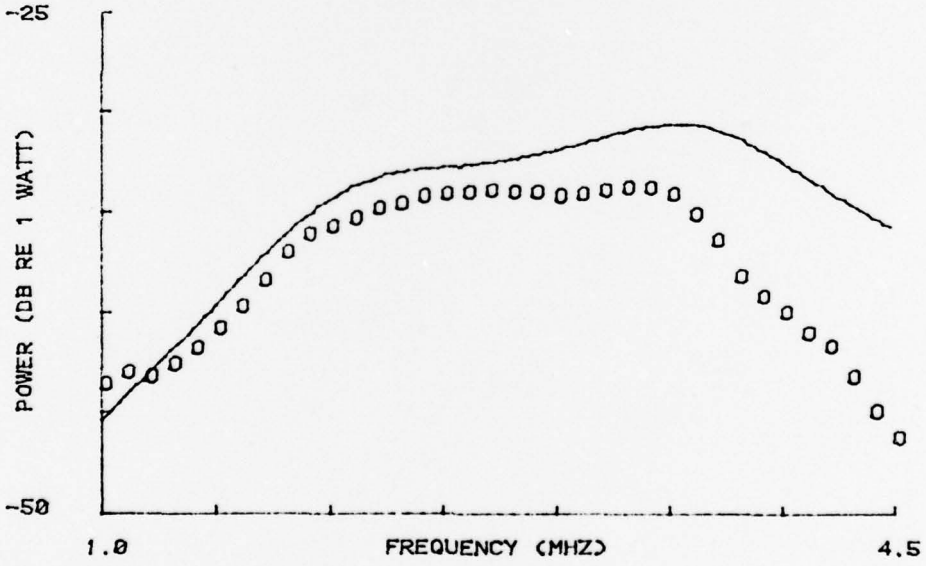

Figure 6.5. A comparison between the theoretical (solid curves) and measured power responses (P_V); with two front-side sections and heavy backing
a. Nonoptimized case (H-2)
b. Optimimized case (H-2-SO)

TABLE 6.4
PHYSICAL CONSTANTS OF THE EPOXY BONDS

System Code	Bond length (m)	Density[1] (kg/m^3)	Speed of sound[1] (m/sec)
H-1 and H-1-O	$0.8X10^{-5}$	$1.15X10^{3}$	$2.60X10^{3}$
All others	$1.1X10^{-5}$	$1.15X10^{3}$	$2.60X10^{3}$

[1]Typical values for the type of epoxy

between the predicted and measured responses indicates a significant but approximately constant difference across the entire frequency band. The loss in the experimental system is directly attributable to a partial breakdown of the conductive adhesive during the pulsing process of system H-1-O (recalling the construction process of Section 6.3). While pulsing, an excessive voltage peak caused the damage. Remeasuring the frequency response of system H-1-O confirmed a constant loss over the band. Likewise, the impulse response measurement suffered only a loss in sensitivity with no appreciable change in its characteristics. Consequently, frequency and time domain measurements of system H-2-SO should and do reflect this level shift.

6.5.2 Time Domain. From the discussion in Section 6.5, it becomes clear that for the model to predict the frequency response accurately, and thus the time response, the epoxy bonds must be included in the equivalent circuit. Another factor to be considered in the time domain is the effect of a non-zero width excitation in the experimental procedure. Figures 6.6a and 6.6b are oscilloscope photographs of the applied excitation across a 50-ohm load measured at the generator and at the transducer, respectively. The time response to a given time excitation, v(t), can be obtained by a discrete convolution:

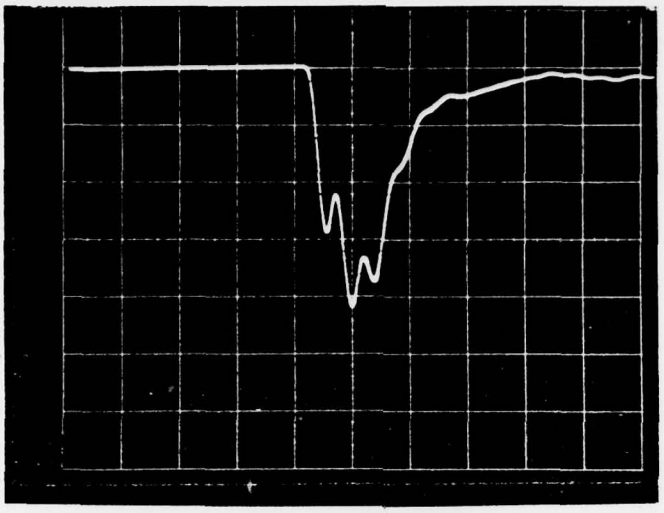

Vertical:
10 v/div

Horizontal:
0.1 μsec/div

(a)

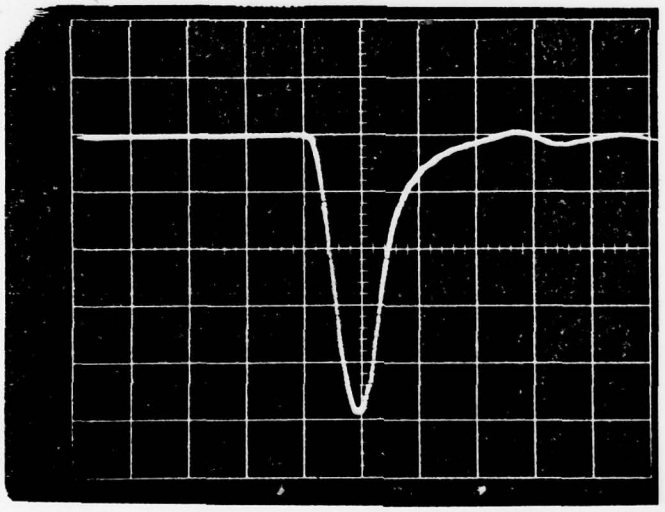

Vertical:
10 v/div

Horizontal:
0.1 μsec/div

(b)

Figure 6.6. The experimental excitation
a. As measured at the generator
b. As measured at the transducer

$$e(t) = \sum_{n=0}^{\infty} h(n\Delta t)v(t-n\Delta t) \quad , \tag{6.9}$$

where h is the impulse response, e is the resulting response, t is the time increment, and t is an integral multiple of Δt. For the purposes of implementation, the infinite summation can be terminated at a point where subsequent values of h can be neglected. System H-2 is selected to demonstrate the effect of using a pulse similar to the one in Figure 6.6b. Figure 6.7 compares the theoretical impulse response of system H-1 (including epoxy bonds) with its theoretical response from the finite amplitude pulse. It demonstrates the importance of including the effects caused by an experimental approximation to an impulse. The amplitude of the finite pulse is normalized so that its time averaged voltage is equal to that of an impulse. As expected, the response to an impulse is more peaked than with a finite width pulse.

With the instrumentation available, the far-field on-axis pressure response can be measured more readily than the face velocity. In the far field ($r_o >> a$), Stepanishen [48] and others have shown that the on-axis pressure from a disc mounted in a planar rigid baffle is proportional to the time differential of the face velocity. This result is due to the diffraction effects from a finite aperture transducer. Stepanishen has extended the analysis to both the near and far fields. He has demonstrated that the on-axis pressure resulting from a velocity impulse at the transducer face consists of two equal and opposite impulses. The arrival of the initial impulse corresponds to the propagation time from the center of the transducer to the observation point, and the arrival of the second one corresponds to the propagation time from the transducer edge. The response is pictured in Figure 6.8.

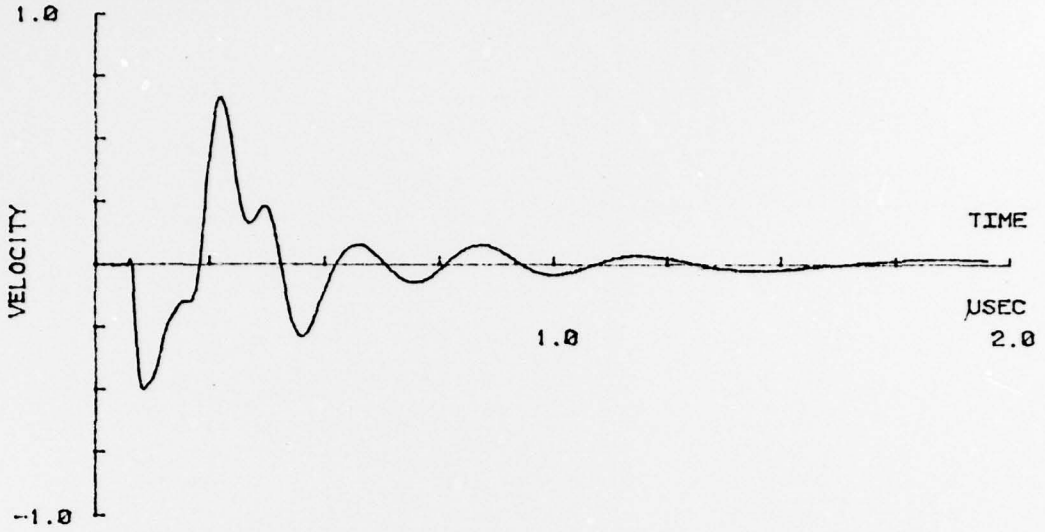

(a)

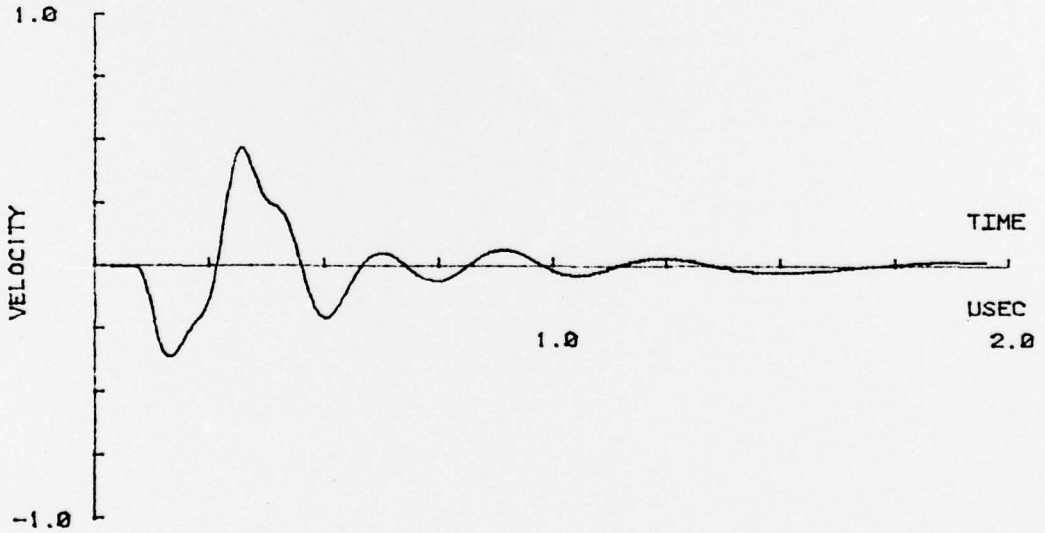

(b)

Figure 6.7. The effects on the face velocity of system H-1 (with epoxy bond included) of a finite width excitation pulse
a. Theoretical impulse response of H-1
b. Theoretical response to a finite width pulse

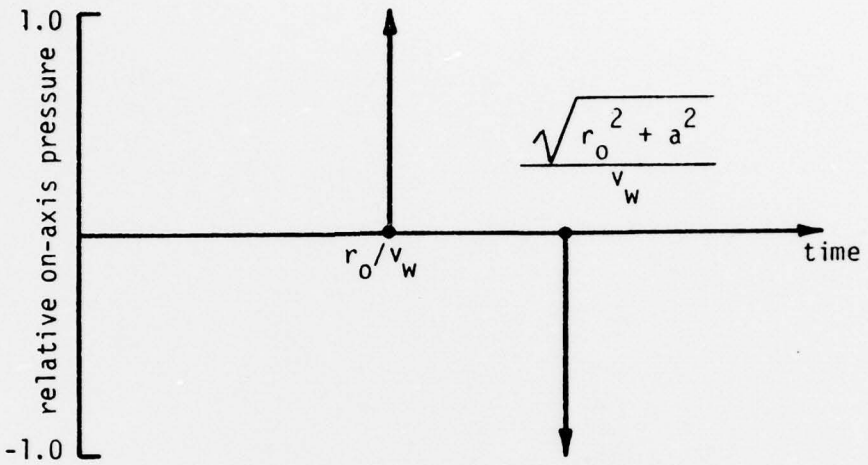

a = radius of transducer

r_o = axial distance from transducer to observer

v_w = speed of sound in water

Figure 6.8. On-axis pressure response from a disc transducer having an impulsive face velocity

The on-axis pressure response to an arbitrary face velocity is proportional to the convolution of the face velocty with the function indicated by Figure 6.8.

The measured pressure responses, with the pulse excitation of Figure 6.6b, are shown in Figures 6.9a to 6.16a. The predicted on-axis pressure responses to that excitation are shown in Figures 6.9b to 6.16b. The epoxy bonds of Table 6.4 are included in the models that have generated those predicted pressure responses. Examination of Figures 6.9 to 6.16 indicates generally good agreement between the experimental and predicted results. In all cases, the first experimental pulse has lower amplitude and longer rise time than predicted. In a few of the cases, there are some variations predicted within a pulse but are not observed. Those differences can be attributed to the limited bandwidth of the receiving system.

A mean squared difference comparison between the predicted and measured pressure responses is possible but is unwarranted. A simple and more meaningful check between the theoretical and observed results can be achieved by examining the characteristics of specific interest. A peaks ratio type calculation using the predicted and observed pressure responses offers that sort of comparison. However, it is first necessary to adapt a modified interpretation of the separation time between early and late energy. A little thought confirms that differentiating the velocity response will result in a pressure response with its first pulse one-half the time-width of the first velocity pulse. After that, the velocity and pressure responses will have the same general time history. This is true to the extent that the velocity response can be characterized as a damped sinusoid. As a matter of

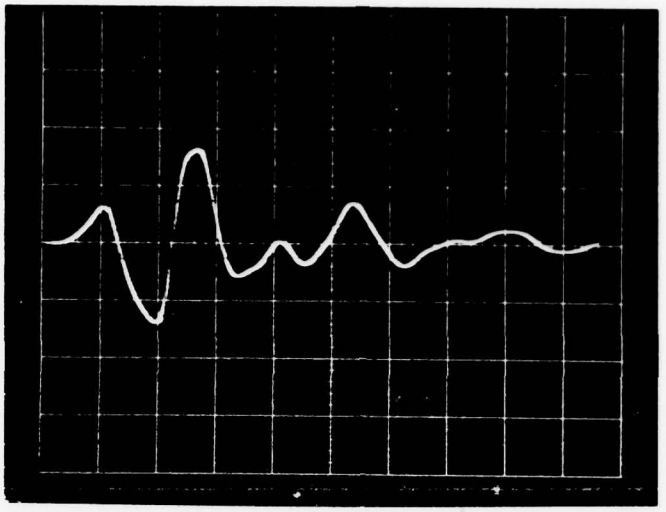

Vertical:
0.05 v/div
(inverted)

Horizontal:
0.2 μsec/div

(a)

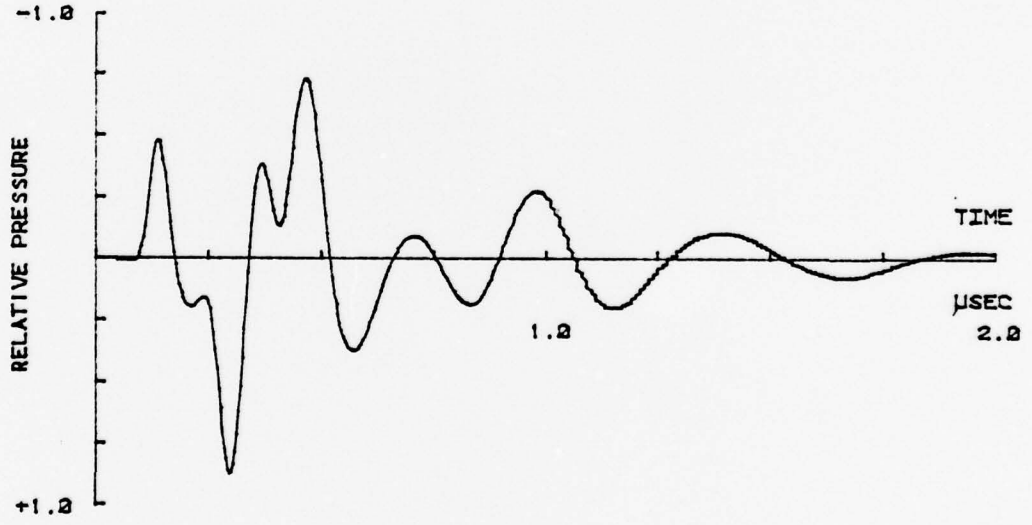

(b)

Figure 6.9. Comparison between the experimental and predicted on-axis transient pressure of system L-1
a. Experimental
b. Predicted

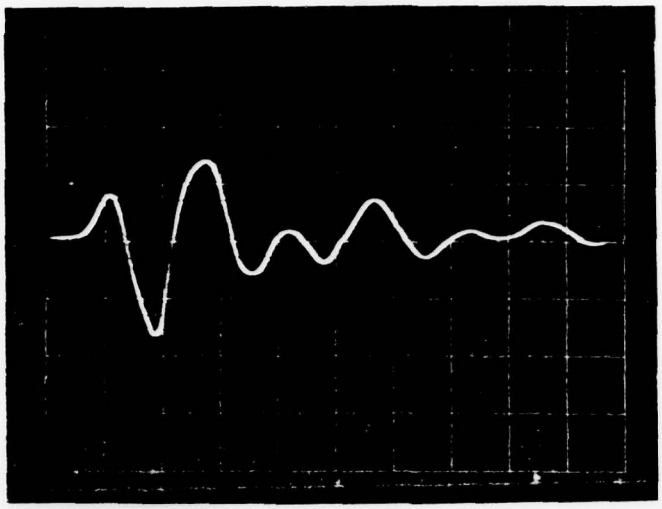

Vertical:
0.05 v/div
(inverted)

Horizontal:
0.2 μsec/div

(a)

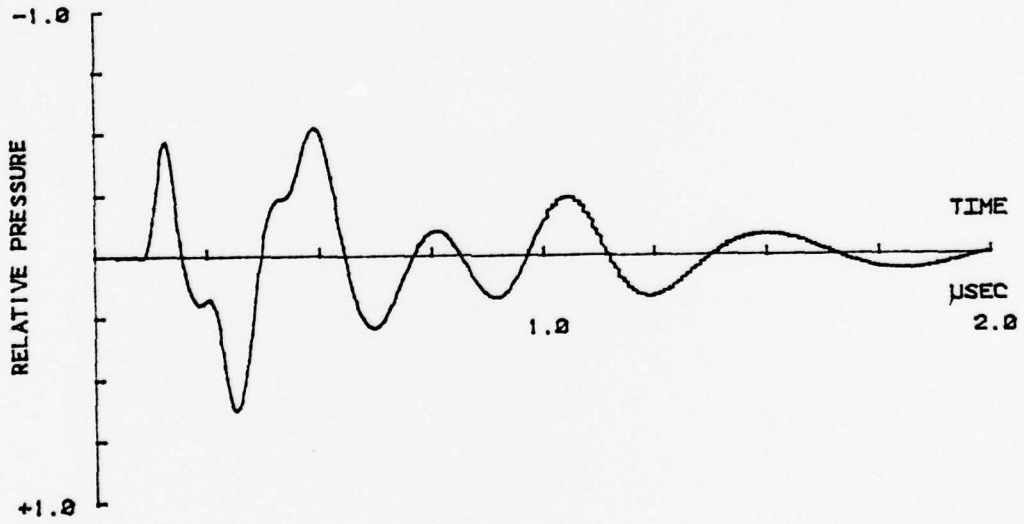

(b)

Figure 6.10. Comparison between the experimental and predicted on-axis transient pressure of system L-1-0
a. Experimental
b. Predicted

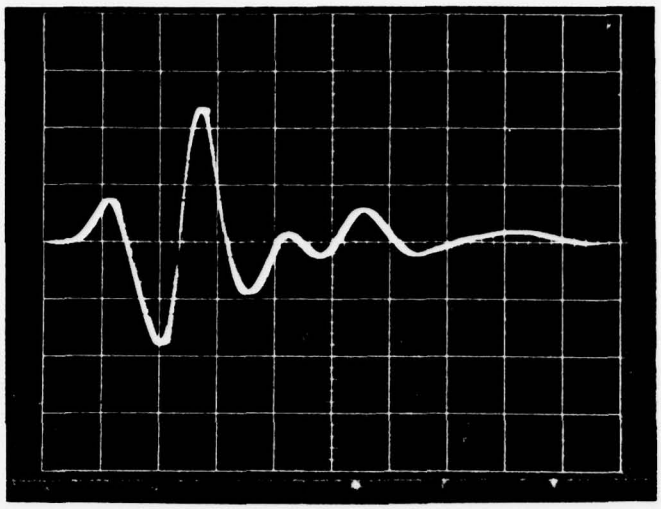

Vertical:
0.05 v/div
(inverted)

Horizontal:
0.2 μsec/div

(a)

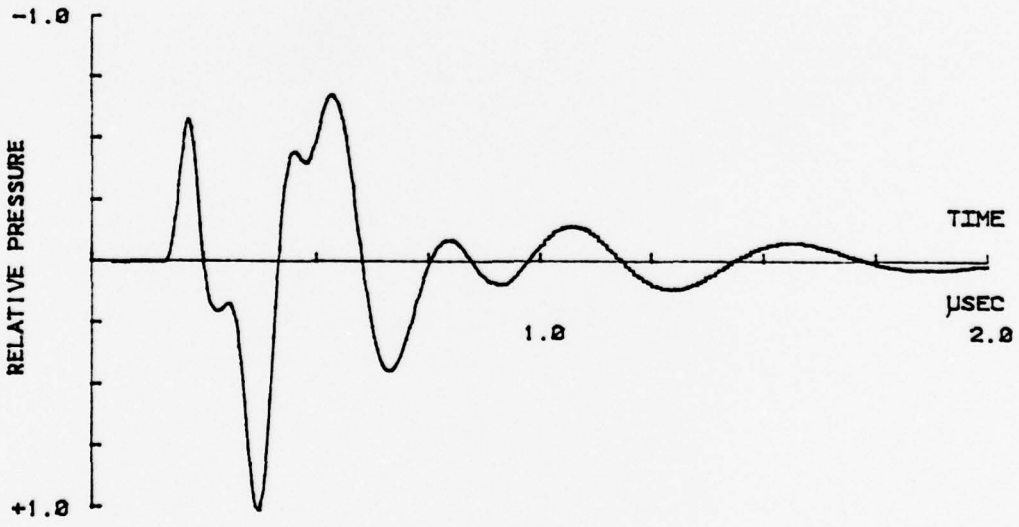

(b)

Figure 6.11. Comparison between the experimental and predicted on-axis transient pressure of system L-2
a. Experimental
b. Predicted

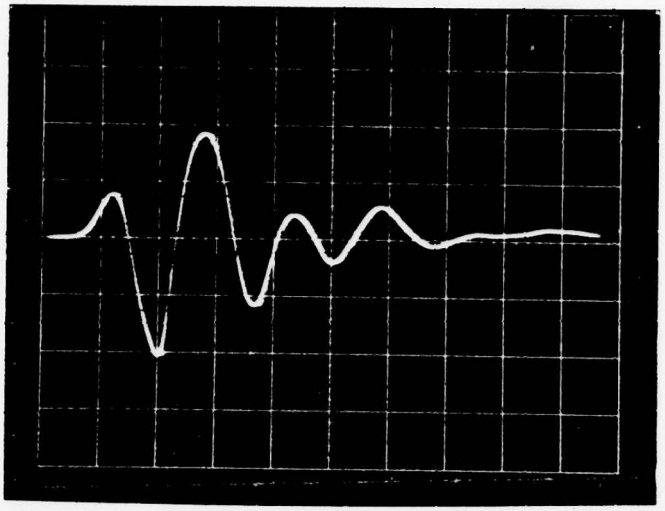

Vertical:
0.05 v/div
(inverted)

Horizontal:
0.2 μsec/div

(a)

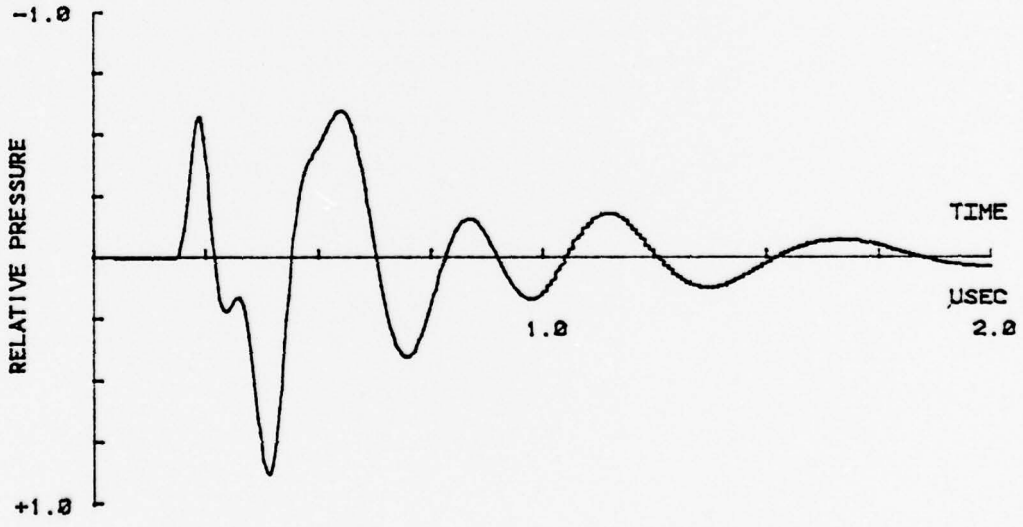

(b)

Figure 6.12. Comparison between the experimental and predicted on-axis transient pressure of system L-2-SO
a. Experimental
b. Predicted

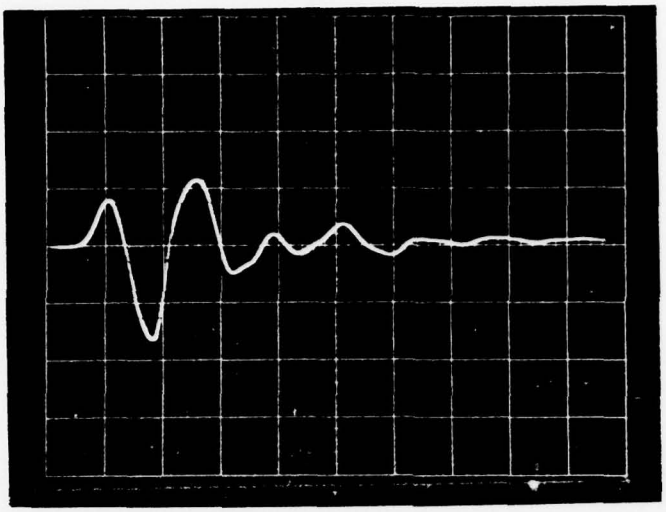

Vertical:
0.05 v/div
(inverted)

Horizontal:
0.2 μsec/div

(a)

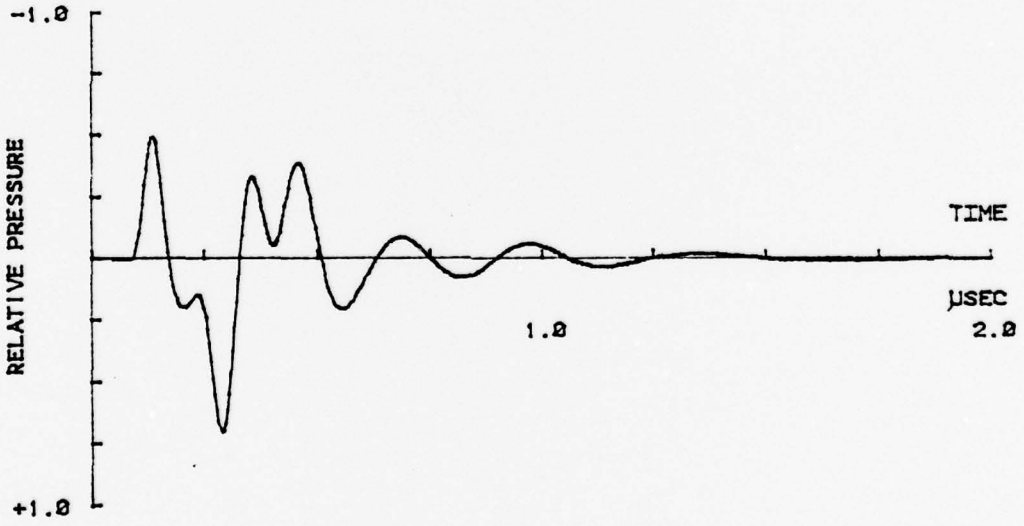

(b)

Figure 6.13. Comparison between the experimental and predicted on-axis transient pressure of system H-1
a. Experimental
b. Predicted

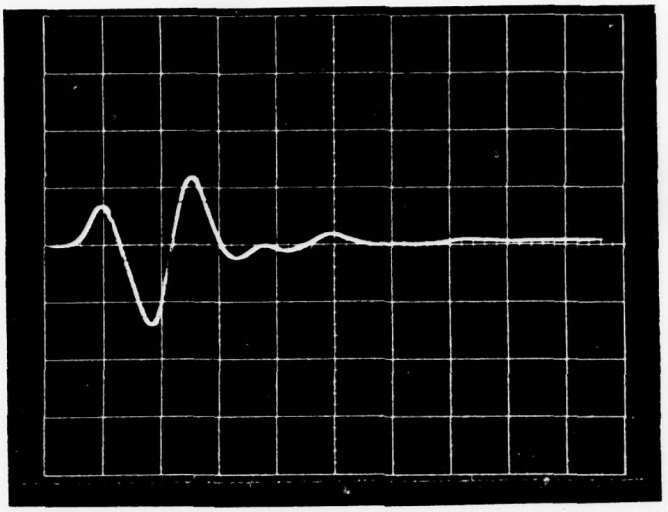

Vertical:
0.05 v/div
(inverted)

Horizontal:
0.2 μsec/div

(a)

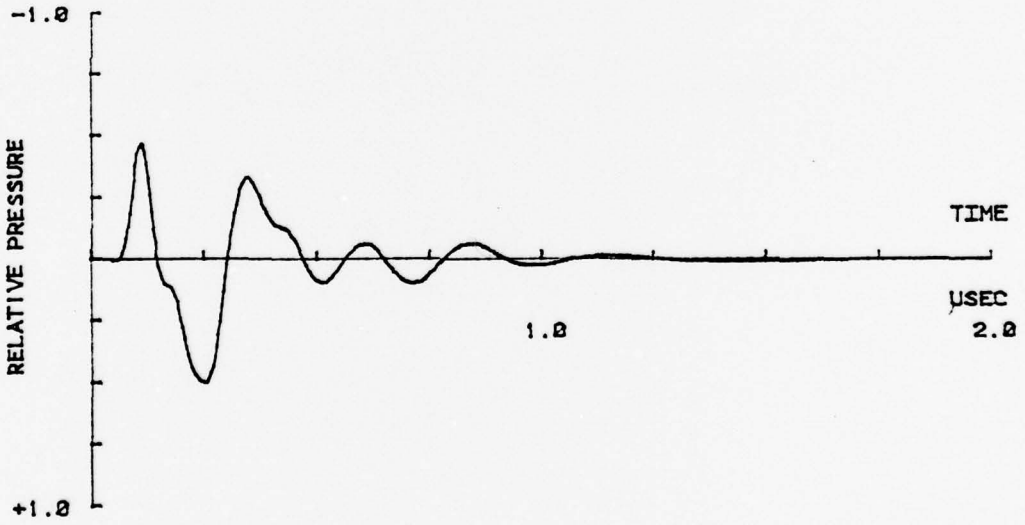

(b)

Figure 6.14. Comparison between the experimental and predicted on-axis transient pressure of system H-1-O
a. Experimental
b. Predicted

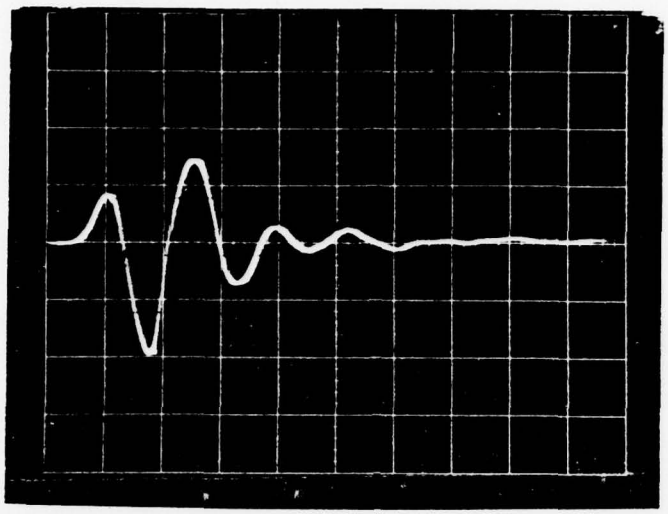

Vertical:
0.05 v/div
(inverted)

Horizontal:
0.2 μsec/div

(a)

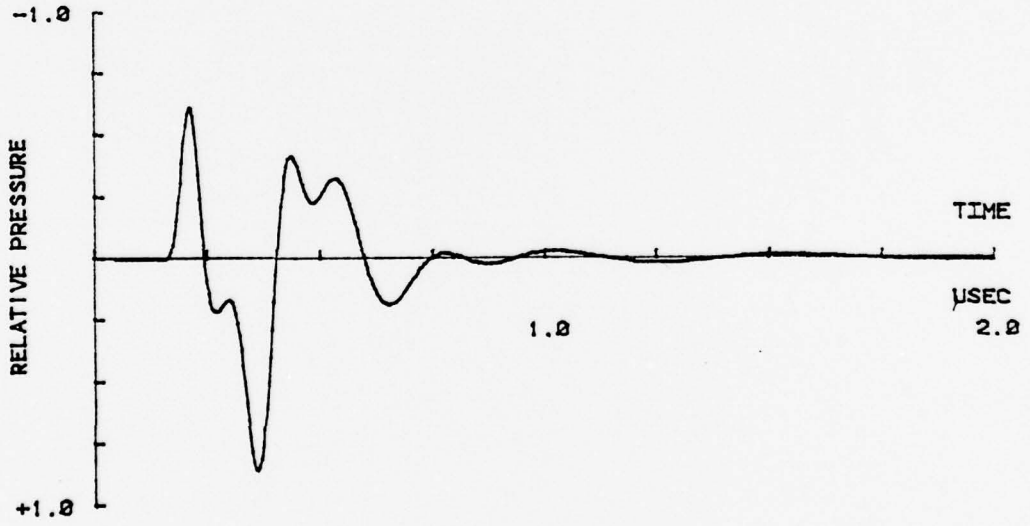

(b)

Figure 6.15. Comparison between the experimental and predicted on-axis transient pressure of system H-2
a. Experimental
b. Predicted

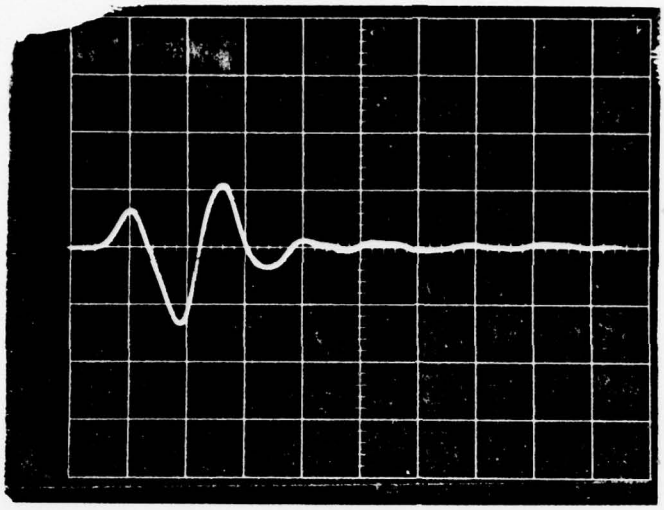

Vertical:
0.05 v/div
(inverted)

Horizontal:
0.2 μsec/div

(a)

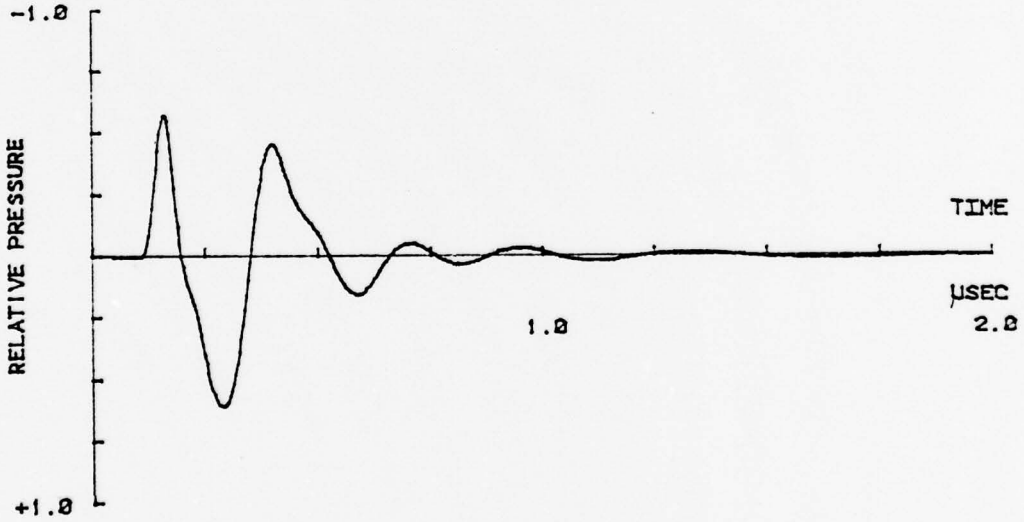

(b)

Figure 6.16. Comparison between the experimental and predicted on-axis transient pressure of system H-2-SO
a. Experimental
b. Predicted

tact, a comparison between the velocity and pressure responses would reveal a good (but sign inverted) pulse by pulse alignment after the first pressure pulse. For the lightly backed situation, it is therefore reasonable to suggest $t_s(4)$ as a separation time for pressure corresponding to a $t_s(3)$ separation time for velocity. Similarly, a $t_s(3)$ separation time for pressure is selected for the heavily backed systems.

Employing the above criteria for determining pressure separation times, the ratios of the third pressure pulse to the peak ring-down pressure pulse is computed for the responses in Figures 6.9 to 6.16. The third pressure pulse most closely corresponds to the second velocity pulse which has been calculted (from the model) to be the peak velocity pulse for the systems of interest. The numerical comparison between those predicted and measured pressure ratios are presented in Table 6.5. Although there is some discrepancy between the actual values of the observed and predicted ratios, the measured relative change due to optimization is in good accord with the theoretical change.

The results in this section demonstrate that the agreement between the theory and the observed results is adequate for achieving the desired time domain characteristics. Inclusion of the epoxy bonds in the model has also been demonstrated to be important. Consequently, it is reasonable to suggest that the optimization procedure should be carried out on a model incorporating the epoxy bonds of Table 6.4. System L-2-SO is an example where optimization without the bonds included in the modeling degrades the performance (see Table 6.5). Table 6.6 shows the results of length optimization on a model including the epoxy bonds. In Table 6.6, the system code suffix, EO, denotes

TABLE 6.5
RESULTS OF OPTIMIZING THE EXPERIMENTAL SYSTEMS

System code[1]	Face velocity peaks ratio (predicted dB)[2]	Pressure ratio (predicted dB)[3]	Pressure ratio (measured dB)[3]
L-1	7.0	8.1	7.4
L-1-O	7.0	6.7	6.8
Change due to optimization	0.0	-1.4	-(
L-2	12.1	13.4	12.7
L-2-SO	10.4	10.7	10.0
Change due to optimization	-1.7	-2.7	-2.7
H-1	8.6	5.8	8.2
H-1-O	12.4	10.5	13.0
Change due to optimization	+3.8	+4.7	+4.8
H-2	8.2	6.0	6.0
H-2-SO	9.0	9.2	9.1
Change due to optimization	+0.8	+3.2	+3.2

[1] The optimized systems are designed without including the epoxy bonds in the model.

[2] The values are the predicted peaks ratio including the epoxy bonds in the model.

[3] The the ratio of the third pressure peak to the peak ring-down pressure in Figures 6.9 to 6.16.

optimization on the quartz and lucite lengths with the epoxy bonds included in the model. A comparison between the EO cases of Table 6.6 (optimization including the epoxy bonds) with the O cases of Table 6.3a (no bonds included in the modeling) shows the impact of optimizing when including the effects of the bonds. The other systems in Table 6.6 (followed by *) are the optimized designs of Table 6.3a with the epoxy bonds considered in the peaks ratio calculations, but not considered in the optimization process. In other words, the comparisons offered by the examples within Table 6.6 demonstrate the consequences of wrongly assuming that the epoxy bonds will impact the transient response but will not affect the final design.

TABLE 6.6
SECTION LENGTHS AND THEORETICAL IMPULSE RESPONSE CHARACTERISTICS OF THE VARIOUS TRANSDUCER SYSTEMS (WITH EPOXY BONDS INCLUDED IN THE MODEL)

System code	Lucite length (m)	Quartz length(m)	V_{peak}	V_{ring}	Peaks ratio (dB)
L-1-EO	-	$4.25X10^{-4}$	0.83	0.29	9.1
L-1-O*	-	$5.31X10^{-4}$	0.66	0.27	7.7
L-2-EO	$2.03X10^{-4}$	$3.67X10^{-4}$	1.08	0.16	16.4
L-2-O*	$2.01X10^{-4}$	$4.91X10^{-4}$	0.94	0.25	11.7
H-1-EO	-	$1.98X10^{-4}$	0.54	0.09	15.5
H-1-O*	-	$3.02X10^{-4}$	0.56	0.20	8.9
H-2-EO	$1.07X10^{-4}$	$1.78X10^{-4}$	0.66	0.14	13.1
H-2-O*	$1.27X10^{-4}$	$2.85X10^{-4}$	0.69	0.26	8.6

* - recalcultions with epoxy bonds appended to the model after optimization

EO - cases that model the epoxy bonds during the optimiztion

CHAPTR VII

SUMMARY AND CONCLUSIONS

7.1 Summary

The goals of this research have been to design and test procedures for improving the acoustical response of piezoelectric disc transducers from an impulsive, electrical excitation. Plane wave propagation is assumed which implies zero output at even harmonics of the half-wave resonance. An impulsive excitation with a characteristic time shorter than the transit time through the ceramic has frequency components higher than that fundamental resonance frequency. Since the transducer cannot be wideband compared to that excitation, the acoustical output must be a distorted version of the electrical input including transient ringing. The methods described in this study yield designs for minimizing that ringing.

The Mason equivalent circuit has been utilized for modeling the piezoelectric disc. The resulting network has two ports corresponding to the disc's two faces, and one port representing the electrical input to the transducer. It is assumed that adjustments can be made at all three ports for achieving the desired improvements to the transient response. Matching at the electrical port is restricted to passive, lumped elements; at the back (nonradiating) mechanical port, purely resistive loading is considered, and up to three front-side matching sections are allowed. The acoustic load medium is modeled resistively. The features of interest in the acoustical output can be characterized by the velocity at the load medium. In the model, the velocity is equal to the current through the resistive load.

The impulse response is calculated by evaluating the inverse Laplace transform of the face velocity from its s-plane representation. Since the transfer function between the acoustical output and electrical input is a complicated expression involving transcendental functions, the Laplace inversion must be performed numerically. The Pade approximation to the exponential function is used for this purpose. Alternatively, the time response can be calculated using the inverse Fourier transform. However, a comparison between the two techniques reveals certain advantages with the Pade approximation. Although the high-order modes influence the transient response, they are observed to have a smaller impact than predicted by the Mason model. The abrupt termination of these modes incurred with the use of the Fourier transform leads to less accurate predictions than the gradual inaccuracies introduced by the Pade method. The errors caused by the Pade approximation compensate for the fact that the Mason Model under-predicts the attenuation of the higher modes.

Having obtained the impulse response, the analysis of various matching configurations can be evaluated once a suitable objective has been determined. An optimizing criterion has been devised to improve the peaks ratio of the velocity response at the interface between the transducer and acoustical load. The peaks ratio is defined as the ratio of the peak velocity to the peak ring-down velocity. The separation between useful energy and ring-down energy is somewhat dependent upon the transducer configuration. Even for matched acoustical loading at both mechanical ports, the mechanics of the transducer dictate that there must be at least two major velocity pulses. Hence, ring-down for heavily backed transducers begins after that second pulse. For a

lightly or air-backed system, an additional pulse is tolerated so that ring-down begins after the third velocity pulse. Due to these different physical situations, the results throughout this dissertation have analyzed the lightly and heavily backed cases separately. With the above definitions for optimization and ring-down, a gradient search is then appended to probe the parameter space for improved solutions. The circuit analysis, Laplace inversion, and gradient search have all been programmed to be calculated on a digital computer.

The numerical data provided for modeling describes a lead metaniobate disc, half-wave resonant in the low megahertz range. Lead metaniobate has been selected as the test material because of its relatively low Q and its low coupling between planar and radial modes. After demonstrating the theoretical utility of the design process, several examples have been built and tested. Because of the potential applications in medical ultrasonics and availablity, water is used as the acoustic load. The impedance mismatch between the ceramic and water is about fifteen to one.

7.2 Conclusions

Electrical matching with lumped elements can improve the impedance match between the electrical generator and transducer, thereby increasing the energy delivered to the acoustical load. Although electrical matching can also broad-band the frequency response, the peaks ratio is decreased. The energy storage elements tend to broaden the pulse that reaches the transducer. The change to the peaks ratio is more detrimental than helpful since peak power is only slightly increased compared to the substantial increase to ring-down energy. It

is believed that proper pulse shaping through an electrical network could improve the transient response. However, active circuits seem more suited to the task of providing rapidly changing pulse amplitude and phase. In effect, the problem is equivalent to finding the appropriate electrical excitation. Since the approach to that problem is considerably different from optimizing the mechanical matching, this work has examined only the latter.

It has already been mentioned that lightly and heavily backed systems have been treated separately. Accordingly, their designs are summarized separately, commencing with the lightly and air-backed transducers. The parameters that have been considered for optimization are the backing impedance and impedances and lengths of the front-side sections. For lightly backed transducers, there is little interaction between the optimization of the front- and back-side matching schemes. Consequently, they can be performed independently. The optimal backing for lightly damped systems has been found to present approximately twice the impedance of the water load. This result is independent of the specific details of the front-side match for one, two, or three matching sections. Selection of the optimal backing has been found to offer a good compromise between losses in peak power and suppression of peak ring-down power. The break point is most discernable for a two-section front-side transformer. For that situation, the optimal backing yields a 1-dB loss in peak power with a 3-dB increase to the peaks ratio. With larger backing impedances, the tradeoff is closer to one to one. These findings regarding the selection of suitable backing impedances substantiate and quantify the conclusions of other investigators.

For air-backed transducers, adjustment of front-side lengths and

impedances can provide considerable improvements to the peaks ratio over the classical maximally flat transformer. With the number of front-side sections fixed at one, two, or three, the possible gain from optimization is 3.0, 3.0, and 7.5 dB, respectively. Qualitatively, the effect of optimization is to redistribute the peak ring-down power throughout the ring-down range. In so doing, the design criteria prevent any major loss to the peak power. The optimization process on the front-side parameter space proceeds in a relatively straightforward manner without severe complications from locally optimal solutions. When considering suboptimal solutions with some parameters fixed, the flexibility afforded by optimization becomes apparent. As an example, length adjustments can only accomplish minor improvements when the impedances are close to being optimal. However, when the proper impedances are not available, length optimization becomes much more important.

With heavily backed transducers, the value of backing impedance does significantly affect the design of the front-side matching scheme. Consequently, the backing impedance must take a more active role in the optimization process. Although this complicates the optimization due to the presence of locally optimal solutions, it is beneficial in providing added flexibility to the finalized design. The results show that even with the backing impedance fixed, there is a considerable range and selection of front-side designs that yield acceptable impulse responses. Removing the restriction of fixed backing supplements this flexibility.

The design procedures do not specifically address the question of determining the optimal number of matching sections. For lightly backed transducers, the greatest improvement in the peaks ratio occurs for

increasing the number of sections from one to two. The addition of a third section only achieves marginal improvement over the two-section transformer. The major effect of increasing the number of sections is to decrease the peak-ring down velocity. There is little change in the peak velocity. With the heavily loaded transducer, the major benefit of a two-section transformer over a single matching section is added flexibility to the design of the front-side transformer. Some increases to the peak power and total energy are also to be gained. Although a third section can continue the increase to peak power and total energy, it may also increase the peak ring-down power. Peak ring-down power is increased due to the increased possiblity for energy storage within the mechanical transformer.

For fixed (resistive) electrical boundary conditions, and for a specific acoustic medium, the results demonstrate the importance of selecting the proper mechanical matching. A suitable choice of mechanical elements can improve and optimize the impulse response over classical frequency domain designs. The techniques also permit a degree of design flexibility for achieving comparable performance. Matching at the electrical port presents special problems with respect to the quality of the transient response. These difficulties have been examined and possible solutions have been suggested; however, no attempt has been made to resolve them.

The sensitivity to parameter variation has also been investigated. In general, the most sensitive front-side element is the section adjacent to the ceramic. In the proximity of an optimized solution, its length and impedance tend to be more critical than for the other sections. The impedance is typically found to be more sensitive than

the length. A useful property associated with the wide ranges of designs is that it also allows for some redistribution of parameter sensitivity.

Several transducer configurations have been constructed and tested to confirm the validity of the design procedure. Lightly and heavily backed systems have been checked, each with one- and two- matching sections. In addition to building a set of length optimized transducers, a control group using quarter-wave sections has also been fabricated. The frequency and time domain measurements have confirmed that the model and numerical Laplace inversion are sufficiently accurate for predicting the performance of the disc transducers. The experimental results therefore prove that the procedures developed in this research can effect the desired changes and improvements to the transient performance. The consequences of diffraction caused by a finite-sized disc are observed and offer direct experimental evidence to the correctness of diffraction theory. It has also been demonstrated that electrode layers and epoxy bonds should be included in the modeling during the optimization process.

7.3 Recommendations for Future Study

One of the most fundamental requirements for effective analysis is the accuracy of the model and associated numerical techniques. Improvements to the modeling are vitally important for better correlation between the theoretical and observed results. Although the Mason model provides an exact representation of a piezoceramic disc, it does not exactly describe the behavior of a physical disc. Radial mode coupling is neglected. Losses are only included by allowing a complex

Young's modulus. Nonuniformities, such as those caused by lead attachment, are not considered. Increased losses at the higher modes are not properly treated. Procedures for incorporating these effects into the model must be devised.

A limited number of mechanical matching schemes have been considered in this work. Although the combination of a resistive backing and a front-side layered match has been extensively examined, there are numerous other possibilities. One addition, which has been previously frequency domain tested, is the use of matching sections between the ceramic and backing. Complex backing, in general, may also be useful for improving the transient response. These mechanisms for transient response improvement merit further study.

A topic which has received little attention with respect to improving the transient response is matching at the electrical port. Traditionally, matching at that port has been approached from the requirements placed upon the reflection coefficient between the matching network and electrical generator. From an applications point of view, the transducer transient problem could justifiably be attacked somewhat differently. A more direct approach is to determine the excitation requirements for producing an acoustical impulse. Another means of adjusting the electrical boundary conditions is achieved by changes to the electrode configuration. It might also be possible to extend the optimization procedures in this dissertation to include an electrical port matching scheme.

Another area for study is the utilization of different optimization criteria. In addition to maximizing the peaks ratio, many different characteristics may be deemed important. Under those circumstances,

goal programming could be useful for assigning weights to the various parameters being monitored. It may even be desirable to incorporate parameter and load sensitivities into the optimization procedures. The search routine itself should be examined from an efficiency point of view. The experiences during this study have demonstrated that the gradient search is effective for reaching improved solutions. However, there have been problems with local maxima and slowness of convergence. The problems of search convergence and locally optimal solutions are directly linked to the optimization goal.

The results have considered the consequences of variability among the transducer's parameters. However, there has been no analysis on the effects of load variability. Since the finalized designs provide broad-band devices, it is expected that small changes to the resistive loading can be tolerated without seriously impacting the impulse response. However, nonhomogeneous load media may not be purely resistive. A nonresistive load is also encountered when the disc's diameter is comparable in size to the fundamental wavelength. Another common application resulting in complex acoustic load impedances is from the interaction between elements within an array. It is anticipated that any significant increase in the reactive component compared to the resistive value of the load would result in deviations from the previously determined designs. However, the procedures developed in this research should be adaptable for generating the new solutions.

This work has demonstrated the importance of including the factors pertaining to the construction of an actual transducer in the optimization process. Bond and electrode characteristics are specific examples. There are also operating requirements, specific to an

application, which may need to be included in the design procedures. Diffraction effects and off-axis operation are examples within this latter category. Although diffraction must be considered in both the near and far fields, it is conjectured that the performance changes due to diffraction would not affect the designs of transducers operating in the far field. For near-field operation, the consequences are more significant. Depending upon the application, new factors may need to be considered to account for diffraction effects in the optimization process. Off-axis operation would also require that additional constraints be incorporated into the optimization. The consequences of these ancillary factors with respect to optimizing the transducer transient response need further study.

REFERENCES

1. Aleksandrov, K.S., Gurovits, L.S., and Kamenskii, E.I., "Effect of an Intermediate Layer on the Frequency Characteristics of Ultrasonic Delay Lines," Sov. Phys.-Acoust. 6 170-177, (1960).

2. Alekseev, B.N., "Increasing the Bandwidth of a Cylindrical Piezoceramic Transducer by Means of Two Transition Layers," Sov. Phys.-Acoust. 22, 101-104, (1976).

3. Berlincourt, D.A., Curran, D.R., and Jaffe, H., "Piezoelectric and Piezomagnetic Materials and Their Function in Transducers," W. Mason and R. Thurston (Eds.), Physical Acoustics (Volume 1A), (Academic Press, Inc., 1964).

4. Bode, H., Network Analysis and Feedback Amplifier Design, (D. Van Nostrand Company Inc., New York, 1947).

5. Boxer, R. and Thaler, S., "A Simplified Method of Solving Linear and Nonlinear Systems," Proc. IRE. 44, 89-101, (1956).

6. Branin, F.H., "Transient Analysis of Lossless Transmission Lines," Proc. IEEE 55, 2012-2013, (1967).

7. Calahan, D., Computer-Aided Network Design, (McGraw-Hill, Inc., New York,1972).

8. Carlin, H.J., "A New Approach to Gain-Bandwidth Problems," IEEE Trans. Circuit & Syst. CAS-24, 170-175, (1977).

9. Cohn, S.B., "Optimum Design of Stepped Transmission-Line Transformers," IRE Trans. Microwave Theory & Tech. MTT-10, 339-359, (1962).

10. Collin, R.E., "Theory and Design of Wide-Band Multisection Quarter-Wave Transformers," Proc. IRE 43, 179-185, (1955).

11. Desilets, C.S., Fraser, J.D., and Kino, G.S., "The Design of Efficient Broad-Band Piezoelectric Transducers," IEEE Trans. Sonics & Ultrason. SU-25, 115-124, (1978).

12. Director, S. and Rohrer, R., "Automated Network Design - The Frequency-Domain Case," IEEE Trans. Circuit & Sys. CT-16, 330-337, (1969). 202-205, (1975).

13. Dvorak, V., "Transient Analysis of Nonuniform Transmission Lines," Proc. IEEE 58, 844-845, (1970).

14. Fano, R.M., "Theoretical Limitations on the Broadband Matching of Arbitrary Load Impedances," J. Franklin Inst. 249, 57-83,139-155, (1950).

15. Foldy, L.L. and Primakoff, H., "General Theory of Passive Linear Electroacoustic Transducers and the Electroacoustic Reciprocity Theorem. I," J. Acoust. Soc. Am. 17, 109-120, (1945).

16. Foster, F.S. and Hunt, J.W., "The Design and Charcaterization of Short Pulse Ultrasound Transducers," Ultrasonics 16, 116-122, (1978).

17. Gledhill, C.S. and Issa, A.M.H., "Exact Solutions of Stepped Impedance Transformers Having Maximally Flat Chebychev Characteristics," IEEE Trans. Microwave Theory & Tech. MTT-17, 379-385, (1969).

18. Goldman, S., Frequency Analysis,Modulation, and Noise, (McGraw Hill Book Company, Inc., New York, 1948).

19. Goll, J.H., Ultrasonic Absorption by Phospholipid Vesicles: Acoustic Impedance Matching and the Design of Broadband Piezoelectric Transducers, (Ph.D. Thesis, Stanford University, Stanford, California, 1974).

20. Goll, J.H. and Auld, B.A., "Multilayer Impedance Matching Schemes for Broadbanding of Water Loaded Piezoelectric Transducers and High Q Resonators," IEEE Trans. Sonics & Utranson. SU-22, 52-53, (1975).

21. Heuter, T.F. and Bolt, R.H., Sonics, (John Wiley & Sons, Inc., New York, 1955).

22. Hjellen, G.A., Anderson, J., and Sigelmann, R.A., "Computer-Aided Design of Ultrasonic Transducer Broadband Matching Networks," IEEE Trans. Sonics & Ultrason. SU-21, 302-305, (1974).

23. International Business Machines, Inc. (IBM), International Mathematical and Statistical Library, (ISML, Houston, 1975).

24. Ho, C., "Time-Domain Sensitivity Computation for Networks Containing Transmission Lines," IEEE Trans. Circuit & Sys. CT-18, 114-122, (1971).

25. Jury, E.I., Theory and Application of the z-Transform Method, (John Wiley & Sons, Inc. New York, 1964).

26. Kasai, C., Okuyama, K., and Kikuchi, Y., "Transient Response Analysis of Piezoelectric Transducers Using Reflection and Transmission Coefficients at Their Surfaces," Electron. & Commun. Jap. 56-A, 19-25, (1973).

27. Kinariwala, B.K., "Theory of Cascaded Structures: Lossless Transmission Lines," Bell Syst. Tech. J. 45, 631-649, (1966).

28. Kinsler, L.E. and Frey, A.R., Fundamentals of Acoustics, (John Wiley & Sons, Inc., New York, 1962).

29. Kittenger, E. and Rehwald, W., "Improvements of Echo Shape in Low Impedance Materials," Ultrasonics 15, 211-215, (1977).

30. Kossoff, G., "The Effects of Backing and Matching on the Performance of Piezoelectric Transducers," IEEE Trans. Sonics & Ulrason. SU-13, 20-30, (1966).

31. Lakestani, F., Beboux, J.C., and Fleischman, P., "Broadening the Bandwidth of Piezoelectric Transducers by Means of Transmission Lines," Ultrasonics 13, 176-180, (1975).

32. Lees, S., Gi lmore, R., and Kranz, P., "Acoustic Propert es Of Tungsten-Vinyl Composites," IEEE Trans. Sonics & Ultrason., SU-20, 1-2, (1972).

33. Lovygin, V.A., "Determination of the Equivalent Parameters of Transducers from Impedance or Admittance Phase Diagrams," Sov. Phys.-Acoust. 16, 357,-360 (1971).

34. Mason, W.P., Electomechanical Transducers and Wave Filters, (D. Van Nostrand Company, Inc., New York, 1948).

35. Merkulov, L.G. and Yablonik, L.M., "Operation of a Damped Piezoelectric Transducer Containing a Number of Intermediate Layers," Sov. Phys.-Acout. 9, 365-372, (1964).

36. Noguchi, T. and Fukumoto, A., "Diagnostic Study of Bonded, Thickness Mode Transducers by Input Impedance Measurement," IEEE Trans. Sonics & Ultrason. SU-20, 365-370, (1973).

37. Onoe, M., "Theory of Ultrsonic Delay Lines for Direct Current Pulse Transmission," J. Acoust. Soc. Am. 34, 1247-1254, (1962).

38. Oppenheim, A.V. and Shaffer, R.W., Digital Signal Processing, (Prentice-Hall, Inc., Englewood Cliffs, N.J., 1975).

39. Peterson, R.G. and Rosen, M., "Use of Thick Transducers to Generate Short-Duration Stress Pulses in Thin Specimens," J. Acoust. Soc. Am. 41, 336-345, (1967).

40. Pirgov, V.A., Reizin, E.S., and Tartakovskii, B.D., "Matching Layers for Electroacoustic Receiving Transducers," Sov. Phys,-Acoust. 19, 478-481, (1974).

41. Redwood, M., "Transient Performance of a Piezoelectric Transducer," J. Acoust. Soc. Am. 33, 527-534, (1961).

42. Redwood, M., "Piezoelectric Generation of an Electrical Impulse," J. Acoust. Soc. Am. 33, 1386-1390, (1961).

43. Riblet, H.J., "General Synthesis of Quarter-Wave Impedance Transformers," IRE Trans. an Microwave Theory and Tech., MTT-5, 36-43, (1957).

44. Seitchik, J.A., "The Determination of Transducer Coupling Coefficients by Time Domain Analysis," IEEE Trans. Sonics & Ultrason. SU-19, 23-27, (1972).

45. Singhal, K. and Vlach, J., "Computation of Time Domain Response by Numerical Inversion of the Laplace Transform," J. Franklin Inst. 299, 109-126, (1975).

46. Sittig, E.K., "High-Speed Ultrasonic Digital Delay Line Design: A Restatement of Some Basic Considerations," Proc. IEEE 55, 1194-1202, (1968).

47. Souquet, J., Defranould, P., and Desbois, J., "Design of Low-Loss Wide-Band Ultrasonic Transducers for Noninvasive Medical Application," IEEE Trans. Sonics & Ultrason. SU-26, 75-81, (1979).

48. Stepanishen, P.R., Transient Analysis of Planar Sonar Arrays, (Ph.D thesis, The Pennsylvania State University, State College, Pennsylvania, 1969).

49. Vlach, J., "Numerical Method for Transient Responses of Linear Networks with Lumped, Distributed, or Mixed Parameters," J. Franklin Inst., 288, 99-113, (1969).

50. Young, L., "Tables for Cascaded Homogeneous Quarter-Wave Transformers," IRE. Trans. Microwave Theory & Tech. MTT-7, 233-237, (1959).

51. Young, L., "Stepped-Impedance Transformers and Filter Prototypes," IRE Trans. Microwave Theory & Tech. MTT-10, 339-359, (1962).

APPENDIX A

LOW-FREQUENCY EVALUATION OF THE PIEZOCERAMIC COUPLING COEFFICIENT

The piezoelectric coupling coefficient can be defined as the ratio of the mutual elastic and dielectric energy density to the geometric mean of the elastic and dielectric self-energy. Its value is not only dependent upon the physical properties of the material but also on the appropriate boundary conditions. For a thin disc transducer, with poling parallel to the applied electric field, the coupling coefficient is typically denoted as k_t. Berlincourt et al. outline the procedure for deriving k_t directly from the piezoelectric equations. For the thin disc under consideration, k_t is evaluated as:

$$k_t = \sqrt{\frac{h}{cb}} \quad . \tag{A.1}$$

The equivalent circuit of Figure 3.3 can also be used to evaluate k_t. Since k_t is assumed to be independent of the mechanical loading and frequency over the range for which the equivalent circuit is valid, it can be calculated for any particular loading and frequency range. For the case of air loading ($Z_L=Z_R=0$), the circuit of Figure 3.3 can be redrawn as shown in Figure A.1a. The total impedance Z_m on the mechanical side of the transformer is given by:

$$Z_m = jZ_o[0.5\tan\frac{kl}{2} - 1/\sin kl] = -j\,\frac{Z_o}{2}\,\frac{\cos\frac{kl}{2}}{\sin\frac{kl}{2}} \quad . \tag{A.2}$$

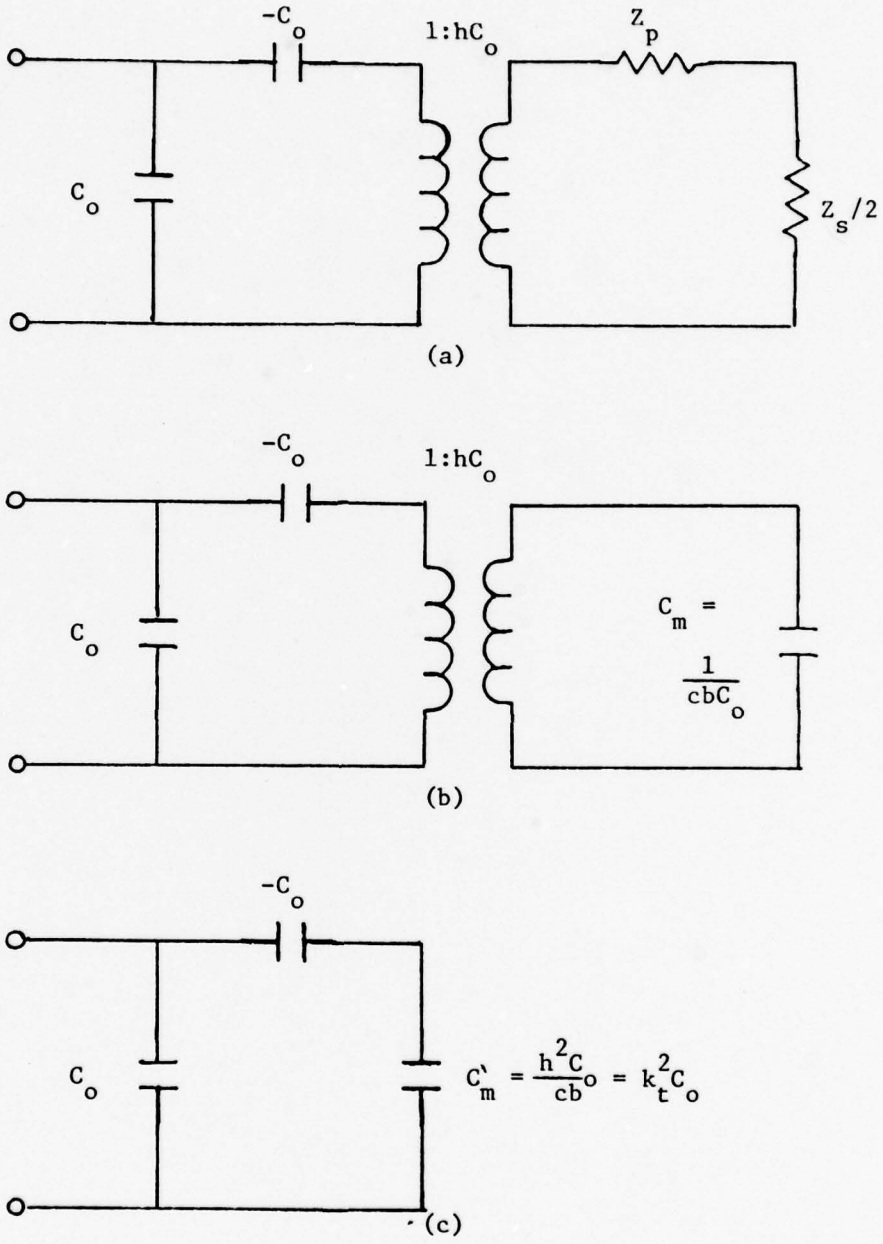

Figure A.1. Equivalent circuit for air loading on each face
a. Mason Equivalent circuit
b. Low-frequency approximation
c. Low-frequency approximation after removal of transformer

At low frequencies, where $\cos\frac{kl}{2}$ is approximately unity and $\sin\frac{kl}{2}$ can be approximated by $\frac{kl}{2}$, Z_m can be expressed as follows:

$$Z_m = -\frac{jZ_o}{kL} = 1/j2\pi f\left(\frac{L}{vZ_o}\right) \quad , \tag{A.3}$$

where L is used to denote the section length l to avoid confusion with the numeral one. Therefore, at low frequencies, the total load on the mechanical side of the transformer responds like a capacitor of value:

$$C_m = \frac{L}{vZ_o} \tag{A.4}$$

as shown in Figure A.1b. Recalling the definitions for Z_o and C_o from Equations (3.15) and (3.18), C_m can be expressed as:

$$C_m = \frac{L}{v^2\rho A} = \frac{1}{v^2\rho C_o b} = \frac{1}{cbC_o} \quad . \tag{A.5}$$

The final simplification of the circuit is shown in Figure A.1c where the transformer has been removed by scaling capacitor C_m by the square of the transformer's turns ratio. The value of the scaled capacitance is:

$$C'_m = \frac{h^2 C_o}{cb} = k_t^2 C_o \quad . \tag{A.6}$$

With the application of a voltage V at the input terminals, the energy stored in the capacitors is readily determined from:

$$\text{Energy} = \frac{1}{2} C_c V_c^2 \quad , \tag{A.7}$$

where V_c is the voltage across a capacitor of capacitance C_c. Applying Equation (A.7) to the circuit of Figure A.1, the ratio of the energy stored in $-C_o$ and C_m' to the total energy stored in the circuit is found to be equal to the square of the coupling coeffficient. From Figure A.1c the effective low-frequency input capacitance is given by

$$C_{eff} = C_o + \frac{C_m' \cdot C_o}{C_o - C_m'} \quad . \tag{A.8}$$

Substituting Equation (A.6) into Equation (A.8) results in:

$$C_{eff} = C_o \frac{1}{(1 - k_t^2)} \tag{A.9}$$

which provides a direct way for calculating k_t.

APPENDIX B

EXPERIMENTAL DETERMINATION OF THE PARAMETERS IN THE EQUIVALENT CIRCUIT

There are several time and frequency domain methods for determining the piezoelectric parameters [33,36,44]. Basically, these approaches adjust the appropriate parameters of the Mason equivalent circuit until the theoretical response agrees with the experimental response. A similar technique is used here. Where available, data offered by the manufacturer is used to determine approximate parameter values. A systematic approach to improve those initial estimates is accomplished by noting that each parameter has its major impact on a particular aspect of the response. The material constants and circuit parameters necessary for describing a piezoelectric disc are defined in Table B.1.

The mechanical constants of density, area, and length can be measured by any suitable means. The main caution in making those measurements is to account for the conductive layer of silver on each face. Because of the relative dimensions and densities, the silver accounts for approximately 20% of the total disc mass. As is shown in Section 3.2, the mass loading caused by the silver results in a significant shift of resonance frequency and should not be neglected. Consequently, the final model of the disc includes a model of the ceramic sandwiched between two silver layers. The thickness of each silver layer must also be determined.

For establishing v, γ, ϕ, and C_o, the transducer's measured electrical input impedance is to be compared to the impedance as predicted by the model. The experimental disc is approximately

TABLE B.1
DEFINITION OF CONSTANTS FOR DESCRIBING A
PIEZOCERAMIC DISC

Symbol	Definition
	Density
v	Speed of sound in the thickness direction
γ	Loss factor which defines the imaginary component of Young's modulus
A	Area
l	Thickness
ϕ	Turns ratio of ideal transformer in Figure 3.3
C_o	Clamped capacitance

$1.27X10^{-2}$ m (0.5 inch) in diameter and approximately $6.75X10^{-4}$ m (0.027 inch) thick including the silver layers. Short leads are attached near the edge of each face by conductive epoxy. Impedance measurements are made with a Hewlett Packard 4815 RF vector impedance meter. Figure B.1a shows the measured input impedance of a nonmounted disc, air loaded on each face. For no other losses in the system, it has been found that v and γ set the frequency of maximum motional impedance and Q, respectively. The frequency of maximum motional impedance, f_z, occurs within the impedance loop and is labeled on Figure B.1 Although the values of v and γ are very specific for establishing the aforementioned parameters, it is desirable to determine γ first. This is because, with γ=0 and with no other system losses, the impedance loop would have an infinite diameter. Once v and γ are set, the next step in the procedure is to adjust ϕ and C_o. The turns ratio, ϕ, primarily adjusts the diameter of the loop, whereas C_o establishes the low-frequency response. Keying in on those aspects of the response, ϕ and C_o are alternately adjusted to match the predicted response with the measured response. Since the adjustments of ϕ and C_o <u>do</u> interact with each other, about four iterations are required to achieve a suitable match between predicted and measured responses. The adjustments of ϕ and C_o cause no appreciable change to Q or f_z. Table B.2 compares the estimated and final values of the various constants. The predicted impedance using those values is shown in Figure B.1b. For the <u>unmounted</u> air-loaded disc, γ is determined to be 0.015.

Two low-frequency data points can be used to verify the dynamically determined values of ϕ and C_o. At 0.5 MHz, the input impedance is approximately -269j ohms corresponding to a capacitance, C_{eff}, of

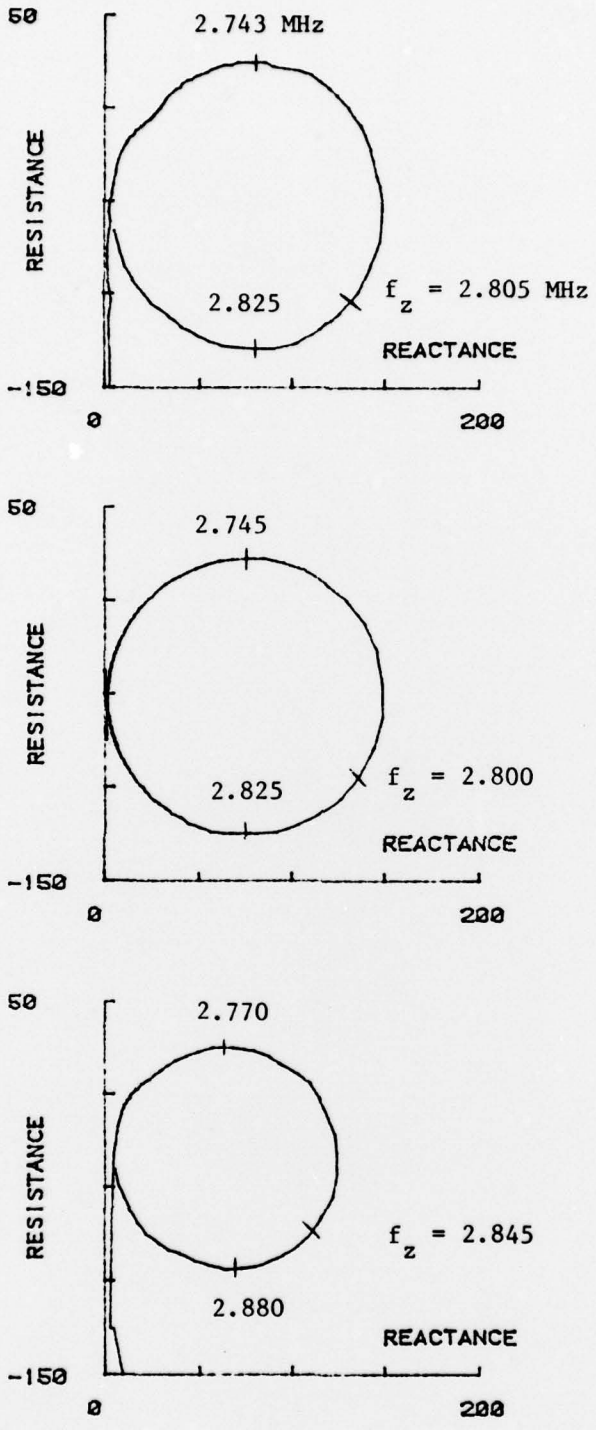

Figure B.1. Electrical input impedances for air loading
a. Measured (unmounted disc)
b. Predicted (= 0.015)
c. Measured (disc mounted in housing)

TABLE B.2
ESTIMATED AND FINAL VALUES OF CONSTANTS
FOR AN UNMOUNTED DISC

Constant	Estimated Value	Actual Value
p (ceramic)	$5.5X10^{3}$ kg/m^{3}	$5.5X10^{3}$ kg/m^{3}
v (ceramic)	$3.31X10^{3}$ m/sec	$4.23X10^{3}$ m/sec
l (ceramic)	------	$6.01X10^{-4}$ m
p (silver)	$10.5X10^{3}$ kg/m^{3}	not measured
v (silver)	$3.7X10^{3}$ m/sec	not measured
l (silver)	------	$4.23X10^{-5}$ m
A	------	$1.29X10^{-4}$ m^{2}
γ	none available	see text
ϕ	4.17 coulomb/m	1.45 coulomb/m
C_o	$1.34X10^{-9}$ Farad	$1.08X10^{-9}$
k_t	0.35	0.30

Note: The values for k_t are calculated from the other parameters using Equations (A.1) and (3.22b).

$1.18X10^{-9}$ Farad. A similar measurement on a depolarized sample has confirmed the value of C_o in Table B.2. With those two values, k_t is calculated from Equation (A.9) to be 0.30. Equations (3.14) and (3.18) can be used for evaluating c and b:

$$c = 9.84X10^{10} \text{ Newtons/m}^2$$

and

$$b = 1.99X10^{8} \text{ m/Farad} \quad .$$

Using Equation (A.1) for calculating h, ϕ is determined from Equation (3.23b) and is found to be 1.42 coulombs/Farad. This low-frequency determination of k_t and ϕ agrees well with their values in Table B.1 which have been determined dynamically.

For the model to be useful, *it must* successfully predict performance under other acoustical load conditions. Since it is ultimately desired to operate the transducer into a water medium, water is a logical selection as an acoustical load. Figure B.2 illustrates the housing and waterproofing so that only one face is loaded by water. Care has been taken to secure the transducer to the housing only near the disc's edge. Figure B.1c shows the measured air impedance of the mounted transducer. Figure B.3a displays the impedance of the water-immersed transducer, while Figure B.3b shows the predicted.

Comparing Figure B.1a with Figure B.1c, it is seen that the housing itself has affected the input impedance and has lowered the effective Q. However, Figure B.3 shows that the model still provides a reasonable prediction to the water-loaded case. Some of the additional loss caused by the mounting can be approximated by increasing gamma from 0.015 to

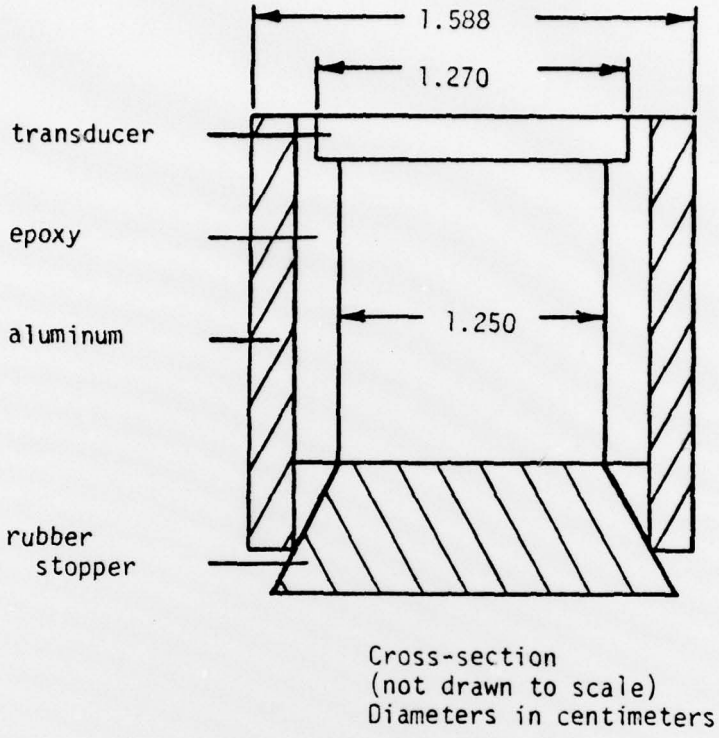

Figure B.2. Housing to waterproof one face of the disc

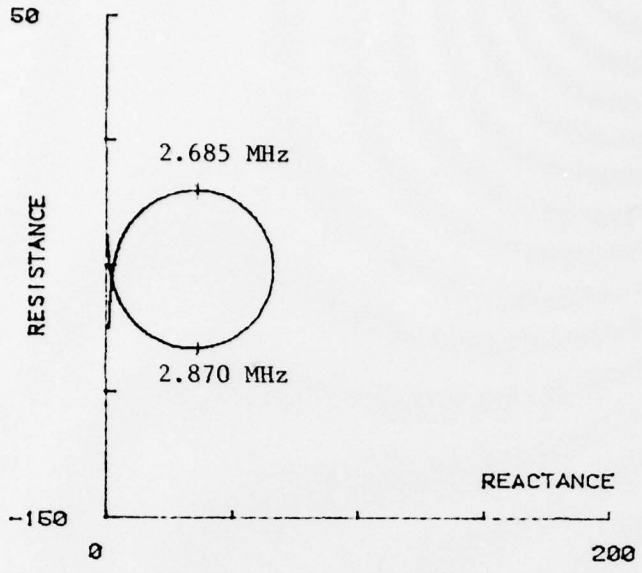

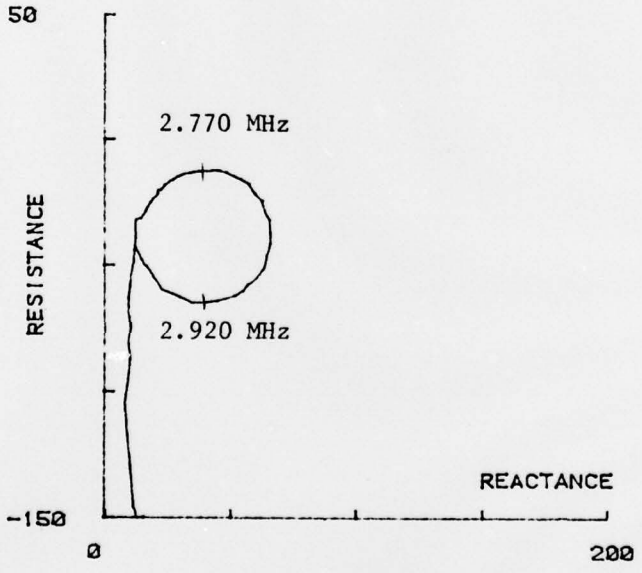

Figure B.3. Electrical input impedance for water loading
a. Measured
b. Predicted values (Y=0.015)

0.018. The impedance diagrams for γ=0.018 with air and water loading are shown in Figure B.4a and B.4b. For subsequent use, the effective value of gamma is considered to be 0.018. This effective γ not only includes the internal losses of the disc, but also accounts for air loading, the losses of mounting, and damping resulting from attaching the leads. As demonstrated in Figures B.3a and B.4b, and as would be expected, the effects of small errors in estimating are reduced as the total loss is increased.

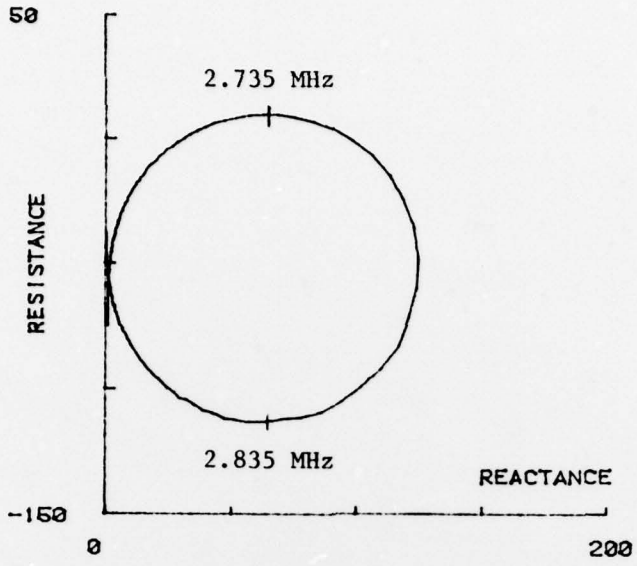

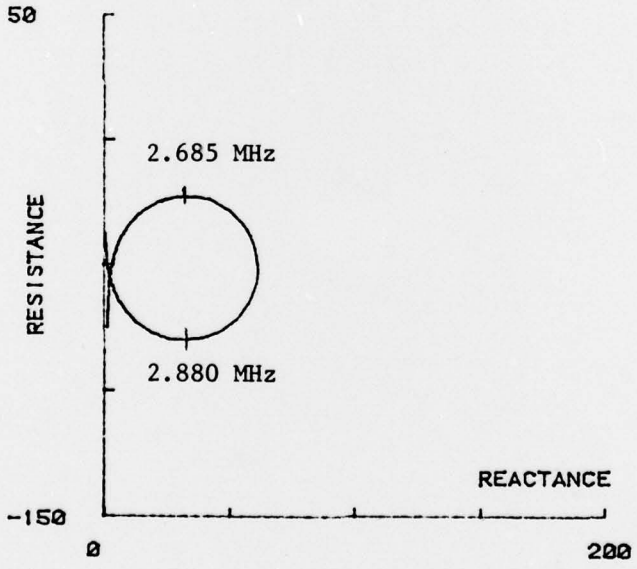

Figure B.4: Predicted input impedances for γ=0.018
a. Air loading
b. Water loading

APPENDIX C

CALCULATION OF THE PADE POLES AND RESIDUES

The Pade poles and residues are found directly from Equation (3.34). A standard polynomial root finder has been used to determine the poles (the zeros of the denominator). The IBM IMSL [23] subroutine ZPOLR was utilized for this purpose. For simple poles it is well known that the residue k_i, corresponding to the pole z_i, is evaluated from:

$$k_i = \left. \frac{\text{Numerator}(z)}{\text{Denomonator}'(z)} \right|_{z=z_i} \qquad \text{(C.1)}$$

where the Numerator(z) is the numerator of Equation (3.34) and Denominator'(z) excludes the factor $(z - z_i)$ from the denominator of Equation (3.34). Implementing the above procedure in double precision arithmetic on an IBM/168 computer yields the results in Table C.1. Comparison with published data shows good agreement to 15 significant figures.

TABLE C.1
POLES AND RESIDUES OF THE PADE EXPANSION

	Poles	Residues
Order (8,10)		
	.42345224947970D+01 + j.14957043781281D+02	.66082970623744D+02 + j.87383739943856D+01
	.77811462644646D+01 + j.11368891649049D+02	-.14352090805158D+04 + j.83705474204212D+03
	.99333837221749D+01 + j.80331063342664D+01	.73148701261718D+04 - j.95909040924992D+04
	.11220853779395D+02 + j.47929641675650D+01	-.14089055856573D+05 + j.37178791186329D+05
	.11830093739168D+02 + j.15937530058873D+01	.81433118401531D+04 - j.69537355775659D+05
Order (12,14)		
	.51178718946201O2D1 + j.2245270182315893D2	.36144301483169922 + j.182295255726616D3
	.9453357916472669D1 + j.1853341976027059D2	-.9293676103759179D4 - j.4343903743137378D4
	.1235050436358592D2 + j.1496568426279466D2	.154332004496505 4D6 - j.208655131876026 4D5
	.1439628584252762D2 + j.11547196565756 00D2	-.9163980344255252D6 + j.562363548191830 9D6
	.1581463383821985D2 + j.8206718813865727D1	.260965182526151 6D7 - j.318944065571841 9D7
	.1671472578531848D2 + j.4909378054420813D1	-.3735643532008891D7 + j.893145941562071 3D7
	.1715262035925535D2 + j.1634176154052124D1	.189731527010183 8D7 - j.145505505410269 8D8
Order (14,16)		
	.5493613186036534D1 + j.2623996550494974D2	.12698129266476 99D3 - j.255930094696068 6D3
	.1015607815170750D2 + j.2217983762574296D2	.12411374367397 82D5 + j.180844288032619 6D5
	.1335447600083716D2 + j.1851173976797145D2	-.4277932850447541D6 - j.138613103247196 1D6
	.1569761834373091D2 + j.1501497891837984D2	.4107789754521790D7 - j.684330748293739 9D6
	.1742055935974349D2 + j.1161123965564184D2	-.1836633432926809D8 + j.111861220072943 7D8
	.1864149510045466D2 + j.8262332819494975D1	.4436330106988009D8 - j.528146013476020 3D8
	.1942600242170738D2 + j.4945905381609919D1	-.5781779934027215D8 + j.134031344700322 9D9
	.1981015743578234D2 + j.16468144772842 56D1	.2812829782396646D8 - j.208871467962816 1D9

The poles in the lower half-plane (and their corresponding residues) are the complex conjugates of those shown above.

VITA

Henry Alan Wolf

Born: March 8, 1951; Paterson, New Jersey

Education: Rutherford Senior High School; Rutherford, New Jersey, 1969

Cornell University; Ithaca, New York, Bachelor of Science in Engineering, January, 1973; and

Master of Engineering (Electrical), January, 1974

Employment: Assistant Engineer with the New Jersey Department of Environmental Protection, Office of Noise Control, Trenton, New Jersey; January, 1974 to September, 1975

Graduate Research Assistant at the Applied Research Laboratory of The Pennsylvania State University; September, 1975 to August 1979

Honoraries and Professional Societies:

Eta Kappa Nu

Tau Beta Pi

Acoustical Society of America

DISTRIBUTION

Commander (NSEA 09G32)
Naval Sea Systems Command
Department of the Navy
Washington, DC 20362 — Copies 1 and 2

Commander (NSEA 0342)
Naval Sea Systems Command
Department of the Navy
Washington, DC 20362 — Copies 3 and 4

Defense Documentation Center
5010 Duke Street
Cameron Station
Alexandria, VA 22314 — Copies 5 through 16